TID-2506(DEL.)

NUCLEAR SCIENCE AND TECHNOLOGY

Extracts from Nuclear Science and Technology,
Volume 1, Issues 1 to 3 (February - June 1955)

Photostat Price $ 28.80
Microfilm Price $ 8.40

Available from the
Office of Technical Services
Department of Commerce
Washington 25, D. C.

Technical Information Service, Oak Ridge, Tennessee

Contents

INTRODUCTION v

ARTICLES

Some Aspects of Stored Energy In Irradiated Graphite. Part I. Kinetics of the Release
William Primak 1

Measurements and Analysis of Uranium – D_2O Lattices
F. B. Estabrook and S. W. Kash 15

Recovery of Fissionable Material from Enriched-uranium Fuels. Part II. Experimental Breeder Reactor Fuel Elements
L. Burris, Jr., S. Lawroski, M. Levenson, R. C. Vogel, and S. Vogler 39

The Variation of $\alpha^{U^{235}}$ with Energy in the Intermediate-energy Range
Sophie Oleksa 57

HRE Experiments on Internal Recombination of Gas with a Homogeneous Catalyst
S. Visner and P. N. Haubenreich 73

REACTOR DATA TABLE 91

REACTOR FUTURES

A Conceptual Design for the Army Package Power Reactor
Robert S. Livingston 103

A Gas-cooled Liquid-metal Reactor
H. L. Falkenberry, C. J. Raseman, W. A. Robba, T. V. Sheehan, and L. D. Stoughton 125

CONTENTS

REACTOR FUTURES

A Hybrid-reactor Proposal — George Safonov — 143

Plutonium Power Reactor with Oxide Fuel and Blanket Elements — J. B. Sampson and E. A. Luebke — 145

TECHNICAL NOTES

Radioactivity in Reactor Cooling Water — W. S. Lyon, Jr., and S. A. Reynolds — 181

A Method of Estimating the N^{16} Content in the Cooling System of an MTR Type Reactor — F. T. Binford — 189

Continuous Repurification of LITR Cooling Water — J. A. Cox, W. R. Casto, and W. H. Tabor — 201

LETTERS TO THE EDITORS — 207

INTRODUCTION

The new classification guide of the Atomic Energy Commission places the majority of information on reactor technology and related subjects in the "Confidential" category. Much of the material in back issues of the Journal of Nuclear Science and Technology and its predecessors, the Journal of Metallurgy and Ceramics and the Journal of Reactor Science and Technology, falls into this category. In order to make such information readily available to those possessing a suitable clearance, articles from these earlier issues are being reissued as Gray Area Journals as follows:

TID-2501	JMC, Issues 1 thru 6 (TID-65 thru 69), July 1948 - January 1951
TID-2502	RST, Vol. 1, Issues 1 thru 3 (TID-71 thru 73), April 1951 - December 1951
TID-2503	RST, Vol. 2, Issues 1 thru 4 (TID-2001 thru 2004), April 1952 - December 1952
TID-2504	RST, Vol. 3, Issues 1 thru 4 (TID-2008 thru 2011), March 1953 - December 1953
TID-2505	RST, Vol. 4, Issues 1 thru 4 (TID-2012 thru 2015), March 1954 - December 1954
TID-2505A	Cumulative Index to all "back issue" JMC and RST Gray Area material
TID-2506 Vol. 1A, Issue 1	NST, Vol. 1, Issues 1 thru 3 (TID-2016 thru 2018), February 1955 - June 1955

Due to the many changes which have taken place on the editorial staff of the Journal during its history, it has been considered inadvisable to specify individual credits for material from early issues. In this regard, the present editors would like to acknowledge the fine work of former editors, Bruce S. Old, George L. Weil and Frank R. Ward, through whose efforts most of the material was originally obtained.

SOME ASPECTS OF STORED ENERGY IN IRRADIATED GRAPHITE

Part I. Kinetics of the Release

WILLIAM PRIMAK

Chemistry Division
Argonne National Laboratory

January 4, 1955

ABSTRACT

Previous scientific studies of the release of stored energy in irradiated graphite are briefly reviewed against the background of studies of the kinetics of the annealing of radiation damage in graphite. It is concluded that the postulation of a quasi-continuous distribution of activation energies for annealing gives the best explanation of the data at present available. The problem of the behavior of kinetic processes distributed in activation energy is considered, and V. Vand's treatment of them is extended. It is shown that most of the stored-energy data gathered in the past are not suitable for detailed kinetic analysis and cannot be used for much more than to derive an approximate activation-energy spectrum. An exception is found in some experimental data reported by J. C. Ballinger. It is shown how data of this kind can afford a means of determining the order of reaction and the frequency factor as well as the activation-energy spectrum. Ballinger's data suggest an order less than unity (the physical conditions from which such a result can arise are suggested) and a frequency factor between 10^{10} and 10^{14} sec^{-1}. However, his data are not sufficiently precise to fix these quantities with certainty.

1. INTRODUCTION

Accounts of the discovery of radiation damage in graphite have been given by Burton,[1] Lees and Neubert,[2] and others.[3] Soon after the discovery of changes in the properties of graphite upon bombardment with neutrons at the St. Louis cyclotron, Neubert et al.[4] heated the irradiated specimens and found that the property changes decreased. In the first preliminary experiments[5] irradiated samples were heated to 100°C until no further change in their electrical resistivity could be observed after long heating times. It was found that only a part of the property change due to irradiation had disappeared. When these samples were heated to 200°C until no further change in their electrical resistivity could be observed, another part of the property change due to irradiation disappeared. Later it was found that the radiation-induced changes in

electrical resistivity and in elastic modulus did not alter proportionately[6] on heating. These experiments suggested that the disturbances in irradiated graphite were not all of one kind. It was proposed by Neubert[7] that the disturbances be considered as if they annealed over a range of activation energies, in the manner considered by Vand[8] for disordered metals, with different weighting functions for the different properties.

Accounts of the discovery of stored energy in irradiated graphite are given by Lees and Neubert[2] and by Fuchs and Primak,[9] among others. The first attempts to find stored energy were made using several methods of differential thermal analysis. Maurer and Ruder[10] reported that the evolution of stored energy accompanied, but was not proportional to, the alterations in the resistance changes found by Neubert et al. Leaf and Novick[11] found that the temperature of maximum stored-energy release per degree varied with the heating rate. Assuming a single activation energy and first-order kinetics, they computed the activation energy to be 28 kcal/mole and the frequency factor to be 10^{13} sec^{-1} from the temperature at which the maximum stored-energy release per degree occurred for two heating rates. However, these values of the activation energy and the frequency factor would not reproduce their stored-energy release per degree as a function of temperature. The experimental curves were much broader than the curves computed from first-order kinetics. They concluded that this was evidence of a distribution of processes over a range of activation energies. A number of samples exposed to neutron irradiation for much larger dosages were subjected to differential thermal analysis by Lees and Neubert.[2] They analyzed the results by Vand's method[8] (which assumes first-order kinetics and a distribution of processes over a range of activation energies), assuming a frequency factor of 10^{13} sec^{-1}. The distribution function giving the stored energy liberated in unit activation energy as a function of activation energy calculated by them rose sharply between 1.2 and 1.4 ev, giving what might be termed "a peak in the activation-energy spectrum." The peak varied somewhat, being depressed and displaced to higher activation energies for samples irradiated at higher temperatures. Following the peak, there was found a broad, somewhat irregular portion in the distribution function of stored energy liberated per unit activation energy, which might be termed a "plateau in the activation-energy spectrum." This plateau was negligible compared to the peak for small irradiation dosages, but, as the dose increased, the height of the plateau increased relative to the peak.

The kinetics of the alteration of the radiation-induced property changes on heating were reconsidered by Brown.[12] He pointed out that, if the analysis of the kinetic data by Vand's method gives a peak in the activation-energy spectrum which is less than 10 per cent wider than would be obtained if the processes annealed at one activation energy according to first-order kinetics, the kinetic data can be equally well fitted by an analysis which assumes that the processes anneal with a single activation energy but follow kinetics of higher order. This suggestion was applied to electrical-resistivity data by Bowen.[13] He found it necessary to assume sixth-order kinetics to explain the behavior of the electrical-resistivity changes on heating irradiated-graphite samples in the 200°C region and to assume other orders of reaction for the behavior at higher temperatures. Brown's suggestion was further examined by Dienes and Parkins,[14] who showed that the experimental data could not be explained by Brown's suggestion if the resistivity changes at the discrete activation energy were proportional to the number of processes involved or to a power of the number of processes involved. They further showed that the discrete activation energies that had to be chosen varied with the dosage of the sample. The stored-energy data obtained by Lees and Neubert were reexamined by Hetrick.[15] To fit the peak with a discrete activation energy, he had to assume that the activation energy depended on the irradiation dosage and that sixth-order kinetics applied. He then attempted to explain the plateau and its irregularities by assuming two higher discrete activation energies. The irregularities introduced into his theoretical curves by these higher activation energies using sixth-order kinetics were much greater than the irregularities in the plateau. Carter, reporting work in progress,[16,17] considered that his stored-energy data in the region of 200 to 475°C could best be interpreted by assuming a large number of overlapping processes following a lower order

kinetics. Austerman[18] reported that graphite irradiated near liquid-nitrogen temperatures showed stored energy liberated at temperatures much lower than had been observed for samples irradiated at temperatures in Hanford cooled test holes.

Measurements of the property changes induced by the irradiation of graphite have been in progress at the Hanford reactors since the inception of their operation[19] for purposes of monitoring the reactor moderator and improving reactor operation. Detailed reports of most of the early studies have not been available. However, a number of interim reports summarizing some of the data have received limited circulation.[20–23] A recent summary has been given by Bupp.[24] Wheeler and O'Connor[25] developed a phenomenological theory of the storage of energy in the reactor graphite in the hope of predicting its future behavior. The stored-energy release on heating was considered to obey first-order kinetics and to be distributed over a range of activation energies, as had been proposed originally by Neubert[7] for the electrical resistivity and elastic modulus. Saturation effects depending upon dose, attributed to heating effects by carbon-atom recoils, were postulated. The theory was based on the results of differential thermal analysis of samples irradiated for exposures up to several hundred megawatt days per central ton.

From very early in the work at Hanford, the stored energy of samples irradiated at various temperatures and subjected to various treatments subsequent to irradiation has been investigated by means of differential thermal analysis,[25] but detailed reports of this work have not been available until the publication of some recent results by Ballinger.[28]

2. DEFINITION OF TERMS

Annealing: This term is herein applied indiscriminately to the heat-treatment of irradiated graphite and to the alterations in the property changes induced by radiation resulting from the heat-treatment.

Isothermal annealing: An annealing conducted by keeping the sample at some fixed temperature.

Tempering: An annealing conducted by raising the temperature of the sample or the surroundings in a gradual manner.

Energy content: The difference in the heats evolved by the irradiated and an unirradiated sample in a reaction in which the end products are in the same state. It is, therefore, the difference between the enthalpies of the irradiated sample and an unirradiated sample at the temperature at which the calorimetry is performed. [This term was given by E. J. Prosen to distinguish the data that he obtained by heat-of-combustion measurements from the internal energy and enthalpy (heat content).]

Stored energy: The irreversible changes in energy content which can be produced by heating an irradiated sample. (This term has been loosely used to include changes in energy content, internal energy, enthalpy, and heat capacity, as well as the definition given here.)

Differential thermal analysis (DTA): This term is herein used to mean the various forms of calorimetry in which the heat is measured by comparing the thermal behavior of two calorimeters placed within thermal barriers. In the typical methods used with geological material, a portion of the substance itself serves as the calorimeter, and another portion is the thermal barrier; a comparison of the thermal behavior of two samples is made by noting their temperatures as the temperature beyond the thermal barrier is raised.[27] For measurements of the stored energy of graphite, almost every investigator has chosen a different method. In all these methods a gas or vacuum has been the thermal barrier. In most of the work the sample with a thermocouple or a thermocouple and a heating coil constituted the calorimeter, but in one set of investigations a calorimeter consisting of a platinum cup containing the sample, sometimes mixed with unirradiated graphite,[26] was used. In some of the work single calorimeters were used, and the behavior of a sample was compared with its behavior after annealing and/or with other substances whose thermal behavior was known.[11] In other work twin calorimeters were used, and a comparison[10] was made of their thermal behavior. In some investigations the thermal behavior was observed by measuring the temperature drop across the

thermal barrier,[10] whereas in other investigations the heat introduced by an electrical heater in the sample[11] or in a twin calorimeter was measured at a particular temperature drop across the thermal barrier.[26] In all the investigations the temperature on one side or on both sides of the thermal barrier was raised gradually; hence they were tempering experiments.

DTA curve: The data of a DTA of irradiated graphite are usually reported as $dQ/dT + (C'-C)$ as a function of temperature, where dQ/dT is the heat released, C' is the heat capacity of the irradiated sample, and C is the heat capacity of the same sample after annealing, as determined by a second DTA. The small distinction between the DTA curve and the stored-energy-release curve (when oxidation of the sample has not occurred during DTA) has usually been disregarded and will be overlooked here.

Catastrophic stored-energy release: The release of stored energy under the condition that the rate of stored-energy release less the rate of heat dissipation exceeds the heat capacity.

Activation-energy spectrum: The distribution in activation energy of the number of kinetic processes per unit activation energy weighted by the property change produced by each type of process. Thus there is an activation-energy spectrum for the annealing of each property and each property change induced by irradiation. The term will be used only when it is desired to imply that the distribution is continuous or quasi-continuous over some range of activation energies.

Discrete activation energy: The single activation energy characterizing a group of kinetic processes when there are no groups of kinetic processes present over a range of contiguous activation energies.

3. EVIDENCE FOR THE ACTIVATION-ENERGY SPECTRUM

The existence of continued annealing over a broad range of temperatures was considered by Vand[8] to be a criterion for the existence of an activation-energy spectrum. Neubert[5] showed that this criterion was obeyed by the annealing of irradiated graphite. However, since then a number of investigators have considered that the annealing data could be explained by assuming a number of discrete activation energies.[13-15] It is therefore desirable to review some of the evidence for the activation-energy spectrum.

It has been shown, by those who have attempted to fit the annealing data for irradiated graphite using discrete activation energies, that it is necessary to displace these discrete activation energies as the irradiation proceeds, presumably in a continuous manner. Furthermore, samples irradiated under different conditions show quite different annealing behavior and would have to be characterized by different discrete activation energies. The discrete activation energies used in these analyses had to be displaced over at least several tenths of an electron volt. Thus, even if an attempt is made to explain the annealing data on the basis of discrete activation energies, one is forced to the conclusion that a continuous range of activation energies is possible. However, there remains the question of whether or not the activation energies over the range coexist in the same sample at the same time. Changes in the discrete activation energies in differently irradiated samples would have to be associated with a change in state of the substance with irradiation. The simultaneous coexistence of different activation energies would merely be a statement of microscopic (i.e., on an atomic scale) inhomogeneity of the solid that has been subjected to irradiation. Such an inhomogeneity of a solid that has been used to stop energetic atomic particles is well established by theoretical work.[28] In addition, artificial graphite is macroscopically inhomogeneous, and this might be expected to contribute to the broadening of an activation-energy spectrum.

Negative evidence for a spectrum of activation energies is to be found in the difficulties encountered in the attempts to explain the annealing data by means of discrete activation energies. The high-order reactions postulated by Bowen[13] and Hetrick[15] seem unacceptable physically. The peculiar functional relation of the property change to the number of processes occurring at a discrete activation energy which had to be invoked by Dienes and Parkins[14] seems like a purely *ad hoc* hypothesis. Attempts by Hetrick to explain the irregularities of the plateau by several discrete activation energies led to irregularities much larger than those

observed. Actually it can be shown that these irregularities arose at least in part from the experimental procedures and may not be present in the actual activation-energy spectrum. Therefore, according to Brown's discussion[12] of the peak width explicable by an increased reaction order, the kinetics in this region cannot be described by a small number of discrete activation energies.

In summary, the small continuous displacement of the low-energy peak which can be made by altering the conditions of irradiation, the broad region of the plateau, the *ad hoc* hypotheses, and the high reaction order needed to even partly fit the annealing data to a small number of discrete activation energies all indicate that the annealing of graphite damaged by energetic atomic particles cannot be described by a small number of discrete activation energies. If the annealing is to be described by a large number of discrete activation energies, the very nature of graphite and the theoretical analysis of the dissipation of the energy of energetic atomic particles, as given by James[28] and others, suggest that it is physically reasonable to expect that the activation energies may be very closely spaced. However, since only a finite number of processes are involved in annealing, the activation-energy spectrum cannot be truly continuous. It is therefore postulated that the annealing of the radiation damage produced in graphite by energetic atomic particles is to be described by a quasi-continuous activation-energy spectrum, which, for practical purposes, may be treated mathematically as a continuum.

4. NATURE OF THE KINETICS PROBLEM

The usual problem in chemical kinetics is resolved into a determination of the order, the activation energy, and the frequency factor from the rate constants. In more complex cases it is necessary to unravel a set of simultaneous reactions and thus find the populations for the various reaction paths. An additional complication may be the presence of consecutive reactions, which are discussed in Sec. 9. The experimental methods of determining the orders, activation energies, frequency factors, populations, and miscellaneous complications when the processes are distributed in activation energy are not established.

To present the data in a simple chemical kinetics system, it is convenient to plot the number of processes completed or remaining against time. When the processes are distributed in activation energy and it is desired to unravel these, another representation must be used. A convenient one is that devised by Vand.[8] The original population of processes among activation energies is plotted as a function of activation energy. Then, if the population is plotted in these coordinates as the annealing proceeds, it can be shown that the area enclosed by the original population is swept out by the advance of the forward portion of the population curve as the annealing proceeds, as shown in part a of Fig. 1. In the absence of complicating

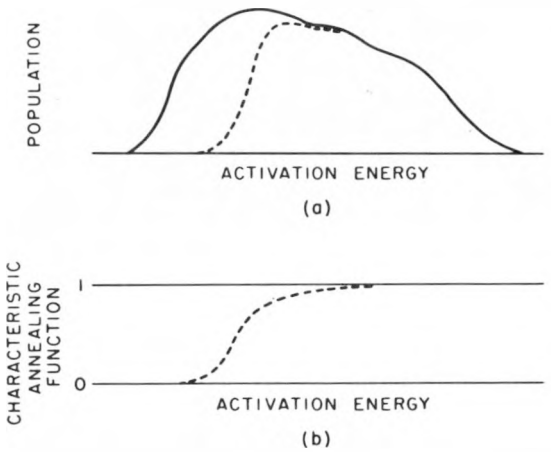

Fig. 1—Annealing of processes distributed in activation energy; schematic representation of the behavior in Vand's coordinates. ——, original distribution. - - - -, distribution after a period of time. (a) Behavior of the population. (b) Behavior of the characteristic annealing function.

factors (like consecutive reactions), the behavior of the broken portion of the curve as a function of time is a complete graphical representation of the kinetic behavior. Its analytical interpretation in the conventional language of kinetics is facilitated by factoring out the arbitrary (arbitrary being used in its mathematical sense) function giving initial population as a function of activation energy and considering the behavior of a population initially uniform

and unity. The curve giving the population during annealing in this case is sigmoid shaped, as shown in part b of Fig. 1, and it is here termed the characteristic annealing function. The following properties of the characteristic annealing function can be demonstrated: Its slope increases as the frequency factor is increased; its slope decreases as the annealing temperature increases; and its slope decreases and the ordinate of its point of inflection increases as the reaction order increases. The shape of the characteristic annealing function is sensitive to the choice of frequency factor over its whole range and in particular over its central portion, which is most accessible to experimental observation. On the other hand, the effect of the order is greatest on the tails of the characteristic annealing function.

Vand's treatment has been branded as physically unsatisfactory,[29] presumably because it has been interpreted as disguising the kinetics, since by its use any annealing curve can be represented as a set of first-order simultaneous reactions. Vand gave two methods for approximately determining the initial population when the frequency factor was sufficiently high and the temperature was sufficiently low. In these approximations the form of the characteristic annealing function was disregarded and was replaced by a step function; yet Vand showed that the resolution of his method in activation energy per atom was within several times Boltzman's constant times the temperature of the annealing. For a broad spectrum of activation energies spread over 20 times this resolution, his result is a useful one. Since his result does not depend on the form of the characteristic annealing function, the general form of his result must be valid (with slightly decreased resolution for higher orders in the reasonable range) for other orders of reaction, although with a small change in the scale of activation energies. It would therefore be best to consider the kinetics of processes distributed in activation energy as incompletely developed rather than physically unsatisfactory. It will be shown here that, although it is possible to describe certain annealing curves by kinetics of various orders, it is not possible to do this when certain sequences of annealings are performed.

Many of the features of the kinetics of processes distributed in activation energy are common to processes of different kinetic order. It will be convenient here to discuss them by showing the behavior of first-order processes (which are easily described by exponential functions) and then indicating the possible deviation of the experimental data from this assumption.

5. TEMPERING AND THE ORIGINAL POPULATION

Vand[8] gave an explicit solution (in approximation) for the small portion of the activation-energy spectrum revealed by an isothermal annealing experiment and a solution in parametric equations for the large portion of the initial activation-energy spectrum revealed by a tempering experiment. A more convenient solution (in approximation), which relates the data of the tempering experiment to the activation-energy spectrum in a simple manner, is developed here.

Since a broad distribution of activation energies with which is associated a distribution of processes (each of which may have a different amount of property change associated with it) is assumed, there is no way of assigning a given amount of property change to a particular process from the behavior of a single property; hence the processes will be counted by means of the property change, the stored energy in the present case. It is thus assumed that the same amount of property change is associated with processes of a given activation energy. Then the annealing of the stored energy q associated with the activation energy ϵ (units of electron volts will be used) will be described by

$$-\frac{dq}{dt} = Ae^{-\epsilon/T}q$$

where T is the product of Boltzman's constant and temperature [in units of electron volts per atom (ev)], t is the time, and A is the frequency factor. Then for an isothermal annealing

$$q = q_0 \exp\left(-Ate^{-\epsilon/T}\right) \qquad (1)$$

where q_0 is the stored energy associated with a particular value of ϵ initially. The approximation given by Vand for determining $q_0(\epsilon)$ from

the data is not given here because it will not be used. In the case of a tempering experiment at a constant rate of temperature rise 1/c, t = cT; hence

$$-\frac{dq}{cdT} = Ae^{-\epsilon/T}q \tag{2}$$

$$-\ln\left(\frac{q}{q_0}\right) = cA\int_0^T e^{-\epsilon/T'}\,dT'$$

where the prime is used to distinguish the variable from the limit and q_0 is the fictitious stored energy associated with T′ = 0. (There is no loss in generality, and some simplification in algebra is made by considering the tempering to have begun at 0°K. For all practical purposes the same experimental result would be achieved by starting the tempering at several T′ below that at which noticeable annealing is observed, and for any experimentally reasonable tempering rates there is practically no difference between the q_0 introduced here and the actual stored energy present in the sample.) Placing $\epsilon/T' = y$, it is seen that the integral is a form of the Gold integral. Using the nomenclature of Placzek's table,[31]

$$E_2\frac{\epsilon}{T} = \frac{\epsilon}{T}\int_{\epsilon/T}^{\infty} e^{-y}\frac{dy}{y^2}$$

the solution becomes

$$q = q_0e^{-cTAE_2(\epsilon/T)} \tag{3}$$

and the total stored energy, Q, is then

$$Q = \int_0^{\infty} q_0e^{-cTAE_2(\epsilon/T)}\,d\epsilon$$

Vand pointed out that the integrand is nearly a step function when A has values in the usual range of values for the frequency factor in chemical reactions; hence, in approximation,

$$Q = \int_{\epsilon_0}^{\infty} q_0\,d\epsilon = \int_{(\epsilon/T)_0}^{\infty} Tq_0\,dy \tag{4}$$

where ϵ_0 is taken from the point of inflection in the exponential part of the integrand (the characteristic annealing function for this case),

$$\Phi = e^{-cTAE_2(\epsilon/T)}$$

which occurs at

$$cTAE_1^2(y_0) = E_0(y_0)$$

where the E values are the exponential integrals[5] and $y_0 = \epsilon_0/T$. [In the case of isothermal annealing the maximum in dq/dt corresponds to the maximum in dq/dϵ. In tempering this is no longer true. Vand places his ϵ_0 at the maximum in dq/dt, although, according to his mathematical argument, it should be placed at the maximum in dq/dϵ. Vand's result, which in some respects is more satisfactory physically,[30] leads to $y_0 + \ln(y_0 + 1) = \ln \beta A$ and gives nearly the same final result as Eq. 9, differing only in having a slightly different numerical value for b.] It is shown later that in its effective range y >> 1. Then, using the first term of the Blanch asymptotic expansion[31] and writing $\beta = cT$,

$$\beta A\left(\frac{e^{-y_0}}{y_0 + 1}\right)^2 = \frac{e^{-y_0}}{y_0}$$

Since y >> 1, if j, k, *l*, and m are near 1 and j + k = *l* + m, then an approximation which is convenient because it preserves the identity of the E functions in the approximation used for them here is

$$(y + j)(y + k) \cong (y + l)(y + m) \tag{5}$$

and hence

$$\beta Ae^{-y_0} \cong y_0 + 2$$

or

$$y_0 + \ln(y_0 + 2) = \ln \beta A \tag{6}$$

The whole tempering process occurs in a very narrow range of y, where $\beta AE_2(y) \sim 1$. Since $y_0 + \ln(y_0 + 2)$ is a very slowly varying function, it is quite permissible to take

$$y_0 + \ln(y_0 + 2) = a + by_0 \tag{7}$$

where a and b are constants appropriate to the range of y under consideration. It is now possible to write an explicit solution for $q_0(\epsilon)$ from the data of the tempering experiment. Differentiating Eq. 4,

$$-\frac{dQ}{dT} = q_0(\epsilon_0)\frac{d\epsilon_0}{dT} \tag{8}$$

From Eq. 6

$$\frac{d\epsilon_0}{dT} = y_0 + \frac{y+2}{y_0+3}$$

and from Eq. 5

$$\frac{d\epsilon_0}{dT} = y_0 + 1$$

From Eqs. 6 and 7, writing ξ for $(\ln cTA - a)$, $y_0 = \xi/b$. Solving Eq. 8 for $q_0(\epsilon_0) = q_0(T\xi/b)$,

$$q_0\frac{T\xi}{b} = -\frac{dQ}{dT}\frac{1}{(\xi/b)+1} \tag{9}$$

Since ξ/b varies only slowly with temperature, the activation-energy spectrum is nearly proportional to the DTA curve which plots $-(dQ/dT)$ against T when the heating rate of the sample has been linear. A similar relation holds for the tempering of other properties or property changes attendant on the irradiation.

6. TEMPERING OF THE CONSTANT-ACTIVATION-ENERGY SPECTRUM

For irradiated graphite the DTA curves obtained between 500 and 800°C are quite flat,[2,24,26] and the activation-energy spectrum for stored energy must therefore be quite flat also. It is therefore of interest to investigate the case of a constant-activation-energy spectrum. Since it is not necessary to approximate Φ with a step function to derive the tempering curve, more detailed information about the kinetic behavior may be expected than is given in Sec. 5. Writing g(T) for $-(dQ/dT)$, it is seen from Eq. 2 that

$$g(T) = q_0\beta A\int_0^\infty \exp\left[-y + \beta A\, E_2(y)\right] dy \tag{10}$$

Again using the first term of the Blanch asymptotic expansion,

$$g(T) = q_0\beta A\int \exp\left(-\frac{y-\beta Ae^{-y}}{y+2}\right) dy$$

Let $v = \exp\left[-A\beta e^{-y}/(y+2)\right]$; then, writing $\ln_2(x)$ for $\ln(\ln x)$,

$$y + \ln(y+2) = \ln A + \ln\beta - \ln_2(1/v) = a + by$$

$$y = \frac{1}{b}\left[\ln\beta A - \ln_2\left(\frac{1}{v}\right) - a\right] = \frac{1}{b}\left(\xi - \ln_2\frac{1}{v}\right)$$

Over the effective range of y, v varies from nearly 0 to nearly 1; hence

$$g(T) = q_0\beta A\int_0^1 e^{-y}\frac{v\,dv}{bv\ln(1/v)}$$

$$= q_0\beta A\int_0^1 \exp\left[-\ln\beta A + \ln_2\left(\frac{1}{v}\right) + \ln(y+2)\right]\frac{dv}{b\ln(1/v)}$$

$$= \frac{q_0}{b}\int_0^1 (y+2)\,dv$$

$$= \frac{q_0}{b^2}\int_0^1 \left[\ln\beta A - \ln_2\left(\frac{1}{v}\right) - a + 2b\right]dv$$

$$= \frac{q_0}{b^2}\left[\ln(\beta A) + \gamma + 2b - a\right] \tag{11}$$

where $\gamma = 0.577\ldots$. Thus g(T) is a very slowly rising function of temperature, increasing about 1 per cent between 500 and 800°C for usual values of A.

7. THE QUALITY OF EXISTING ANNEALING DATA

The release of stored energy has been a subject of special interest to the engineer because of its implications in reactor operation. It has been of special interest to theoretical physicists because it has been believed to be simpler to interpret than other effects of irradiation. It also has a special interest to the experimental physicist because of its unique and central position in any annealing experiment. This arises from the fact that it is of the order of magnitude of the heat capacity. Its release on annealing modifies the heating program and thus affects

all the annealing data. Thus irregularities in the stored-energy-release curves should be reflected in the annealing of other properties or in property changes. Some of these effects are readily seen by considering the behavior of the law (Eq. 11). These considerations even apply to the cases where the activation-energy spectrum $q_0(\epsilon)$ is not constant because the law (Eq. 11) shows the behavior of the characteristic annealing function.

The behavior of the law (Eq. 11) shows the effect noted by Bupp[24] from physical considerations, i.e., the heat-release rates are greater for lower tempering rates, because β is inversely proportional to the tempering rate. If the tempering rate is not constant but starts changing, an exaggerated effect is observed. The qualitative nature of the effect is easily shown for an increasing tempering rate such as that governed by the law $t = cT^p$, where p is a small integer. The equations corresponding to Eqs. 3 and 11, respectively, are now

$$q = q_0 \exp\left[-A\zeta E_{(p+1)}(y)\right]$$

$$g(T) = \frac{q_0}{s^2}\left[\ln(\zeta A) + \gamma - r + (p+1)s\right]$$

where $\zeta = pcT^p$ and $y + \ln(y + p + 1) \cong r + sy$. Since r and s have nearly the same values as a and b, the major effect is due to the power of the temperature appearing in the logarithm term. If the tempering rate were parabolic (p = 2), g(T) would be about 10 per cent less than if the tempering rate were constant. However, if the tempering rate were originally constant and were to change to a parabolic one at some temperature T_c, the decline in g(T) would obviously be greater than the difference between the values of g(T) for the two powers of p since the distribution $q(T_c)$ for the constant tempering rate is smaller than it would have been had the parabolic law operated from the beginning. Such an increase in tempering rate is common at the initiation of a DTA, and, since the DTA curve is usually interpreted as if the tempering rates were constant, it may be said that the initial portion is depressed. As the constant tempering rate is approached, there is a declining law, and here the DTA curve is elevated. The same effect occurs at the end of the heating range when the tempering rate usually declines. The effect is seen in the data of Lees and Neubert[2] and is demonstrated by the maximum in their F_0 at the end of their heating range and also in the g(T) derived by Hetrick[15] from the F_0 of Lees and Neubert. It will be assumed that this fault is present in all DTA data near the end of the heating range unless the investigators have specifically indicated how they avoided it.

Even greater effects occur where there is a sudden release of stored energy (a peak in the DTA). Usually the heating rates rise so rapidly on the low-temperature side of the sudden release and decline so rapidly on the high-temperature side that they are more easily described by exponentials than by powers. In such a case there is the additional complication of q_0 being a steep function of ϵ. However, the qualitative nature of the distortion of the DTA curve is seen to be some depression of the low-temperature side of the DTA peak and some elevation of the high-temperature side of the peak, followed by a depression as the normal heating rate is restored. The second depression can give rise to the impression that there is a small subsidiary peak at a higher temperature than that of the major peak or that there is a shoulder on the high-temperature side of the major peak. Samples in which the stored energy in a range of annealing temperatures exceeds the heat capacity were first reported by Wheeler and O'Connor[25] and are quite common in the region of the DTA peak that appears between 150 and 400°C. In such samples catastrophic stored-energy release can occur; the DTA curves then have little relation to the activation-energy spectrums present in the samples and can vary greatly with the heating program, the sample size, and the annealing arrangement. The development of spurious peaks in the DTA curves as a result of catastrophic stored-energy release has been discussed by Primak.[32] Some of the theoretical implications of stored energy in excess of the heat capacity will be discussed in a report now being written.[33]

It must be concluded that most of the DTA data available for irradiated graphite are distortions of the ideal tempering curves that would be obtained if the sample temperature were varied in a simple, known manner. This is especially true for most data obtained for the peak that appears between 150 and 400°C. It

cannot be expected that these data are suitable for anything more than to obtain an approximate activation-energy spectrum as was done by Lees and Neubert.[2] Recently Ballinger[26] has reported the DTA of some irradiated graphite having a DTA curve that showed no peak and possessed a fairly flat region between 500 and 800°C. He subjected samples of this irradiated graphite to isothermal annealing and subsequently subjected the isothermally annealed samples to DTA. Since the original activation-energy spectrum was quite flat, it might be expected that the form of the initial portion of the activation-energy spectrum present subsequent to isothermal annealing for a sufficiently long time would be proportional to the characteristic annealing function for isothermal annealing at that temperature and that this form would be revealed by the DTA. If this were so, additional information about the kinetics would be obtained, as is shown in Sec. 8.

8. TEMPERING OF A PREVIOUSLY ISOTHERMALLY ANNEALED SAMPLE

The result (Eq. 11) derived for constant tempering assumed $q_0(\epsilon)$ to be constant from $\epsilon = 0$ to ∞. In practice samples are stored at some temperature for a long time; hence they are subjected to isothermal annealing at that temperature. Furthermore, release of stored energy ceases at some upper temperature, indicating an upper bound for $q_0(\epsilon)$. However, the range of temperatures is sufficiently great so that in the central region it may be assumed that the law applies. A case in which 220 cal/g is released between 0.05 and 0.11 ev (300 to 1000°C) will be considered. Then,

$$220 = \int_{0.05}^{0.11} g(T)\, dT = \frac{q_0}{b^2}(0.06G - 0.93)$$

where $G = 10.75 + \ln(A) + 2b - a$. For the cases $A = 10^{14}$ and 10^{10}, y ranges about 37.3 and 28.3, respectively; hence a is 2.74 and 2.48, respectively, and b is 1.025 and 1.033, respectively. [The values of a and b are calculated most conveniently from the slope and value of $y + \ln(y + 2)$ in the middle range of y.] Then it is found that q_0 is 94 and 123 cal/g/ev, respectively. These values yield approximately the release rate above 500°C found by Ballinger[26] for one of his samples. He subjected other samples of this material to isothermal annealing and then investigated them by DTA.

In the Vand approximation, if a sample possessing a constant q_0 were subjected to isothermal annealing and subsequently tempered, the tempering curve would be a step function. Similarly, if the actual experimental isothermal annealing law were used for q_0 and the Vand approximation were used to derive the tempering curve, the curve so obtained would be much steeper than the exact solution, as can be seen by considering the nature of the exponential functions involved. The approximations used by Vand are not suitable for obtaining the form of g(T) in any region where q_0 is steep and where they would, in general, yield a g(T) which is steeper than the exact solution. After the isothermal annealing, Eq. 1 applies. This q may be taken as the q_0 of Eq. 10. Then, for tempering following isothermal annealing for a time t at a temperature T_0,

$$g(T) = \beta A q_0 \int_0^\infty \exp\left\{-y - A\left[te^{-\epsilon/T_0} + \beta E_2(y)\right]\right\} dy$$

$$\cong \beta A q_0 \int_0^\infty \exp\left(-y - A\frac{te^{-\sigma y} + \beta e^{-y}}{y + 2}\right) dy \quad (12)$$

where $\sigma = T/T_0$. For Ballinger's tempering rate (10°/min), $c = 7.1(10^4)$, and hence $cT_0 = 5.10(10^3)$. To affect the tempering at T_0 by means of a previous isothermal annealing at T_0, it is seen that the isothermal annealing must be conducted for a length of time such that

$$t \sim \frac{cT_0}{y + 2}$$

which, for $A = 10^{14}$ to 10^{10}, would be 125 to 170 sec. Ballinger found that after his first isothermal annealing (t_1 = 300 sec) practically no stored energy was released at T_0, in accord with the estimate given here. No attempt will be made to analyze this case further since experimental details of raising the temperature to 560°C are absent and from the present analysis it is seen that this would be important for so short an annealing. Ballinger gives the DTA following two other isothermal annealings at 560°C, $t_2 = 7.2(10^3)$ and $t_3 = 8.6(10^4)$ sec. The

initial portion of the tempering curve is easily obtained because then $t >> \beta/(y + 2)$ and Eq. 12 becomes

$$g(T) = \frac{\rho q_0 \beta A^{1-\rho}}{t^{\rho}} \int_0^{At} z^{(\rho-1)} e^{-z} \, dz$$

where $z = Ate^{-\sigma y}$ and $\rho = 1/\sigma$. Thus, since At is large,

$$g(T) = q_0 \beta t^{-\rho} \rho \, \Gamma(\rho) \, A^{(1-\rho)} \tag{13}$$

where $\Gamma(\rho) = (\rho - 1)!$ The further portion of the tempering curve can be obtained at some particular temperature by computing the integrand of Eq. 12 over the range of y up to y_m in which $Ate^{-\sigma y} + \beta e^{-y}/(y + 2)$ makes an appreciable contribution, integrating graphically, and then adding $\exp(-y_m)$ to this.

9. FREQUENCY FACTOR, ORDER, CONSECUTIVE REACTIONS, AND POPULATION FROM BALLINGER'S EXPERIMENT

The results obtained for the calculated tempering curve g(T) following isothermal annealings for times $t_2 = 7.2(10^3)$ and $t_3 = 8.6(10^4)$ sec are given in Table 1 for two values of the frequency factor $A = 10^{10}$ and $A = 10^{14}$ sec^{-1}. In Fig. 2 these results are plotted on the reproduction of Ballinger's figure[26] giving his experimental results. It is seen that the experimental data indicate that A must be between 10^{10} and 10^{14} sec^{-1}. The frequency factor at this temperature thus seems to be about the same which Wheeler and O'Connor[25] claimed (without giving their reasoning) best suited the data which they obtained at lower temperatures.

The experimental curves of Fig. 1 rise rather more steeply than do the theoretical ones. Part of this must be attributed to the effects of thermal lags and other lags which would be appreciable in the DTA of a powder by Ballinger's method, where a manual balance is made following the appearance of an effect. To the extent that the deviations cannot be explained by the lags, it would be necessary to postulate an order less than unity, according to the discussion of Sec. 4. This effect might arise from the physical situation suggested by a number of investigators (see, for example, reference 34) at the Metallurgical Laboratory and the Argonne National Laboratory, among whom were O. C. Simpson, T. J. Neubert, and G. R. Hennig, that some of the stored energy observed at higher activation energies is not present originally but results from the annealing of stored energy at lower activation energies. The effect cannot be a large one because the observation of some property change at a given activation energy can leave only a fraction of the actual total property change associated with a particular activation energy to be distributed over the range of remaining activation energies. The total result would be the observation of a smaller apparent q_0 for lower ϵ than the actual q_0, the observation of a larger apparent $q_0(\epsilon)$ for larger ϵ than the actual q_0, and the observation of a lower apparent order of kinetics than the actual one for larger ϵ.

Since A is so large, the Vand approximation is fairly good except when the details of sudden changes of q_0 or of g(T) are involved, and it may therefore be taken to apply to the DTA of Ballinger's sample between 400 and 750°C before isothermal annealing. The activation-energy spectrums of stored energies released between 500 and 750°C, the range over which the values given for a and b may be taken to apply, as calculated from Eq. 9 using the data of the first curve of Fig. 2, assuming frequency factors of $A = 10^{10}$ and 10^{14} sec^{-1}, are given in Fig. 3. The activation-energy spectrum for the release of stored energy $q_0(\epsilon)$ which is revealed exhibits a slight rise with activation energy (part of which may be due to a nonconstant tempering rate). This small rise is not considered sufficient to affect the discussion given here.

10. CONCLUSIONS

From the investigations and discussions given here, it is evident that the detailed kinetics of the release of stored energy in irradiated graphite is not yet known and that most of the experimental annealing data available are not suitable for investigating the detailed kinetics. The data thus far available can be most easily explained with the fewest *ad hoc* assumptions as resulting from processes distributed in activation energy. The data are suitable for deriving the approximate general form of the

Table 1—Calculated Tempering Curve Following Isothermal Annealing

Tempering temperature (T), °C	Stored-energy release rate (at indicated time* and frequency factor†), cal/g/ev			
	t_2; 10^{10}	t_3; 10^{10}	t_2; 10^{14}	t_3; 10^{14}
Tempering curve g(T) from Eq. 13				
560	87	7	67	5
580	160	15	150	14
600	320	32	350	34
620	850	79	1200	120
650		230		
Tempering curve g(T) by graphical integration				
650	1400		2000	410
700	2600	770	3200	1600
750	3300	1800	3500	3000

*Isothermal annealing time.
†Frequency factor A.

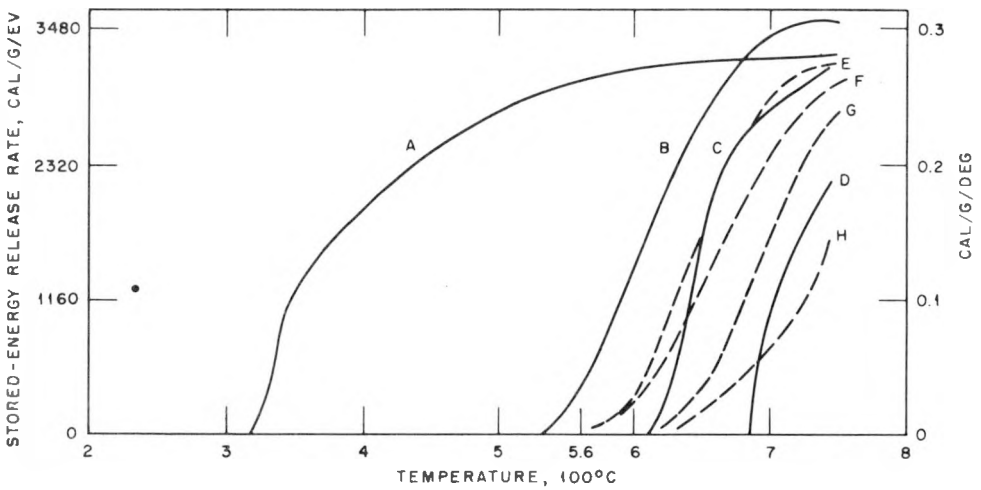

Fig. 2—Comparison of g(T) calculated theoretically with the results of Ballinger's differential thermal analysis. ——, experimental data given by Ballinger.[26] – – – –, g(T) calculated theoretically. A, before isothermal annealing. B, isothermally annealed for 300 sec. C, isothermally annealed for $7.2(10^3)$ sec. D, isothermally annealed for $8.6(10^4)$ sec. E, $t = 7.2(10^3)$; $A = 10^{14}$. F, $t = 7.2(10^3)$; $A = 10^{10}$. G, $t = 8.6(10^4)$; $A = 10^{14}$. H, $t = 8.6(10^4)$; $A = 10^{10}$.

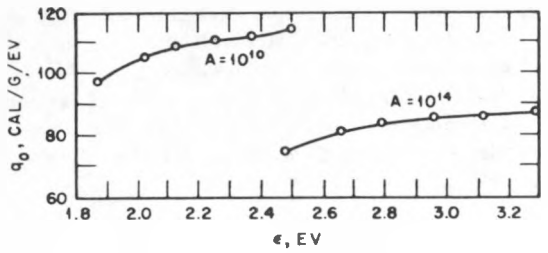

Fig. 3 — Activation-energy spectrums calculated from Ballinger's DTA of a sample of graphite using his dQ/dT at 500, 560, 600, 650, 700, and 750°C as taken from curve A of Fig. 2.

activation-energy spectrum and an approximate frequency factor, but the order of reaction and the complication of consecutive reactions are unknown.

ACKNOWLEDGMENTS

The author is indebted to O. C. Simpson, T. J. Neubert, and G. R. Hennig for discussions of various aspects of the subjects treated here and to O. C. Simpson, Sidney Siegel, R. L. Carter, D. L. Hetrick, W. H Sullivan, W. K. Woods, J. M. Davidson, L. P. Bupp, M. Lewis, J. H. Crawford, and G. R. Hennig for criticism of the manuscript in various stages of its preparation.

REFERENCES

1. M. Burton, Radiation Chemistry, J. Phys. & Colloid Chem., 51: 611(1947).
2. R. B. Lees and T. J. Neubert, Stored Energy in HEW Irradiated Graphite, Report ANL-4307, June 1949.
3. Metallurgical Laboratory, Reports CP-387, CC-418, CC-446, CC-465, CC-520, CC-577, CC-649, CC-734, CP-773, CP-773A, CC-784, CC-841, CC-918, CP-961, CC-983, CC-1036, CC-1139, CC-1195, CC-1320, CC-1338, CC-1390, and M-CC-1538.
4. T. J. Neubert et al., Thermal Annealing of Irradiated Graphite, Report CC-918, Sec. 3.1.3, and Report CC-983, Sec. 3.1.3.
5. T. J. Neubert, Thermal Annealing of Neutron-induced Discomposition in Artificial Graphite. I. Rate of Healing Experiments, Report ANL-4369, Nov. 18, 1949.
6. T. J. Neubert, Thermal Annealing of Neutron-induced Discomposition in Artificial Graphite. II. Asymptotic Annealing Experiments, Report ANL-4477, July 7, 1950.
7. T. J. Neubert, 1944 (private communication by M. Burton, 1954).
8. V. Vand, A Theory of the Irreversible Electrical Resistance Changes of Metallic Films Evaporated in Vacuum, Proc. Phys. Soc. (London), 55: 222 (1943).
9. L. H. Fuchs and W. Primak, The Increase in Heat Content of Diamond on Irradiation, Report ANL-4466, June 1950.
10. R. J. Maurer and R. C. Ruder, The Increase in Internal Energy of Graphite as a Result of Fast-neutron Bombardment, Report CP-2889, Apr. 25, 1945.
11. B. Leaf and A. Novick, Measurement of Specific Heat of Graphite; Determination of Energy Stored During Fast-neutron Bombardment, Report CC-3086, Jan. 29, 1947.
12. F. W. Brown, Some Methods for Analysis of Annealing Data, Report NAA-SR-16, Jan. 17, 1950.
13. D. Bowen, On the Mechanism of Thermal Annealing of Irradiated Graphite, Report NAA-SR-41, Aug. 4, 1950.
14. G. J. Dienes and W. E. Parkins, An Improved Method for Determining Activation Energies of Relaxation Processes, Report NAA-SR-60, Apr. 12, 1950.
15. D. L. Hetrick, Technical Cooperation Program Report of Washington Meeting on Graphite, May 22, 1953, Report WASH-345, September 1953, pp. 38-71.
16. R. L. Carter, Asymptotic Aging Experiments, Progress Report, Report NAA-SR-1013, Aug. 15, 1954, p. 25.
17. R. L. Carter and S. B. Austerman, Asymptotic Aging Experiments, Progress Report, Report NAA-SR-1056, Nov. 1, 1954.
18. S. B. Austerman, draft of U.S./U.K. progress letter (cover letter dated Dec. 15, 1954).
19. W. E. Jordan, Interim Report on Production Test 105-1-P, Report HW-3-2305, Apr. 30, 1945.
20. J. J. O'Connor and H. A. Fowler, Interim Report on Production Test 105-1-P, Supplement A, Report HW-3-3359, Jan. 2, 1946.
21. H. A. Fowler and J. J. O'Connor, Interim Report on Production Test 105-1-P, Report HW-3-3475, Mar. 1, 1946.
22. H. A. Fowler, Interim Report on Production Test 105-1-P, Report HW-9128, Mar. 8, 1948.
23. D. H. Curtiss et al., Interim Report on Production Test 105-1-P, Report HW-13117, Apr. 29, 1949.
24. L. P. Bupp, Technical Cooperation Program Report of Washington Meeting on Graphite, May 22, 1953, Report WASH-345, September 1953, pp. 27-37.

25. J. A. Wheeler and J. J. O'Connor, Interim Report on Production Test 105-1-P, Report HW-7-3020, Nov. 9, 1945.
26. J. C. Ballinger, Graphite-stored Energy, Reactor Sci. Technol., 3(4): 55-66 (December 1953).
27. R. E. Grim, Method and Application of Differential Thermal Analysis, Ann. N. Y. Acad. Sci., 53: 1031 (Jan. 20, 1951).
28. H. M. James, Neutron Damage in Graphite, Report ORNL-307, Mar. 22, 1949.
29. Sidney Siegel, private communication.
30. W. Primak, Annealing Involving a Range of Activation Energies (submitted to The Physical Review).
31. G. Placzek, The Functions $E_n(x)$, National Research Council of Canada Report MT-1 (NRC-1547).
32. W. L. Primak, DTA of Irradiated Diamond and Silicon Carbide, Report ANL-5249 (to be published).
33. W. Primak, Some Aspects of Stored Energy in Irradiated Graphite. Part II. The Storage of Energy on Irradiation (to be published).
34. R. L. Seifert, Energy of Activation of Dislocated Carbon Atoms as Determined from the Irreversible Resistance Changes in Irradiated Graphite, Report ANL-4196, September 1948, p. 22.

ABOUT THE AUTHOR

William Primak has been employed as an associate chemist at the Argonne National Laboratory since 1946. During this time he has been engaged in various studies associated with irradiation effects. He received the B.S. degree from the College of the City of New York in 1937, the M.S. degree from the Polytechnic Institute of Brooklyn in 1943, and the Ph.D. degree from the Polytechnic Institute of Brooklyn in 1946.

Begin
TRG, Inc.

TID-2506 (Del)
(EXCERPT)

MEASUREMENTS AND ANALYSIS OF URANIUM-D_2O LATTICES

F. B. ESTABROOK and S. W. KASH

North American Aviation, Inc.
Downey, California

November 8, 1954

ABSTRACT

During the past few years an extensive series of measurements on low-enrichment uranium-rod lattices in D_2O has been carried out at North American Aviation, Inc. This article briefly summarizes the measured values of the material bucklings, the fuel and moderator disadvantage factors, and the activity ratios for all the lattices and then gives the details and results of a careful two-group analysis into the consistency and significance of the measurements.

The effective thermal-neutron temperature of each lattice is obtained from the ratio of absorption cross section to low-energy slowing-down power. The slowing-down power of D_2O in the thermal region is shown to be 0.173 cm^{-1}, and some agreement with experimental values of the average cosine in a scattering collision is adduced.

Thermal utilizations are obtained from the experimental intracell measurements. Comparison is made with diffusion calculations of rod disadvantage factors and with excess absorption calculations for the moderator.

Calculated in conventional fashion are η, ϵ, and L^2; in L^2 it may be noted that experimental disadvantage factors are used. The ratio of thermal to epithermal foil activities is shown to be a parameter characteristic of the asymptotic lattice spectrum and is successfully correlated with the predictions of two-group theory. The possible use of this experimental ratio for determining lattice diffusion lengths is critically examined.

The neutron ages in the various lattices are computed by taking the lower limit of the age integral at an effective thermal energy some 16 times greater than would be proper in a nonmultiplying medium. This is the correction for thermal absorption and multiplication recently worked out by E. R. Cohen.

The resonance escape probabilities that can be computed from the above quantities are then compared with resonance escape probabilities computed from the usual Fermi-Wigner-Weinberg theory. A series of small, but definite, discrepancies, functions of rod uranium enrichment, are found. These are believed to be real and independent of experimental scatter.

Three supplemental experiments are recorded in the appendixes. These indicate the presence of a small amount of anisotropic diffusion, show the thermal utilization to be independent of large flux gradients that exist near

the boundary of an exponential tank, and support the method used for computing effective neutron ages.

1. INTRODUCTION

The program of exponential experiments at North American Aviation, Inc. (NAA), has now accumulated a large amount of data on uranium lattices in D_2O moderator. The 35 lattices that have been investigated to date embrace a range of enrichments, rod sizes, and rod spacings. The experimental results, consisting of the bucklings (B^2), uranium and moderator disadvantage factors (F and F_m), and activity ratios (R), will be briefly described and tabulated. These can be of immediate engineering use in the design of reactors of this type. The main body of this article will present a two-group analysis of the data which may possibly throw some light on both the shortcomings of, and the accuracies that can be expected from, the conventional procedures of inhomogeneous-reactor calculation.

Three enrichments of fuel material were used: 0.49, 0.71, and 0.90 wt. % U^{235}. Hereafter these will be referred to as depleted, natural, and enriched uranium, respectively. The uranium fuel rods ranged from $\frac{3}{4}$ to 2 in. in diameter. The lattice cell spacings were varied from 3 to 12 in. Table 1 lists the lattices which have been measured.

Table 1 — Summary of Lattices Measured*

Rod diameter, in.	Cell spacing, in.								
	3	3.625	4.5	4.9	6.0	7.25	7.5	9.0	12.0
0.75	N		N		N				
1.00		N,E	D, N	D, N, E	N, E		D, N, E	N, E	D, N, E
1.25			N		N		N	N	N
1.50					N	N		N	N
2.00						N	D	D, N	D, N

*D is depleted uranium (0.49% U^{235}); N is natural uranium (0.71% U^{235}); E is enriched uranium (0.90% U^{235}).

2. MEASUREMENTS

The exponential experimental arrangement has been fully described in previous reports.[1,2] Most of the data on the natural-uranium lattices has also been reported.[2–4] The lattices are contained in a cadmium-covered cylindrical aluminum tank 5 ft in diameter* and 6 ft high into which D_2O can be admitted. The tank rests on the 3-ft-high thermal column atop the Water Boiler Neutron Source. To form a lattice, the fuel rods are held vertically in a square array by special grid plates at the top and bottom of the aluminum tank. Each rod consists of 4-in.-long slugs of uranium contained in 0.040-in.-wall aluminum tube.

Flux readings were taken by exposing indium foils along the axis of the cylinder and along horizontal diameters to measure the bucklings. To measure the disadvantage factors, horizontal flux traverses were made across a central cell and through a rod. In both cases thermal fluxes were obtained by correcting the bare-foil data with data from similarly exposed foils shielded by 0.020-in. cadmium boxes. The analysis of the buckling measurements is described in reference 3, and the analysis of the intracell thermal data for the disadvantage factors is de-

*A 4-ft-diameter tank was used for the three enriched-uranium lattices with the largest bucklings. Measurements on three other lattices were repeated in this smaller tank to investigate the possibility of anisotropic diffusion (see Sec. 7, Appendix A).

scribed in reference 2. Recent experimental work[5] has verified that F and F_m are not significantly affected by the finite size of our flux-measuring foils.

The ratio of thermal to epithermal activities on the tank axis (and hence at the center of a lattice cell which has rods at its corners) obtained during the analysis of the axial-buckling data was denoted by R, the activity ratio. This ratio was constant over the central 2 or 3 ft of axis, indicating that the measurements made in the central region of the exponential tank were sufficiently far from the boundaries to represent actual properties of the lattice. R is thus a parameter characteristic of the asymptotic lattice neutron spectrum and will be further considered in Sec. 4.

Table 2 summarizes the data for the 35 lattices. In addition, the results are graphically represented in Figs. 1 to 4. The moderator to uranium volume ratios, V_m/V_U, obtained from the dimensions of an individual cell are also shown in Table 2. Because of lattice irregularities near the edge of the tank, these ratios differ somewhat from the ratios obtained using the number of rods and the dimensions of the tank. However, measurements have shown that the buckling is relatively insensitive to the presence of the peripheral rods.

Throughout the course of the measurements a cooperative exchange of information and data was carried on with the Canadian group at Chalk River, which was making related criticality measurements with the ZEEP reactor. For comparable lattices the ZEEP buckling measurements were consistently lower than the NAA measurements by a few per cent (see, for example, reference 6). To date all attempts to understand the discrepancy have been unsuccessful. Samples of NAA D_2O were sent to Chalk River for mass spectrographic confirmation of H_2O content. Samples of the Canadian uranium were compared with NAA samples by danger coefficient techniques at NAA; the differences observed were too small to reconcile the disagreement. Finally, sufficient NAA natural uranium for an entire lattice was sent to Chalk River; the bucklings obtained by their critical-assembly methods for three different lattice spacings still fell about 4 per cent under the NAA values. Since the ZEEP measurements were made on a critical rather than an exponential assembly, it was thought that anisotropic diffusion or changes in the thermal utilization because of streaming might be the cause. Experiments to check these possibilities (see Secs. 7 and 8, Appendixes A and B) yielded effects too small to account for the observed discrepancies. It is, of course, quite possible that the disagreement results from a number of small effects. In any case the observed differences are too small to appreciably affect the resonance-escape or multiplication-constant calculations presented in this article.

3. ANALYSIS

In his analysis of the natural-uranium lattice measurements, Cohen[4] adopted the following procedure: Treating the transport mean free path (λ_m) of the moderator as a parameter, he obtained η as a function of λ_m for each natural lattice. He then derived the particular value of λ_m that gave the most constant value of η. This value of η agreed well with the then accepted cross-section values.[7]

Recently revised cross-section values[8] now indicate a somewhat higher value of η for the natural uranium. Furthermore the value of λ_m has since been measured[9] at this laboratory; therefore it need no longer be considered an unknown. In fact it now seems that the most poorly known quantity in this kind of reactor calculation is p, the resonance escape probability. In our lattices p should be independent of the small enrichment variations; all our material is 99+ per cent U^{238}, and it is U^{238} resonances that give the parasitic capture.

In view of these facts we adopted the following approach: For each lattice the resonance escape probability was calculated according to the formula

$$p_{exp} = \frac{(1 + B^2L^2)\, e^{B^2\tau}}{\epsilon \eta f} \tag{1}$$

and also according to the formula

$$p_{theo} = \text{neg exp} \left[\frac{V_m \Sigma_{s,m} \xi}{V_U N_U \left(\frac{C_1}{F_r} + C_2 \frac{S}{M} \right)} + S_r \right]^{-1} \tag{2}$$

Table 2—Summary of Measurements and Computations

Enrichment, wt. %	Rod diameter, in.	Cell side, in.	Number of rods in tank	$\frac{V_m}{V_U}$	B^2, meters^{-2}	F	FF_m	R	$\Sigma_a \times 10^3$, cm^{-1}	$\bar{\Sigma}_U$, cm^{-1}	$\frac{T_{eff}}{T_0}$	η	ϵ	f	L^2, cm^2	τ, cm^2	k	p_{exp}	p_{theo}
0.490	1.00	4.50	120	24.82	1.76	1.162	1.537	5.5	6.454	0.4040	1.064	1.142	1.024	0.977	128	109	1.042	0.912	0.902
0.490	1.00	4.90	120	29.64	2.10	1.162	1.563	6.3	5.385	0.4035	1.054	1.142	1.024	0.974	153	108	1.056	0.927	0.918
0.490	1.00	7.50	52	71.02	1.60	1.162	1.633	16.4	2.278	0.4023	1.024	1.142	1.024	0.947	364	106	1.076	0.971	0.964
0.490	1.00	12.00	16	183.7	0.105	1.162	1.792	44.5	0.881	0.4019	1.009	1.142	1.024	0.875	942	105	1.011	0.988	0.987
0.490	2.00	7.25	52	15.71	1.61	1.420	2.427	5.7	6.444	0.4045	1.064	1.142	1.045	0.980	128	110	1.039	0.888	0.884
0.490	2.00	9.00	32	24.80	2.25	1.420	2.594	8.9	3.952	0.4034	1.039	1.142	1.045	0.970	209	108	1.072	0.926	0.926
0.490	2.00	12.00	16	44.94	1.28	1.420	2.796	19.4	2.110	0.4025	1.021	1.142	1.045	0.947	392	106	1.064	0.942	0.959
0.711	0.75	3.00	285	19.35	7.60	1.133	1.406	3.0	10.89	0.4060	1.102	1.332	1.018	0.983	75.4	110	1.149	0.862	0.864
0.711	0.75	4.50	120	45.09	7.48	1.133	1.474	7.0	4.753	0.4032	1.048	1.332	1.018	0.971	174	107	1.224	0.930	0.940
0.711	0.75	6.00	80	81.13	5.40	1.133	1.508	11.1	2.678	0.4025	1.027	1.332	1.018	0.954	309	106	1.236	0.955	0.966
0.711	1.00	3.625	208	15.69	7.31	1.190	1.520	2.7	12.20	0.4074	1.114	1.332	1.024	0.986	67.0	111	1.137	0.846	0.849
0.711	1.00	4.50	120	24.82	8.47	1.190	1.578	4.5	7.789	0.4050	1.076	1.332	1.024	0.981	106	109	1.195	0.893	0.902
0.711	1.00	4.90	120	29.64	8.36	1.190	1.598	5.7	6.517	0.4045	1.067	1.332	1.024	0.978	126	108	1.210	0.907	0.918
0.711	1.00	6.00	80	45.03	7.25	1.190	1.657	8.4	4.259	0.4033	1.043	1.332	1.024	0.970	194	107	1.232	0.932	0.945
0.711	1.00	7.50	52	71.02	5.36	1.190	1.718	12.7	2.671	0.4027	1.027	1.332	1.024	0.955	310	106	1.234	0.947	0.965
0.711	1.00	9.00	32	102.8	3.92	1.190	1.789	21.0	1.827	0.4022	1.019	1.332	1.024	0.937	454	106	1.228	0.961	0.976
0.711	1.00	12.00	16	183.7	2.11	1.190	1.901	39.3	1.019	0.4019	1.010	1.332	1.024	0.892	814	105	1.198	0.985	0.987
0.711	1.25	4.50	120	15.47	8.32	1.290	1.809	3.0	10.61	0.4068	1.101	1.332	1.029	0.985	77.2	111	1.167	0.863	0.857
0.711	1.25	6.00	80	28.39	8.30	1.290	1.918	6.3	5.727	0.4042	1.056	1.332	1.029	0.977	144	108	1.224	0.914	0.921
0.711	1.25	7.50	52	44.99	6.84	1.290	1.976	9.8	3.611	0.4032	1.036	1.332	1.029	0.966	229	107	1.244	0.938	0.950
0.711	1.25	9.00	32	65.29	5.35	1.290	2.064	14.2	2.440	0.4026	1.025	1.332	1.029	0.952	339	106	1.250	0.957	0.965
0.711	1.25	12.00	16	117.0	2.92	1.290	2.237	25.7	1.320	0.4021	1.014	1.332	1.029	0.916	628	105	1.220	0.971	0.981
0.711	1.50	6.00	81	19.36	8.65	1.356	2.139	4.4	7.389	0.4052	1.072	1.332	1.035	0.982	111	109	1.205	0.891	0.892
0.711	1.50	7.25	52	28.79	7.94	1.356	2.221	6.9	4.922	0.4038	1.049	1.332	1.035	0.975	168	108	1.234	0.919	0.927
0.711	1.50	9.00	32	44.97	6.29	1.356	2.341	11.1	3.077	0.4030	1.031	1.332	1.035	0.962	269	106	1.250	0.942	0.953
0.711	1.50	12.00	16	80.81	3.69	1.356	2.527	22.0	1.656	0.4023	1.017	1.332	1.035	0.933	500	105	1.231	0.958	0.974
0.711	2.00	7.25	52	15.71	8.23	1.502	2.560	4.7	7.593	0.4055	1.074	1.332	1.045	0.983	108	110	1.192	0.872	0.884
0.711	2.00	9.00	32	24.80	7.22	1.502	2.806	8.0	4.534	0.4036	1.049	1.332	1.045	0.974	182	108	1.221	0.901	0.929
0.711	2.00	12.00	16	44.94	4.76	1.502	3.174	16.1	2.311	0.4026	1.024	1.332	1.045	0.951	358	106	1.230	0.929	0.959
0.901	1.00	3.625	124*	15.69	12.6	1.238	1.721	2.6	12.82	0.4083	1.119	1.443	1.024	0.986	63.7	111	1.242	0.852	0.848
0.901	1.00	4.90	68*	29.64	12.5	1.238	1.829	4.9	6.580	0.4048	1.065	1.443	1.024	0.979	125	108	1.323	0.915	0.917
0.901	1.00	6.00	52*	45.03	10.6	1.238	1.924	7.1	4.325	0.4035	1.043	1.443	1.024	0.970	191	107	1.347	0.940	0.945
0.901	1.00	7.50	52	71.02	7.81	1.238	1.968	11.2	2.751	0.4027	1.028	1.443	1.024	0.957	301	106	1.341	0.948	0.965
0.901	1.00	9.00	32	102.8	5.85	1.238	2.009	16.0	1.907	0.4023	1.020	1.443	1.024	0.940	434	105	1.334	0.959	0.976
0.901	1.00	12.00	16	183.7	3.13	1.238	2.131	33.0	1.062	0.4019	1.011	1.443	1.024	0.897	781	105	1.286	0.970	0.986

*Measurements made in 4-ft tank.

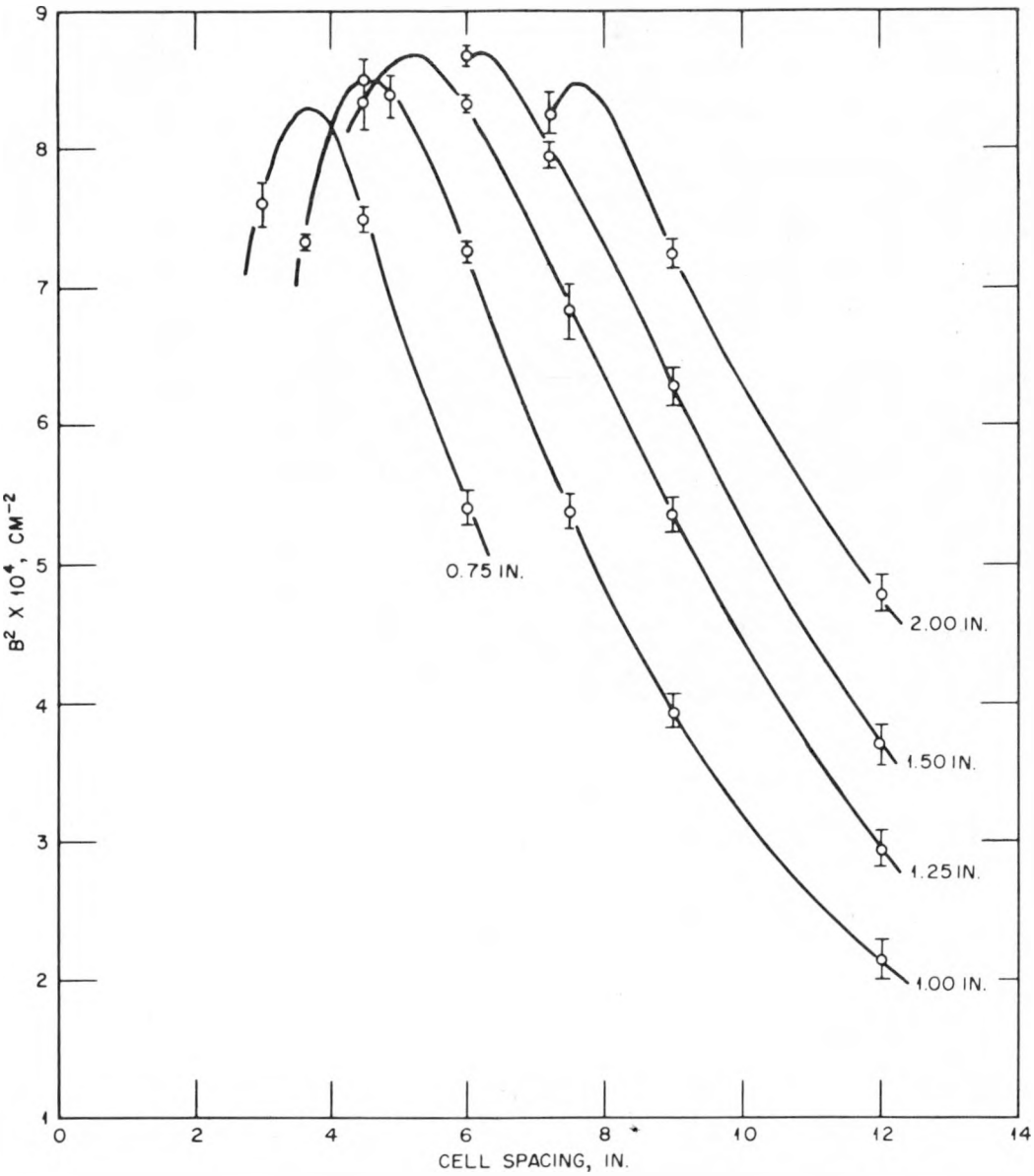

Fig. 1 — Material buckling for natural-uranium lattices. The largest buckling is obtained with 1.50-in.-diameter rods on about a 6-in. lattice spacing.

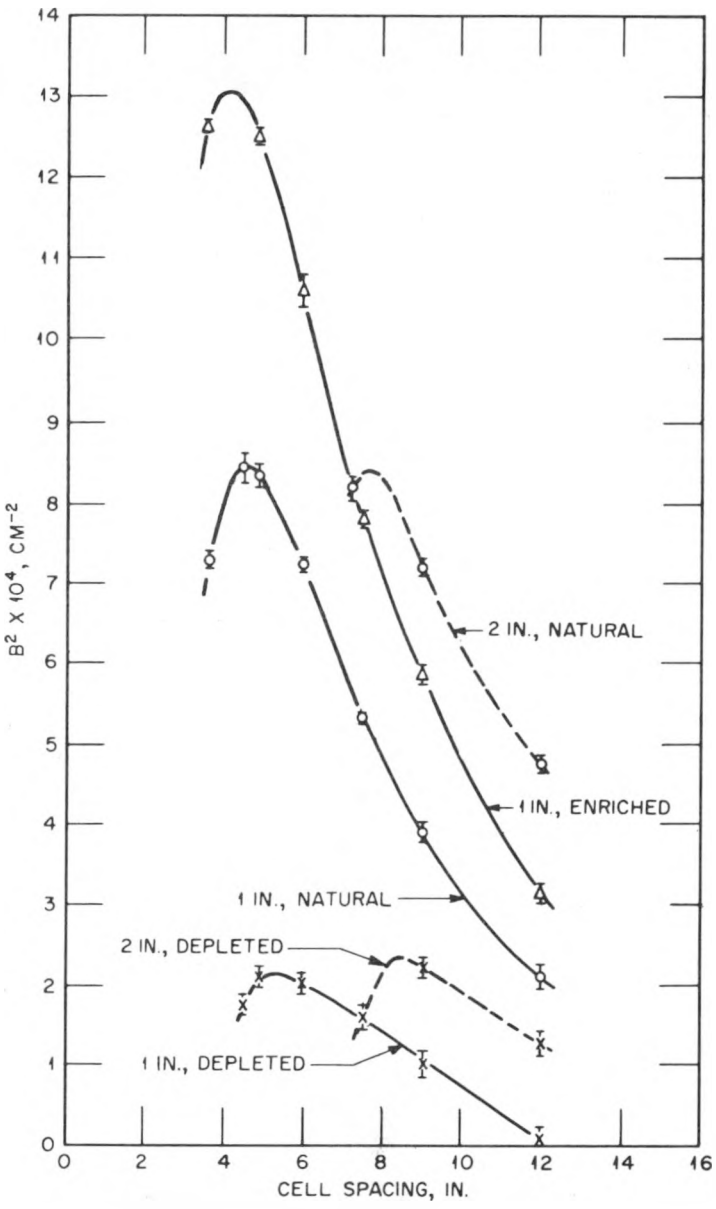

Fig. 2 — Material buckling for lattices of 1- and 2-in. rods. It is perhaps noteworthy that, for a given rod size, the cell spacing for maximum buckling is not greatly dependent on enrichment. The graph shows buckling data for two depleted lattices, D-1-6 and D-1-9, which were not included in the general computations because of the lack of satisfactory intracell data.

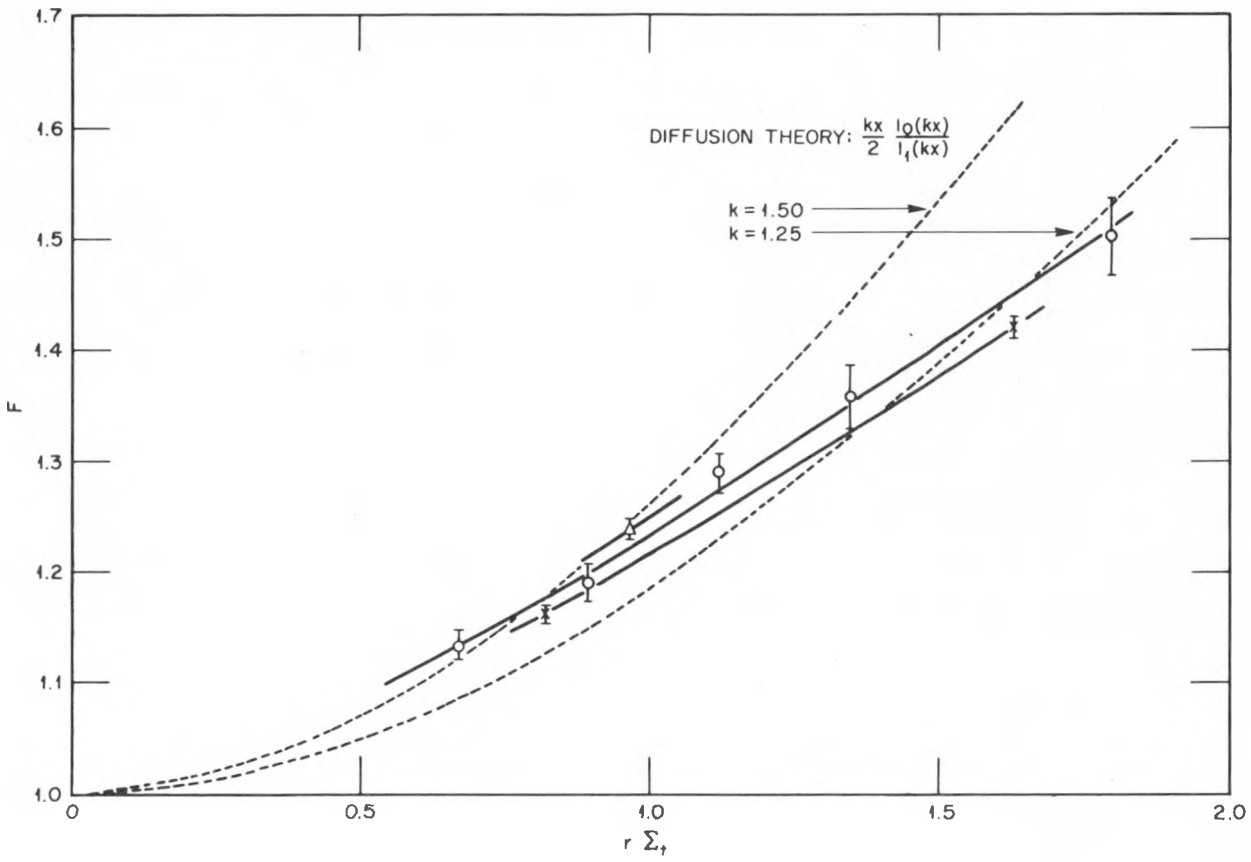

Fig. 3—Rod disadvantage factors vs. radius in mean free paths. Two diffusion theory solutions are shown for comparison, with k = 1.25 and 1.50, respectively. Asymptotic diffusion theory would evaluate the k's for our three enrichments as between 0.90 and 0.95; it is apparent, however, that no family of such solutions can be fitted to the data for these rods, which all have radii that are not large compared to a mean free path. ×, depleted. ○, natural. △, enriched.

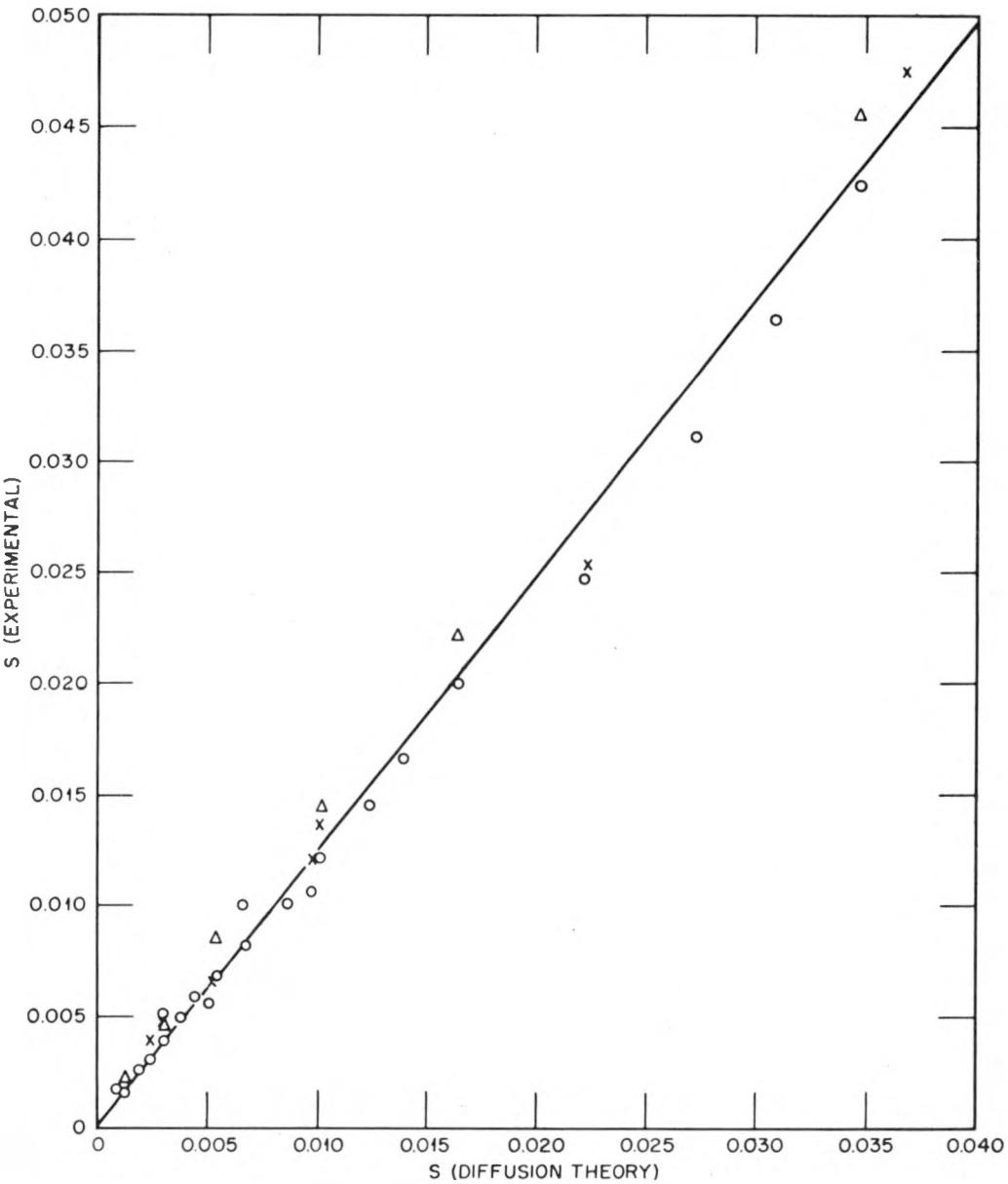

Fig. 4 — Excess absorption. It is confirmed that S is independent of fuel enrichment and is a function only of moderator and geometry. Diffusion theory, however, will underestimate the flux dip near a rod and, in fact, appears to underestimate S by about 25 per cent. ×, depleted. ○, natural. △, enriched.

Equation 1, which we will consider as giving the experimental p, follows from the usual four-factor compatibility relation

$$k = \eta\epsilon pf = 1 + L \tag{3}$$

and the continuous-slowing-down thermal-diffusion leakage formulation for homogeneous mediums

$$1 + L = (1 + B^2L^2)\, e^{B^2\tau} \tag{4}$$

Wherever possible experimentally measured values have been inserted in Eq. 1. The computational details are explained at length in the following sections. Equation 2, which gives a theoretical p, is the customary Fermi equation as modified by Wigner and Weinberg. Comparison of p_{exp} and p_{theo} is then a test of the applicability of the modified two-group theory as well as of the customary method of computing p_{theo}. Table 2 lists p_{exp} and p_{theo} for all the lattices. Graphs of p_{exp} vs. p_{theo} are presented in Figs. 5 and 6. Again, it should be noted that for all our 99+ per cent U^{238} materials we expect p to be independent of rod enrichment.

The experimental values for p appear to agree fairly well with the theoretical values, indicating that the homogeneous two-group model could be made satisfactory for D_2O–uranium lattices. There remain to be explained, however, some differences, systematic with enrichment, of the order of 1 to 2 per cent. As will be shown in the error analysis, it appears difficult to attribute these systematic differences to experimental errors.

The values of k listed in Table 2 were obtained from the leakage expression in Eq. 4.

4. COMPUTATIONAL DETAILS

4.1 Effective Thermal-neutron Temperature

A knowledge of the nuclear cross sections is necessary for the computation of f, η, and the leakage term $1 + B^2L^2$. The effective cross sections, in particular the absorption cross sections, of the materials of our heterogeneous mediums are dependent on the spectrum of neutron velocities. This spectrum varies from point to point in a lattice and from lattice to lattice. For the thermal neutrons (say, those with energy less than 0.4 ev), it appears that we may describe the spectrum at any point by a single parameter T, the temperature of a Maxwellian neutron-velocity distribution. Thus we may speak of the thermal-neutron temperature, T, as varying from point to point in a lattice and from lattice to lattice, and we can use Maxwellian averaged macroscopic thermal absorption cross sections, which will be functions of T.

The point-to-point variation will not unduly concern us in this analysis because our so-called "flux"-measuring foils themselves have microscopic absorption cross sections whose velocity dependence is close to that of the materials in the lattice. In most cases this dependence is an inverse velocity dependence; therefore the absorption rates for the materials involved depend only on the neutron densities and are independent of T. The experimental foil activities, therefore, also give relative neutron densities throughout a lattice. Thus the experimental disadvantage factors, F and F_m, will give correct relative absorptions, and, in particular, they will give correct thermal utilizations, f, providing the effective cross sections used are all computed at the same temperature.

To compute the thermal-diffusion length, however, we must know absolute cross sections and, hence, thermal-neutron temperatures. The leakage term $1 + L$ is quite insensitive to small changes in the cross sections; therefore we may ignore the point-to-point variation of the temperature in the lattice (see Sec. 4.5). As a first-order correction, however, a proper effective value of T should be used for computing all cross sections in a given lattice. For this we have recourse to the recent result of E. R. Cohen[10] for homogeneous mediums (that the thermal-neutron temperature T is slightly elevated) in a ratio which he has calculated numerically and which for small absorption is closely given by

$$\frac{T}{T_0} \approx 1 + 1.35\,\frac{\Sigma_a(T_0)}{\xi\Sigma_s} \tag{5}$$

where T_0 is the ambient or moderator temperature, i.e., 20°C, and $\Sigma_a(T_0)$ is the macroscopic absorption cross section of the medium for a Maxwellian neutron distribution at the ambient

temperature. (An equation of this form was first given by K. Cohen in Report HKF-102.) For the heterogeneous situation we will replace $\Sigma_a(T_0)$ by a flux-weighted volume average (see Sec. 4.5).

It is necessary at this point to make explicit the convention that will be followed consistently in this article: all macroscopic absorption cross sections used will be effective cross sections for Maxwellian distributions. When no temperature is indicated, the Maxwellian distribution is understood to be that for effective thermal-neutron temperature, T. In other words, the macroscopic absorption cross sections corresponding to effective temperature T are obtained by multiplying tabulated microscopic monoenergetic 2200 m/sec values (σ^0) by the atomic densities, by $\sqrt{T_0/T}$, and by the factor $\sqrt{\pi}/2$. For U^{235} a small additional correction due to its deviation from v^{-1} dependence is included (see Sec. 4.3).

Returning to Eq. 5, we require the slowing-down power of D_2O for thermal neutrons. The result given by Cohen already includes the effects due to the thermal motion of the moderator, and a correction for the small volume of uranium hardly seems warranted in the presence of other uncertainties; therefore we may use the usual monatomic formula $\xi = 2/(M + 2/3)$, and we will take the simple average $\overline{\xi\Sigma}_s = \xi^D\Sigma_s^D + \xi^O\Sigma_s^O$, where the superscripts stand for deuterium and oxygen, respectively.

In a recent report H. D. Brown and D. S. St. John[11] point out that, in the important part of the thermal velocity range, D_2O molecules behave as rigid rotators and that consequently the actual velocity distribution of the bound deuterons can be computed from an appropriate

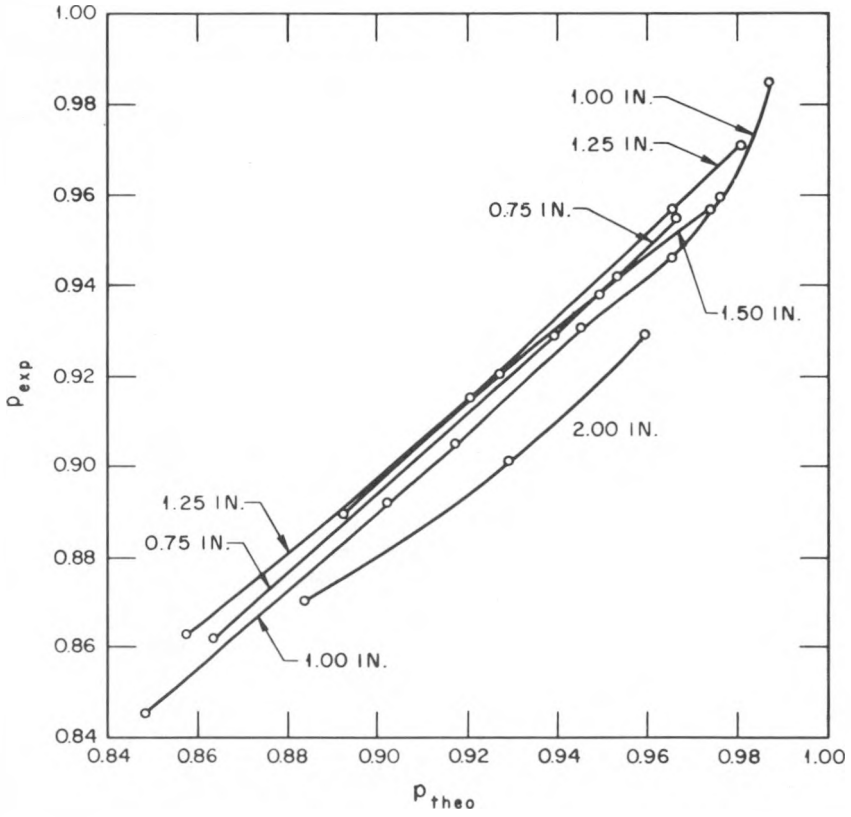

Fig. 5—Compatibility calculations for natural-uranium lattices. For most of the cases p_{exp} appears to be about 0.9 per cent below p_{theo}.

Maxwellian for a medium of free nonrotating point masses. The temperature of this Maxwellian is to be taken as ambient, but the mass value required is 3.595, which might be called the "effective" mass of the bound deuteron in the rotator. Secondly, they point to earlier work of Sachs and Teller,[12] which shows that the effective deuteron mass, so far as energy and momentum transfer in an average collision with an incident neutron, is again 3.595. Thus for the purpose of Eq. 5, which applies to the thermal velocity range, the bound deuterons in D_2O are completely equivalent to free particles of weight 3.595 amu (atomic mass units). A similar calculation gives the bound oxygen mass in a D_2O molecule as equivalent to a free mass of 18.03 amu. Combining these with the thermal values $\Sigma_s^D = 0.340$ cm^{-1} and $\Sigma_s^O = 0.127$ cm^{-1}, we get $\overline{\xi\Sigma}_s = 0.173$ cm^{-1}.

For fast neutrons, where molecular binding effects are unimportant, the free-atom values $M^D = 2$, $\Sigma_s^D = 0.223$ cm^{-1}, $M^O = 16$, and $\Sigma_s^O = 0.127$ give $\overline{\xi\Sigma}_s = 0.177$ cm^{-1}; although $\bar{\xi}$ and $\bar{\Sigma}_s$ individually are considerably changed, $\overline{\xi\Sigma}_s$, surprisingly, is not greatly different from the thermal value. It is this circumstance that has encouraged us to use Cohen's result, which, properly, applies only to mediums in which Σ_s and ξ (apart from thermal effects) are constant. Using, then, the flux-weighted average $\bar{\Sigma}_a(T_0)$ (see Sec. 4.5) and the thermal value $\overline{\xi\Sigma}_s = 0.173$ cm^{-1} in Eq. 5, we can compute T/T_0. The values thus obtained are given in Table 2.

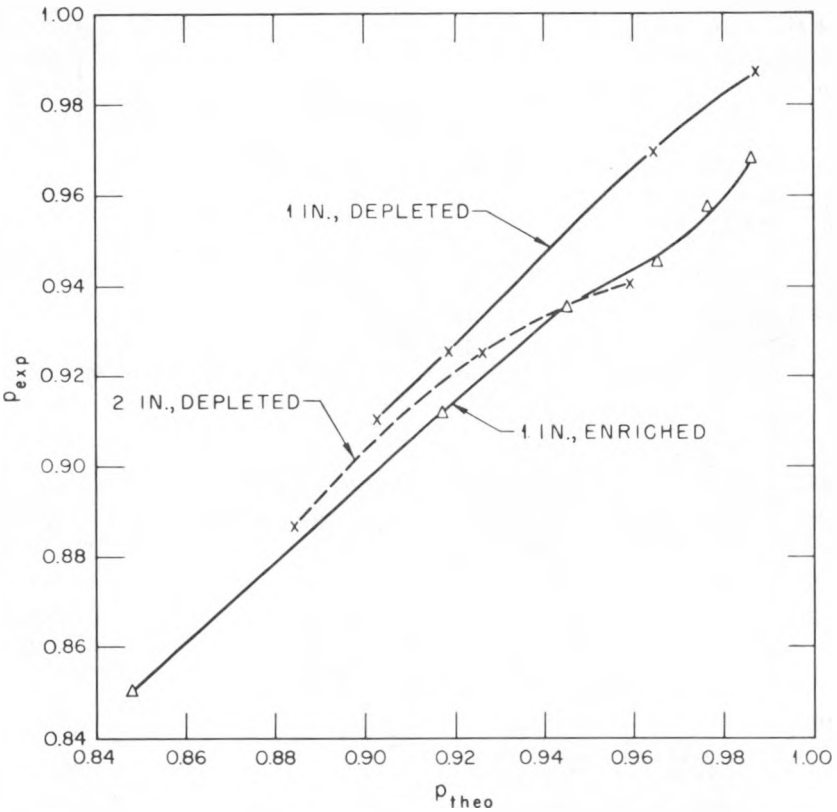

Fig. 6—Compatibility calculations for depleted- and enriched-uranium lattices. For most of the depleted cases p_{exp} is about 0.6 per cent high, whereas for the enriched lattices it averages 1.0 per cent low. This discrepancy is quite marked and is difficult to ascribe to error other than in the theory.

Corroboration of the results of Brown and

St. John may be obtained from scattering and transport cross-section measurements for D_2O.[9] These yielded, for the average cosine in the scattering of a thermal neutron in D_2O, $\bar{\mu} = 0.15 \pm 0.03$. On the other hand, the theoretical value obtained from the above effective thermal masses is $\bar{\mu} = [\Sigma_s^D(2/3M^D) + \Sigma_s^O(2/3M^O)]/\Sigma_s = 0.145$. For comparison, the free-atom values would give $\bar{\mu} = 0.227$, which does not agree at all. It is also worth noting that cross-section measurements for light water support the above considerations. The equivalent masses for hydrogen and oxygen nuclei in light water are, respectively, 1.884 and 17.06. Combining these with the effective thermal values $\Sigma_s^H = 3.03\,cm^{-1}$ and $\Sigma_s^O = 0.13\ cm^{-1}$, we get a theoretical $\bar{\mu} = 0.341$. Experimentally the values $\Sigma_s(H_2O) = 3.16 \pm 0.06\,cm^{-1}$ and $\Sigma_{tr}(H_2O) = 2.08 \pm 0.04\,cm^{-1}$ give $\bar{\mu} = 0.34 \pm 0.02$.

The rod diameters listed in Table 1 are actually the inside diameters of the aluminum tubes and, therefore, are only nominal values for the uranium slugs. In the computation allowance was made for the machining tolerances employed, and all slug diameters were taken 4 mils less than the stated nominal values. The residual annular air volumes were lumped in with the 0.040-in. thickness of aluminum cladding.

For $\Sigma_{Al}(T_0)$ and $\Sigma_m(T_0)$ the values 0.01021 cm^{-1} and 0.000105 cm^{-1}, respectively, were used. The value of $\Sigma_m(T_0)$ for our D_2O was obtained during the recent measurement of λ_{tr} by the boron-poisoning experiment[9] and corresponds to a D_2O purity of 99.70 at. %. This value has been confirmed by mass spectrographic measurements at Chalk River and by additional D_2O diffusion-length measurements at this laboratory.

Table 3 — Effective Fuel Absorption Cross Sections at 20°C

Fuel	Uranium density, g/cm³	$E = \frac{100\,N^{U^{235}}}{N^{U^{235}} + N^{U^{238}}}$	$\Sigma_U(T_0)$, cm^{-1}
Depleted uranium	18.80	0.4962	0.2557
Natural uranium	18.88	0.7205	0.3200
Enriched uranium	18.83	0.9124	0.3763

4.2 Thermal Utilization

The thermal utilizations were computed from the intracell data according to the formula

$$f = \frac{\Sigma_U V_U}{\Sigma_U V_U + \Sigma_{Al} V_{Al} F + \Sigma_m V_m F F_m} \qquad (6)$$

and the values tabulated in Table 2. The macroscopic uranium cross sections used are listed in Table 3. For the computations the 2200 m/sec values of $\sigma_a^0(U^{235})$ and $\sigma_a^0(U^{238})$ were taken to be 680 and 2.77 barns, respectively.[8] The U^{235} percentage atomic enrichments, E, were taken from data accompanying the fuel material; they have been checked by mass spectrographic analyses. $N^{U^{235}}$ and $N^{U^{238}}$ denote the atomic densities of U^{235} and U^{238}, respectively, in the fuel slugs. The maximum uncertainty in E is estimated to be 0.3 per cent.

A subsidiary check both on our choice of $\Sigma_m(T_0)$ and on the applicability of diffusion theory to the moderator volume can be obtained by writing Eq. 6 as

$$\frac{1}{f} = 1 + \frac{\Sigma_{Al} V_{Al} + \Sigma_m V_m}{\Sigma_U V_U} F + \frac{\Sigma_m V_m}{\Sigma_U V_U} F(F_m - 1) \qquad (7)$$

The last term of this is often denoted the "excess absorption" S (see, for example, Guggenheim and Pryce[13]); if diffusion theory is strictly applicable in the moderator volume, S is a function only of moderator properties and lattice dimensions, i.e., S is independent of rod

material. In Fig. 4 we have plotted our experimental values of S from Eq. 7 vs. theoretical values given by diffusion theory. The data are indeed independent of enrichment and are consistent to ±0.002. The ratio is apparently not unity, however, but rather S(experiment)/S(diffusion theory) = 1.25 ± 0.05. This discrepancy could immediately be resolved if we adopted $0.84 \times 10^{-4}\,cm^{-1}$ for $\Sigma_m(T_0)$ instead of our value of $1.05 \times 10^{-4}\,cm^{-1}$; however, there is no other justification for such a considerable change. From transport theory we would expect somewhat larger flux dips near the rods than simple diffusion theory predicts, and then S(experiment) would exceed S(diffusion). We have consequently left $\Sigma_m(T_0)$ unchanged and will merely remark here that, if S were computed from simple diffusion theory, our data indicate that about a 25 per cent underestimate would occur, leading to an overestimate in the thermal utilization of, at most, 1 per cent.

4.3 Calculation of η

The value of η was computed by the usual formula

$$\eta = \frac{E\sigma_a^{U^{235}} g}{E\sigma_a^{U^{235}} g + (100 - E)\sigma_a^{U^{238}}} \frac{\nu}{1 + \alpha} \tag{8}$$

where $\nu = 2.48$ and $\alpha = 0.184$. The values of σ are the 2200 m/sec values. The factor

$$g(T) = \int_0^\infty \frac{v\, M(v,T)\, \sigma(v)\, dv}{\sigma^0 v^0} \tag{9}$$

is essentially the quantity denoted by f in references 7 and 8 and corrects for the non 1/v dependence of the U^{235} cross section. M(v,T) is a normalized Maxwellian velocity distribution for effective neutron temperature T; the superscript zeros indicate 2200 m/sec values. Since our maximum effective neutron temperature increase was in all cases less than 12 per cent, g was essentially constant at 0.98.

4.4 Fast Effect

The values of ϵ used for our lattices have been taken from calculations by J. E. Garvey[14] at this laboratory. They are given in Table 2. Garvey calculated the U^{238} cross sections averaged over the fission spectrum to be $\sigma_c = 0.09$, $\sigma_f = 0.28$, $\sigma_e = 4.88$, $\sigma_{inel} = 1.85$, and $\sigma_t = 7.10$, and he used the expression for P, the probability of a fission neutron having its first collision in the parent rod, given in Report CP-644. It is to be noted that, for the lattices under discussion, ϵ is independent of enrichment.

4.5 Calculation of L^2

The diffusion length, L, for each lattice was computed according to the formula

$$\frac{1}{L^2} = 3\overline{\Sigma}_a\overline{\Sigma}_{tr} \tag{10}$$

$\overline{\Sigma}_a$ and $\overline{\Sigma}_{tr}$ represent flux-weighted volume averages; as an example we have

$$\overline{\Sigma} = \frac{\Sigma_U V_U + \Sigma_{Al} V_{Al} F + \Sigma_m V_m F F_m}{V_U + V_{Al}\, F + V_m F F_m} \tag{11}$$

The subscripts refer to uranium, aluminum, and moderator (D_2O), respectively, and the V's are the corresponding volume fractions of the lattice cell. The values for $\overline{\Sigma}_a$, $\overline{\Sigma}_{tr}$, and L^2 are all tabulated in Table 2.

Equations 10 and 11 are examples of the homogenization procedure used in reactor calculations in which the heterogeneous lattice is replaced by some equivalent homogeneous medium. For the validity of this process suitable means of averaging the lattice properties must be established. Now a flux-weighted average of the absorption cross sections, $\overline{\Sigma}_a$, is unexceptionable since the absorption rates in the various parts of the lattice structure are just proportional to the corresponding fluxes. There has been, however, some doubt as to the accuracy of flux weighting $\overline{\Sigma}_{tr}$ and of computing L^2 by such a simple formula as Eq. 10. Again, it is to be noted that the averaging procedure is somewhat inaccurate because the effect of point-to-point temperature variation does not cancel out of Eq. 11. However, recent experimental measurements made at this laboratory[15] have demonstrated that, for our lattices at least, Eq. 10 is completely adequate when the averaging is done according to Eq. 11.

Since the moderator occupies a preponderant portion of the volume, $\overline{\Sigma}_{tr} \approx \Sigma_{tr,m}$, and the above expression for L^2 then differs very little from the simpler form $L^2 = L_m^2 f_m$, where L_m

is the diffusion length of pure moderator and f_m is the thermal utilization of the moderator in the lattice. However, it should be noted that for flux weighting we have been able to use experimental values of F and F_m.

4.6 Activity Ratio

It is sometimes thought that L^2 can be determined experimentally from R, the activity ratio. Actually, this is not quite correct. Suppose A_b and A_{Cd} are the experimental saturated activities obtained with bare indium foils and cadmium-shielded indium foils, respectively. Then, using the result of Kunstadter[16] that, for 95 mg/cm^2 foils and 0.020-in. cadmium covers, the indium resonance activity is attenuated some 7 per cent by the shielding, an experimental activity ratio can be defined by

$$R = \frac{\text{thermal activity}}{\text{epithermal activity}} = \frac{A_b - 1.07\,A_{Cd}}{1.07\,A_{Cd}} \qquad (12)$$

This ratio is a function of the effective position of the cadmium cutoff ($E_c \sim 0.35$ ev) and of the relative thermal to epithermal flux response of indium and may, in principle, be computed by setting

$$R = \frac{\int_0^\infty \sigma_{In}\,\rho\,M(v)\,v\,dv}{\int_{E_c}^\infty \sigma_{In}\,(q/\overline{\xi\Sigma}_s)\,(dE/E)} \qquad (13)$$

In the numerator a normalized Maxwellian thermal-neutron velocity distribution M(v) has been used. Since M(v) drops exponentially at higher speeds, the integral has, with little error, been extended past the cadmium cutoff to infinity. The microscopic thermal absorption cross section of indium was taken to have the dependence $\sigma_{In} = \sigma_{In}^0\,(v^0/v)^{0.75}$; the superscript zeros refer to values at 2200 m/sec, and ρ is the thermal-neutron density. In the denominator q is the standard slowing-down density, and $\overline{\xi\Sigma}_s$ is the averaged slowing-down power of the medium. The large indium resonance just above cadmium cutoff is responsible for most of the integral; hence q can be taken as effectively constant at its cadmium cutoff value. With these considerations

$$R = \frac{\rho v^0}{q}\,\overline{\xi\Sigma}_s\,\frac{1.013\,\sigma_{In}^0}{\int_{E_c}^\infty \sigma_{In}(dE/E)} \qquad (14)$$

Now q is the source for thermal neutrons and must equal the sum of the thermal absorption and thermal leakage rates; therefore

$$q = \rho v^0 \overline{N\sigma^0}\,(1 + B^2L^2) \qquad (15)$$

The bar indicates a spatial average. Combining Eqs. 14 and 15 gives

$$\overline{N\sigma^0}\,\frac{1 + B^2L^2}{1.013\,\overline{\xi\Sigma}_s} = \left[\frac{\sigma_{In}^0}{\int_{E_c}^\infty \sigma_{In}\,(dE/E)}\right]_{eff}\frac{1}{R} \qquad (16)$$

B^2L^2 is of the order of 0.1 to 0.3 for many of our lattices. Hence, if this last equation were used to get L^2 from experimental values of R, a very high accuracy in R would be required. In fact, our determinations of R are good to only ±3 per cent; therefore they are of no direct use in the present analysis.

Some authors substitute

$$\overline{N\sigma^0} = \frac{1}{3\overline{\Sigma}_{tr}L^2}\,\frac{2}{\sqrt{\pi}}\,\sqrt{\frac{T}{T_0}}$$

in Eq. 16 and thereby get a relation in which L^2 appears almost directly proportional to R. To obtain L^2 in this way would, however, be self-deluding since it assumes we know how to calculate $\overline{\Sigma}_{tr}$. We must, indeed, assume this, but then it is more direct to calculate L^2 from Eq. 10. However, if we did not have reliable intracell data to use in flux weighting $\overline{\Sigma}_a$, the computation of L^2 from R would be pertinent. It should be noted that the values listed for R were obtained only from the activities at the tank center, i.e., at the center of a cell that has rods at its corners. No attempt has been made to average R over a cell. Not only is it uncertain how such an average is to be taken but also the limited usefulness of this concept for heterogeneous mediums does not seem to justify further refinement.

The ratio in the brackets on the right side of Eq. 16 has been labeled "eff" because our indium foils (~95 mg/cm^2) are not thin for neutrons at the indium resonance energies. At

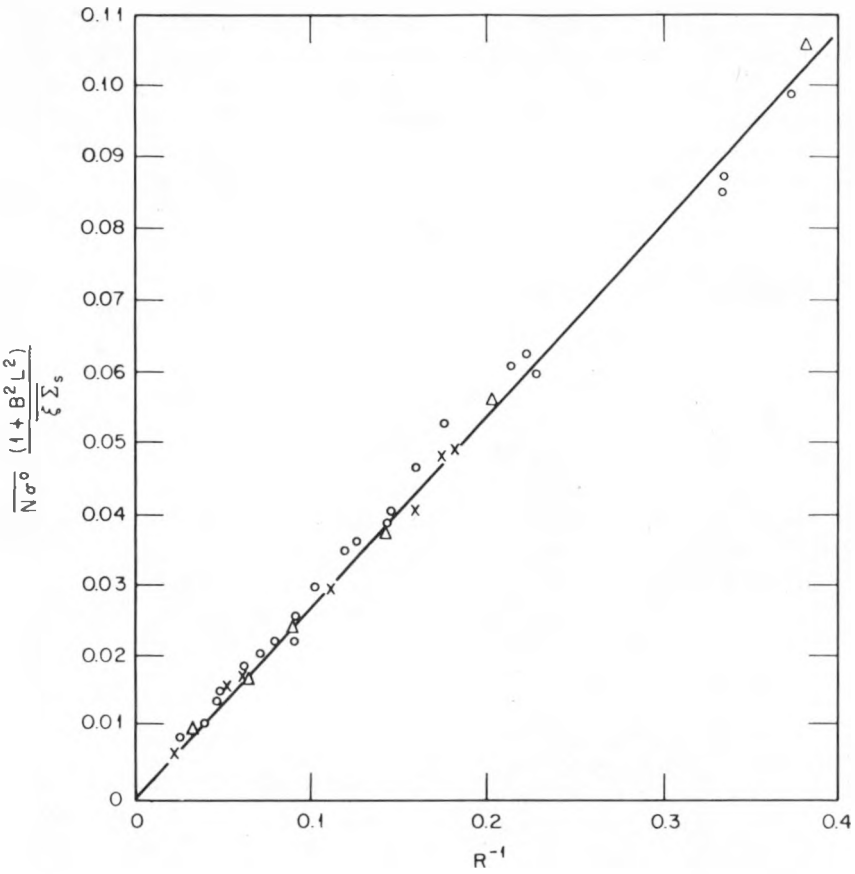

Fig. 7—Activity ratio data for 35 lattices. R is the ratio of thermal to epithermal indium-foil activities, $(A_b - 1.07\,A_{Cd})/1.07\,A_{Cd}$, at the center of a lattice cell. The slope of 0.272 ± 0.010 is characteristic of our 95 mg/cm^2 indium foils and 0.020-in.-thick cadmium covers. ×, depleted. ○, natural. △, enriched. Note that the ordinate does not include the factor 1.013 on the left side of Eq. 16.

these energies we must have considerable self-shielding in the epithermal activation process, which will raise the value of the ratio. We have, in fact, found the self-shielding to result in an increase of this ratio by a factor of 3.9 for our 95 mg/cm^2 foils. Other laboratories have reported factors of 3.88 for 92 mg/cm^2 foils[17] and 3.66 for 88 mg/cm^2 foils.[18]

Figure 7 is a graph of the left side of Eq. 16 vs. 1/R for our 35 lattices. The linear relation is thought to be an encouraging complement to our lattice calculations. The slope of this line is 0.272 ± 0.010, which can be combined with the self-shielding factor of 3.9 to get the ratio of the (thin-foil) resonance integral of indium to the 2200 m/sec cross section

$$\frac{\int_{E_c}^{\infty} \sigma_{In}\,(dE/E)}{\sigma_{In}^{\theta}} = 14.5 \pm 0.5 \qquad (17)$$

This may be compared to the value of 13.9 computed directly from cross-section data.[18]

4.7 Age

In a lattice the age or migration area of the moderator must be corrected for inelastic scattering in the fuel rods and for dilution of the moderator by the fuel rods. A correction must also be applied for the absorption of neutrons above thermal energies by fissionable material. It is convenient, therefore, to express the age

from fission to thermal energies in pure moderator as the sum of the age from fission energy E_0 to the lowest energy E_{inel} for which a neutron can be inelastically scattered, the age from E_{inel} to the indium resonance energy, E_{res}, and the age from E_{res} down to thermal energy, E_{th}; i.e.,

$$\tau_0 = \tau(E_0,E_{inel}) + \tau(E_{inel},E_{res}) + \tau(E_{res},E_{th}) \quad (18)$$

In making the corrections, it is reasonable for a light moderator to neglect elastic moderation in the fuel and to assume that a neutron can be slowed from E_0 to E_{inel} by inelastic scattering in the fuel or by elastic scattering in the moderator but that it can be slowed from E_{inel} to E_{th} only by elastic scattering in the moderator. It can also be assumed that a fission neutron having undergone inelastic collision will most likely be slowed past E_{inel} before returning to a fuel rod.

A neutron suffering an inelastic collision will undergo a large degradation in energy without migrating appreciably. The possibility of such a neutron leaking out before being thermalized will be correspondingly reduced. On the other hand, a fast neutron undergoing elastic collisions in a fuel rod will be able to migrate without being degraded and thereby will increase its probability for leaking before being thermalized. In the first case the age would effectively be decreased, whereas in the second it would be effectively increased. Accordingly, in a lattice $\tau(E_0,E_{inel})$ should be decreased by $P\sigma_{inel}/\sigma_{total}$, the fraction of fission neutrons having inelastic collisions before entering the moderator, and $\tau(E_{inel},E_{res})$ and $\tau(E_{res},E_{th})$ should be increased by the reciprocal of the moderator volume fraction.

In plain D_2O, $\tau(E_{res},E_{th})$ is usually taken to be of the order of 25 cm^2. In a multiplying medium, however, this age is considerably decreased as an effective result of the epithermal absorption of neutrons. In the usual two-group theory the fast group is treated by Fermi age theory; fast neutrons either are moderated to thermal energies or are lost by leakage. No true absorption is envisaged, although for multiplicative mediums, such as our lattices, this undoubtedly does occur in the epithermal region of, say, 0.1 to 10 volts. E. R. Cohen has pointed out that this epithermal true absorption competes only with the fairly low fast leakage probability and therefore results in additional neutron production. The correction for epithermal absorption may thus be described as an effective increase in η and has been so used previously.[4] It now appears that for multiplying mediums this epithermal absorption correction should more properly be applied to the age below indium resonance. In a recent computation Cohen[10] has shown that for D_2O lattices the age from indium resonance energy to the effective thermal energy, $\tau(E_{res},E'_{th})$, is more likely to be about 6 cm^2.

Combining the several corrections discussed, the effective age in the lattice may be taken as

$$\tau = \tau(E_0,E_{inel})\left(1 - \frac{P\sigma_{inel}}{\sigma_{total}}\right) + \left[\tau(E_{inel},E_{res}) + \tau(E_{res},E'_{th})\right]\frac{1}{V_m} \quad (19)$$

The values of τ computed according to Eq. 19 are listed in Table 2. The age in D_2O from E_0 to E_{res} was taken[7] as 100 cm^2. Using $E_0 = 2 \times 10^6$ ev, $E_{inel} = 2 \times 10^5$ ev, and $E_{res} = 1.44$ ev and assuming $D/\xi\Sigma_s$ constant over this energy region, $\tau(E_0,E_{inel}) = 16$ cm^2 and $\tau(E_{inel},E_{res}) = 84$ cm^2. P was obtained from fast-effect calculations by Garvey[14]; $\sigma_{inel}/\sigma_{total}$ was taken to be $1.85/7.10 = 0.26$.

For a subsidiary experiment providing some corroboration for our age computations see Sec. 9, Appendix C.

4.8 Resonance Escape Probability

The theoretical value of the resonance escape probability was computed in the usual way for heterogeneous mediums. That is, if

$$p_{theo} = e^{-1/T} \quad (20)$$

the analogy of T to be the quantity $(1 - f)/f$ (see Eq. 7) in the thermal-utilization calculation suggests that one can set

$$T = \frac{V_m\Sigma_{s,m}\xi}{V_U N_U\left[(C_1/F_r) + C_2(S/M)\right]} + S_r \quad (21)$$

This model ascribes to the resonance flux a spatial distribution which would be obtained by diffusion theory from a uniform source distribution in the moderator. The "absorption" of the moderator is due to the scattering cross section, $\Sigma_{s,m}$, which moderates the neutrons through the resonance-energy region. The absorption of the uranium rod is real, and, in fact, it is so strong at the resonance peaks in this region that the over-all uranium absorption cross section is regarded as having both a volume and a surface dependence; hence we have the quantity S/M, the surface to mass ratio of the rod, in Eq. 21.

F_r and S_r are the rod resonance disadvantage factor and moderator resonance excess absorption, respectively. In terms of rod and cell radii, a and b, and rod and moderator reciprocal resonance diffusion lengths, $\varkappa_U$ and $\varkappa_m$, we have

$$F_r = \frac{\varkappa_U a\, I_0(\varkappa_U a)}{2I_1(\varkappa_U a)} \tag{22}$$

and

$$1 + S_r = \varkappa_m \frac{b^2 - a^2}{2a} \times \frac{I_1(\varkappa_m b)\, K_0(\varkappa_m a) + K_1(\varkappa_m b)\, I_0(\varkappa_m a)}{I_1(\varkappa_m b)\, K_1(\varkappa_m a) - K_1(\varkappa_m b)\, I_1(\varkappa_m a)} \tag{23}$$

In these computations the customary numbers $\varkappa_m = 0.154\ cm^{-1}$ and $\varkappa_U = 0.420\ cm^{-1}$ have been used. C_1 and C_2 were recomputed from the data of Goldstein and Hughes,[19] using the result given in Eq. 17, the newer cross-section value[8] $\sigma^{U^{238}} = 2.77$, and a 1.50-barn correction for that part of the resonance integral that is due to the normal 1/v tail, and hence that should not be regarded as being parasitic. The result was

$C_1 = 7.3$ barns

and

$C_2 = 25.0 \times 10^{-24}$ g

The values of p computed according to Eqs. 20 to 23 are listed in Table 2. They also are used as the abscissas in the compatibility graphs, Figs. 5 and 6.

5. ERRORS

One reason for the present series of measurements can be seen by inspecting the two equations

$$k = \eta\epsilon fp = (1 + B^2L^2)e^{B^2\tau} \tag{24}$$

and

$$\frac{1}{f} = 1 + \frac{\Sigma_{Al}V_{Al}}{\Sigma_U V_U} F + \frac{\Sigma_m V_m}{\Sigma_U V_U} FF_m \tag{25}$$

In the first of these, $1 + B^2L^2$ is less than 1.25 (for the "hottest" enriched lattice) and, in fact, more usually about 1.10. This means that if k were known to but 1 per cent and if L^2 could be exactly computed, B^2 would only be known to within 10 per cent. Thus, at the present stage of our knowledge, it is difficult to compute B^2 (and hence critical sizes) for this type of inhomogeneous lattice. Furthermore, because of poorly understood deviations of the intracell neutron distribution from the predictions of simple diffusion theory, computation of F and FF_m can be greatly in error, and, although f does not greatly differ from unity (f is always greater than 0.86 and usually about 0.95), this ambiguity in f can still amount to several per cent. For both the buckling and disadvantage factors, therefore, our program has, of necessity, been experimental and empirical.

The foregoing recital has an inverse import when applied to our theoretical analysis of the data, the theoretical analysis being based precisely on Eqs. 24 and 25. The inversion is that our experimental errors in B^2, F, and F_m are greatly diminished in importance when we compute p_{exp}. In fact, if we made a pessimistic estimate $\pm 0.12 \times 10^{-4}\ cm^{-2}$ for the uncertainty in B^2, the uncertainty in p_{exp} would be but 1 per cent for a few lattices with large L^2. For most lattices it will be considerably under 0.5 per cent. This conclusion follows from the error approximation for the leakage term

$$\frac{\delta(1 + B^2L^2)e^{B^2\tau}}{(1 + B^2L^2)e^{B^2\tau}} = \left(\frac{L^2}{1 + B^2L^2} + \tau\right)\delta B^2 + \frac{B^2}{1 + B^2L^2}\,\delta L^2 + B^2\delta\tau \quad (26)$$

Again, we believe the reliability of our intracell measurements to be within 1 per cent in F and F_m. If a rather complete error analysis is made on the quantity ηf, we obtain

$$\frac{\delta(\eta f)}{\eta f} = (1 - af)\frac{\delta E}{E} + (1 - a)f \times \left(\frac{\delta\sigma^{U^{235}}}{\sigma^{U^{235}}} - \frac{\delta\sigma^{U^{238}}}{\sigma^{U^{238}}}\right) + \frac{\delta[\nu/(1 + \alpha)]}{\nu/(1 + \alpha)} + (1 - f)\left(\frac{\delta\sigma^{U^{235}}}{\sigma^{U^{235}}} - \frac{\delta\Sigma_m}{\Sigma_m} - \frac{\delta(FF_m)}{FF_m}\right) \quad (27)$$

where $a = \Sigma_{U^{235}}/\Sigma_U = 0.55$ for the depleted lattices, 0.64 for the natural lattices, and 0.69 for the enriched lattices. In this it can be seen that the factor $1 - f$ makes the term in $\delta(FF_m)/FF_m$ completely negligible in varying ηf.

Equation 27 also gives the expected variations if cross sections were to be blamed. This seems inadequate since we suspect that most of the remaining uncertainty in uranium cross sections is such that $\delta\sigma^{U^{235}}/\sigma^{U^{235}} = \delta\sigma^{U^{238}}/\sigma^{U^{238}}$, and for this case the factor $1 - f$ again appears in Eq. 27.

6. RESULTS

The graphs of p_{exp} vs. p_{theo} (Figs. 5 and 6) show what seem to be systematic deviations from the equality that we could hope for. Omitting the anomalous 2-in. rod cases, the enriched-uranium lattice values of p_{exp} are, on the average, about 1.0 per cent low, the natural lattice values are about 0.9 per cent low, and the depleted lattice values are about 0.6 per cent high.

Although there is considerable scatter in our p_{exp} values, the trends of deviation (from equality with p_{theo}) seem unmistakable and real. Most of the experimental scatter afflicts the natural-uranium data (these data were largely taken before the higher flux of the Water Boiler Neutron Source was available). The systematic deviation between the newer data on depleted and enriched uranium is quite marked.

It appears that this deviation is not new; if we had used a traditional value or so-called "lattice value" of η about 1 per cent below that computable from cross-section data, we could have achieved agreement for the natural-uranium data. However, this artifice now seems particularly forced since our data on other than the natural enrichment show that a different correction to the cross section η would be required for each enrichment.

In conclusion, we have not been able to rationalize the systematic deviations, apparently functions of enrichment, that the program has turned up. We do believe the deviations to be real and to indicate a real defect in the present theory. Whether this defect is to be found in the computation of the infinite lattice multiplication constant or in computation of the leakage probability is unclear. Further experimental and theoretical work on these topics is required.

7. APPENDIX A: ANISOTROPY

One of the persistent uncertainties of lattice calculation is the magnitude of anisotropy effects. The material bucklings of three lattices were measured in both the 4- and 5-ft exponential tanks to check this possibility. The agreement between the buckling values obtained indicates that such an effect very likely exists for our lattices, but it is, nevertheless, quite small.

The one-group multiplying diffusion equation

$$\nabla \cdot \vec{D} \cdot \nabla\phi + (k - 1)\,\Sigma_a\phi = 0 \quad (28)$$

has, in the geometry of our tank, the "fundamental" solution

$$\phi = A\,J_0(\mu r)\sinh\nu(h - z) \quad (29)$$

where

$$D_{\parallel}\nu^2 - D_{\perp}\mu^2 + (k - 1)\,\Sigma_a = 0 \quad (30)$$

Setting

$$\frac{D_{\parallel}}{\Sigma_a} = M_{\parallel}^2 \qquad \frac{D_{\perp}}{\Sigma_a} = M_{\perp}^2 \quad (31)$$

we may take as a measure of the anisotropy (or nonanisotropy) the ratio

$$r = \frac{M_{\parallel}^2}{M_{\perp}^2} \tag{32}$$

Thus

$$M_{\perp}^2 \mu^2 - M_{\parallel}^2 \nu^2 = M_{\perp}^2(\mu^2 - r\nu^2) = k - 1 \tag{33}$$

If r is unity, a lattice buckling can be unambiguously defined as

$$B^2 = \mu^2 - \nu^2 \tag{34}$$

If r is not unity, B^2 as so defined will no longer be a constant characteristic of the medium but will depend somewhat upon the macroscopic dimensions of the lattice. Using subscripts to denote measurements in the 4- and 5-ft tanks, from Eq. 33

$$r = \frac{\mu_4^2 - \mu_5^2}{\nu_4^2 - \nu_5^2} \tag{35}$$

Table 4 presents the results of the data obtained. The error limitations of the measurements preclude a definite conclusion but seem to indicate a small anisotropic effect for tighter lattice spacings.

The introduction of anisotropy will decrease the computed leakage B^2M^2. If we assume that the average migration area, M_0^2, defined by

$$M_0^2 = \tfrac{1}{3}(2M_{\perp}^2 + M_{\parallel}^2) \tag{36}$$

is to a first-order approximation equal to the homogenized value $L^2 + \tau$, previously computed, the decrease will be approximately

$$B^2M_0^2 - (M_{\perp}^2 \mu^2 - M_{\parallel}^2 \nu^2) \sim \frac{r - 1}{3} \times M_0^2 (\mu^2 + 2\nu^2) \tag{37}$$

For the lattice with the largest r (N-1-4.9, Table 4), this amounts to 0.006 (5-ft tank) and would decrease p_{exp} by about 0.5 per cent. Although the correction may well be significant for the more closely spaced lattices, it has not been applied to the lattice calculations because of the large experimental uncertainty in r − 1.

Table 4—Results of Anisotropy Measurements

	5-ft tank			4-ft tank			
Lattice*	μ, meter^{-1}	ν, meter^{-1}	B^2, meter^{-2}	μ, meter^{-1}	ν, meter^{-1}	B^2, meter^{-2}	r
N-1-4.9	3.10 ± 0.01	1.122 ± 0.02	8.35 ± 0.08	3.86 ± 0.01	2.51 ± 0.04	8.63 ± 0.21	1.06 ± 0.05
N-1-6.0	3.10 ± 0.01	1.546 ± 0.02	7.22 ± 0.08	3.86 ± 0.01	2.74 ± 0.03	7.39 ± 0.17	1.03 ± 0.03
E-1-7.5	3.10 ± 0.01	1.341 ± 0.01	7.81 ± 0.07	3.86 ± 0.01	2.64 ± 0.03	7.94 ± 0.16	1.02 ± 0.03

*The letter indicates the type (normal or enriched) rod; the first number indicates the rod diameter; and the final number indicates the cell spacing.

8. APPENDIX B: CONSTANCY OF THERMAL UTILIZATION

We have considered the possibility that the conditions of the exponential experiment are such that f is not constant over the lattice. This would vitiate the use of homogeneous diffusion theory and conceivably might occur because of the high radial currents near the side of the exponential tank, currents which are transverse to the rods and to the cell structure of the medium. Consequently a series of intracell flux measurements was made in a rod-centered square lattice cell near the edge of the 4-ft tank. The lattice consisted of 1-in. enriched-uranium rods on a 4.9-in. spacing. Flux traverses were taken along three different directions through the rod, allowing accurate experimental flux

contours to be drawn throughout this peripheral cell. These are shown in Fig. 8.

There is, of course, no a priori reason why a lattice cell need be defined so that a rod is at its center, and, in the outer portions of the tank where there is a considerable radial current and consequently a large gross flux variation superposed on the lattice intracell flux pattern, the choice of cell can greatly influence the relative magnitudes of the average moderator and uranium fluxes. However, in harmony with the assumption that heterogeneous mediums such as ours can be treated by using suitable averages in homogeneous theory, we might expect the observed intracell flux pattern to be the product of (1) the intracell pattern in an infinite lattice and (2) the homogeneous pattern appropriate to the tank, $J_0(\mu r)$. Dividing the observed fluxes by this latter function should then give an infinite lattice flux distribution in which no radial current exists and, consequently, in which the thermal utilization is well defined and is independent of the choice of cell boundary. This procedure has, in fact, always been followed in our analysis of intracell data near the tank center, where it is a small correction. In the peripheral cell analysis the $J_0(\mu r)$ correction effectively removed the large radial current; the corrected flux pattern shown in Fig. 9 appears only slightly distorted from what might have been expected for an infinite lattice.

Table 5 — Disadvantage Factor Measurements on Lattice E-1-4.9

	Central-cell values with J_0 correction	Peripheral-cell values	
		With J_0 correction	Without J_0 correction
F	1.245	1.209	1.217
F_m	1.469	1.505	1.490
FF_m	1.829	1.820	1.813

Disadvantage factors for the peripheral cell were obtained by mechanically integrating the flux over the rod and the moderator portion of the cell. Table 5 compares the peripheral lattice-cell disadvantage-factor measurements with the corresponding values for a central lattice cell; the peripheral-cell values are considered accurate to ±2 per cent and the central-cell values to ±1 per cent. The agreement between the two sets of values is quite good; in fact, the values of FF_m, the quantity most significantly affecting the thermal utilization, differ by only about 0.5 per cent. It is apparently coincidental that, for the rod-centered choice of lattice cell, the uncorrected flux values agree with the corrected flux values.

We conclude that the usual assumption of f constant over the lattice is, indeed, valid and that the multiplying mediums of our exponential experiment can be suitably averaged and treated as homogeneous.

9. APPENDIX C: MEASUREMENT OF AGE

As has been previously mentioned, $\lambda_{tr}(D_2O)$ was measured at this laboratory by the boron-poisoning method.[9] At the conclusion of that experiment, when the D_2O contained approximately 150 mg of B_2O_3 per liter of solution, a natural-uranium lattice was placed in the tank, and the bucklings and disadvantage factors were obtained. This lattice, 1-in.-diameter rods on a 4.9-in. square spacing, was one which had been previously investigated in the unpoisoned D_2O.

The only important effect of the added boron was to increase the moderator absorption for thermal neutrons. This, in turn, would affect the quantities B^2, L^2, and f. Presumably η, ϵ, p, and τ would remain unchanged, and we would expect

$$\eta\epsilon p = \frac{(1 + B^2L^2)e^{B^2\tau}}{f} \tag{38}$$

to be the same for the borated and unborated lattices. Now B^2 is directly measurable, and L^2 and f can be computed from known cross sections and the measured disadvantage factors; hence the experiment can be used to check the value of τ. Combining the unborated (unbarred) values with the borated (barred) values, we have

$$(B^2 - \bar{B}^2)\tau = \ln\left[\frac{1 + \bar{B}^2\bar{L}^2}{1 + B^2L^2}\,\frac{f}{\bar{f}}\right] \tag{39}$$

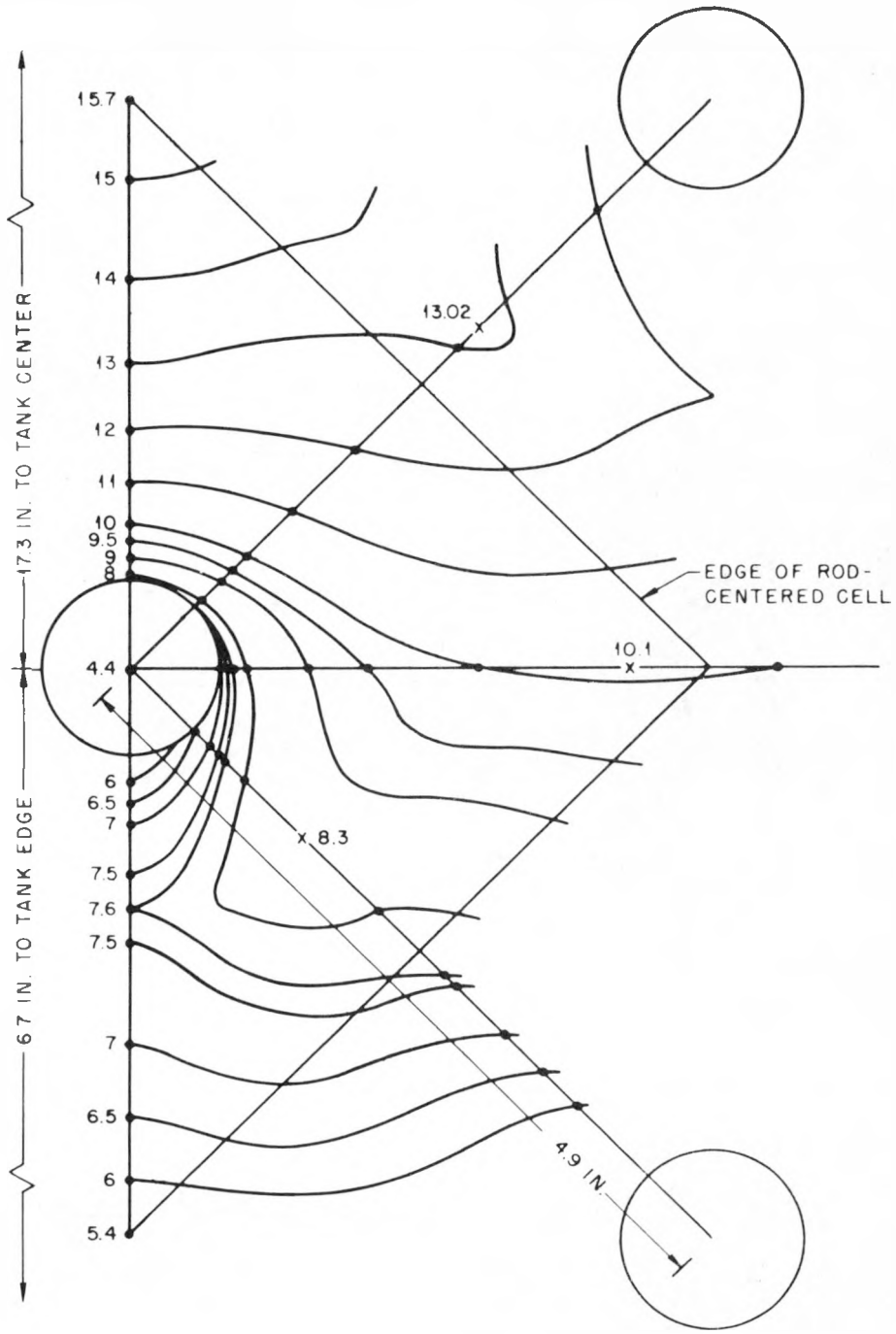

Fig. 8—Experimental flux contours in peripheral cell. The cell is symmetrically oriented about a tank diameter, and dots indicate the smoothed data points from which the contours were drawn. The large radial gradient present is evident.

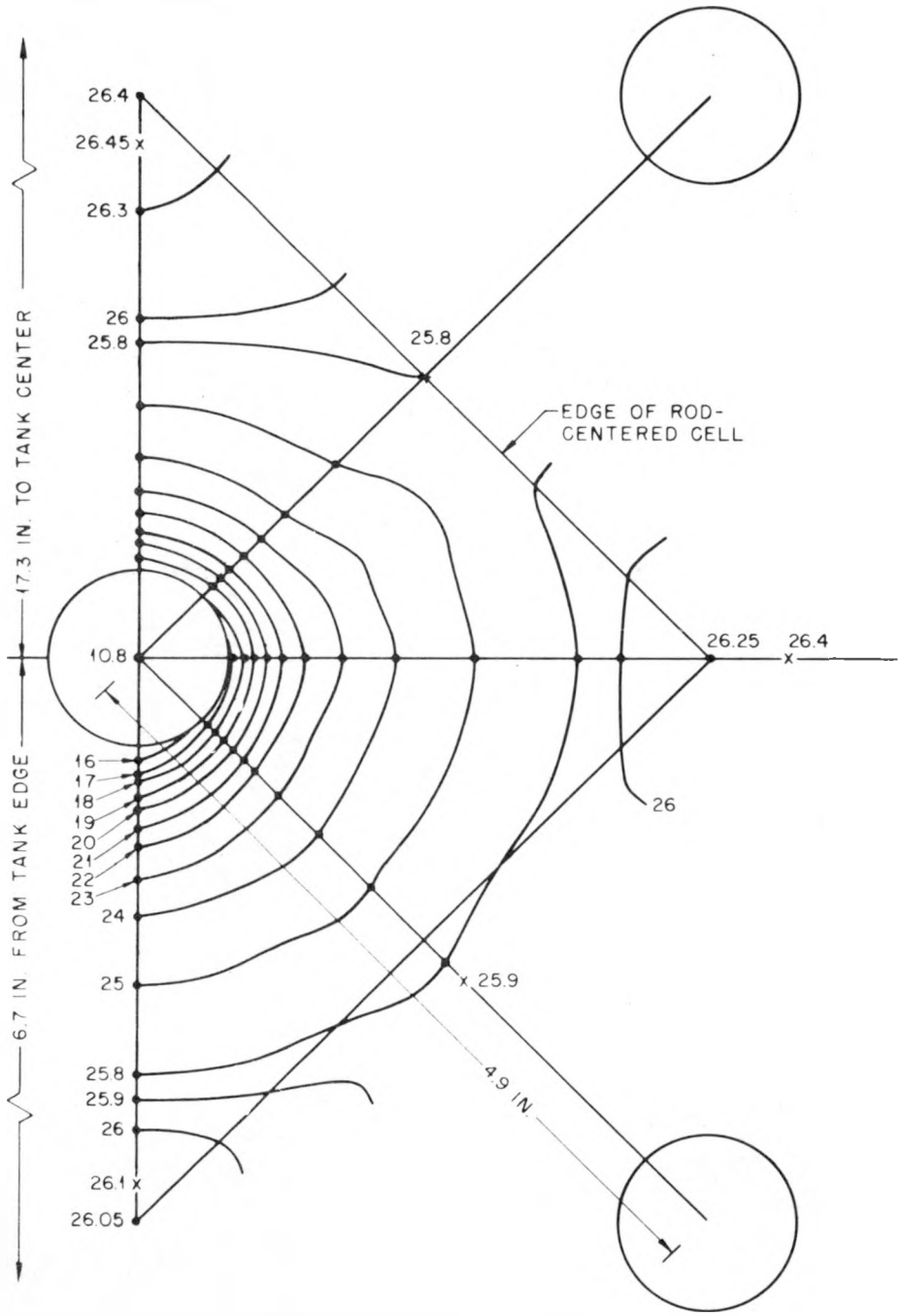

Fig. 9—Contours of corrected flux in peripheral cell. Division by $J_0(\mu r)$ effectively removes the radial flux gradient; some asymmetry is, however, still evident.

The parameters obtained for the two lattices are listed in Table 6. Substituting these into Eq. 39 we obtain

$\tau = 107 \pm 5$ cm^2

Table 6 — Measurements on Lattice N-1-4.9

Lattice parameter	Plain D_2O	Borated D_2O
B^2, meters^{-2}	8.36 ± 0.15	−1.85 ± 0.12
F	1.19 ± 0.01	1.20 ± 0.01
FF_m	1.60 ± 0.01	1.69 ± 0.01
f	0.978 ± 0.002	0.778 ± 0.006
L^2, cm^2	125 ± 3	106 ± 3

The major contributor to the uncertainty in this value is the uncertainty in the cross sections involved, in particular the uranium absorption cross sections. The effect of our experimental uncertainties is reduced considerably because some of the errors entering the computations are related; for example, the quantity $B^2 - \overline{B}^2$ is just the difference of the respective vertical bucklings, a more accurately known quantity than is implied by the errors listed for the bucklings themselves.

The total age computed for this lattice by the methods described in Sec. 4.7 is 108 ± 6 cm^2, a most satisfactory, if possibly fortuitous, agreement. The partial age from fission to indium resonance energies for this lattice was computed to be 102 ± 5 cm^2. Subtracting this from the measured age, we obtain an effective age from indium resonance to thermal of 5 ± 7 cm^2. This is hardly an accurate determination, but it does favor the value 6 cm^2 used in our lattice calculations as opposed to the value of about 25 cm^2 that has often been used but which more properly applies to plain D_2O.

REFERENCES

1. A. T. Biehl and E. R. Cohen, The NAA Exponential Assembly. Part I. Apparatus and Preliminary Procedure, Report NAA-SR-103, June 22, 1951.
2. A. T. Biehl and D. Woods, Intracell Neutron Densities. Part I. 1-in.-diameter Natural-uranium Rods, Report NAA-SR-138, Sept. 25, 1951.
3. S. W. Kash, Buckling Measurements of Thermal Neutrons in Natural Uranium−D_2O Square Lattices, Report NAA-SR-209, Feb. 12, 1953.
4. E. R. Cohen, An Analysis of D_2O−Natural Uranium Lattices, NAA-SR-Memo-457, reprinted as Paper A.2 in Report on Reactor Calculations Held at Chalk River, Ontario, on Jan. 26 to 28, 1953, Report CRR-546.
5. D. H. Martin, Reactor Physics Quarterly Progress Report for February−April, 1954, Report NAA-SR-1016, Aug. 1, 1954.
6. D. W. Hone, Paper A.1.a, Report CRR-546, Jan. 26, 1953.
7. D. J. Hughes et al., Neutron Cross Sections, Report BNL-170, May 15, 1952.
8. J. A. Harvey and D. J. Hughes, Effect of Recent Cross-section Measurements on Pile Constants, Report BNL-221, Jan. 26, 1953.
9. S. W. Kash and D. C. Woods, Measurement of the Transport Mean Free Path of Thermal Neutrons in D_2O by a Boron Poisoning Method, Phys. Rev., 90: 564-566 (May 1953).
10. E. R. Cohen, work reported at Oak Ridge, Symposium on Reactor Physics and Shielding, October 1954, Reactor Sci. Technol., 4(4): 124 (December 1954).
11. H. D. Brown and D. S. St. John, Neutron-energy Spectrum in D_2O, Report DP-33, February 1954.
12. R. G. Sachs and E. Teller, Scattering of Slow Neutrons by Molecular Gases, Phys. Rev., 60: 19 (July 1941).
13. E. A. Guggenheim and M. H. L. Pryce, A Quantitative Study of Uranium−Graphite Lattices, Report A.E.R.E. R/R 922, Aug. 11, 1945.
14. J. E. Garvey, unpublished work.
15. S. W. Kash and F. B. Estabrook, Thermal Diffusion Length in Heterogeneous Mediums, Reactor Sci. Technol., 4(4): 107 (December 1954).
16. John W. Kunstadter, A Correction To Be Applied to the Activity of Neutron Activated Cadmium-Covered Indium Foils, Phys. Rev., 78: 484 (May 1950).
17. W. H. Zinn, Report for Period May and June 1945, Report CP-3195, Aug. 24, 1945.
18. B. W. Sargent and J. C. Duckworth, Cadmium Ratios with Thin and Thick Indium Foils in the NRX Pile and in Other Lattices, Report CRP-459, Sept. 12, 1950.
19. N. Goldstein and D. J. Hughes, Resonance Absorption of Uranium, Report CP-3580, Aug. 10, 1946.

ABOUT THE AUTHORS

Frank B. Estabrook is a physicist in the theoretical physics group at North American Aviation, Inc. Prior to this he was an Associate Professor of Physics at Miami University. He obtained the Ph.D. degree in

1950 from the California Institute of Technology and the A.B. degree from Miami University in 1943. His research interests have included microwave propagation at sea, spectroscopic determination of oscillator strengths, relativity theory, and neutron physics.

Sidney W. Kash is a physicist presently engaged in nuclear energy research at North American Aviation, Inc. During the latter part of World War II, he worked on mine sweeping and degaussing problems at the Naval Ordnance Laboratory in Washington, D. C. After the war he returned to the University of California at Los Angeles, where he received the Ph. D. degree in physics in 1950. While at the university he was employed at the Institute of Geophysics on an upper-atmosphere project sponsored by the Office of Naval Research. After receiving his degree, Dr. Kash worked a short time with the Meteorology Department at UCLA on a problem concerning skylight polarization.

End for TR & Inc.

RECOVERY OF FISSIONABLE MATERIAL FROM ENRICHED-URANIUM FUELS

Part II. Experimental Breeder Reactor Fuel Elements

L. BURRIS, JR., S. LAWROSKI, M. LEVENSON,
R. C. VOGEL, and S. VOGLER

Argonne National Laboratory

March 1955

ABSTRACT

The first core loading of the Experimental Breeder Reactor was of unalloyed enriched uranium. A solvent-extraction recovery scheme for this core material using tri-n-butyl phosphate is described. The process consists of a single extraction-scrub-strip cycle. The extraction of fission-product zirconium is minimized by complexing with oxalate ion, and the extraction of the small amounts of plutonium is minimized by reducing to the trivalent state. The laboratory data leading to the process flow sheet are presented. The results of the semi-works investigation of the process at the West Stands and the operation of a second unit at Lemont are described.

1. INTRODUCTION

The fuel for the first loading of the Experimental Breeder Reactor (EBR) core was unalloyed enriched (94 per cent) uranium. In order to determine the conversion ratio by radiochemical analysis, it was required that the reactor be sampled liberally. It was necessary to provide decontamination and recovery facilities for these samples. Also, at the time the EBR fuel loading was being prepared and during the early phases of the reactor operation, it was necessary to guarantee the prompt return of the enriched uranium to the national stockpile. During the period of reactor design the Idaho processing facility under consideration was restricted to the Materials Testing Reactor (MTR) fuel; thus it was necessary to have available an EBR recovery process.

The MTR hexone-extraction process developed at Oak Ridge National Laboratory (ORNL) for use at the Idaho processing facility[1] might have been used for the recovery and decontamination of the EBR fuel. In this process a fission-product decontamination of about 10^4 is realized in one solvent-extraction cycle and 10^6 or more in two extraction cycles. Therefore two solvent-extraction cycles would be required to achieve the decontamination factor of 10^5 necessary, as explained later, for the EBR fuel.

After each hexone cycle ruthenium activity predominates, being greater than 90 per cent of the total.[1] The promise of a considerably greater decontamination from ruthenium with a tri-*n*-butyl phosphate (TBP) solvent pointed to the possibility of achieving adequate decontamination of EBR fuel in a single solvent-extraction cycle. Another highly desirable feature of a TBP-extraction process is that, since nitric acid is used as the uranium salting agent, the wastes are comparatively free of salts and can be easily concentrated. Accordingly, since a one-cycle TBP process for recovery of the U^{235}, taken for the conversion-ratio determination, appeared both feasible and advantageous, laboratory and semiworks development of such a process was commenced at Argonne National Laboratory (ANL). This task was finished in 1950 and has been reported[2] in detail.

Late in the developmental program at Argonne on the EBR separations scheme, an AEC policy decision was made to convert the MTR processing installation to a central processing plant, the Idaho Chemical Processing Plant (ICPP), for U^{235} and to process the bulk of the EBR fuel there. Since a considerable time lapse was inevitable before the ICPP would be in operation, it was necessary to build, earlier, an installation at the new Argonne site at Lemont. This installation was ready to operate by the summer of 1951 and has been used, as planned, in the recovery of the analytical samples taken from the EBR for the conversion-ratio determination.[3] Even if the semiworks unit had been adequately shielded, it was unfortunately impossible to use it for this task since it had to be dismantled in the move of the group from the West Stands to the Lemont installation.

This article reports, briefly, the laboratory development, the semiworks testing of this process, and the operation of the analytical facility. It is believed that this information will be instructive since this process is one of the simplest of solvent-extraction recovery schemes and since it is unusual in the use of carbon tetrachloride as a diluent for TBP.

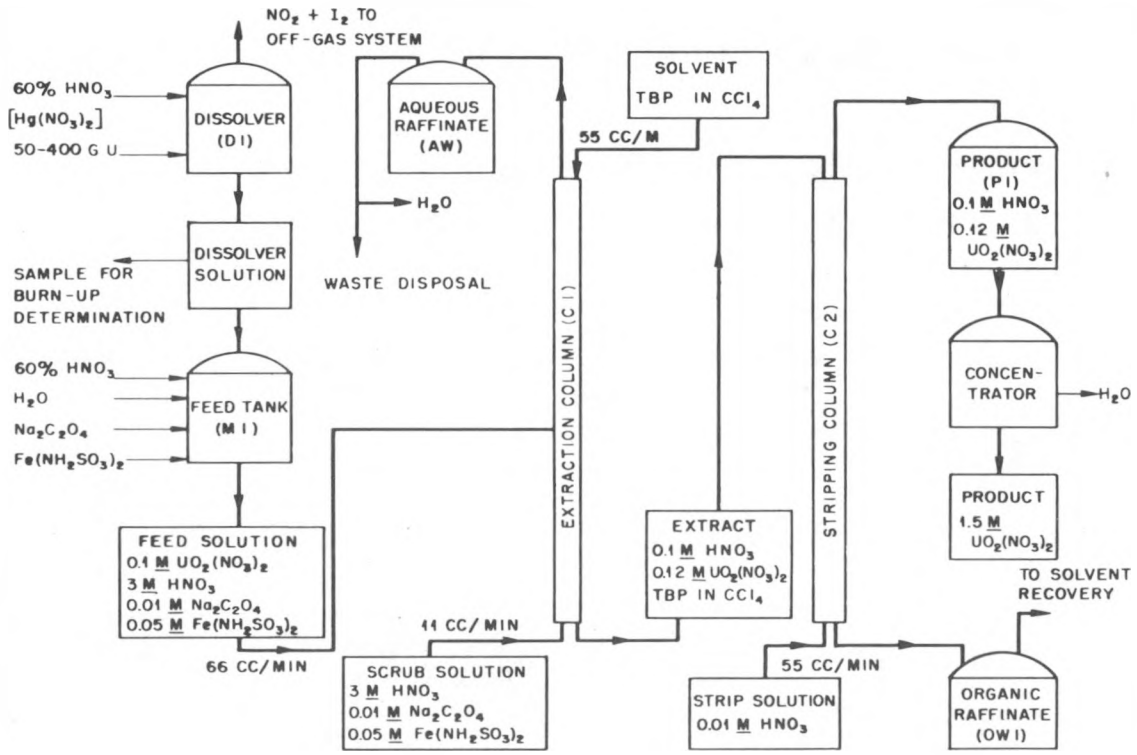

Fig. 1 — Flow sheet for one-cycle unit solvent-extraction plant.

2. ARGONNE EBR FUEL-RECOVERY PROCESS

2.1 Factors Circumscribing the Process

The EBR fuel elements in the first loading consisted of small cylindrical pieces of 94 per cent enriched uranium. These slugs were placed end-to-end in an EBR fuel rod and were sandwiched between natural-uranium slugs. These natural-uranium slugs were canned in 5-mil-thick stainless-steel jackets to prevent dilution of the enriched uranium if migration of uranium within the fuel-rod jacket occurred. All the slugs of a fuel rod were contained in a stainless-steel tube having a wall thickness of 0.56 mm and an outside diameter of 1.138 cm. The space between the uranium and the stainless-steel jacket was filled with sodium-potassium alloy as a liquid bond. After discharge the fuel was mechanically decanned, the sodium potassium alloy was removed, and the slugs were placed in aluminum shipping containers at the Argonne facility at Idaho. The fuel received for analytical investigations at Lemont was in the form of bare slugs in aluminum containers.

It was planned that the reactor might operate, on its first loading, to 0.1 per cent burn-up of the uranium. For this low burn-up of uranium a decontamination factor of 10^5 from fission-product activity, after cooling at least 60 days to allow decay of the active U^{237}, suffices to reduce the beta and gamma activities to a safe level for hand operation in subsequent metallurgical steps.[2] The plutonium produced in the enriched-uranium fuel was estimated to be low and not worthy of recovery; after the core was finally analyzed, the plutonium was found to total 0.1 g in the 54-kg core. A decontamination factor of 200 is sufficient to reduce the amount of plutonium to the required value of

2.2 Flow Sheet for Argonne EBR Process

In the Argonne process for recovering the enriched uranium, the core metal is dissolved in nitric acid. The uranium is extracted from the feed solution which is 0.1M in uranyl nitrate, 3M in nitric acid, 0.05M in ferrous sulfamate, and 0.01M in sodium fluosilicate or sodium oxalate. The organic solvent is 0.4M TBP in carbon tetrachloride. This extraction is performed continuously in an extraction column with the lighter aqueous phase as the continuous phase. In the lower portion of the column, the uranium-bearing organic solvent is scrubbed with an aqueous solution to effect further removal of fission products from the uranium. This scrub solution has the same composition as that of the feed solution except that no uranyl nitrate is present. In a second column the uranium is stripped from the organic solvent into a dilute nitric acid (0.01M) solution. These two columns thus represent one cycle. The flow sheet that was, in general, followed in the analytical recovery unit is shown in Fig. 1. In actual practice the aluminum shipping containers for the slugs were also dissolved with the uranium in nitric acid. The resulting aluminum concentration was about 0.05 moles/liter. To facilitate the dissolution a small amount of mercuric nitrate catalyst in the nitric acid was used. Slightly different volume ratios were employed in the flow sheet used for semi-works testing of the process.

3. LABORATORY DATA LEADING TO FLOW SHEET

Some of the laboratory data leading to the ANL procedure for recovery of the EBR fuel are covered below. Since data of a similar nature and the method of interpretation to lead to a solvent-extraction flow sheet are already available in the literature,[1,2] an attempt will be made to emphasize those points which are considered unique.

3.1 Basic Principles of the Solvent-extraction Procedure

TBP forms complexes with uranyl nitrate and Pu(IV) nitrate. These complexes are sufficiently specific that they can be used to separate uranium and plutonium from fission products. If a complex is formed when the plutonium is reduced to the III state, it is very unstable, and a separation of the uranium from the plutonium and the fission products may be made. TBP itself is too viscous a material for a continuous-extraction unit; thus it requires a diluent to produce favorable physical characteristics.

TBP, when dissolved in a diluent, extracts uranium and nitric acid according to the following equations:

$$UO_2^{+2}(aq) + 2NO_3^-(aq) + 2TBP(org) \rightleftharpoons (TBP)_2 \cdot UO_2(NO_3)_2(org) \quad (1)$$

$$H^+(aq) + NO_3^-(aq) + TBP(org) \rightleftharpoons TBP \cdot HNO_3(org) \quad (2)$$

Eq. 1 shows the maximum solubility of uranium in the organic phase to be 1 mole of uranium to 2 moles of TBP.

Whereas the equilibrium constants for these reactions in the appropriate diluent describe the system over a moderate concentration range,[4] experimental distribution data that take into account the mutual effects of varying uranium, nitric acid, and TBP concentrations were actually used for process design.

From Eq. 1, it is seen that extraction of uranium into the organic layer can be enhanced by increasing the nitrate concentration. Stripping into water is accomplished by reversing this reaction, i.e., by using low nitrate-ion concentrations.

3.2 Selection of Diluent for TBP

Favorable characteristics of a TBP diluent are good stability to nitric acid and irradiation, reasonably low viscosity, specific gravity lower than 0.8 or higher than 1.2, noncorrosivity to stainless steel, high flash point (greater than 80°F), ready availability, easy attainment of high purity, and lack of reactive groups which might lead to extraction of fission products. In the Purex process[5] the diluent for the TBP is a hydrocarbon mixture, whereas, in the ANL process for recovery of uranium from the EBR fuel and in the Halex process,[6] the diluent is carbon tetrachloride. Since the diluent is an important difference between this process and other solvent-extraction processes, some detail of the work leading to its selection will be given. In order to present complete information, data are taken from the Halex process development program;[6] however this program was not finished until considerably after the development of the EBR separations process was completed.

(a) General Types of Compounds Considered for Diluents. Because of the many requirements necessary for a suitable diluent, serious consideration was given to only two main groups of compounds, halocarbons and hydrocarbons. As a result of preliminary screening tests to determine stability and TBP miscibility of various compounds, the following observations were made.

Tests of TBP solubility in fluorocarbons confirmed the suspicion that these compounds have low solubility for TBP. For example, at room temperature the solubilities of TBP in perfluoroheptane, perfluorotriethylamine, and perfluorodiethylpropylamine are 0.2, 2.1, and 4 vol. %, respectively. Compounds of this type were therefore eliminated from further consideration.

A number of fluorochlorocarbon compounds were tested and were found to exhibit a reasonable solubility for TBP. Since this type of compound was known to be highly stable under many conditions, several of these liquids were chosen for corrosion and stability tests. However, the uranium-TBP complex formed in extraction must also be soluble in the diluent selected. Experiments were performed to determine whether the solubilities of these complexes in various diluents were adequate for an extraction process. It appeared that all fluorochlorocarbon diluents considered, with the exception of Fluorolube-FS, had satisfactory solubility characteristics. In this case a third phase was formed when an extraction was attempted. The top phase was mainly water, the middle phase TBP, and the bottom phase Fluorolube-FS. Uranium was present in all three phases.

During the consideration of the hydrocarbons it was felt that the use of a diluent which was a mixture of organic compounds would lead to difficulty in setting solvent specifications and also to poorer decontamination. Therefore consideration was limited to pure hydrocarbons only. The pure suitable hydrocarbons were found to be unavailable in quantity at that time. Furthermore, because of their flammability, these compounds were considered less desirable than the halocarbons. No additional consideration was given to hydrocarbons.

Chlorocarbons received extensive consideration as diluents, and carbon tetrachloride is

typical of this group. Additional compounds investigated and eliminated were *o*-dichlorobenzene, ethylene dichloride, and tetrachloroethylene.

As a result of these considerations and investigation of the availability of various materials, the group of compounds listed in Table 1 was selected for further testing.

Table 1—Physical Properties of Possible TBP Diluents

Compound	Boiling point, °C	Freezing point, °C	Specific gravity at 20°C
Carbon tetrachloride	77	−23	1.60
Freon-112 ($CFCl_2-CFCl_2$)	92	26	1.65
Freon-113 ($CFCl_2-CF_2Cl$)	48	−31	1.64
Freon-316 (dichlorohexafluorocyclobutane)	60	−15	1.62

Table 2—Corrosion of Stainless Steel in Nitric Acid–TBP Solvent Mixtures at 50°C*

	Cumulative penetration, mils/year					
	Type 304 stainless steel			Type 347 stainless steel		
Organic phase	100-hr exp.	200-hr exp.	400-hr exp.	100-hr exp.	200-hr exp.	400-hr exp.
None†	0.1	0.04				
70% CCl_4–30% TBP	0.4‡	0.04‡			0.1	0.06
70% F-112–30% TBP	0.05	0.04	0.02	0.03	0.04	0.05
70% F-113–30% TBP	0.48	0.22		0.16	0.09	0.05
70% F-316–30% TBP	0.03	0.05	0.02	0.12	0.03	0.08

*Two-phase system rapidly stirred; aqueous phase, 3M nitric acid.
†Single phase, 3M nitric acid.
‡10 per cent TBP in CCl_4; data from Report ANL-4463.

(b) Relative Acid Stabilities of Carbon Tetrachloride and Fluorochlorocarbons. The relative stabilities of the compounds listed in Table 1 to acid were compared in the presence of 347 stainless steel in two-phase systems consisting of diluent, TBP, and 3M nitric acid. The concentration of chloride ion in the aqueous phase was considered to be a measure of the extent of decomposition of the organic compound. At 50°C the decomposition of each of the four diluents listed in Table 1 led to about 40 ppm of chloride in an equal volume of the aqueous phase after a period of 400 hr. It was also found that the rate of decomposition was independent of nitric acid concentration in the dilute region. More strenuous tests[6] were carried out, and it was found that the stabilities to acid of the diluents under consideration did not differ greatly.

(c) Corrosion of Stainless Steel by Nitric Acid–TBP Solvent Systems. The rate of corrosion of stainless steel (types 304 and 347) in nitric acid–TBP solvent systems at 50°C were preliminarily determined (see Table 2). These data indicate that the corrosion rates for all the diluents tested are about the same as those for 3M nitric acid alone under the experimental conditions employed. In all cases the stainless steel remained untarnished at the conclusion of

the test, and no evidence of pitting was apparent to the naked eye. Further data on corrosion of stainless steel are available in the Halex process development work.[6] The most significant corrosion test, of course, was the lack of corrosion difficulty in running the EBR semiworks, EBR analytical facility, and Halex semiworks units with the carbon tetrachloride diluent.

At the completion of these simple screening tests, it appeared that carbon tetrachloride would very likely be the best diluent. Carbon tetrachloride is easily obtained in a pure form; is as good as, or better than, from the stability and corrosion standpoints, any of the other halocarbons; and is not flammable. The use of a nonflammable diluent is, of course, of considerable importance in a plant handling high levels of radioactivity. Carbon tetrachloride alone was therefore subjected to a more thorough investigation.

(d) Photochemical Decomposition of Carbon Tetrachloride in the Presence of Uranyl Ion. Before discussing the irradiation stability of carbon tetrachloride, it is appropriate to mention a complicating factor. It has been observed that carbon tetrachloride undergoes photochemical decomposition in the presence of uranyl ion when exposed to light in the visible region. It is believed that this effect has at other laboratories led to erroneous results in irradiation decomposition studies and also may have caused some erroneously high corrosion effects.

It was found, for example, that a typical organic phase containing TBP and uranium, when exposed to ordinary laboratory fluorescent light, would form 50 ppm of chloride in 20 min with a rate of formation decreasing with time.[6] It was established that this photochemical decomposition does not take place except in the presence of uranium.

Thus, if the investigator were unaware of this photochemical reaction, invalid data could be obtained. Erroneously high corrosion could be observed if the experiment were done in the presence of light and uranium. If analytical samples for chloride analysis were improperly stored, the results would be meaningless.

The mechanism of this reaction is different from that on exposure to gamma irradiation. In plant operation these solvent systems are not exposed to light except, perhaps, in sample bottles.

(e) Radiation Stability of Carbon Tetrachloride. A number of different types of laboratory experiments have been carried out in an effort to evaluate the seriousness of the radiation damage of carbon tetrachloride. Appropriate systems have been irradiated at a rather low level in a Van de Graaff accelerator.[2] Experiments have also been carried out at ANL[6] and at Hanford[7] in which the appropriate organic phase was contacted with a highly active solution of fission products and uranium in nitric acid for extended periods. Irradiations were carried out at Argonne and at Knolls Atomic Power Laboratory[8] using Co^{60} irradiations. Experiments were also carried out at Hanford in which the appropriate two-phase systems were irradiated in the slug-cooling basin. These experiments were compared and brought into general agreement by G. Starr Nichols of E. I. du Pont de Nemours & Company and were reported by Burris et al.[6]

Semiworks runs in establishing the Halex process provide good information on carbon tetrachloride radiation stability since these runs were made under typical solvent-extraction-process conditions. The semiworks runs at full-process Savannah River activity levels showed carbon tetrachloride to have high stability to irradiation damage as indicated by the presence of only 10 to 20 ppm of chloride ion in the first-cycle aqueous wastes. Chloride ion equivalent to a concentration of 5 to 10 ppm can easily be introduced into influent streams, particularly in the active feed solution. This arises from the decanning operation in the Halex or Purex processes in which commercial sodium hydroxide containing 1 to 2 per cent sodium chloride is used. It is difficult to wash the bare slugs completely free of this chloride-containing solution.

The beta-gamma irradiation levels of an EBR process are considerably less than those of a Halex type process if the more dilute feed used in the EBR process is considered. Thus the above data constitute a very thorough test of the use of carbon tetrachloride in an EBR process.

3.3 Uranium and Fission-product Extraction

In the study of the extraction of uranium, plutonium, and fission products by TBP, it was decided to carry out preliminary work with

methylcyclohexane as a diluent. It was appreciated that this diluent had too low a flash point to be desirable in a solvent-extraction process. It was, however, necessary to obtain pertinent data while the experimental work leading to final diluent selection was being carried out.

A thorough distribution study was conducted[2] and used in establishing the flow sheet given in Fig. 1. It is appropriate in this article to indicate only the general tenor of these data.

(a) Uranium Equilibriums. It was found that the extraction of uranyl nitrate behaved in a straightforward manner. Either increasing the uranium concentration in the aqueous phase, increasing the TBP concentration in the organic phase, or increasing the aqueous nitric acid concentration increased the uranyl nitrate concentration in the organic phase. There was only one exception to the above statement in that increasing the nitric acid from 5 to 7 moles/liter decreased the uranyl nitrate extraction very slightly. Thus for all TBP concentrations 0.1 to 0.4 moles/liter at aqueous-phase uranyl nitrate equilibrium concentration of 0.1 moles/liter, the maximum distribution ratio (organic/aqueous) occurs at about 5 moles/liter. Another qualification that should be mentioned is the somewhat obvious fact that the organic phase becomes saturated with uranyl nitrate [i.e., $(TBP)_2 \cdot UO_2(NO_3)_2$, thus limiting the uranyl nitrate concentration for any given TBP concentration].

(b) Gross Beta and Gamma Activities. Rather complete experiments were carried out to elucidate the behavior of fission products in the extraction process.[2] It was found that the extraction of gross beta and gamma activities decreases slightly as the solvent uranium concentration increases, with other variables being held constant. The extraction of the gross beta and gamma activities increases markedly with increase in the nitric acid concentration of the aqueous phase. Thus for a constant (60 per cent) uranium saturation of the organic phase, gross gamma-activity ratios (organic/aqueous) were nearly 100-fold greater for an aqueous phase 7M in nitric acid than for one 1M in nitric acid. In the aqueous acidity range of 1 to 7 moles/liter, beta ratios are much less affected by acidity than are gamma ratios, increasing 20- to 30-fold instead of 100-fold.

The decontamination of uranium from fission products depends upon both the uranium and gross-activity ratios. This separation is sometimes expressed quantitatively as the separation factor, i.e., uranium distribution ratio (organic/aqueous) divided by the gross beta- or gross gamma-activity ratio. This separation factor, although not readily achievable in continuous countercurrent extraction, is a convenient indication of the relative effects of a particular variable on the achievable separation of uranium from gross beta or gamma activities.

The effect of the aqueous-phase nitric acid concentration, at 60 per cent uranium saturation of the organic phase on the separation factor for gross beta and gamma activities, is shown in Fig. 2. The maximum separation factor of uranium from gross beta activity occurred at an aqueous equilibrium nitric acid concentration of 2 to 3 moles/liter. A different maximum occurred for each TBP concentration, the highest separation factor being 1.2×10^4 for a solvent 0.2M in TBP and the lowest 6×10^2 for a solvent 0.4M in TBP. No such maximum in the separation factor of uranium from gamma activity occurred with change in the aqueous nitric acid concentration. Instead the separation factor decreased from 2.3×10^3 to 100, with increase in nitric acid concentration from 1 to 7 moles/liter.

(c) Individual Fission-product Equilibriums: the Use of Complexing Agents. The concentrations of zirconium, cerium, and ruthenium were measured only for the series of extractions made with 0.4M TBP in methylcyclohexane since, only for this series, was sufficient activity extracted into the organic phase to justify individual fission-product analyses. Even so the counts of ruthenium present in the organic phase were too low for results to be meaningful, and too few cerium analyses were obtained for satisfactory interpretation.

It was found that the extraction of zirconium, which constitutes a major portion of the beta activity in the extract as compared to only 5 to 10 per cent in the feed, decreases as the solvent uranium concentration increases and is increased by an increase in the aqueous-phase nitric acid concentration. For an aqueous phase 0.1M in uranium, the zirconium ratio increases about 10-fold, from about 0.001 to 0.01, as the nitric acid concentration is increased from 1 to 6.5 moles/liter, with a consequent decrease of

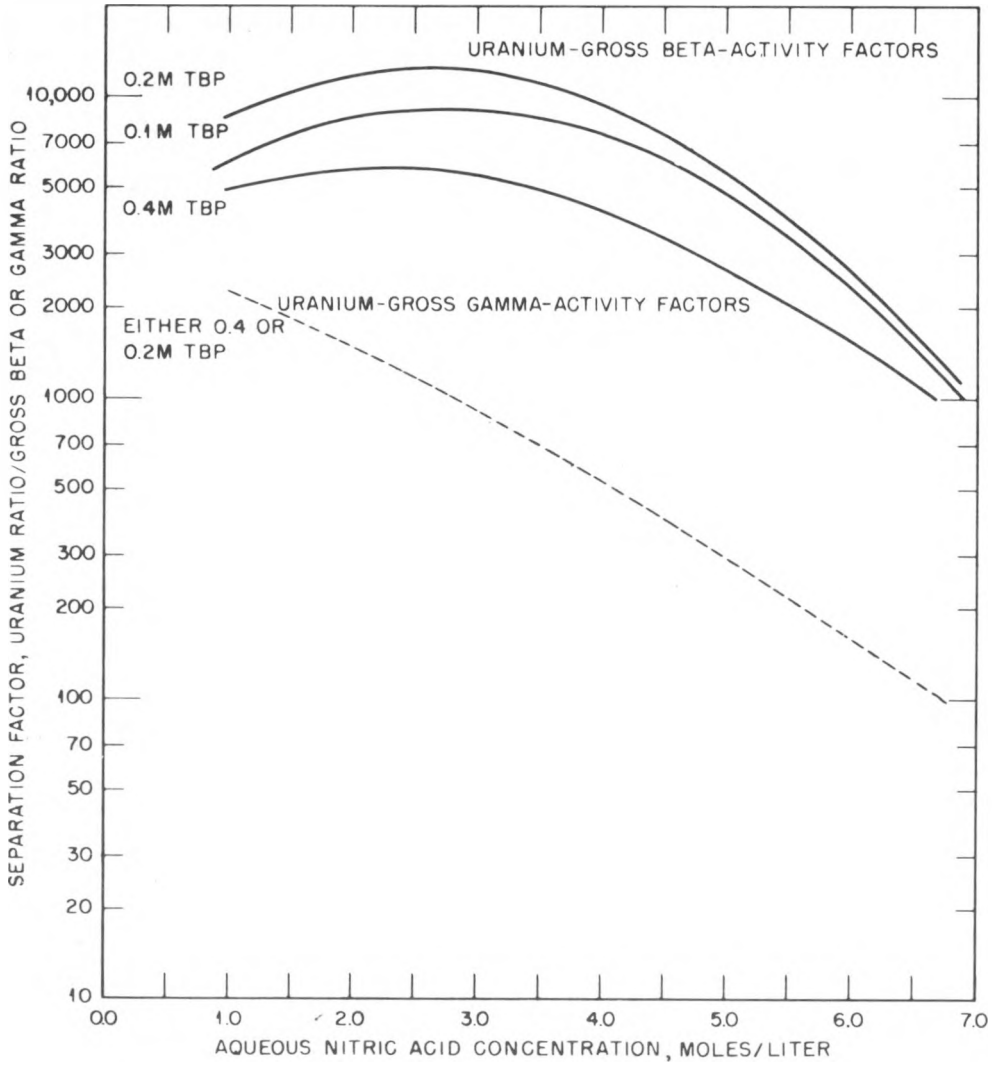

Fig. 2—Separation factors of uranium from gross beta and gamma activities as a function of aqueous nitric acid concentration. (Curves for solvent 60 per cent saturated with uranium at equilibrium.) Solvent: TBP in methylcyclohexane. Activity: from 100-day-irradiated, 270-day-cooled ORNL slugs.

1000 to about 50 in the uranium-zirconium separation factor.

Since zirconium is one of the principal fission products which is extracted by TBP, it was anticipated that the high extraction of zirconium relative to that of the other fission products would limit the decontamination obtainable in an extraction cycle. A search, therefore, was made for an aqueous-soluble zirconium complexing agent that would lessen the extraction of zirconium without limiting the extraction of uranium. As shown in Table 3, at a concentration of 0.01 mole/liter, oxalate in the aqueous phase decreased the extraction of zirconium by a factor of about 60, compared with a factor of about 20 for fluosilicate. The presence of oxalate does not interfere with extraction of the uranium to an aqueous uranium concentration of

10^{-6} mole/liter which represents a uranium loss of 0.001 per cent for a feed uranium concentration of 0.1 mole/liter.

(d) Pu(IV) Equilibriums: the Reduction to the III State. Since a small amount of Pu^{239} is formed in the enriched-uranium core of the EBR, a modest decontamination factor of about 200 is necessary. Laboratory extraction data indicated that the presence of oxalate or fluosilicate would lead to adequate complexing of the plutonium so that the decontamination requirements would be met. Contrary to the satisfactory tetravalent plutonium decontamination predicted by the laboratory data, decontamination from plutonium in the first fifteen semiworks runs with either oxalate or fluosilicate was very poor, generally less than ten.

Since trivalent plutonium is essentially nonextractable, it was decided to guarantee decontamination from the plutonium by reducing it to the trivalent state with ferrous sulfamate rather than to attempt to resolve the reasons for the difference between laboratory predictions and semiworks results with tetravalent plutonium. This treatment reduced plutonium laboratory distribution ratios in the presence of oxalate by a factor of about 500, giving a thoroughly adequate opportunity for good plutonium decontamination. This procedure was successful as described in Sec. 4.

(e) Substitution of Carbon Tetrachloride Diluent for Methylcyclohexane. The data cited above, except for the plutonium distribution studies, were determined using methylcyclohexane as the diluent. It was realized that this diluent would not ultimately be satisfactory. After it had been determined that carbon tetrachloride was a satisfactory diluent, key data were redetermined using carbon tetrachloride. It was found that the change of diluents neither appreciably affected that data nor invalidated the above conclusions.

Table 3—Comparison of Zirconium Complexing Agents*

Complexing agent†	HNO_3 conc. in aqueous, moles/liter	Zr beta ratio, org/aq	Decrease factor in Zr beta ratio relative to blank	U ratio, org/aq
None	3	6.7×10^{-3}		4.1
None	5	1.9×10^{-2}		4.7
Citrate	3	2.1×10^{-3}	3.2	3.9
Citrate	5	1.6×10^{-2}	1.2	4.8
Fluoride	3	5.4×10^{-4}	12	3.8
Fluoride	5	1.1×10^{-3}	17	4.7
Fluosilicate	3	4.4×10^{-4}	15	3.8
Fluosilicate	5	7.9×10^{-4}	24	4.7
Oxalate	3	8.5×10^{-5}	79	3.5
Oxalate	5	3.3×10^{-4}	58	4.5

*Aqueous: 0.1M uranyl nitrate, 3M or 5M nitric acid, and 3.4×10^6 counts/min/ml Zr tracer; solvent: 0.4M TBP in methylcyclohexane; and equal volume extractions.

†Concentration = 0.01 mole/liter.

(f) Selection of First Contactor (Extraction and Scrubbing) Conditions. As a result of the laboratory investigations outlined above, the compositions of the various streams were selected and are as follows:

Feed solution: 0.1M uranyl nitrate; 3M nitric acid; and 0.01M sodium oxalate or sodium fluosilicate.

Scrub solution: Same as feed solution except that no uranyl nitrate is present.

Organic solvent: 0.4M TBP in carbon tetrachloride.

The method of selection of the flow ratios has been described in detail in reference 2; therefore it will not be covered here. It is possible to use many different flow-ratio combinations. In the early semiworks runs a volume ratio of feed to scrub to solvent of 4:1:5 was employed.

In later runs the amount of organic extractant was gradually and successfully decreased until the ratios of feed to scrub to solvent were 5.5 : 1 : 5.

The solvent of 0.4M TBP was chosen because of the lower solvent consumption required despite the lower separation of uranium from beta activity with a 0.4M TBP solvent than with either a 0.1M or a 0.2M TBP solvent (by a maximum factor of 2).

As mentioned above, when it became known later that decontamination from plutonium was unsatisfactory in semiworks operations, ferrous sulfamate at a concentration of 0.05 mole/liter was incorporated as a constituent of the feed and scrub streams.

3.4 Stripping of Uranium from a TBP–Carbon Tetrachloride Solvent

Data for the stripping of uranium from the 0.4M TBP–carbon tetrachloride solvent system have been obtained and extend over a uranyl nitrate concentration of from 10^{-8} mole/liter to about 0.1 mole/liter. For water the uranyl nitrate ratio increases from about 10 (aqueous/organic) with 0.01M uranyl nitrate in the organic phase at equilibrium to several hundred for solvent uranyl nitrate concentrations in the range of 5×10^{-3} to 10^{-7} mole/liter. Although distribution ratios are highest with pure water, the use of a dilute nitric acid strip solution, e.g., 0.01 mole/liter is believed advisable in order to ensure a reasonably low pH throughout the stripping system.

4. DEMONSTRATION OF TBP-EXTRACTION PROCESS IN SEMIWORKS OPERATIONS AT WEST STANDS

Sixteen active semiworks runs were made in developing and demonstrating the ANL recovery process for the EBR fuel. Sufficient information was obtained to make feasible the design of full-scale plant facilities for recovery of uranium by this process. Over-all uranium losses in this series of runs were consistently 0.1 per cent or less. From the data obtained the column heights necessary to reduce over-all uranium losses to less than 0.1 per cent in plant operation can be safely predicted.

Very high fission-product decontamination factors were obtained for a single extraction cycle. With optimum conditions using Hanford slugs cooled 85 days, beta decontamination factors were $10^{5.3}$ whereas the gross gamma decontamination factors were $10^{4.9}$.

The results of the semiworks investigations will be briefly outlined, as were the laboratory results. For more detailed information it is suggested that the original report[2] be consulted.

4.1 Description of Semiworks Equipment

The semiworks studies were conducted in 1-in. stainless-steel columns packed with ¼-in. stainless-steel Raschig rings. The packed height in the extraction-scrubbing column was 23 ft, which could be divided into a 14-ft extraction section and a 9-ft scrubbing section or a 17-ft extraction section and a 6-ft scrubbing section. The packed height in the stripping column was 15 ft. Interface control was effected by means of Taylor Fulscope Interface controllers.

Solutions were pumped with Milton Roy pumps and, with the exception of the aqueous scrub stream, were all pumped to spill-over points from which they flowed by gravity into the column. The aqueous scrub stream was pumped directly into the column. The active feed solution was pumped by displacement with methylcyclohexane.

A schematic diagram of the equipment is shown in Fig. 3.

4.2 Results of Semiworks Studies

(a) Decontamination from Individual Fission Products. Although changes throughout the series of sixteen runs were made in various variables, the effects of these changes were small in comparison with the dependence of gross decontamination factors on slug-cooling time. Decontamination improved with a slug-cooling time up to about 70 days, with further aging having little or no effect. For example, using 50- to 120-day-cooled Clinton slugs, the beta factors increased from $10^{4.2}$ to $10^{4.7}$ and gamma factors from $10^{3.8}$ to $10^{4.7}$.

The lower decontamination with the shorter cooled slugs is due to the 8-day I^{131} activity. This activity is very poorly removed, and it limits the gross beta and gamma decontamina-

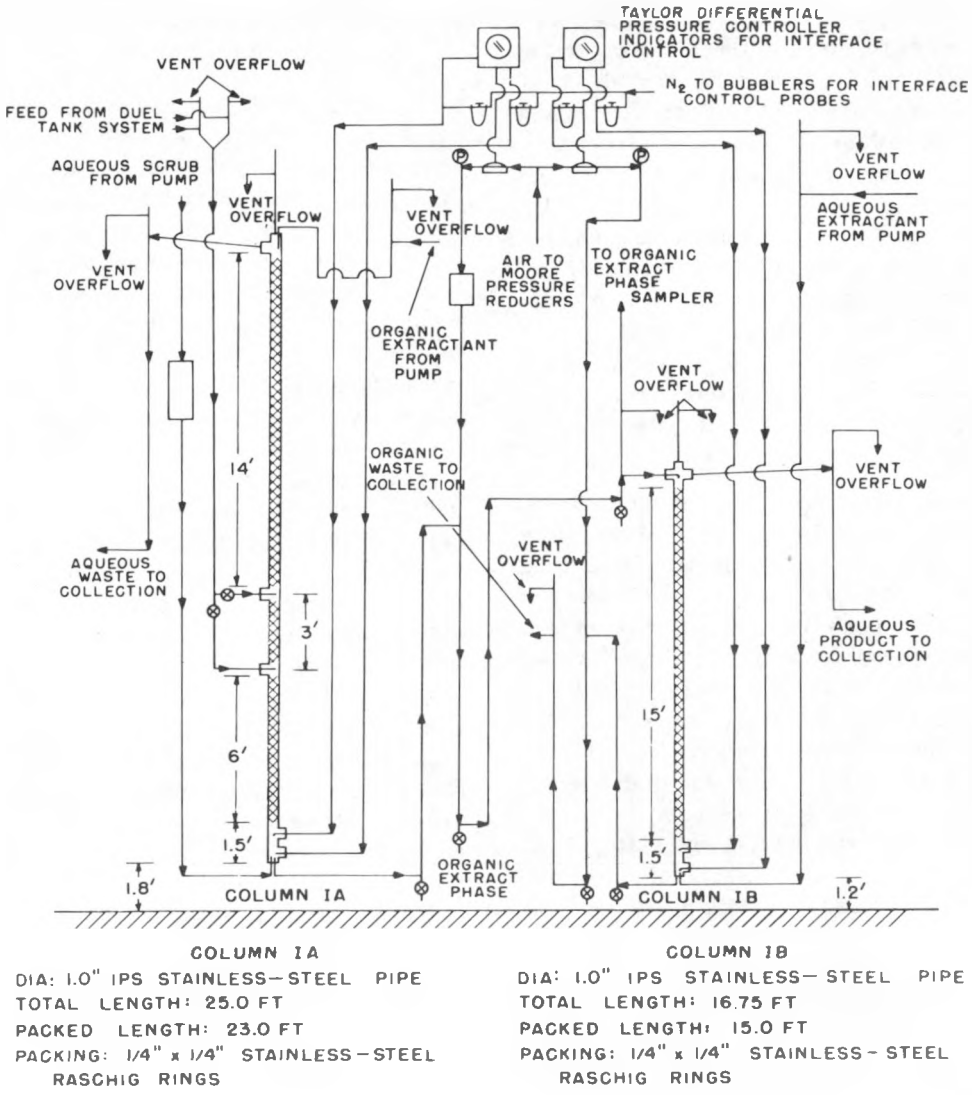

Fig. 3—Schematic diagram of EBR separations columns.

tion achievable. For example, fission-product analysis demonstrated that the decontamination from iodine varied from $10^{1.5}$ to $10^{2.4}$.

Consistently high decontamination from other major fission products (cerium, ruthenium, and zirconium) was found in the runs. In the absence of iodine these fission products account for most of the activity associated with the separated uranium. Thus there is the indication that the ultimate level of activity associated with the uranium would be independent of slug-cooling time, provided the iodine activity were allowed to decay out either before or after processing. If aging time is defined as the time from discharge of fuel to the start of hand-manipulated operations on the uranium, a decontamination factor for iodine of 600 would be required for 60-day-aged EBR fuel, 100 for 80-day-aged, and 20 for 100-day-aged material. In its present state of development, therefore, processing of EBR fuel in conjunction with an over-all cooling time of 100 days is needed to ensure sufficient reduction of fission-product activity for safe handling in direct operations.

An examination of the complete data[2] reveals very uniform decontamination factors for ruthenium, zirconium, and cerium. In runs with Clinton slugs ruthenium decontamination is

about $10^{4.1}$, cerium $10^{5.6}$, and zirconium 10^{5}. The use of Hanford slugs allowed the detection of higher decontamination factors than was possible with Clinton slugs. The decontamination factors for ruthenium, cerium, and zirconium, using Hanford slugs, are about $10^{4.3}$, $10^{5.7}$, and $10^{5.5}$, respectively.

Semiworks runs were also made to compare the decontaminations found for zirconium in the presence of either sodium fluosilicate or sodium oxalate. The results obtained for each were essentially the same. It was therefore concluded that either reagent could be used. In the operation of the unit at Lemont, described in Sec. 5, the oxalate was used.

(b) Decontamination from Plutonium. Plutonium-decontamination factors in the runs without ferrous sulfamate were generally less than 10 which is considerably below the required value (about 200); however, one value of 38 was obtained. As discussed previously these factors were much poorer than the values of 200 expected on the basis of laboratory data. The reasons for this were not discovered. In later runs 0.05M ferrous sulfamate was employed in feed and scrub streams to reduce the plutonium to the inextractable trivalent state. High plutonium-decontamination factors of 180 to 680 demonstrated the success of this measure.

(c) Number of Theoretical Stages Present in Extraction and Stripping Columns. For the extraction column it was found that the height equivalent to a theoretical stage (HETS) varied from 2.2 to 3.3 ft, the average being 2.7 ft. A safe design value for the HETS is regarded as 3 ft. It is felt that the length of the extraction section in plant operations should be a minimum of 20 ft and preferably 25 ft. A 10-ft scrubbing section in conjunction with the extraction section is believed adequate. The details of the calculations are given in the complete report.[2]

It was difficult to determine the number of theoretical stages present in the stripping column since the nitric acid concentration of the stripping solution changed continuously as it passed through the column. However, it was estimated that the HETS was in the neighborhood of 6 ft. For plant operations it was recommended that 20 ft of packing be employed in the stripping column to ensure a low loss of uranium in the organic phase.

5. THE ENRICHED-URANIUM RECOVERY FACILITIES AT LEMONT

As explained in Sec. 1, it was necessary to build an installation at ANL which could recover the core of the EBR in case of a national emergency. This installation has been used for the recovery of the analytical samples taken for the burn-up determination. It would not have been possible to use the semiworks equipment described in the previous section since the group had to vacate the West Stands, where it was located. The new facilities were subsequently designed, were erected, and were ready for operation at the end of the summer of 1951. The design philosophy called for a batch size that is limited to one-half of criticality. The capacity of the installation with three-shift operation is 1 kg of uranium per day. However, if this unit were to operate on highly irradiated material over an extended period, there would be a serious problem of waste disposal at the Lemont site. The operating area of this unit is shown in Fig. 4. The equipment installed provides means of (1) dissolving EBR fuel elements, (2) decontaminating the enriched-uranium dissolver solution by the solvent-extraction process, (3) reducing the product-solution volume so that the final concentration is 200 to 300 g of uranium per liter, (4) removing residual trace fission products (mostly zirconium) and clarifying the product solution by passing it through a silica gel column, and (5) reducing the volume of the fission-product aqueous-waste stream. The flow sheet used is shown in Fig. 1.

5.1 Description of EBR Fuel Processing Facilities

The sampling of the enriched core of the EBR consisted of a complete traverse. This represents about 4 kg of U^{235} per sampling. At the date of this writing the processing of the enriched uranium for one burn-up determination has been completed, and a second similar experiment is now under way.

Most of the equipment in the EBR processing facility is standard with the exception of the solution-sampling and the active-feed metering devices. These will be described in some detail whereas the other equipment will be discussed only briefly.

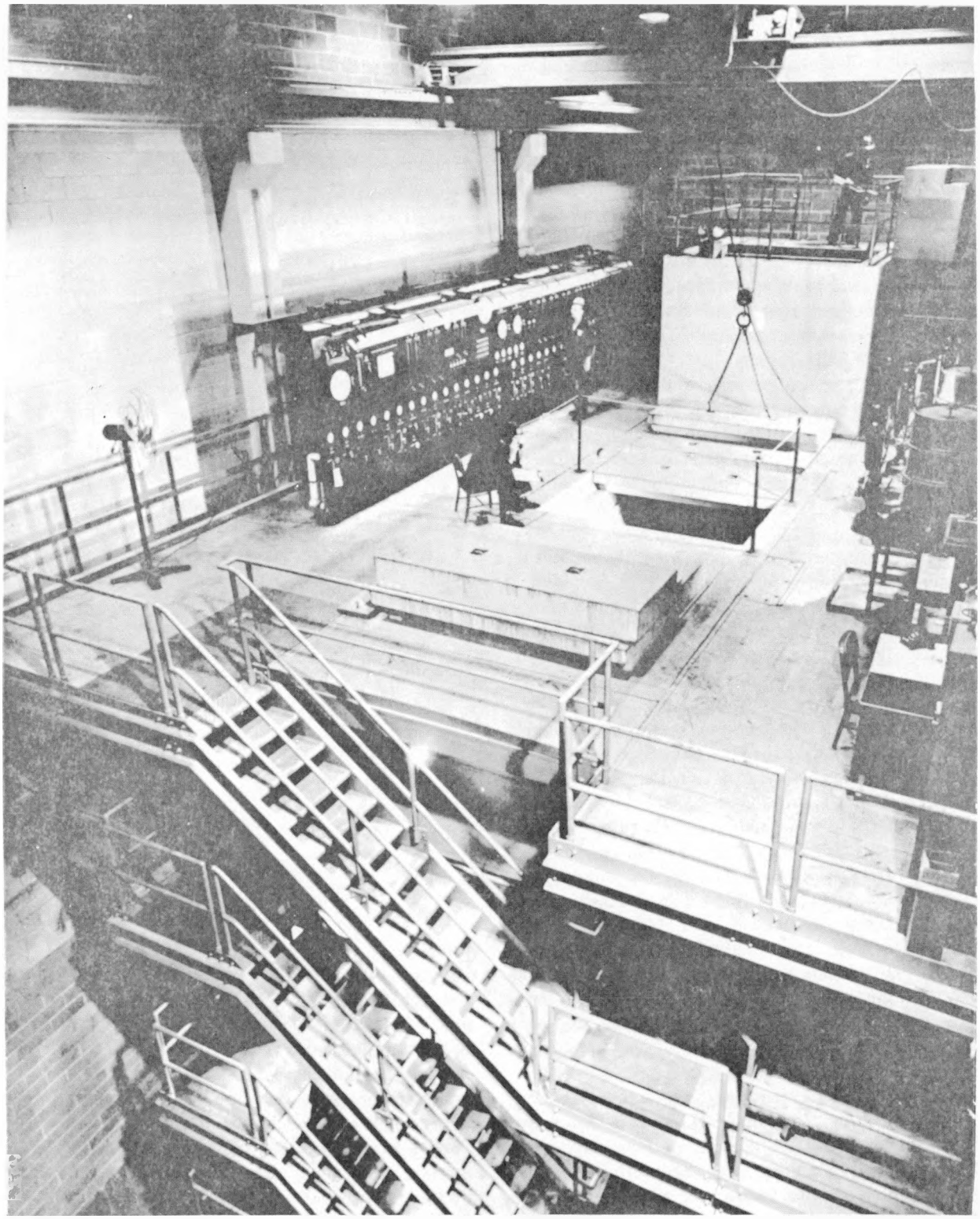

Fig. 4—Recovery facility control area.

The dissolver is capable of dissolving completely from one to eight slugs (50 to 400 g) at a time. In order to get significant analytical samples, it is essential that each dissolving be complete so that there is no opportunity for cross contamination of batches. The solvent-extraction plant is a one-cycle unit consisting of a feed make-up tank, two packed towers, and collection tanks. These tanks are for the organic raffinate, aqueous fission-product waste, and the aqueous-product solution. The uranyl nitrate solution, after collection, is concentrated to an approximately 1M solution. The aqueous waste is concentrated as a preliminary step to further disposal.

The fumes and off-gases are caustic scrubbed in a packed tower, drawn through a steam jet ejector, and discharged into a surface condenser. The condensate flows through a mixed-bed ion-exchange column and into the monitored drain system. The noncondensables are vented via a CWS filter back to the atmosphere.

The solution samplers have been described in detail.[9] The basic principles are those of the Q-Smith sampler designed by du Pont personnel for the original Oak Ridge (X-10) bismuth phosphate pilot plant. An air jet is used to circulate solution from a process vessel through a sample vial and back into the vessel. Some of the drawbacks of this original sampler were the high radiation exposure while removing a sample vial, the relatively high percentage of broken or spilled samples, and the problem of sample disposal. In the modification of this sampler these problems were largely overcome.

Figure 5 is a schematic diagram of the improved sampling device. The improvements are accomplished in the following manner: The caps for the vials contain a self-sealing rubber diaphragm, which is punctured with hypodermic needles for solution addition and removal. The capped vial is retained in the shielded carrier by a retaining ring, which is inserted and removed by a screwdriver mounted on the bottom of the cover of the shielded pot.

The sampling operation is carried out in the following manner: A clean capped vial is placed in the shielded carrier, and the retaining ring is added. This assembly is placed in the sampling enclosure and lifted into place hydraulically. When raised into position, two hypodermic needles puncture the diaphragm, one needle going to the bottom of the vial and the other being a preset distance from the bottom. The air jet is then turned on, and liquid is drawn into the vial via the longer needle and leaves via the short needle, thus agitating the solution in the vial. The air jet is turned off, and the carrier is removed and taken to the analytical

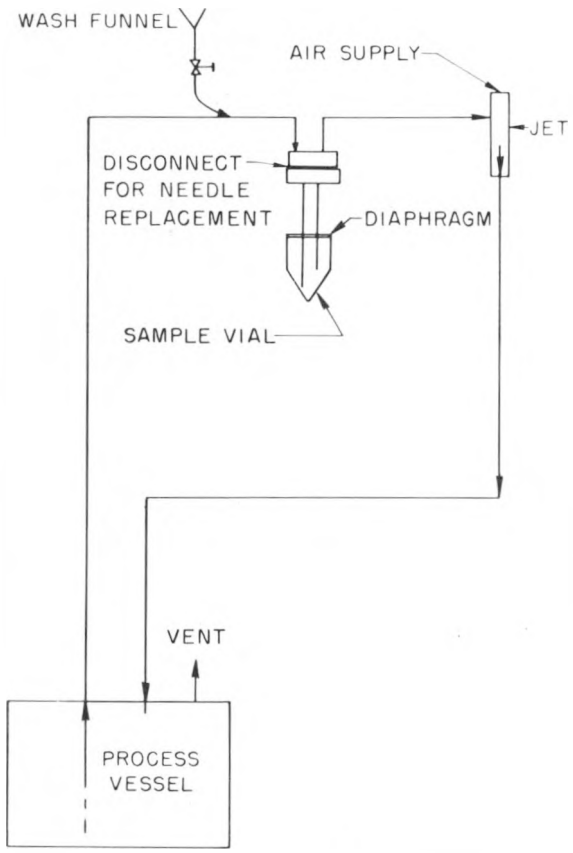

Fig. 5—Sampling device for radioactive materials.

laboratory. After an aliquot is removed, the carrier is returned to the sampler. A valve in the suction line is opened, and the air jet is again turned on. Instead of sucking on the process vessel, the wash solution in the funnel is sucked through the sample vial via the needles, recovering the material in the original sample and rinsing the vial and needles.

The same type of sampler can be used to sample inactive solutions that contain valuable or dangerous material, such as plutonium.

The active-feed metering device is the other somewhat unusual equipment feature of the EBR

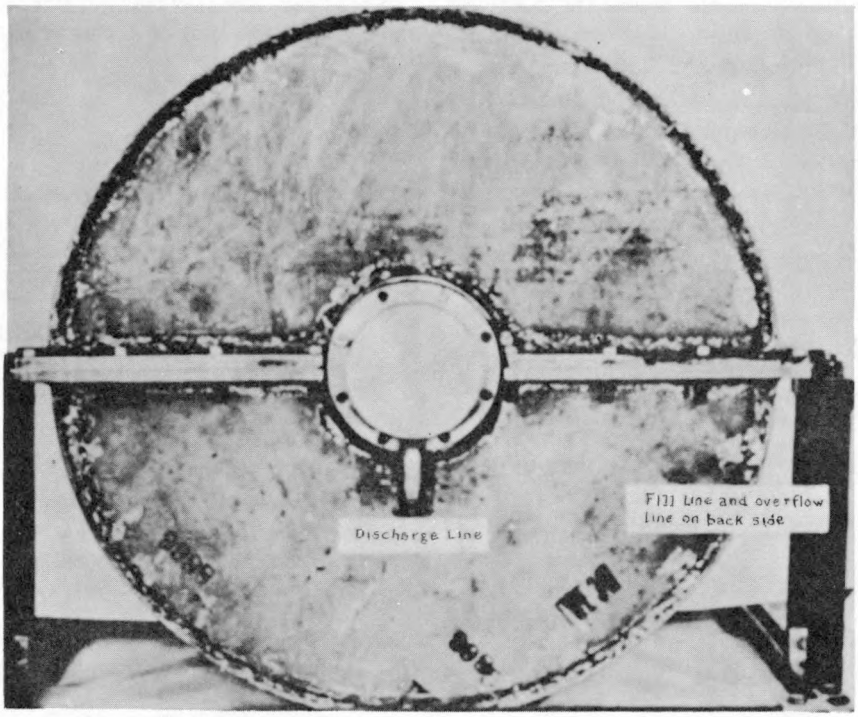

A

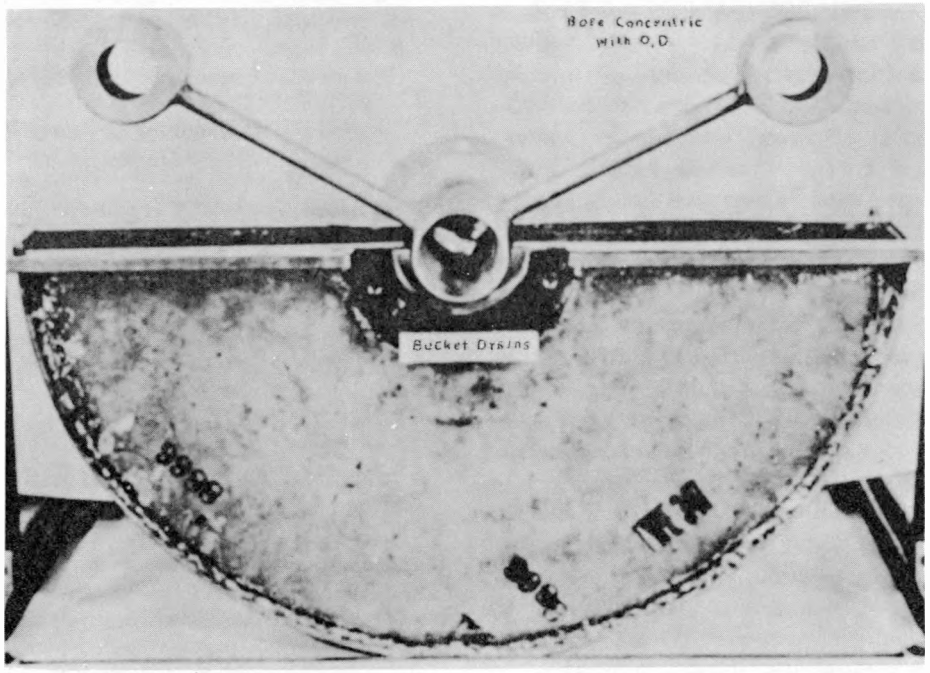

B

Fig. 6—Rotating bucket type feed metering device. A, assembled feeder-discharge side. B, feeder showing buckets (upper housing removed).

fuel recovery unit at Lemont. It is a modified wet feeder mounted above the top of the extraction column and is supplied by a nonmetering pump (a remote Pulsafeeder). The modification consists of a bucket design such that the "pumping" rate is independent of the liquid level in the reservoir. The apparatus is shown in Fig. 6. Some of the advantages of such a device are the elimination of check valves, bellows, or seals with their problems and freedom from effects of particles in the stream. Rate adjustment is provided through speed control of the driving mechanism.

5.2 Performance of Recovery Unit at Lemont

The performance of the unit at Lemont has been thoroughly satisfactory. The recovery of the enriched uranium from individual fuel rods of the EBR, based on the potentiometric and precision colorimetric analytical methods, ranged from 98.4 to 100.0 per cent, whereas the corresponding material balance range was 99.0 to 100.9 per cent. The average material balance for the twenty runs was 100.4, and the average recovery was 100.1 per cent.

Extraction losses (which include uranium in the aqueous- and organic-waste streams and in the condensate from the 50-to-1 volume reduction of the uranium-bearing product stream by evaporation) totaled 0.0056 per cent of the uranium dissolved in all runs. Purification losses in the silica gel treatment of the product solution were 0.1 per cent. Over one-fourth of the total loss was incurred on one of the first batches purified before operating techniques had been perfected.

The beta activity of the decontaminated product solution was 2.1 times that of unirradiated enriched uranium, whereas the corresponding gamma activity ratio was 2.2. The over-all decontamination factors for both beta and gamma activities were about 5×10^4. These decontamination factors are somewhat lower than those found in long runs using the semiworks equipment. This occurs because of the lower decontamination factors that are obtained toward the completion of a batch run when the uranium content of the solvent has been depleted. The reduction in uranium content of the solvent is accompanied by an increase in solvent uptake of fission products still remaining in the column. When small batches of 200 to 300 g are processed, the contamination of the accumulated product at the end of a run is significant.

REFERENCES

1. A. M. Rom, Terminal Report of ORNL Pilot-plant Development of the Materials Testing Reactor—25 Recovery Process, Report ORNL-676, May 23, 1950.
2. L. Burris and R. C. Vogel, Tributyl Phosphate Solvent-extraction Process for Recovery and Decontamination of Uranium-235 Fuel Discharged from Experimental Breeder Reactor, Report ANL-4530, Sept. 15, 1950.
3. M. Levenson, Determination of the Conversion Ratio of the Experimental Breeder Reactor by Radiochemical Methods, Report ANL-5095, Dec. 23, 1953.
4. R. L. Moore, The Mechanism of the Extraction of Uranium by Tributyl Phosphate, Report HW-15230, Sept. 1, 1949.
5. W. B. Lanham and T. C. Runion, Purex Process for Plutonium and Uranium Recovery, Report ORNL-479, Oct. 7, 1949.
6. L. Burris, I. G. Dillion, and V. G. Trice, Halex Solvent-extraction Process for Uranium and Plutonium Recovery from Discharged Reactor Fuels, Report ANL-5218, Jan. 1, 1954.
7. F. W. Woodfield, Progress Report, Chemical Development, Separation Technology, Report HW-24321, April 1952.
8. Report of the Chemistry and Chemical Engineering Section for February, March, April, 1952, Report KAPL-747.
9. S. Lawroski and C. E. Stevenson, Summary Report, Argonne National Laboratory Chemical Engineering Division, January, February, March, 1952, Report ANL-4820, May 5, 1952.

ABOUT THE AUTHORS

Leslie Burris, Jr., is an associate chemical engineer in the Chemical Engineering Division of ANL. He has been associated with the development of separations processes for uranium and plutonium since 1945 and served as Project Leader for the development of the uranium recovery process described in this article and for the Halex process (a uranium-plutonium separations process using TBP diluted with carbon tetrachloride as the solvent). He has been employed by ANL since 1948, having previously worked a short time for Tracerlab, Inc., and five

years for the Monsanto Chemical Company (three years at ORNL and two years in St. Louis). He received the B.S. degree in chemical engineering from the University of Colorado in 1943 and has since engaged in graduate study at the Illinois Institute of Technology and the University of Tennessee.

M. Levenson is a chemical engineer in the Chemical Engineering Division of ANL. He received the B.Ch.E. degree from the University of Minnesota in 1943. Prior to joining ANL in 1948, he was with ORNL (1944 to 1948) and the Houdaille-Hershey Corporation (1944). He was Project Engineer in charge of the EBR fuel processing facility described in this article and the interhalogen volatility pilot plant built at Argonne. He is now on special assignment in the Chemical Engineering Division Director's office.

Biographical sketches for S. Lawroski, R. C. Vogel, and S. Vogler are given with Part I.

THE VARIATION OF $\alpha^{U^{235}}$ WITH ENERGY IN THE INTERMEDIATE-ENERGY RANGE

SOPHIE OLEKSA

Brookhaven National Laboratory

December 1954

ABSTRACT

Recent experiments have made possible a new evaluation of resonance parameters for some of the low energy levels of U^{235}. The data permit a numerical calculation of the variation of $\alpha^{U^{235}}$ with energy in the range from 100 to 100,000 ev in accordance with a method proposed by E. P. Wigner. We examined the effects of fitting the experimental data with several different distributions, and the results are as follows:

1. The variation of $\alpha^{U^{235}}$ with energy is a slow one, no matter which of several distributions is assumed to hold for the fission and scattering widths.

2. The different distributions used give values of α that do not differ markedly.

3. The values obtained by means of Wigner's theory are in good agreement with results of the Knolls Atomic Power Laboratory integral experiments.

4. The theory can be applied with confidence to fissionable materials other than U^{235} for which comparable information about low-energy resonances is available.

1. INTRODUCTION

The ratio of the radiative-capture cross section of a fissionable material to the fission cross section is one of the important parameters of any chain-reacting assembly based on nuclear fission. This ratio, usually denoted by α, appears in the quantity η, which is defined by

$$\eta = \frac{\nu}{1 + \alpha}$$

where ν is the average number of neutrons produced per fission. Then η is the number of fission neutrons produced for each neutron absorbed in the fissionable material. The neutron economy of a chain-reacting system depends strongly on the value[1] of η and, therefore, on the value of α. For example, the possibility of breeding is a consequence of the fact that the value of η is greater than 2 under certain conditions.

The neutron economy of a nuclear reactor actually depends on the values of ν, α, and η as functions of energy over the entire range of neutron energy in the system. It follows that one of the most important nuclear properties of a reactor is the variation of α with neutron energy. The value of $\eta^{U^{235}}$ has been measured[2] by a direct method in the thermal-energy region, i.e., the region covered by the slow chopper, up to about 0.2 ev. Since ν is not expected to vary in this region, the measurement actually gives α as a function of energy in the range 0.006 to 0.2 ev. The results of the measurement

show α for U^{235} to be practically constant in this range.

The measurement of α in the resonance region is a more difficult problem because the partial reaction widths can vary from resonance to resonance and they are hard to measure. The development of the fast chopper has made possible the location and resolution of many resonances in the lower part of the resonance region,[3,4] and more information is now available than ever before. Thus about 35 resonances in U^{235} have been resolved between 0.3 and 35 ev, and the total and some fission widths, as well as some values of α, are listed for these resonances in the latest compilation of cross sections.[5] Although the values of α listed vary widely and the uncertainties cited are relatively large, the presence of such a list represents a great step forward in reactor physics.

The resonances at higher energies, i.e., at energies greater than a few hundred electron volts, present a serious problem because it is extremely difficult to obtain partial level widths with any precision and values of α can be obtained only with great difficulty, if at all. Because of the importance of α as a reactor parameter, integral experiments have been made in which average or cutoff values[6,7] of α have been obtained for Pu^{239} and U^{235}. In these experiments shielded samples of the fissionable material were irradiated in a Hanford reactor, and the amount of Pu^{240} or U^{236} formed was measured. Depending on the way in which a sample is shielded, a value of α can be obtained which corresponds to an average over the energy range above a certain cutoff energy. Values of α obtained in this way have proved to be useful; but their precise meaning is far from clear, and their usefulness in refined reactor-design calculations is open to question.

Wigner[8] showed that it is possible to calculate the value of α as a function of energy in the

Table 1 — Fission and Neutron Scattering Widths of $_{92}U^{235}$*

E_0, ev	Γ_f, mv	$2g\Gamma_n$, mv	$2g\Gamma_n^0$, mv
0.29 ± 0.01	120 ± 30	0.0040 ± 0.0006	0.007 ± 0.001
1.12 ± 0.02	130 ± 20	0.016 ± 0.003	0.015 ± 0.003
2.04 ± 0.01	30 ± 13	0.009 ± 0.002	0.006 ± 0.001
2.86 ± 0.07	60 ± 40	0.004 ± 0.001	0.002 ± 0.001
3.17 ± 0.02	130 ± 40	0.024 ± 0.003	0.014 ± 0.002
3.60 ± 0.02	110 ± 20	0.050 ± 0.005	0.027 ± 0.003
4.85 ± 0.05	20 ± 10	0.052 ± 0.004	0.024 ± 0.002
5.4 ± 0.2, 5.9 ± 0.2		0.04 ± 0.02	0.017 ± 0.009
6.2 ± 0.2		0.04 ± 0.02	0.016 ± 0.008
6.4 ± 0.1	16 ± 6	0.34 ± 0.03	0.13 ± 0.01
7.1 ± 0.1	30 ± 20	0.13 ± 0.01	0.049 ± 0.005
8.8 ± 0.1	100 ± 30	1.08 ± 0.09	0.36 ± 0.03
9.3 ± 0.1		0.14 ± 0.02	0.046 ± 0.005
9.5 ± 0.2, 9.8 ± 0.2		0.06 ± 0.03	0.02 ± 0.01
10.2 ± 0.1		0.09 ± 0.02	0.027 ± 0.005
11.7 ± 0.1	50 ± 20		
12.5 ± 0.1	40 ± 20		
19.3 ± 0.2	45 ± 20		
21.2 ± 0.2	90 ± 30		
23.7 ± 0.3	140 ± 70		
35.3 ± 0.6	110 ± 50		

*$\Gamma\gamma$ = 30 ± 6 mv; g = ½ for all practical purposes; and $\Gamma_n^0 = \Gamma_n\ (\epsilon/E_0)^{1/2}$, where ϵ = 1 ev.

range 100 to 100,000 ev, provided that the total and fission widths of a reasonable number of resonance levels are known at neutron energies less than 100 ev and that the number of neutrons emitted per fission is assumed the same for all levels. The absence of experimental information prevented the adequate application of Wigner's ideas, but his work stimulated the further measurement of the necessary widths. The work of the Brookhaven fast-chopper group[5] supplied enough data to make it seem worth while to apply Wigner's theory to these data.

2. DISCUSSION OF THE EXPERIMENTAL DATA

The experimental data[9] on which the present study is based are listed in Table 1, which gives the values of parameters for 21 of the low-energy resonance levels of U^{235}. Most of the measurements were made by the Brookhaven fast-chopper group, and the values are the result of the methods of analysis used by that group.[4]

The cross section at the peak of the resonance, σ_0, and the total width, Γ, were determined by means of shape analysis of the transmission curve at energies up to about 4 ev; at energies greater than 4 ev the method of thick and thin samples was used. The neutron-scattering width, Γ_n, was obtained from the experiments with thin samples. The capture width, Γ_γ, varies somewhat from level to level, but the variation is not large and Γ_γ is assumed to be constant. The value given, 0.030 ± 0.006 ev, is an average of the capture widths obtained from the analysis of the first few resonances of the total and fission cross-section curves. The fission width, Γ_f, was then found by subtracting the constant capture width and the scattering width from the total width. The fission widths obtained in this way were checked, wherever possible, against the fission cross-section curve. The errors assigned to the widths are often large, in some cases as large as 60 to 70 per cent of the widths themselves, and the values listed must be considered preliminary in nature.

It can be seen from Table 1 that Γ_f varies from level to level with a factor of about 9 from the smallest to the largest width. The calculation of α involves the differential spectrum produced by this fluctuation, i.e., the probability that Γ_f lies between Γ_f and $\Gamma_f + d\Gamma_f$. Only 16 fission widths were available for the present analysis, and these are not enough to allow an adequate fitting of the differential spectrum. Consequently it is necessary to fit the less sensitive integral spectrum, in which the ordinate is the probability that Γ_f is greater than, or equal to, a given value. Unfortunately the integral spectrum is often not sensitive enough to permit clear distinctions to be made between the effects of different distributions. Instead of finding the distribution of widths which fits the data best, several differential distributions can be considered. The integral form of each of these distributions fits the data reasonably well. The results of the theoretical treatment can then be examined to find useful particular results or trends. In addition, the theoretical results can be checked against the results of the Knolls Atomic Power Laboratory (KAPL) integral experiments.[6,7] This procedure has been adopted in the present study.

Three differential distributions have been used for the fission widths in this study. These are

$$P(\Gamma_f)\, d\Gamma_f = \frac{1}{a}\, d\Gamma_f \qquad \text{for } 0 \le \Gamma_f \le a$$

$$= 0 \qquad \text{for } \Gamma_f > a \tag{1a}$$

$$P(\Gamma_f)\, d\Gamma_f = a e^{-a\Gamma_f}\, d\Gamma_f \tag{1b}$$

$$P(\Gamma_f)\, d\Gamma_f = a^2 \Gamma_f e^{-a\Gamma_f}\, d\Gamma_f \tag{1c}$$

The constant a has somewhat different meanings in Eqs. 1a, 1b, and 1c. Its value is determined by the condition

$$\frac{1}{\bar{\Gamma}_f} \int_0^\infty \Gamma_f\, P(\Gamma_f)\, d\Gamma_f = 1 \tag{1d}$$

For the constant distribution, Eq. 1a,

$$a = 2\bar{\Gamma}_f$$

For the exponential distribution, Eq. 1b,

$$a = \frac{1}{\bar{\Gamma}_f}$$

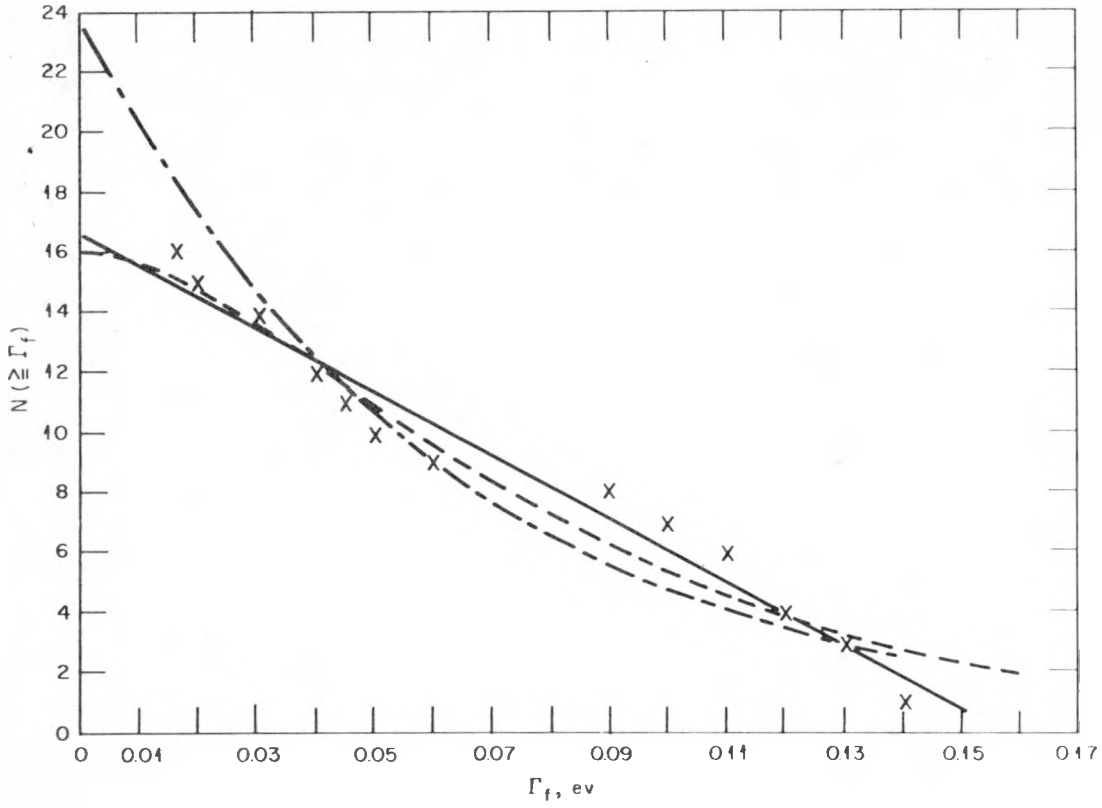

Fig. 1—Integral spectrum of the fission widths in $_{92}U^{235}$. ×, experimental points. – – –, $N = 24e^{-16\,\Gamma_f}$ (average $\Gamma_f = 0.063$ ev). ———, $N = 16e^{-23\,\Gamma_f}\ (23\,\Gamma_f + 1)$ (average $\Gamma_f = 0.087$ ev). ——, $N = 17 - 105\,\Gamma_f$ (average $\Gamma_f = 0.079$ ev).

For the xe^{-cx} distribution, Eq. 1c,

$$a = \frac{2}{\overline{\Gamma}_f}$$

The integral forms of these distributions are compared in Fig. 1 with the experimental values of the fission widths. The fit may be regarded as reasonably good in each case, in view of the number of fission widths available and the uncertainties in their values.

The theoretical results obtained with the distributions of Eq. 1 will be compared with those obtained for a distribution used by Wigner in his original study. He assumed a distribution that is symmetrical and constant on the logarithmic scale, i.e.,

$$P(\Gamma_f)\,d\Gamma_f = 0 \qquad \text{for } \Gamma_f < \frac{f_0}{t}$$

$$P(\Gamma_f)\,d\Gamma_f = (2\Gamma_f \ln t)^{-1}\,d\Gamma_f \quad \text{for } \frac{f_0}{t} < \Gamma_f < f_0 t$$

$$= 0 \qquad \text{for } \Gamma_f > f_0 t \qquad (1e)$$

where f_0 = the geometric center of the fission-width distribution

t^2 = the spread in the values of the fission widths

$$\overline{\Gamma}_f = f_0\,\frac{t - (1/t)}{(2 \ln t)}$$

It can be seen from Table 1 that the scattering widths fluctuate much more strongly than the fission widths; the largest value is about 250 times as large as the smallest value. The integral spectrum for Γ_n has an extremely long tail because of the large widths of the resonances at 6.4 and 8.8 ev. In the absence of better information and for the sake of convenience and simplicity, the same functional form

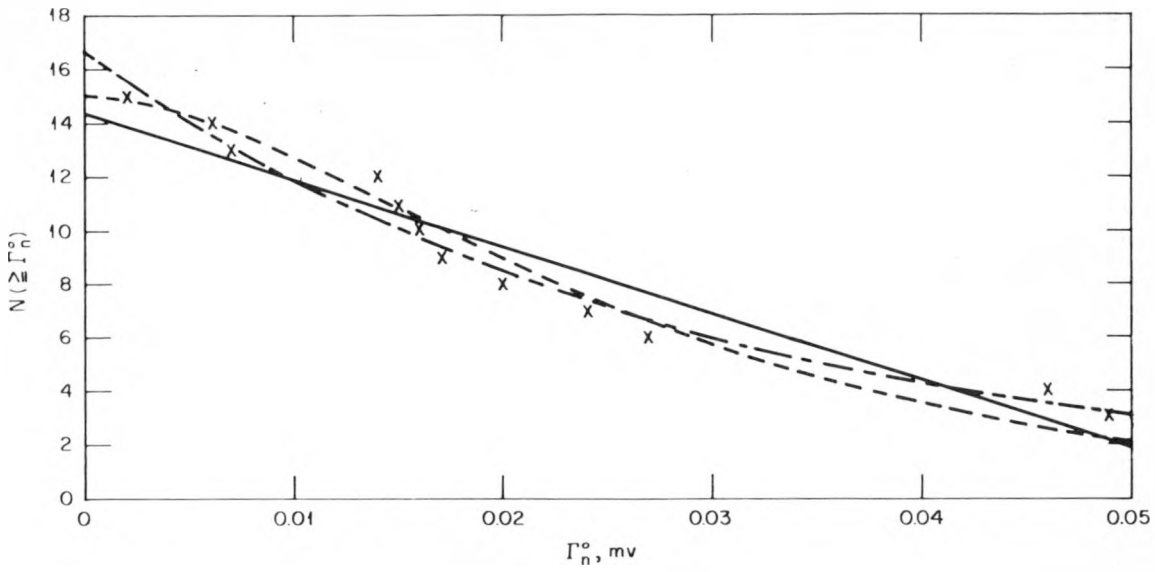

Fig. 2—Integral spectrum of the reduced scattering widths in $_{92}U^{235}$. ×, experimental data. – – –, $N = 17e^{-34\,\Gamma_n^0}$. - - - -, $N = 15e^{-70\Gamma_n^0}$ $(70\Gamma_n^0 + 1)$. ——, $N = 14 - 250\Gamma_n^0$..

of the distribution has been used for the scattering widths which was used for the fission widths, except, of course, that the constants are different. This does not mean that the distributions for Γ_f and Γ_n must be the same. Thus

$$P(\Gamma_n)\,d\Gamma_n = \frac{1}{b}\,d\Gamma_n \qquad \text{for } 0 \leq \Gamma_n \leq b$$

$$= 0 \qquad \text{for } \Gamma_n > b \qquad (2a)$$

$$P(\Gamma_n)\,d\Gamma_n = be^{-b\Gamma_n}\,d\Gamma_n \qquad (2b)$$

$$P(\Gamma_n)\,d\Gamma_n = b^2\Gamma_n e^{-b\Gamma_n}\,d\Gamma_n \qquad (2c)$$

The constant b has different meanings in Eqs. 2a, 2b, and 2c, just as does the constant a in Eqs. 1a, 1b, and 1c. Its value is determined by the condition

$$\frac{1}{\overline{\Gamma}_n}\int_0^\infty \Gamma_n\,P(\Gamma_n)\,d\Gamma_n = 1 \qquad (2d)$$

Then b has the values $2\overline{\Gamma}_n$, $1/\overline{\Gamma}_n$, and $2/\overline{\Gamma}_n$ for the constant, exponential, and xe^{-cx} distributions, respectively. The integral forms of these distributions are compared with the experimental neutron widths in Fig. 2; actually, the reduced neutron widths Γ_n^0 are used, where

$$\Gamma_n^0 = \Gamma_n(\epsilon/E)^{1/2}$$

with ϵ being equal to 1 ev. The tail of the spectrum has been ignored. (If the tail really exists and is not caused by the superposition of the widths of several resonances, then the best fit to the present neutron-scattering data of $_{92}U^{235}$ is the integrated form of the differential distribution $[K/(b^2 + \Gamma_n^2)]\,d\Gamma_n$. This distribution, however, is both uncertain and difficult to use. J. Harvey and D. J. Hughes have considered the distribution of $\Gamma_n^0/\overline{\Gamma}_n^0$ for 150 resonances of several isotopes, where $\overline{\Gamma}_n^0$ is the average reduced neutron width of a particular isotope, and they find that the exponential distribution agrees well with the experimental differential spectrum.) The reduced neutron widths are used because Γ_n varies very nearly directly as the square root of the energy, as shown by the experimental values. The average neutron-scattering width $\overline{\Gamma}_n$ is then equal to the product of the average reduced neutron width $\overline{\Gamma}_n^0$ and the square root of the energy.

The distribution of the neutron widths which corresponds to Wigner's distribution for the fission width is

$$P(\Gamma_n)\, d\Gamma_n = 0 \qquad \text{for } \Gamma_n < \frac{n_0}{s}$$

$$= (2\Gamma_n \ln s)^{-1}\, d\Gamma_n \qquad \text{for } \frac{n_0}{s} < \Gamma_n < n_0 s$$

$$= 0 \qquad \text{for } \Gamma_n > n_0 s \quad (2e)$$

where n_0 = the geometric center of the neutron-width distribution

s^2 = the spread in the values of the neutron widths

$$\bar{\Gamma}_n = n_0 \frac{s - (1/s)}{2 \ln s}$$

3. THEORY

According to the usual theory of compound nucleus formation, the cross section $\sigma(n,x)$ is given by

$$\sigma(n,x) = \sigma_c \frac{\Gamma_x}{\Gamma} \qquad (3)$$

where σ_c = the cross section for the formation of the compound nucleus

Γ_x = the partial width for the process x

Γ = the total width

According to resonance theory

$$\sigma_c = \frac{\pi \lambda\!\!\!^{-2} g \Gamma_n \Gamma}{(E - E_r)^2 + (\Gamma^2/4)} \qquad (4)$$

Thus

$$\sigma(n,x) = \frac{\pi \lambda\!\!\!^{-2} g \Gamma_n \Gamma_x}{(E - E_r)^2 + (\Gamma^2/4)} \qquad (5)$$

which is the one-level Breit-Wigner formula, where $\lambda\!\!\!^{-}$ is the wavelength, E is the energy of the incoming neutron, E_r is the energy of the neutron at resonance, and g, a statistical weighting factor, is equal to $(2J + 1)(2S + 1)(2I + 1)$, where J is the spin of the compound nucleus, I is the spin of the target nucleus, and S is the spin of the neutron.

If it is assumed that $\lambda\!\!\!^{-}$, Γ_n, and Γ_x are constant over the energy spread dE of the neutron source, then the average of Eq. 5 over a single level gives

$$\int \sigma(n,x)\, dE = 2\pi^2 \lambda\!\!\!^{-2} g \frac{\Gamma_n \Gamma_x}{\Gamma} \quad \text{barns ev}$$

$$= \frac{4.1 \times 10^6\, g}{E} \frac{\Gamma_n \Gamma_x}{\Gamma} \quad \text{barns ev} \qquad (6)$$

where E now is the energy of the level. The energy and the widths should be expressed in electron volts.

For the energy range 100 to 100,000 ev, only neutrons with $l = 0$ need be considered. Since $I = 7/2$ for U^{235}, g will have the values $7/16$ and $9/16$; but for all practical purposes g can be taken as $1/2$. The partial width, Γ_x, will be Γ_γ or Γ_f, depending on whether the radiation cross section or the fission cross section is wanted. The total width, Γ, is equal to the fission width, Γ_f, plus the radiation width, Γ_γ, plus the scattering width, Γ_n.

It is believed that the average values of the radiation and fission widths do not vary appreciably with energy. This would seem to imply that α should not change with energy since $\alpha = \Gamma_\gamma/\Gamma_f$ for an individual level. However, if Γ_f fluctuates from level to level, around some average value, α will have different values for different levels. The data of Table 1 show that Γ_f does fluctuate in this way. This variation of Γ_f from level to level, together with the weighting of each level with the probability that a reaction will occur, is the basis for the variation of the average value of α with energy. (This point is discussed in greater detail by Wigner in reference 8.) At low energies Γ_n, which varies with the square root of the energy, is negligible compared with Γ_γ and Γ_f. The probability for a reaction $(\Gamma_f + \Gamma_\gamma)/(\Gamma_f + \Gamma_\gamma + \Gamma_n)$ is then practically equal to unity. At higher energies Γ_n approaches $\Gamma_\gamma + \Gamma_f$. Since Γ_γ is constant, the probability of the reaction will be affected mainly by the fluctuation of Γ_f. The effect of the fluctuations on $\bar{\sigma}(n,\gamma)$ and $\bar{\sigma}(n,f)$ can be expressed as

$$\bar{\sigma}(n,\gamma) = \sigma' \int_0^\infty \int_0^\infty P(\Gamma_n)\, P(\Gamma_f) \times \frac{\Gamma_n \Gamma_\gamma}{\Gamma_n + \Gamma_f + \Gamma_\gamma}\, d\Gamma_f\, d\Gamma_n \qquad (7)$$

and

$$\bar{\sigma}(n,f) = \sigma' \int_0^\infty \int_0^\infty P(\Gamma_n)\, P(\Gamma_f) \times \frac{\Gamma_n \Gamma_f}{\Gamma_n + \Gamma_f + \Gamma_\gamma}\, d\Gamma_f\, d\Gamma_n \quad (8)$$

where $\sigma' = (4.1 \times 10^6\ g)/DE$ barns/ev and the averages are over many levels. The average spacing of the levels, D, is assumed to be larger than the widths; it appears in the expression because the averaging is taken over many levels. The capture to fission ratio is then given by

$$\alpha = \frac{\bar{\sigma}(n,\gamma)}{\bar{\sigma}(n,f)} \quad (9)$$

The integrations of Eqs. 7 and 8 give the $\bar{\sigma}(n,\gamma)$ and $\bar{\sigma}(n,f)$ in terms of the average fission width and the average neutron-scattering width, and α is then obtained as a function of those parameters. The value of α obtained in this way depends on the energy because of the dependence of $\bar{\Gamma}_n$ on energy.

It will be seen shortly that the formulas for α become quite complicated when the expressions for the distributions are inserted. Some of the main features of the results can be seen much more easily in the limits of zero and very large energy. In the limit $E \to \infty$ the neutron width becomes much larger than the fission and radiation widths, and α approaches the same limit for all the distributions. This limit is

$$\alpha = \frac{\int_0^\infty \int_0^\infty P(\Gamma_f)\, P(\Gamma_n)\, \Gamma_\gamma\, d\Gamma_n\, d\Gamma_f}{\int_0^\infty \int_0^\infty P(\Gamma_f)\, P(\Gamma_n)\, \Gamma_f\, d\Gamma_n\, d\Gamma_f} = \frac{\Gamma_\gamma}{\int_0^\infty P(\Gamma_f)\, \Gamma_f\, d\Gamma_f} = \frac{\Gamma_\gamma}{\bar{\Gamma}_f} \quad (10)$$

In the limit $E \to 0$ the average neutron width approaches zero. For each of the distributions used here, α, as $E \to 0$, is given by

$$\alpha = \frac{\int_0^\infty P(\Gamma_f)\, \frac{\Gamma_\gamma}{\Gamma_f + \Gamma_\gamma}\, d\Gamma_f}{\int_0^\infty P(\Gamma_f)\, \frac{\Gamma_f}{\Gamma_f + \Gamma_\gamma}\, d\Gamma_f} \quad (11)$$

or

$$\alpha = \frac{\int_0^\infty P(\Gamma_f)\, \frac{\Gamma_\gamma}{\Gamma_f + \Gamma_\gamma}\, d\Gamma_f}{1 - \int_0^\infty P(\Gamma_f)\, \frac{\Gamma_\gamma}{\Gamma_f + \Gamma_\gamma}\, d\Gamma_f}$$

The next step in the analysis is the derivation of the actual expressions for $\bar{\sigma}(n,\gamma)$, $\bar{\sigma}(n,f)$, and α for the different distributions. This is done in the Appendix, where the expressions for the various quantities of interest are given in some detail to save other workers the trouble of deriving them.

4. RESULTS

It is evident from Sec. 3 that the calculations can be tedious, especially when several distributions are used. Some of the general properties of the behavior of α can be seen more easily by looking at the behavior of α in the limits $E \to 0$ and $E \to \infty$. In particular, a good idea can be obtained of the possible range of variation of α, and the effects of differences in the distributions can be estimated.

In the limiting cases of very large and very small values of the neutron energy, α can be expressed as a function of the ratio $\Gamma_\gamma/\bar{\Gamma}_f$, and the variation of α with the parameter is shown in Fig. 3. All the distributions give the same result in the limit $E \to \infty$, and α increases from zero to unity as $\Gamma_\gamma/\bar{\Gamma}_f$ increases from zero to unity. Each distribution gives a different curve in the limit $E \to 0$, and in each case the value of α is greater in the lower limit than in the higher limit.

The best value of Γ_γ at present is 0.030 ± 0.006 ev.* The values of Γ_f shown in Fig. 1 vary from 0.060 to 0.085 ev, depending on the choice of the distribution. These values, together with their uncertainties, put the region of interest for $\Gamma_\gamma/\bar{\Gamma}_f$ between 0.3 and 0.5. The best value of the ratio is, at present, in the

*At the time many of these calculations were performed, the average values of the widths were different, e.g., $\Gamma_\gamma = 0.025 \pm 0.005$ ev. Since these values are still not rigidly settled, we have used the old values wherever possible to avoid repeating calculations. For example, although Fig. 1 indicates that the best fit for the constant distribution is $\Gamma_\gamma/\bar{\Gamma}_f = 0.38$, we have used the old value of $\Gamma_\gamma/\bar{\Gamma}_f = 0.33$ for the reason just stated. The change in α for a change in $\Gamma_\gamma/\bar{\Gamma}_f$ from 0.33 to 0.38 can easily be obtained from Fig. 3 or Table 2.

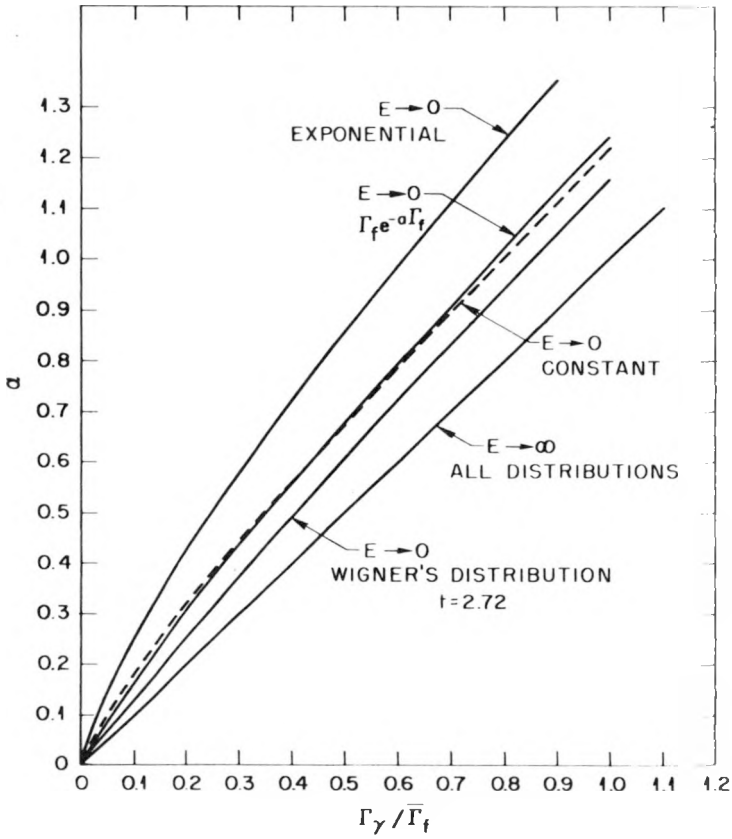

Fig. 3—Variation of α of $_{92}U^{235}$ with $\Gamma_\gamma/\overline{\Gamma}_f$ for $E \to 0$ and $E \to \infty$.

neighborhood of 0.35 to 0.40. For $\Gamma_\gamma/\overline{\Gamma}_f = 0.35$, α varies from 0.5 to 0.35 for the constant and xe^{-cx} distributions, from 0.65 to 0.35 for the exponential distribution, and from 0.43 to 0.35 for Wigner's distribution. The results for the variation of α with $\Gamma_\gamma/\overline{\Gamma}_f$ are listed in Table 2; the ratio $\alpha(E \to 0)/\alpha(E \to \infty)$ is plotted for the different distributions in Fig. 4.

The exponential distribution gives the greatest spread in the possible values of α, and the Wigner distribution gives the smallest spread. When the Wigner distribution is used, the value of α depends on the value of the parameter t, which is a measure of the spread in the fission widths. In the results presented so far for this distribution, the value of t was taken as 2.72. This value was used by Wigner, and its use here permits comparison with his results. At the same time the value t = 2.72 fits the new experimental data quite well. The effect on the value of α of varying t is shown in Table 3 for $\Gamma_\gamma/f_0 = 0.40$ and in the limits $E \to 0$ and $E \to \infty$.

Although, for simplicity, the limits $E \to 0$ and $E \to \infty$ have been used, the calculation of α is valid only in the range 100 to 100,000 ev. (It will be seen from the graphs that the value of α at 100 differs very little from the value obtained at E = 0. This, in addition to the ease of calculation, is another reason why we studied α in the limit $E \to 0$.) At higher neutron energies the effects of neutrons with angular momentum greater than zero must be taken into account, and reactions such as inelastic scattering must be considered. The actual variation of α with energy is shown in Fig. 5 for a particular case of practical interest; the case is that of the constant distribution, with $\Gamma_\gamma/\overline{\Gamma}_f = 0.33$ and $\overline{\Gamma}_n = 0.13\sqrt{E} \times 10^{-3}$ ev. (Because we had to give less weight to the tail of the distribution, our $\overline{\Gamma}_n = 0.03\sqrt{E} \times 10^{-3}$ ev. We prefer the value of

Table 2 — Variation of α with $\Gamma_\gamma/\overline{\Gamma}_f$ for $E \to 0$ and $E \to \infty$

	$\alpha(E \to 0)$				$\alpha(E \to \infty)$	$\Delta\alpha$			
$\Gamma_\gamma/\overline{\Gamma}_f$	Expon. dist.	Const. dist.	Xe^{-cx} dist.	Wigner dist.*	for all dist.	Expon. dist.	Const. dist.	Xe^{-cx} dist.	Wigner dist.*
0	0	0	0	0	0	0	0	0	0
0.1	0.25	0.18	0.16	0.13	0.1	0.15	0.08	0.06	0.03
0.2	0.43	0.32	0.30	0.26	0.2	0.23	0.12	0.10	0.06
0.3	0.58	0.44	0.43	0.38	0.3	0.28	0.14	0.13	0.08
0.4	0.72	0.56	0.56	0.50	0.4	0.32	0.16	0.16	0.10
0.5	0.86	0.67	0.68	0.61	0.5	0.36	0.17	0.18	0.11
0.6	0.99	0.79	0.79	0.72	0.6	0.39	0.19	0.19	0.12
0.7	1.11	0.90	0.91	0.83	0.7	0.41	0.20	0.21	0.13
0.8	1.24	1.00	1.02	0.94	0.8	0.44	0.20	0.22	0.14
0.9	1.36	1.11	1.14	1.05	0.9	0.46	0.21	0.24	0.15
1.0	1.48	1.22	1.25	1.16	1.0	0.48	0.22	0.25	0.16

*t = 2.72.

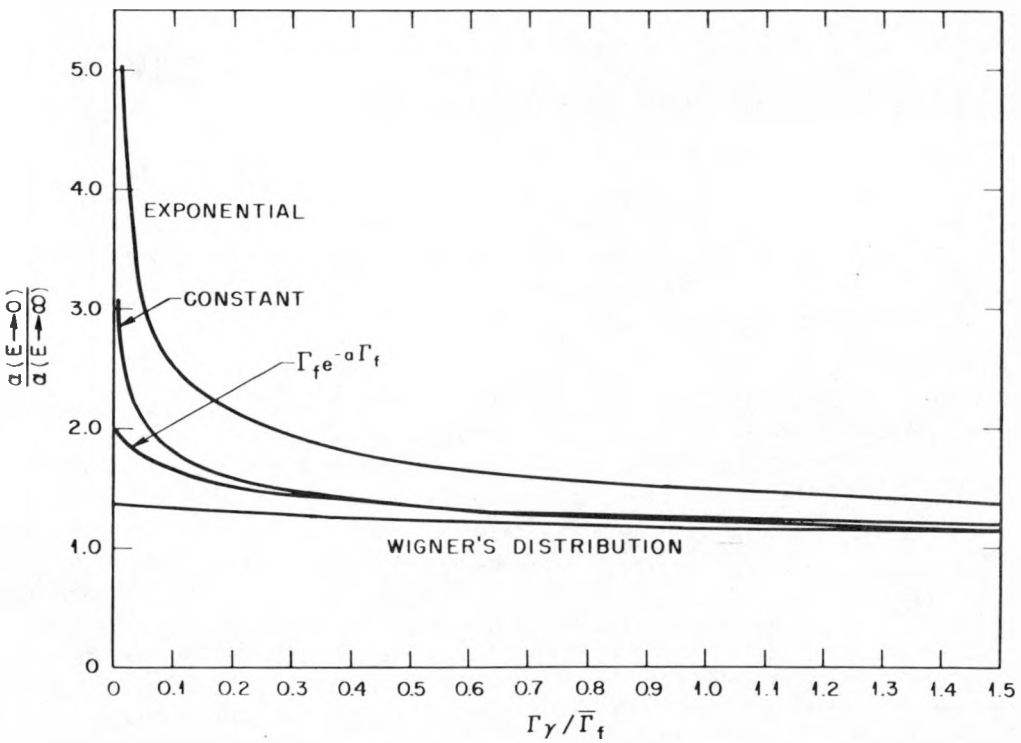

Fig. 4 — Variation of $\alpha(E \to 0)/\alpha(E \to \infty)$ with $\Gamma_\gamma/\overline{\Gamma}_f$.

Table 3 — Variation of α with t for $E \to 0$ and $E \to \infty$ ($\Gamma_\gamma / f_0 = 0.40$)

t	$\alpha(E \to 0)$	$\alpha(E \to \infty)$	$\Delta\alpha$
1.50	0.41	0.39	0.02
2.00	0.41	0.37	0.04
2.50	0.42	0.35	0.07
2.72	0.43	0.34	0.09
3.00	0.43	0.33	0.10
3.50	0.44	0.32	0.12

J. Harvey and V. E. Pilcher, $\overline{\Gamma}_n = 0.13\sqrt{E} \times 10^{-3}$ ev, which is obtained by taking more resonances into consideration.) The same results hold for the xe^{-cx} distribution since there turns out to be little difference in the results for these two distributions.

The theoretical results are also compared with the values obtained for α in the KAPL integral experiments; the latter values are denoted by the circles. The KAPL values are also listed in Table 4, where the energies given are

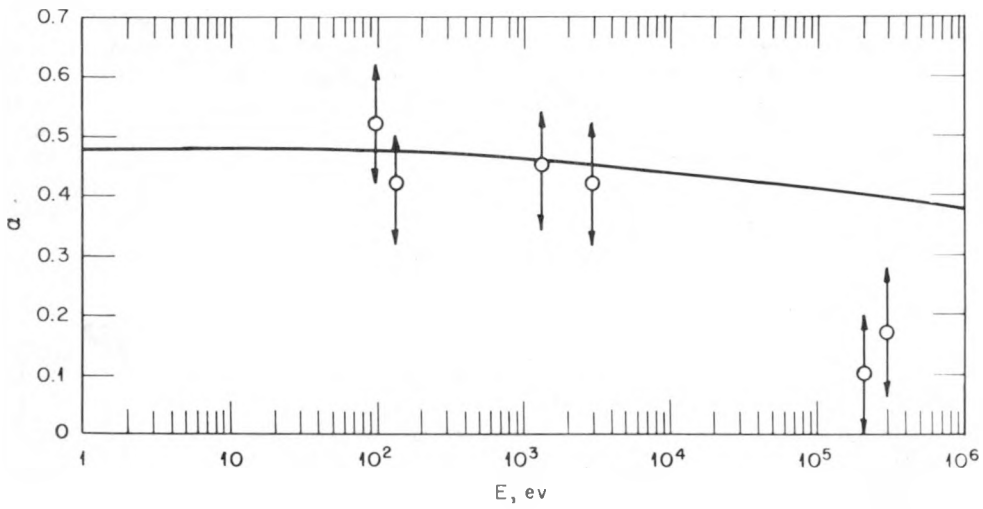

Fig. 5 — Variation of α of $_{92}U^{235}$ with energy for the constant distribution. $\Gamma_\gamma / \overline{\Gamma}_f = 0.33$. $\overline{\Gamma}_n = 0.13\sqrt{E} \times 10^{-3}$ ev. The points indicated by circles are the values determined in the KAPL integral experiments.

Table 4 — Variation of α with Energy* (Experimental values)

Energy, ev	α
100	0.52
150	0.42
1,500	0.45
3,000	0.42
215,000	0.10
300,000	0.17

*The energies given are median energies. The median energy is defined such that half the neutron flux is below this energy. J. R. Stehn states that the values of α given here are seldom better than 20 per cent.

median energies, the median energy is defined so that half the neutron flux is below the median energy. According to J. R. Stehn in a private communication, the values of α obtained in the KAPL integral experiments seldom have uncertainties smaller than 20 per cent of the value of α itself. It is evident from Fig. 5 that theory and experiment agree quite well in the range 100 to 10,000 ev. At 100,000 ev the experimental value is much smaller than the theoretical value. Similar results are shown in Fig. 6, for which the exponential distribution was used. At the higher energies the effects of higher angular momentums and inelastic scattering have undoubtedly started to become important. Weisskopf[10] considered these effects and ob-

tained agreement with experiment at 100,000 ev. We have also examined the variation of the average fission cross section with energy for the several distributions. The theoretical values agree within a constant factor with the experimental values from 100 to 10,000 ev. At 100,000 ev the same constant factor does not apply, thereby lending support to the belief that higher angular momentums have begun to appear.

Figure 6 also shows how a change in $\overline{\Gamma}_n$ affects the variation of α with energy. The case

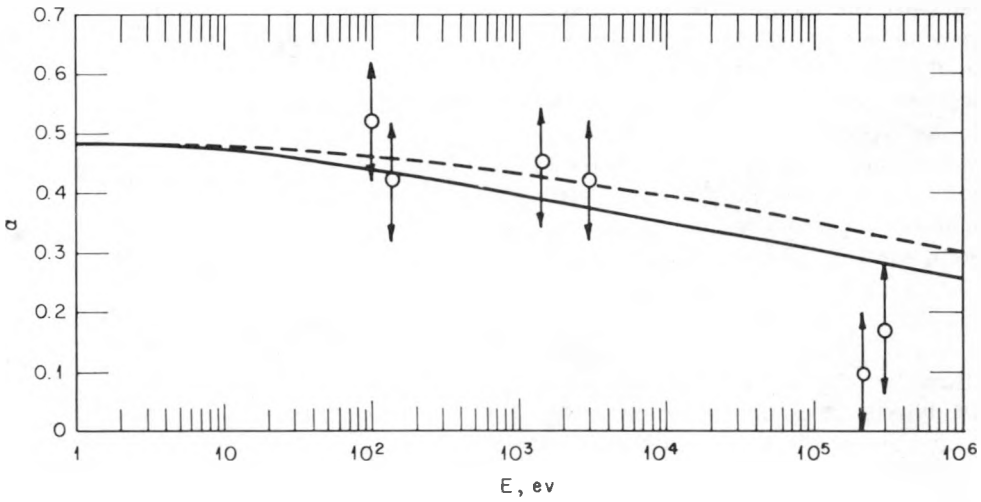

Fig. 6—Variation of α of $_{92}U^{235}$ with energy for the exponential distribution. ——, $\Gamma_\gamma/\overline{\Gamma}_f = 0.23$; $\overline{\Gamma}_n = 0.67\sqrt{E} \times 10^{-3}$ ev. - - - -, $\Gamma_\gamma/\overline{\Gamma}_f = 0.23$; $\overline{\Gamma}_n = 0.2\sqrt{E} \times 10^{-3}$ ev.

chosen is the exponential distribution with $\Gamma_\gamma/\overline{\Gamma}_f = 0.23$ and $\overline{\Gamma}_n = 0.67\sqrt{E} \times 10^{-3}$ ev and $\overline{\Gamma}_n = 0.2\sqrt{E} \times 10^{-3}$ ev.

Since 1949, when Wigner wrote his original report, there have been many changes in the average values. The present values and the 1949 values are listed below because the comparison is interesting:

Present values	1949 values
$\Gamma\gamma = 0.030 \pm 0.006$ ev	$\Gamma\gamma = 0.017$ ev
$\overline{\Gamma}_f = 0.075 \pm 0.015$ ev	$\overline{\Gamma}_f = 0.12$ ev
$\overline{\Gamma}_n = (0.13 \pm 0.02) \times 10^{-3}\sqrt{E}$ ev	$\overline{\Gamma}_n = 6.6 \times 10^{-3}\sqrt{E}$ ev
t = 2.72	t = 2.72
s = at least 10	s = 8

5. CONCLUSIONS

The theory and results treated in Secs. 3 and 4 can be summarized briefly in the statements that follow.

1. The variation of $\alpha^{U^{235}}$ with energy is a slow one, no matter which of several distributions is assumed to hold for the fission and scattering widths.

2. The different distributions used give values of α that do not differ markedly.

3. The values obtained by means of Wigner's theory are in good agreement with results of the KAPL integral experiments.

4. The theory can be applied with confidence to fissionable materials other than U^{235} for which comparable information about low-energy resonances is available.

Although the preceding conclusions are highly favorable, there is still some room for improvement. Despite the fact that more experimental data are available than ever before, this information still leaves some questions open. Thus it would be highly desirable to have enough information so that differential distributions could be obtained which fit the experimental fission and scattering widths well. More precise measurements on more resonances are

needed to accomplish this. For a more detailed understanding of the variation of α with energy, a better understanding of the partial widths is needed. Thus Γ_γ has been assumed to be constant; actually it fluctuates slightly from level to level, but the radiation process involves such a large number of final states that Γ_γ is already an average quantity. The variation of Γ_γ with energy is not large, and Γ_γ increases at most by a factor of 1.3 over the energy range[10] up to 1 mev. The assumption of constant Γ_γ is, therefore, probably a good one, but more detailed information would be helpful. Similarly, it has been assumed that the systematic variation of Γ_f with energy is too small to be considered and that the fluctuations in Γ_f from level to level are responsible for the variation of α with energy. More information bearing on this assumption would also be helpful. With regard to Γ_n, statistical theory predicts that this width should vary as the square root of the energy, and the experimental data seem to support this prediction. Again, a more thorough test of the assumption would help in understanding the behavior of α. Finally, it has been assumed that the distributions for Γ_f and Γ_n are the same. The available data point in the direction of different distributions for the fission and scattering widths, and this point should be settled.

The preceding remarks bear on the problem of understanding the behavior of α, a problem that is different from that of obtaining reasonable values for use in reactor-design calculations. The fact that the different distributions used in this report lead to values of α which do not vary greatly indicates that many subtleties which are of interest from the viewpoint of nuclear theory would not have any serious effects on reactor calculations. Thus some calculations have been made by us in which different distributions were used for Γ_f and Γ_n; the results for α were not significantly different. Results such as this one increase our confidence in the application of Wigner's theory to the problem of getting values of α as a function of energy for use in reactor calculations.

6. APPENDIX: EXPRESSIONS FOR $\bar{\sigma}(n,\gamma)$, $\bar{\sigma}(n,f)$, AND α

For the constant distribution defined by Eqs. 1a and 2a, the average neutron-radiation cross section is

$$\bar{\sigma}(n,\gamma) = \frac{\sigma'}{ab}\int_0^b\int_0^a \frac{\Gamma_n\Gamma_\gamma}{\Gamma_n+\Gamma_f+\Gamma_\gamma}\,d\Gamma_f\,d\Gamma_n \qquad (12)$$

which gives, on integration,

$$\bar{\sigma}(n,\gamma) = \frac{\sigma'\Gamma_\gamma}{2ab}\left[ab + (a+\Gamma_\gamma)^2 \ln\frac{a+\Gamma_\gamma}{a+b+\Gamma_\gamma} - b^2\ln\frac{b+\Gamma_\gamma}{a+b+\Gamma_\gamma} - \Gamma_\gamma^2\ln\frac{\Gamma_\gamma}{b+\Gamma_\gamma}\right] \qquad (13)$$

The average fission cross section is

$$\bar{\sigma}(n,f) = \frac{\sigma'}{ab}\int_0^b\int_0^a \frac{\Gamma_n\Gamma_f}{\Gamma_n+\Gamma_f+\Gamma_\gamma}\,d\Gamma_f\,d\Gamma_n \qquad (14)$$

which gives, on integration,

$$\bar{\sigma}(n,f) = \frac{\sigma'}{6ab}\left[2(a^2b+ab^2) + ab\Gamma_\gamma + (2a^3+3a^2\Gamma_\gamma-\Gamma_\gamma^3)\ln\frac{a+\Gamma_\gamma}{a+b+\Gamma_\gamma} + (2b^3+3b^2\Gamma_\gamma-\Gamma_\gamma^3)\ln\frac{b+\Gamma_\gamma}{a+b+\Gamma_\gamma} + \Gamma_\gamma^3\ln\frac{\Gamma_\gamma}{a+b+\Gamma_\gamma}\right] \qquad (15)$$

Then

$$\alpha = \frac{\bar{\sigma}(n,\gamma)}{\bar{\sigma}(n,f)} \qquad (16)$$

As $E \to \infty$, $b \to \infty$, and

$$\alpha = \frac{2\Gamma_\gamma}{a} = \frac{\Gamma_\gamma}{\Gamma_f} \qquad (17)$$

As $E \to 0$, $b \to 0$, and

$$\alpha = \frac{\frac{\Gamma_\gamma}{a}\ln\left(\frac{a+\Gamma_\gamma}{\Gamma_\gamma}\right)}{1-\frac{\Gamma_\gamma}{a}\ln\left(\frac{a+\Gamma_\gamma}{\Gamma_\gamma}\right)} \qquad (18)$$

In the case of the exponential distribution defined by Eqs. 1b and 2b, the average radiation cross section is given by

$$\bar{\sigma}(n,\gamma) = \sigma' ab\int_0^\infty\int_0^\infty e^{-b\Gamma_n}\,e^{-a\Gamma_f} \times \frac{\Gamma_n\Gamma_\gamma}{\Gamma_n+\Gamma_f+\Gamma_\gamma}\,d\Gamma_f\,d\Gamma_n \qquad (19)$$

which gives

$$\bar{\sigma}(n,\gamma) = \frac{\sigma'}{b-a}\left[-\Gamma_\gamma a + \Gamma_\gamma abe^{b\Gamma\gamma} \times E_1(b\Gamma_\gamma)\left(\Gamma_\gamma - \frac{1}{b-a}\right) + \frac{\Gamma_\gamma abe^{a\Gamma\gamma}\ E_1(a\Gamma_\gamma)}{b-a}\right] \quad (20)$$

where $E_1(a\Gamma_\gamma)$ is the exponential integral

$$\int_{a\Gamma_\gamma}^{\infty} e^{-x}\frac{dx}{x}$$

$E_1(a\Gamma_\gamma) = -E_i(-a\Gamma_\gamma)$ $(a\Gamma_\gamma > 0)$.

The average fission cross section is

$$\bar{\sigma}(n,f) = \sigma' ab \int_0^\infty\int_0^\infty e^{-b\Gamma_n} e^{-a\Gamma_f} \times \frac{\Gamma_n\Gamma_f}{\Gamma_n+\Gamma_f+\Gamma_\gamma} d\Gamma_f\, d\Gamma_n \quad (21)$$

Thus

$$\bar{\sigma}(n,f) = \frac{\sigma'}{(b-a)^2}\left[(b+a) - abe^{b\Gamma\gamma} \times E_1(b\Gamma_\gamma)\left(\Gamma_\gamma - \frac{2}{b-a}\right) - abe^{a\Gamma\gamma} \times E_1(a\Gamma_\gamma)\left(\frac{2}{b-a} + \Gamma_\gamma\right)\right] \quad (22)$$

Finally, for $\alpha = \bar{\sigma}(n,\gamma)/\bar{\sigma}(n,f)$, we get

$$\alpha = \Gamma_\gamma(b-a)\left[-1 + be^{b\Gamma\gamma}\ E_1(b\Gamma_\gamma)\left(\Gamma_\gamma - \frac{1}{b-a}\right) + be^{a\Gamma\gamma}\ E_1(a\Gamma_\gamma)\frac{1}{b-a}\right]\left[\frac{1}{a}(b+a) - be^{b\Gamma\gamma}\ E_1(b\Gamma_\gamma)\left(\Gamma_\gamma - \frac{2}{b-a}\right) - be^{a\Gamma\gamma}\ E_1(a\Gamma_\gamma)\left(\frac{2}{b-a} + \Gamma_\gamma\right)\right]^{-1} \quad (23)$$

In the limiting case $E \to \infty$, $b \to 0$, and

$$\alpha = a\Gamma_\gamma = \frac{\Gamma_\gamma}{\bar{\Gamma}_f} \quad (24)$$

For $E \to 0$, $b \to \infty$, and

$$\alpha = \frac{a\Gamma_\gamma e^{a\Gamma\gamma}\ E_1(a\Gamma_\gamma)}{1 - a\Gamma_\gamma e^{a\Gamma\gamma}\ E_1(a\Gamma_\gamma)} \quad (25)$$

or

$$\alpha = \frac{\frac{\Gamma_\gamma}{\bar{\Gamma}_f}\, e^{\Gamma\gamma/\bar{\Gamma}_f}\ E_1\left(\frac{\Gamma_\gamma}{\bar{\Gamma}_f}\right)}{1 - \frac{\Gamma_\gamma}{\bar{\Gamma}_f} e^{\Gamma\gamma/\bar{\Gamma}_f}\ E_1\left(\frac{\Gamma_\gamma}{\bar{\Gamma}_f}\right)} \quad (26)$$

It is sometimes interesting to consider the special case in which the constants a and b are the same. This can be done by finding limiting forms of the expressions for $\bar{\sigma}(n,\gamma)$, $\bar{\sigma}(n,f)$, and α.

For $b \to a$

$$\lim_{b\to a}\bar{\sigma}(n,\gamma) = \frac{\sigma'\Gamma_\gamma}{2}\left[1 - a\Gamma_\gamma + (a\Gamma_\gamma)^2 e^{a\Gamma\gamma}\ E_1(a\Gamma_\gamma)\right] \quad (27)$$

and

$$\lim_{b\to a}\bar{\sigma}(n,f) = \frac{\sigma'\Gamma_\gamma}{6}\left[\frac{2}{a\Gamma_\gamma} - 1 + a\Gamma_\gamma - (a\Gamma_\gamma)^2 e^{a\Gamma\gamma}\ E_1(a\Gamma_\nu)\right] \quad (28)$$

and therefore for $b \to a$

$$\lim_{b\to a}\alpha = 3\left[1 - a\Gamma_\gamma + (a\Gamma_\gamma)^2 e^{a\Gamma\gamma} \times E_1(a\Gamma_\gamma)\right]\left[\frac{2}{a\Gamma_\gamma} - 1 + a\Gamma_\gamma - (a\Gamma_\gamma)^2 e^{a\Gamma\gamma}\ E_1(a\Gamma_\gamma)\right]^{-1} \quad (29)$$

In the case of the xe^{-cx} distribution, the average radiation cross section is

$$\bar{\sigma}(n,\gamma) = \sigma' a^2 b^2 \Gamma_\gamma \int_0^\infty\int_0^\infty e^{-b\Gamma_n} e^{-a\Gamma_f} \times \frac{\Gamma_n^2\Gamma_f}{\Gamma_n+\Gamma_f+\Gamma_\gamma} d\Gamma_f\, d\Gamma_n \quad (30)$$

Thus

$$\bar{\sigma}(n,\gamma) = \sigma' a^2 b^2 \Gamma_\gamma \left\{ \frac{2}{(a-b)^3} \left[\Gamma_\gamma e^{a\Gamma_\gamma} \; E_1(a\Gamma_\gamma) - \frac{1}{a} \right] + \frac{4}{(a-b)^3} \left[\Gamma_\gamma e^{b\Gamma_\gamma} \; E_1(b\Gamma_\gamma) - \frac{1}{b} \right] + \frac{6}{(a-b)^4} \left[e^{b\Gamma_\gamma} \; E_1(b\Gamma_\gamma) - e^{a\Gamma_\gamma} \; E_1(a\Gamma_\gamma) \right] + \frac{1}{(a-b)^2} \left[\Gamma_\gamma^2 e^{b\Gamma_\gamma} \; E_1(b\Gamma_\gamma) - \frac{\Gamma_\gamma}{b} + \frac{1}{b^2} \right] \right\} \quad (31)$$

The average fission cross section is given by

$$\bar{\sigma}(n,f) = \sigma' a^2 b^2 \int_0^\infty \int_0^\infty e^{-b\Gamma_n} e^{-a\Gamma_f} \times \frac{\Gamma_n^2 \Gamma_f^2}{\Gamma_n + \Gamma_f + \Gamma_\gamma} \, d\Gamma_f \, d\Gamma_n \quad (32)$$

or

$$\bar{\sigma}(n,f) = \sigma' a^2 b^2 \left\{ \frac{2}{(a-b)^3} \left[-\Gamma_\gamma^2 e^{a\Gamma_\gamma} \; E_1(a\Gamma_\gamma) + \frac{\Gamma_\gamma}{a} - \frac{1}{a^2} + \Gamma_\gamma^2 e^{b\Gamma_\gamma} \; E_1(b\Gamma_\gamma) - \frac{\Gamma_\gamma}{b} + \frac{1}{b^2} \right] + \frac{12}{(a-b)^4} \left[\Gamma_\gamma e^{b\Gamma_\gamma} \; E_1(b\Gamma_\gamma) - \frac{1}{b} + \Gamma_\gamma e^{a\Gamma_\gamma} \; E_1(a\Gamma_\gamma) - \frac{1}{a} \right] + \frac{24}{(a-b)^5} \times \left[e^{b\Gamma_\gamma} \; E_1(b\Gamma_\gamma) - e^{a\Gamma_\gamma} \; E_1(a\Gamma_\gamma) \right] \right\} \quad (33)$$

In the special case for which b → a,

$$\lim_{b\to a} \bar{\sigma}(n,\gamma) = \frac{\sigma' \Gamma_\gamma (a\Gamma_\gamma)^2}{12} \left[\frac{3!}{(a\Gamma_\gamma)^2} - \frac{2!}{a\Gamma_\gamma} + 1 - a\Gamma_\gamma + (a\Gamma_\gamma)^2 e^{a\Gamma_\gamma} \; E_1(a\Gamma_\gamma) \right] \quad (34)$$

and

$$\lim_{b\to a} \bar{\sigma}(n,f) = \frac{\sigma' \Gamma_\gamma \, (a\Gamma_\gamma)^2}{30} \left[\frac{4!}{(a\Gamma_\gamma)^3} - \frac{3!}{(a\Gamma_\gamma)^2} + \frac{2!}{a\Gamma_\gamma} - 1 + a\Gamma_\gamma - (a\Gamma_\gamma)^2 e^{a\Gamma_\gamma} \; E_1(a\Gamma_\gamma) \right] \quad (35)$$

Thus, for b → a,

$$\lim \alpha = \frac{5}{2} \left[\frac{3!}{(a\Gamma_\gamma)^2} - \frac{2!}{a\Gamma_\gamma} + 1 - a\Gamma_\gamma + (a\Gamma_\gamma)^2 e^{a\Gamma_\gamma} \; E_1(a\Gamma_\gamma) \right] \left[\frac{4!}{(a\Gamma_\gamma)^3} - \frac{3!}{(a\Gamma_\gamma)^2} + \frac{2!}{a\Gamma_\gamma} - 1 + a\Gamma_\gamma - (a\Gamma_\gamma)^2 e^{a\Gamma_\gamma} \; E_1(a\Gamma_\gamma) \right]^{-1} \quad (36)$$

In the limiting case E → ∞, b → 0, and

$$\alpha = \frac{a\Gamma_\gamma}{2} = \frac{\Gamma_\gamma}{\bar{\Gamma}_f} \quad (37)$$

For E → 0, b → ∞, and

$$\alpha = \frac{a\Gamma_\gamma [1 - a\Gamma_\gamma e^{a\Gamma_\gamma} \; E_1(a\Gamma_\gamma)]}{1 - a\Gamma_\gamma [1 - a\Gamma_\gamma e^{a\Gamma_\gamma} \; E_1(a\Gamma_\gamma)]} \quad (38)$$

or

$$\alpha = \frac{\frac{2\Gamma_\gamma}{\bar{\Gamma}_f} \left[1 - \frac{2\Gamma_\gamma}{\bar{\Gamma}_f} e^{2\Gamma_\gamma/\bar{\Gamma}_f} \; E_1\left(\frac{2\Gamma_\gamma}{\bar{\Gamma}_f}\right) \right]}{1 - \frac{2\Gamma_\gamma}{\bar{\Gamma}_f} \left[1 - \frac{2\Gamma_\gamma}{\bar{\Gamma}_f} e^{2\Gamma_\gamma/\bar{\Gamma}_f} \; E_1\left(\frac{2\Gamma_\gamma}{\bar{\Gamma}_f}\right) \right]} \quad (39)$$

For the Wigner distribution we are interested mainly in the limiting values of α for very large and very small energies. Wigner found that with his distributions (Eqs. 1e and 2e), α in the limit E → ∞ is given by

$$\alpha = \frac{\Gamma_\gamma}{\int_{f_0/t}^{f_0 t} P(\Gamma_f) \, \Gamma_f \, d\Gamma_f} = \frac{\Gamma_\gamma}{\bar{\Gamma}_f} = \frac{\Gamma_\gamma}{f_0} \frac{2 \ln t}{t - \frac{1}{t}} \quad (40)$$

and in the limit E → 0

$$\alpha = \frac{2 \ln t}{\ln \left(\frac{\Gamma_\gamma + f_0 t}{\Gamma_\gamma + \frac{f_0}{t}} \right)} - 1 \quad (41)$$

ACKNOWLEDGMENTS

I am particularly indebted to Norman Bauman for his help with the calculations and to Jack Harvey for his advice, for many interesting discussions, and for making the experimental data available. I wish to thank Jack Chernick for suggesting the problem and for discussions, Irving Kaplan for discussions and encouragement, Ennis Pilcher for help with the data, and J. R. Stehn for supplying the values of α obtained in the integral experiments.

REFERENCES

1. F. T. Miles and I. Kaplan, Evaluation of Reactor Designs, Reactor Sci. Technol., 2(2): 93-120 (August 1952).
2. H. Palevsky, R. M. Eisberg, T. I. Taylor, and D. J. Hughes, The Variation of $1 + \alpha$ for U^{235} in the Energy Region from 0.006 to 0.2 Ev, Report BNL-276, January 1954.
3. W. Selove, Resonance-region Neutron Spectrometer Measurements on Silver and Tungsten, Phys. Rev., 84(5): 869-876 (Dec. 1, 1951).
4. F. G. P. Seidl, D. J. Hughes, H. Palevsky, J. S. Levin, W. Y. Kato, and N. G. Sjostrand, Fast Chopper Time of Flight Measurement of Neutron Resonances, Phys. Rev., 95(2): 476-499 (July 15, 1954).
5. Neutron Cross Sections, Report BNL-250, Aug. 1, 1954.
6. Reports KAPL-183, KAPL-238, KAPL-394, and KAPL-706.
7. Report KAPL-806 and J. R. Stehn, private communication.
8. E. P. Wigner, On the Variation of η with Energy in the 100 to 1000 Ev Region, Report BNL-25, November 1949.
9. J. Harvey and V. E. Pilcher, private communication.
10. V. F. Weisskopf, A Preliminary Discussion of the Ratio of Capture to Fission, NDA Memo-15-B-1, July 1952.

ABOUT THE AUTHOR

Sophie Oleksa received the Ph. D. degree in physics from the University of Minnesota in 1951. She is now employed as an associate physicist in the Nuclear Engineering Department at the Brookhaven National Laboratory.

HRE EXPERIMENTS ON INTERNAL RECOMBINATION OF GAS WITH A HOMOGENEOUS CATALYST*

S. VISNER† and P. N. HAUBENREICH

Oak Ridge National Laboratory

January 31, 1955

ABSTRACT

The use of copper dissolved in the reactor fuel for the complete recombination of radiolytic gas has been successfully demonstrated in the Homogeneous Reactor Experiment. Copper ion was added as copper sulfate on four occasions, increasing the copper concentration to 10, 25, 75, and 150 per cent of the estimated concentration necessary for complete recombination in a static system at 250°C, at 1000-psig total pressure, and at a uniform power density of 20 kw/liter. The investigation was conducted at temperatures from 185 to 260°C, at pressures from 765 to 1200 psig, and at power levels as high as 1600 kw.

In the main the copper behaved as expected from previous static bomb tests; the reactor data have been shown to be consistent with the laboratory data if it is postulated that a small but relatively stagnant region exists in the core with characteristics predicted from mixing experiments with a plastic model. The highest power level for which all the gas was internally recombined was 1350 kw. In the course of all copper experiments, including 350 hr of operation at the highest copper concentration, 0.06 mole/liter, no deleterious effects due to the presence of copper observed.

1. INTRODUCTION

In an aqueous homogeneous reactor the water is continually dissociated by the fission fragments into H_2 and O_2. During the early operation of the Homogeneous Reactor Experiment (HRE),[1] this gas was continuously removed from the core and bled to the low-pressure system, where it was recombined both by burning and by contact with a catalyst bed. The water was returned to the reactor system to maintain a constant fuel concentration. For 1000-kw operation gas was formed at the rate of 10.3 cfm at S.T.P., the rate being independent of temperature. This corresponds to a G_{H_2} value (the number of hydrogen molecules produced

*Upon successful conclusion of the Homogeneous Reactor Experiment, the reactor was dismantled in June 1954 to make room for the Homogeneous Reactor Test.

†Presently affiliated with Combustion Engineering–Superheater, Inc.

for each 100 ev of energy absorbed in solution) of 1.4, which is in agreement with predictions based on in-pile ampoule tests.[2]

It had been reported that, in the presence of dissolved copper salts as homogeneous catalysts, hydrogen and oxygen when dissolved in aqueous solutions at elevated temperatures recombine smoothly to form water.[3,4]

The dependence of the rate constant on various parameters had been studied in in-pile static bombs and in rocking bombs primarily out-of-pile where the gas is charged into the bomb from supply cylinders. The rate of the recombination reaction was found to be first order in both the concentration of dissolved copper and the concentration of dissolved hydrogen. Since the concentration of dissolved hydrogen is proportional to the partial pressure of hydrogen (the constant of proportionality being related to the solubility at the temperature), the recombination rate is also proportional to the partial pressure of hydrogen. The rate of recombination for a given hydrogen and copper concentration increases with temperature. There is a doubling of the rate constant, for example, from 240 to 256°C, corresponding to an activation energy of 24.4 kcal/mole.

It is a relatively simple matter to compute for a static isothermal system at equilibrium the minimum concentration of copper ion that is required for complete recombination at a specified temperature, power density, and total pressure (to prevent the accumulation of radiolytic gas in the gas phase). If the effects of increasing the temperature with the total pressure of gas and steam remaining constant are considered, it is found that the concentration of gas in solution goes through a maximum and decreases rapidly as the boiling point is approached since the increase in solubility constant is outweighed by the decrease in gas pressure. Although the reaction-rate constant increases with temperature, the effectiveness of the copper as a recombiner catalyst also goes through a maximum and decreases due to the rapid decline in the gas in solution. The higher the total pressure, the higher will be the temperature at which the maximum effectiveness of the copper occurs.

The conditions that are obtained in a circulating homogeneous reactor are, in general, quite removed from those in a static test bomb. As the fuel solution circulates through the core, pump, heat exchanger, and other auxiliary equipment, the solution experiences changes in temperature, pressure, and power density. Reactors under consideration call for a temperature increase from core inlet to outlet of about 40°C, a pressure drop of about 40 psi in the circulating loop, a residence time of 2 to 4 sec inside the core where the average power density is 50 to 100 kw/liter, and a residence time of 3 sec outside where the power density is negligible. As an additional complication a slug of solution during circulation may alternately experience conditions where the maximum concentration of dissolved gas from solubility considerations either exceeds or is less than that carried by the solution, with the result that equilibrium conditions may not prevail. A method has been worked out for computing the effect of residence in the external portion of the circulating system, assuming uniform pressure and equilibrium conditions;[5] the results are the same as those obtained by considering the reactor as a static system but with a volume 15 to 20 per cent larger. This has the effect of decreasing the average specific power for a given total power and therefore increasing the the apparent effectiveness of the copper by 15 to 20 per cent.

In a homogeneous-reactor fuel solution the copper is concentrated or diluted along with the uranium. For a given copper loading the Cu^{+2} concentration is always proportional to the concentration of U^{235}. Thus the Cu^{+2} concentration varies with operating temperature in the same manner as does the critical fuel concentration.

The copper experiments were undertaken in the HRE primarily to show that the results of laboratory experiments on gas recombination in static bombs could be used to predict rates of recombination in a reactor. It was also desired to demonstrate in a reactor operating at full power density the over-all feasibility of internal recombination of the gases that are formed from the radiolytic dissociation of water.

Although on the basis of laboratory and static in-pile tests no difficulty was anticipated with respect to the compatibility of copper and the reactor system (the stability of copper in solution, the stability of the fuel, and the effects on corrosion), the appearance of exotic effects

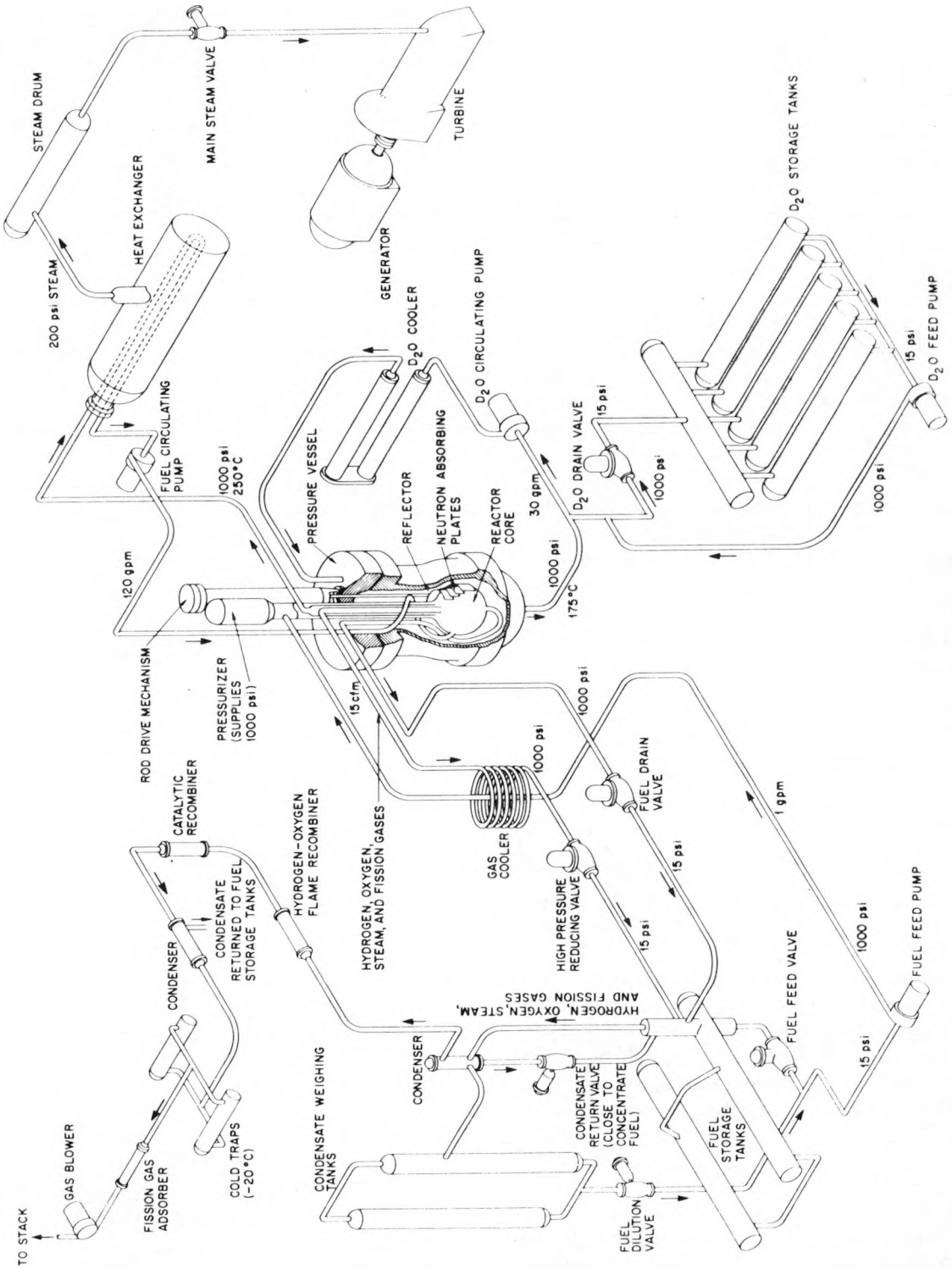

Fig. 1—Schematic flow diagram for HRE.

within the reactor environment could not be completely ruled out in advance.

2. EXPERIMENTAL PROCEDURE

2.1 High-pressure System

Figure 1 is a schematic flow diagram for the HRE. The high-pressure fuel system consists essentially of an 18-in.-diameter spherical core, a tube-and-shell heat exchanger, and a centrifugal pump. The volumes and residence times for a pumping rate of 120 gal/min are given in Table 1.

The pressure is controlled by means of a steam pressurizer, which is a vertical pipe above the core and which is heated with steam. There is a pressure drop of 60 psi in the circulating high-pressure system at 120 gal/min; and at 1000 kw, corresponding to an average power density of 20 kw/liter in the core, the temperature rise across the core is 30°C. With the solution outlet at the north pole of the core, the inlet is located at 45 deg north latitude and is so designed as to impart a tangential flow component. The gases that are produced are centrifuged toward a central vortex and withdrawn at the north pole.

2.2 Low-pressure System

The low-pressure system operates near atmospheric pressure and consists of the fuel-storage tanks and the equipment for handling the reactor gases. In the tanks, which have a capacity of 285 liters, there is normally present 20 to 40 liters of fuel solution, which is continually recirculated to the high-pressure system at a rate of 1 gal/min. The quantity of water in the fuel solution and therefore the concentration of uranium can be varied by changing the holdup of condensate in the weigh tanks. The concentration of the copper is therefore always proportional to the concentration of uranium and increases with the operating temperature as shown in Fig. 2.

2.3 Gas Handling

The gases that are centrifuged toward the central vortex in the core are let down to the low-pressure system along with excess fuel solution. Steam that is generated in an evaporator appendage to the storage tanks at a rate of 0.5 kg/min dilutes the gases in the dump tanks. The gases then flow to a condenser where the steam is removed, and, before entering the flame recombiner where the hydrogen and oxygen are burned, the gases are again diluted with steam from a steamer pot (not shown) for the purpose of maintaining a sufficient velocity at the burner nozzle for low gas flows. Cooling water flows through the jacket of the flame recombiner, the flow rate and the temperature

Table 1 — High-pressure Components of HRE

Equipment	Fuel volume, liters	Residence time, sec
Core	50	6.6
Piping from core to heat exchanger	4	0.53
Heat exchanger	5.5	0.73
Pump and return piping to core	6.1	0.80

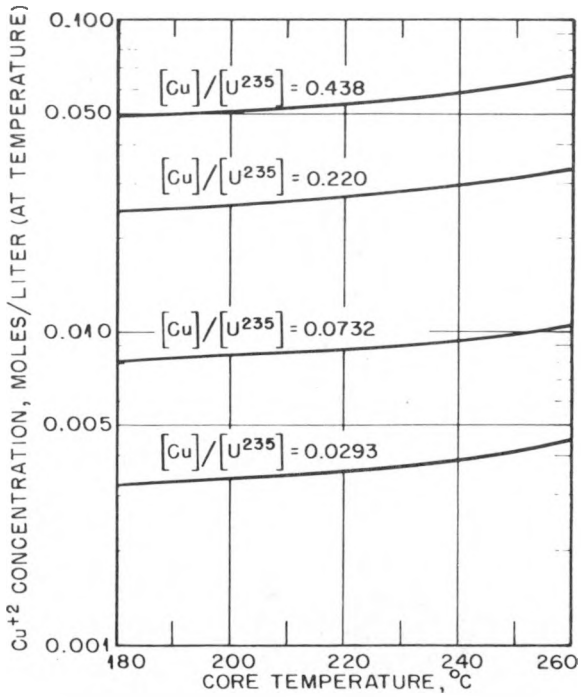

Fig. 2 — Variation of copper concentration with core temperature.

rise being measurable for the purpose of determining the rate of heat removal. If it is necessary to avoid hot spots in the bed, steam from a second steam pot (not shown) can be injected into the gas stream upstream of the catalytic recombiner, which follows the flame recombiner. The catalytic recombiner, steam jacketed to keep the catalyst dry, is followed by a second condenser, where a heat balance on the cooling water can also be made. Residual gases are discharged through a cold trap to the charcoal absorbing bed and thence to the stack. The recombined water from the second condenser is continuously returned to the fuel-storage tanks. On the basis of a survey of temperatures in the catalyst bed, it has been established that all the dissociation gases from the reactor are recombined.

2.4 Measurement of Gas Production

The rate of evolution of gas from the radiolytic dissociation of water in the reactor is measured by the rate of recombination in the off-gas system. This, in turn, is measured by the rate of removal of the heat of recombination. A correction is made for the heat contributed by the various extraneous heat sources, such as the steamer pots. This can be readily calculated and is also checked by measuring the heat balance when no gas is produced in the reactor. The correction (3.7 kw) is 9 per cent of the heat removed from recombining the gas when the reactor operates at 1000 kw.

2.5 Experimental Procedure

After the inventory of reactor fuel solution was established as 185 kg of water and 3.75 kg of U^{235}, the first of four additions of copper sulfate was made. For a given quantity of copper the concentration in solution, as mentioned earlier, is proportional to the concentration of U^{235}. These concentrations vary with the reactor operating temperature. For example, from 200 to 260°C, the critical U^{235} concentration in grams per kilogram of H_2O increases from 33.5 to 44.0 or 31 per cent. It has proved more reliable to infer the U^{235} concentration and therefore the copper concentration from the critical temperature of the core rather than from fuel samples or from considerations of inventory. The quantity of copper added on each occasion was that estimated to give approximately 10, 25, 75, and 150 per cent recombination for a static system at 250°C, 1000-psig total pressure, and a power density of 20 kw/liter. The quantities and concentrations are listed in Table 2.

Table 2—Copper Additions to HRE

Date	$CuSO_4$ added, g	Cumulative $CuSO_4$ in reactor, g	Cu conc. at 250°C, moles/liter	Molar ratio, $[Cu]/[U^{235}]$	Gas estimated to be recombined,* %
12/5/53	74.6	74.6	0.00417	0.0293	9.5
12/6/53	111.4	186.5	0.0104	0.0732	23.7
12/18/53	373.0	559.5	0.0313	0.220	71
1/5/54	555.1	1114.6	0.0624	0.438	142

*In a static system at 250°C, 1000 psig, and 20 kw/liter.

At each copper concentration the reactor was operated over a range of power levels at various temperatures and pressures, and the net gas production was measured. By comparison with the gas production at the same power level in the absence of copper, the effectiveness of the copper as a catalyst for internal recombination could be inferred.

3. RESULTS AND DISCUSSION

3.1 Recombination Data

The data obtained on the net gas yield from the reactor at various power levels for the four copper concentrations are plotted in Figs. 3 to 9. The line representing the gas production in the reactor in the absence of copper is shown in the figures. Also shown is a dotted line rep-

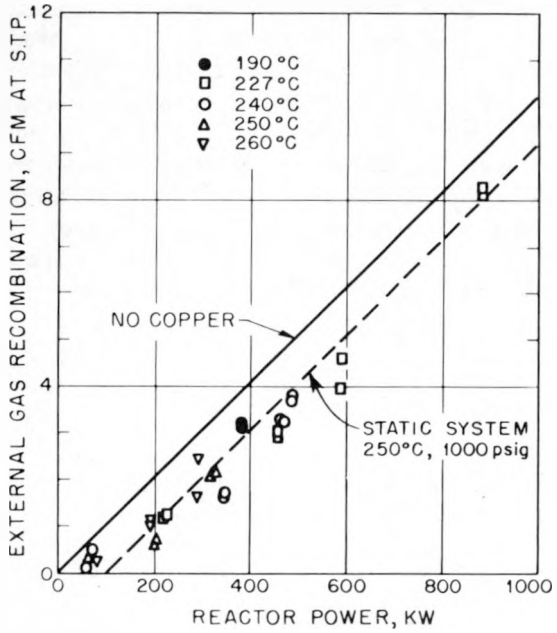

Fig. 3—Internal gas recombination in HRE with 0.004M Cu^{+2}. Total pressure, 1000 psig. $[Cu]/[U^{235}]$ = 0.0293.

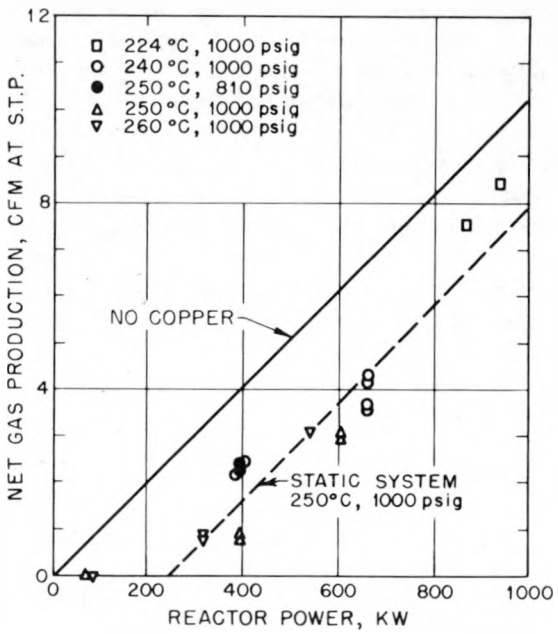

Fig. 4—Internal gas recombination in HRE with 0.01M Cu^{+2}. $[Cu]/[U^{235}]$ = 0.0732.

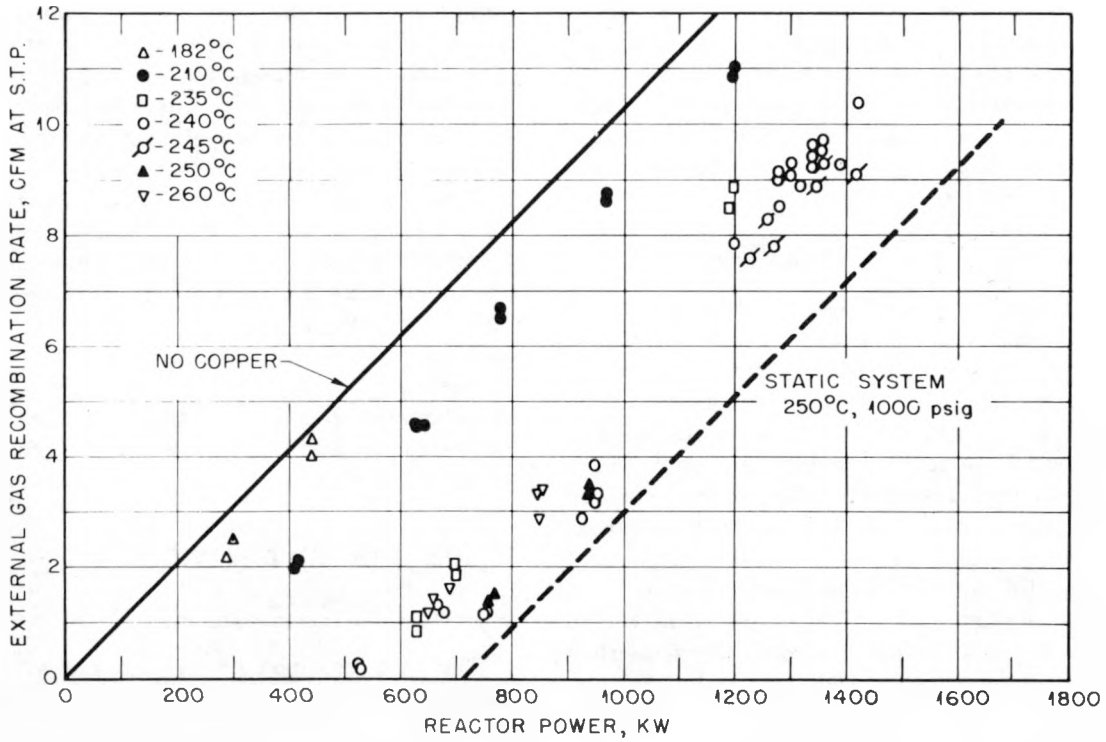

Fig. 5—Internal gas recombination in HRE with 0.03M Cu^{+2}. Total pressure, 1000 psig. $[Cu]/[U^{235}]$ = 0.220.

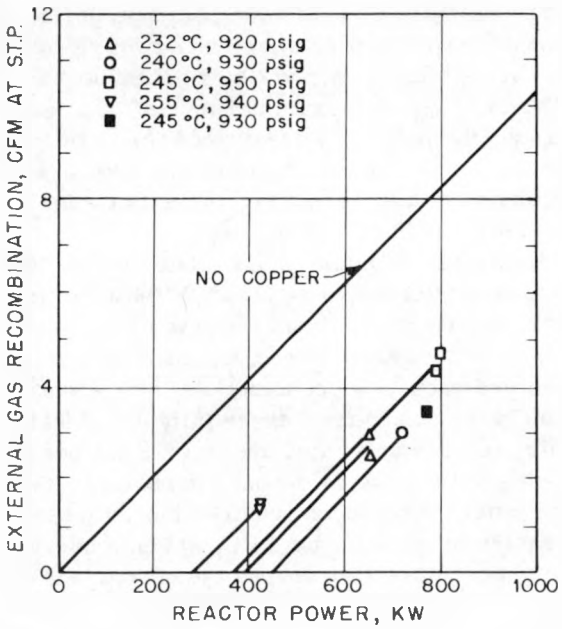

Fig. 6—Internal gas recombination in HRE with 0.03M Cu^{+2}. $[Cu]/[U^{235}] = 0.220$.

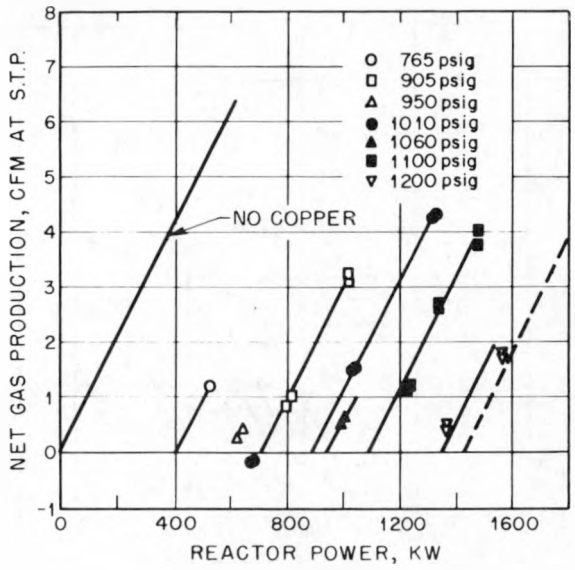

Fig. 7—Gas production in HRE with 0.06M Cu^{+2} at 235°C core outlet temperature. $[Cu]/[U^{235}] = 0.438$. ---, static system, 250°C, 1000 psig.

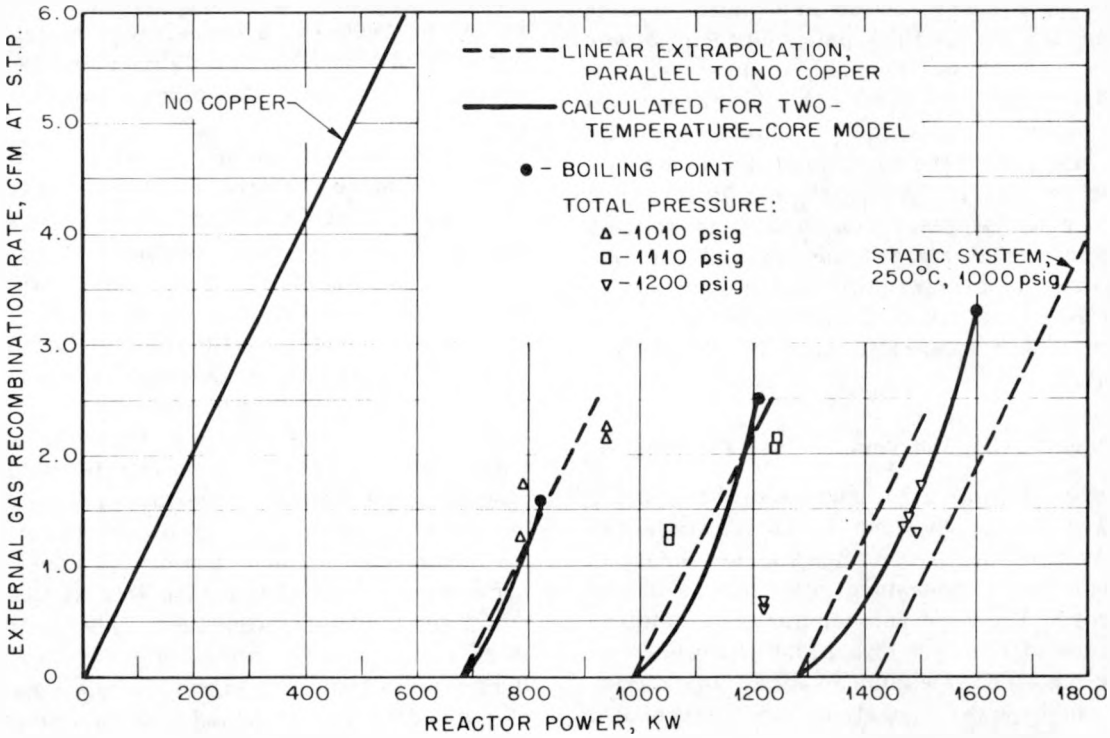

Fig. 8—Internal gas recombination in HRE with 0.06M Cu^{+2} at 260°C core outlet temperature. $[Cu]/[U^{235}] = 0.438$.

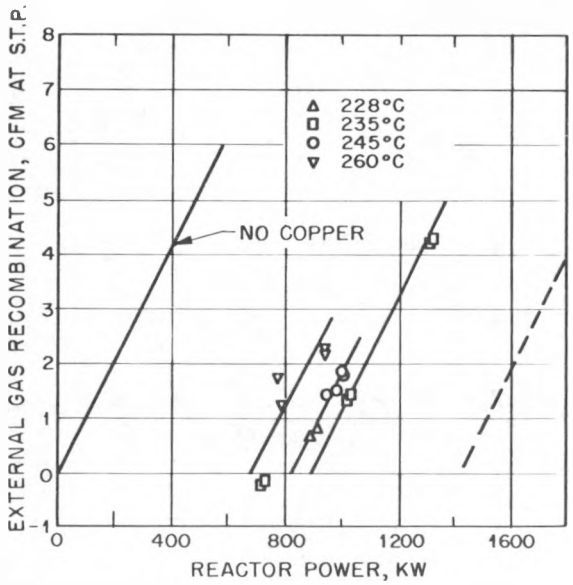

Fig. 9—Internal gas recombination in HRE with 0.06M Cu^{+2}. Total pressure, 1010 psig. $[Cu]/[U^{235}] = 0.438$. ———, static system, 250°C, 1000 psig.

resenting the calculated performance with the same copper concentration in a static 50-liter reactor at 250°C, 1000 psig, uniform power density, and without circulation. In general, it is possible to draw a straight line through all points taken at the same pressure and outlet temperature from the core. This line is roughly parallel to that for no copper, and its intercept at zero external gas recombination represents the highest reactor power for which all the dissociation gas is internally recombined and is therefore a measure of the effectiveness of the copper. These intercepts have been compiled in Table 3.

3.2 Core Mixing and Temperature Distribution

Before attempting to correlate the reactor data with the predictions based on static experiments in the laboratory, it is necessary to examine the temperature distribution in the HRE core. The flow and temperature patterns inside the core are somewhat ambiguous because it has not been feasible to study the mixing during high-power operation when gas bubbles and volume heat generation become important factors. Early mixing experiments at room temperature with a plastic model of the HRE core[6] indicated that the main body was perfectly mixed except for a relatively stagnant region of 7.5-liter volume, shaped like a doughnut, 16 cm I.D. and 22 cm O.D., with the vertical axis going through the poles. The residence time and temperature rise for the liquid in this region were estimated as approximately twice those for the main body of the 50-liter core.

Additional information on mixing in the HRE core is available from operating the reactor at high power. It has been observed that, within the error of measurement, the core outlet temperature remains constant as the power is rapidly increased from essentially 0 to 1000 kw. This would imply that there is near perfect mixing in the core as opposed to pure slug flow. The latter would have required the outlet temperature to increase by 15°C, which is one-half the temperature rise across the core, since the average nuclear temperature, which depends only on the fuel concentration, must remain constant. From considerations of criticality and conservation of energy, it can be shown that the presence of a hot region of the size and residence time indicated by the tests with the plastic sphere would cause, as the power is raised to 1000 kw, a decrease in outlet temperature of only 2°C. This is comparable to the error in observing the temperature for this type of test.

Another phenomenon at high power sheds additional light on the core temperature distribution. It has been noted that the fuel concentration in the core becomes enhanced owing to the removal of radiolytic gases and associated steam.[7] Although for no internal recombination the mass rate of removal of the radiolytic gases is proportional only to the reactor power, the removal of steam depends also on the temperature. In order to account quantitatively for the enhancement in concentration as reflected by the rise in core outlet temperature, it has been necessary to postulate that the temperature of the steam-gas mixture leaving the core is approximately 20°C higher than that at the core outlet for the circulating fuel. This hypothesis is also supported by data from heat balances on the let-down heat exchanger where the mixture of gas and solution returned to the low-pressure system is cooled by the upcoming stream. A hotter region surrounding the vortex is implied. However, the thickness of this region need only

Table 3 — Effectiveness of Copper from Intercepts

Molar conc. of Cu^{+2} at temp.	Molar ratio, $[Cu]/[U^{235}]$	Fuel temp., °C	Fuel pressure, psig	Maximum reactor power where all gas is recombined, kw
0.0045	0.0293	260	1000	85
0.0042	0.0293	250	1000	120
0.0040	0.0293	240	1000	160
0.0038	0.0293	227	1000	90
0.0034	0.0293	190	1000	70
0.0112	0.0732	260	1000	240
0.0104	0.0732	250	1000	320
0.0104	0.0732	250	810	170
0.0099	0.0732	240	1000	240
0.0093	0.0732	224	1000	110
0.0336	0.220	260	1000	530
0.0313	0.220	250	1000	615
0.0298	0.220	240	1000	600
0.0292	0.220	235	1000	530
0.0265	0.220	210	1000	200
0.0243	0.220	182	1000	50
0.0298	0.220	240	945	440
0.0290	0.220	232	920	380
0.058	0.438	235	1200	1350
0.058	0.438	235	1100	1100
0.058	0.438	235	1060	940
0.058	0.438	235	1010	890
0.058	0.438	235	905	710
0.058	0.438	235	760	410
0.067	0.438	260	1010	690
0.061	0.438	245	1010	820
0.056	0.438	228	1010	830
0.067	0.438	260	1110	980
0.067	0.438	260	1200	1280

be sufficient to saturate the radiolytic gas passing through to the vortex. The volume of the region must be greater than 0.5 liter to satisfy the power requirements for saturating the gas with steam.

In summary, the main body of the HRE core is in a state of perfect mixing with the temperature approximately the same as the outlet temperature. In addition, there is probably a region near the center with perhaps 15 per cent of the core volume for which the residence time and temperature rise at 1-megawatt operation are approximately twice those of the main body.

3.3 Effect of Temperature

It appears from Figs. 3 to 5 and 9 and Table 3 that, at a total pressure of 1000 psig and for a given copper loading, the most effective internal recombination is with the core outlet temperature between 230 and 250°C. That is, the power at which gas first begins to be recombined externally is highest when the temperature is in this range. This is more readily seen in Fig. 10.

Also shown in Fig. 10 are theoretical curves for the HRE (calculated as in reference 5).

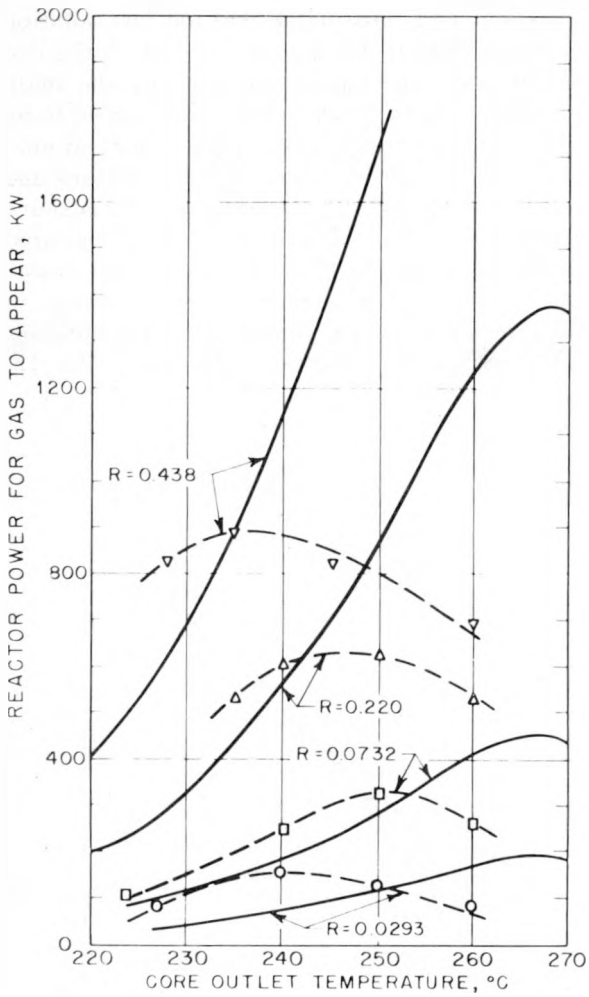

Fig. 10 — Internal gas recombination in HRE as a function of core outlet temperature. Total pressure, 1000 psig. R = [Cu]/[U^{235}]. ——, calculated for static isothermal core with recombination in external core. – – –, experimental.

These curves are based on a completely isothermal core and take into account recombination in the circulating system. For reasons discussed earlier, these curves all have maximums at the same temperature, 268°C. The experimental data indicate maximum effectiveness at lower temperatures.

A qualitative explanation for the shifting of the maximum to lower core outlet temperatures would be the presence in the core of a region which is at a considerably higher temperature than the main body. In this case the effectiveness of the copper in the hotter region would follow the temperature there and not the core outlet temperature, which was measured. The intercepts plotted in Fig. 10 occur at higher power levels for the higher copper concentrations. Therefore, if the temperature difference between the hot region and the core outlet increases with power level, the effect of the hot region should be more pronounced at the higher copper concentrations. This is in agreement with the experimental data which show that generally the higher the copper content, the lower the temperature at which the maximum effectiveness occurs. The effect of a two-temperature region core will be discussed more fully in the discussion of the effect of pressure.

In Fig. 11, the recombination rate constant calculated from the HRE data for 25 and 75 per cent nominal copper content is compared at various core outlet temperatures with that obtained by static bomb investigators. The only correction applied to the reactor data was for the recombination in the external high-pressure loop. The agreement is, in general, very encouraging, ignoring the decrease at high temperatures, which probably reflects the effect of the hot region in the core. This effect seems more pronounced for the data taken with 75 per cent copper, probably for the reason that the temperature increase in the stagnant region is greater at the higher power levels associated with the higher copper content.

3.4 Effect of Pressure

With the highest copper concentration in the fuel, 0.06 moles/liter nominal, an investigation was made of the effect of the total reactor pressure on the effectiveness of the copper for gas recombination. Although it would have been desirable to conduct this study at a number of temperatures, it was possible because of equipment limitations to achieve a sizable range of pressures at only one temperature, 235°C. The data obtained are shown in Fig. 7. The extrapolated reactor power for gas first to appear, which is a measure of the effectiveness of the copper, is plotted in Fig. 12 against total reactor pressure.

Also shown in Fig. 12 is a theoretical curve that was calculated on the basis of a completely isothermal core with recombination also occurring in the external high-pressure system.

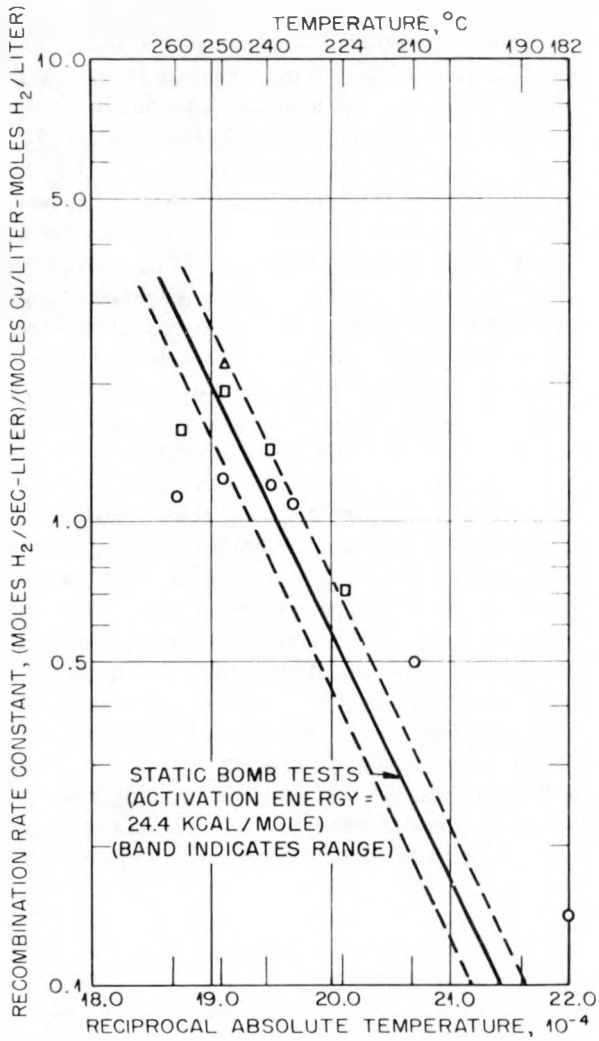

Fig. 11 — Effect of temperature on recombination rate constant at low power. Data interpreted on basis of isothermal core with recombination in external system.

Molar ratio, $[Cu]/[U^{235}]$	Pressure, psig
□, 0.0732	1000
△, 0.0732	810
○, 0.220	1000

In general, the experimental data agree well with the curve with indications that, at the higher pressures, the copper was somewhat less effective than had been predicted by this model.

The data were also analyzed on the basis of a core model in which there is a relatively stagnant region where 15 per cent of the power is generated. It is postulated that the fuel solution entering the core divides into two streams, one for the stagnant region and one for the main body of the core. Each region is assumed to be separate, perfectly mixed, and therefore at uniform but, in general, different temperature and gas concentration. For each region the pressure required for total recombination is calculated, as shown in Sec. 5, as a function of the power density. The curve giving the performance of the stagnant or hotter region at a constant core outlet temperature of 235°C is shown in Fig. 12,

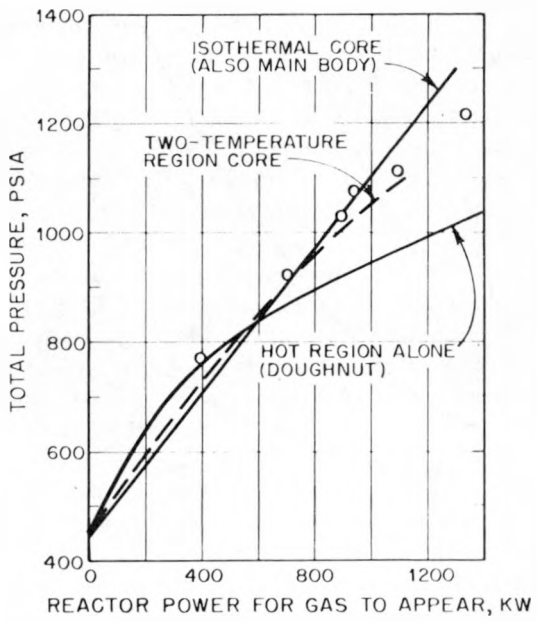

Fig. 12 — Gas recombination in HRE at 235°C core outlet temperature with 0.058M Cu^{+2}. $[Cu]/[U^{235}] = 0.438$.

and that for the main body is adequately represented by the curve already drawn for the isothermal-core model. For pressures up to 840 psia, gas bubbles by the two-region model are formed first in the stagnant region when the reactor power is increased. At higher pressures, they appear first in the main body.

It is now necessary to discuss more fully the significance of the intercepts listed in Table 3. These were obtained by extrapolating the experimental data to zero external recombination by a straight line parallel to the line which gives the gas generation for the reactor in the absence of

copper. In this there is the implicit assumption that, with or without copper, once gas begins to appear, increases in the rate of external recombination are proportional to the increase in total reactor power. This is not generally true in the two-temperature model. If gas is generated in one region before the other, the initial rate of increase should, to a first approximation, be proportional to the fraction of the total power which is generated in the region where the gas is being produced. As gas begins to appear in the second region, the slope should change and become parallel to the no-copper line—provided the temperature of neither region changes. If this part of the curve were extrapolated to zero external recombination, the intercept would lie between the powers at which gas first appeared in the two regions. In those cases where, as the power is increased, gas is first produced in the main body (in which 85 per cent of the power is produced), the intercept should be 15 per cent of the way between the power for the appearance of gas in the main body and the power for appearance in the stagnant region. In the experiments where the dependence of gas production on power was followed over an appreciable range, it is impossible to detect any significant deviation from the slope of the no-copper line. However, the predicted change in slope would be only 15 per cent, which could not be seen because of experimental error.

The intercept power as a function of total pressure, calculated as described in the preceding paragraph, is shown in Fig. 12 as a dashed line. It appears that the experimental data support the two-temperature-core model. Additional data at higher pressures, which were not obtainable, would have been more conclusive. Also data at lower pressures would have been helpful in verifying that the intercept on the pressure axis for no internal recombination is the steam pressure for 235°C.

A limited amount of data was taken at 260°C outlet temperature at total pressures from 1010 to 1200 psig with a nominal copper concentration of 0.06 mole/liter. These data are shown in Fig. 8. At the highest power level attained at each pressure, the reactor was on the verge of instability owing to the fuel-concentration effect in the core.

The analysis of the 260°C case using the two-temperature-core model predicts somewhat different behavior than that for a 235°C core outlet. For the 260°C outlet temperature as the power is raised gas bubbles are generated first in the hotter region at all pressures. Furthermore, as the power is increased from the point at which gas first emerges to the point at which the solution boils in the stagnant region, the gas production, as shown by the solid curves in Fig. 8, increases as rapidly as if the gas were generated throughout the reactor core. This arises from the fact that the gas generation in the stagnant region is supplemented by two other phenomena: first, a fraction of the solution which leaves the main body enters the bottom stagnant region where the gas dissolved in the solution is stripped; second, as the boiling point is approached in the stagnant region, the recombination rate falls off rapidly. It so happens here that the linear extrapolation of the data in the usual manner yields intercepts that are identical to the threshold powers for gas production, which are calculated on the basis of the two-temperature-core model. The effectiveness of the copper as measured by this threshold power is plotted in Fig. 13 against the total pressure in the reactor. The data are in excellent agreement with the predictions based on the two-temperature-core model, whereas the calculations for an isothermal core predict an effectiveness for the copper three to four times greater than observed.

The two-temperature model also explains the incipient instability in the reactor at the highest power levels achieved at 260°C on the basis of incipient boiling in the stagnant region. This results in an inordinately large rate of steam removal from the core and a corresponding enhancement of the fuel concentration.

This experiment at the 260°C core outlet temperature thus demonstrates in a striking manner the necessity of taking into account the detailed temperature pattern in the core and also the validity of the assumptions concerning the stagnant region in the HRE core.

Shown in Fig. 14 are some data on pressure dependence obtained with a 0.0104M concentration of Cu^{+2} at relatively low power levels where the effect of the stagnant region would not be too important. The agreement with the predictions based on an isothermal-core model is reasonably good.

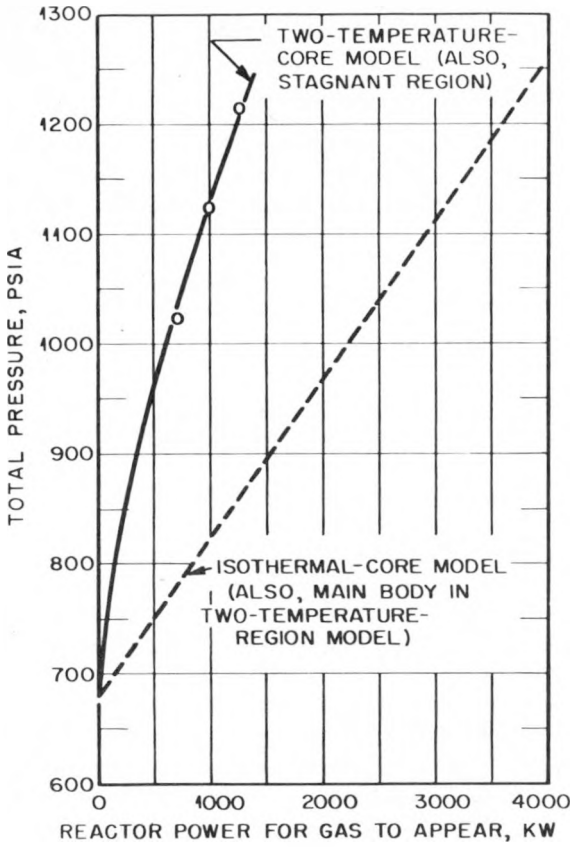

Fig. 13 — Effect of total pressure on internal gas recombination at 260°C fuel outlet temperature with 0.067M Cu^{+2}. $[Cu]/[U^{235}] = 0.438$.

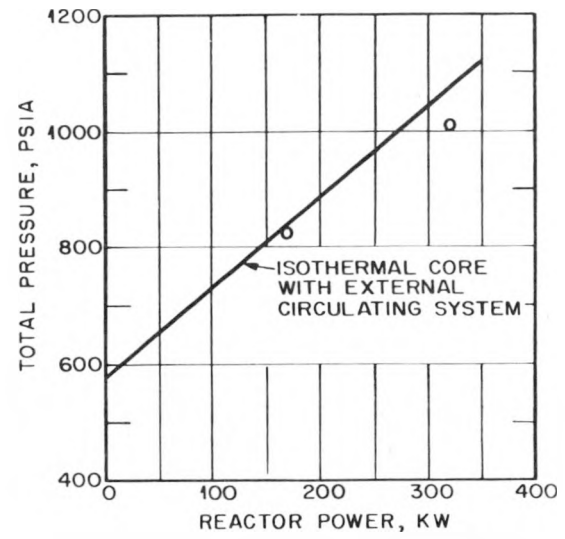

Fig. 14 — Pressure dependence of internal gas recombination in HRE at 250°C with 0.0104M Cu^{+2}. $[Cu]/[U^{235}] = 0.0732$.

4. CONCLUSIONS

The use of copper dissolved in the reactor fuel for the complete recombination of radiolytic gas has been successfully demonstrated in the HRE. In the main, the results obtained over a sizable range of temperatures, power levels, and pressures are consistent with the findings of the static-system experiments.

The quantitative interpretation of the HRE data has been complicated by the flow and temperature distribution in the reactor core. There appears to have been a region near the center of the core for which the residence time and temperature rise at 1-megawatt operation were approximately twice those for the main body. The existence of such a region was indicated by mixing experiments on a plastic model. At low power levels the temperature in the stagnant region would not be expected to be much above the remainder of the core. This was borne out by the HRE experiments with low copper concentrations. Here the powers at which gas began to appear were low, and there was good agreement between the observed dependence on temperature and that predicted for a static isothermal system. At higher copper concentrations, where the power was raised quite high before the appearance of gas, the data had to be analyzed on the basis of a two-temperature region core model.

Because of the copper it was possible to extend the permissible power level of the HRE from 1000 to 1500 kw. The removal from the core of the decomposition gases with associated steam tended to increase the concentration of fuel in the core with respect to the low-pressure system. Because the region about the vortex apparently ran 20 to 30° hotter than the remainder of the core, the removal of steam and the concentration effect were enhanced to the point where an instability developed in the operation of the reactor.[8] By reducing the net gas production by means of the copper, the concentration effect in the core was also reduced permitting the operation of the reactor at high power levels.

Finally, no harmful effects from the copper were found in the operation of the reactor for 350 hr with 0.06M Cu^{+2}. There was no significant change in the corrosion rate as determined

from the nickel concentration in the fuel solution, and there was no evidence of any chemical instability either with respect to the copper or the uranium.

5. APPENDIX: RECOMBINATION IN A TWO-TEMPERATURE REGION HRE CORE MODEL

5.1 Calculation of Doughnut Temperatures

The behavior of flow in the HRE core under the influence of density differences had been investigated in the full-scale plastic model by Spiewak and Bradfute.[6] They report a characteristic stagnant region coaxial with the vortex with the following average dimensions:

Radius, 9.5 cm
Thickness, 3 cm
Height, 41.6 cm
Volume, 7.45 liters

Bradfute and Spiewak also give an expression by which the temperature in the stagnant region or "doughnut" can be estimated. The density in the doughnut is given by

$$a_1(\rho_1 - \rho) + \frac{a_2}{\rho_0}(\rho_0 - \rho)^2 - \frac{\phi x}{C_P \rho_0} = 0 \qquad (1)$$

where ρ = density in doughnut, grams per cubic centimeter
ρ_1 = core inlet density, grams per cubic centimeter
ρ_0 = core outlet density, grams per cubic centimeter
ϕ = specific power in doughnut, calories per cubic centimeter per second
x = temperature coefficient of density, grams per cubic centimeter per degree centigrade
C_P = specific heat, calories per gram per degree centigrade
a_1 = experimentally determined mixing coefficient, sec^{-1}
a_2 = experimentally determined mixing coefficient, sec^{-1}

The specific heat and temperature coefficient of density are evaluated at the core outlet temperature, which is usually about halfway between inlet and doughnut temperatures. The doughnut temperature can be found from the density by

$$T = T_0 + (\rho_0 - \rho)x$$

The mixing coefficients a_1 and a_2 were found to be directly proportional to the flow through the core.

$a_1 = 0.0227$ g/100 sec^{-1}

$a_2 = 1.65$ g/100 sec^{-1}

where g is the flow rate in gallons per minute. For the HRE the flow rate is 120 gal/min and

$a_1 = 0.02724\ sec^{-1}$

$a_2 = 1.98\ sec^{-1}$

Spiewak and Bradfute also made a calculation of the power density in the doughnut compared to the average for the core. Taking into account the flux distribution and density differences, they found that at 1000 kw the doughnut power density was only 10 per cent above the average for the core. In calculating temperatures for this report, the power density in the doughnut was assumed to equal the core average.

The inlet temperature is less than the outlet temperature by an amount which depends upon the power. For the HRE the difference has been found to be 0.030°C per kilowatt.

Other constants that were used in evaluating the doughnut temperatures are given in the following table. Densities are for water at 75 atm and are taken from N. E. Dorsey, "Properties of Ordinary Water Substance." Specific heats are from Report ORNL 156-12.

Temp., °C	ρ, g/cm³	x, g/cm³/°C	C_P, cal/g/°C
220	0.8449	0.001275	1.102
230	0.8318	0.001345	1.120
235	0.8251	0.001380	1.129
240	0.8180	0.001425	1.139
250	0.8033	0.001510	1.162
260	0.7878	0.001615	1.188

The differences in doughnut temperature and core outlet temperature which were calculated

using the above information are shown in Fig. 15. This particular curve is for a 250°C outlet; curves for other temperatures are only slightly different because of small differences in specific heat and temperature coefficient of density.

5.2 Calculation of Total Pressure

The following model is assumed for the purpose of calculating the relation between total pressure and the reactor power at which gas first appears. As the fluid enters the core it is assumed to be divided into two streams: one through the doughnut and the other through the main body of the core. Each region is assumed to be perfectly mixed, at uniform temperature, pressure, power density, and hydrogen concentration. The following procedure is then used:

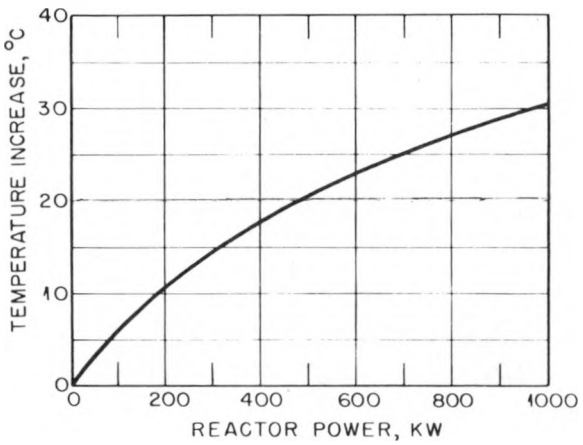

Fig. 15 — Calculated increase in doughnut temperature with respect to main body.

1. For a specified power density and outlet temperature, the temperatures in the two regions are estimated. For all practical purposes the temperature of the main body can be taken equal to the outlet temperature. The temperature of the doughnut can be calculated as shown in the previous section. Also the power densities in the two regions can be taken as equal.

2. The copper concentration in the main body is obtained from the copper and uranium inventories and the critical uranium concentration for the particular outlet temperature. The ratio of the copper concentration in the doughnut region to that in the main body is given by the ratio of the liquid densities.

3. The residence time in the doughnut is calculated from the temperature rise, power density, specific heat, and density of the solution. From the residence time and assumed volume the flow rate through this region can be obtained.

4. The required concentration of H_2 for complete recombination in solution is then calculated for each region.

5. From solubility data the required partial pressure of H_2 is calculated; the pressure due to $2H_2$ and O_2 is 50 per cent greater.

6. The total pressure in the region is then the sum of the gas pressure and the steam pressure.

Denote by the subscript 1 all properties pertaining to the main body and by 2 the properties in the hot region or doughnut.

Let p^t = total pressure of gas and steam, pounds per square inch absolute
p^s = steam pressure, pounds per square inch absolute
p^{H_2} = H_2 partial pressure, pounds per square inch
y = concentration of H_2 in solution, moles per liter
x = concentration of Cu^{+2} in solution, moles per liter
α = Henry's law coefficient for H_2, pounds per square inch per mole per liter
T = temperature in core, degrees centigrade
P = power density, kilowatts per liter
f = fraction of flow through region 1
t = residence time in core, seconds
$1 - \beta$ = fractional reduction in H_2 concentration in external loop due to recombination, about 0.08
A = rate of formation of H_2 by dissociation of water, 1.47×10^{-4} moles of H_2 per kilowatt

The specific rate constant for Cu^{+2} ions, k, is a function of temperature. The data from McDuffie et al.[3] were used to obtain

$$k = 7.16 \times 10^9 \exp(-12{,}200/T_{abs})$$

At equilibrium the rate of production of H_2 in each region is equal to the rate it is being removed. The removal is due both to recombination and to transport in and out of the region.

$$0 = AP_1 - k_1x_1y_1 - (y_1 - y_0)\frac{1}{t_1} \tag{2}$$

$$0 = AP_2 - k_2x_2y_2 + (y_0 - y_2)\frac{1}{t_2} \tag{3}$$

$$y_0 = \beta[fy_1 + (1 - f)y_2] \tag{4}$$

After substituting for y_0 from Eq. 3, subtract Eq. 2 from Eq. 1;

$$0 = y_1\left(\beta f\frac{t_2 - t_1}{t_1t_2} - \frac{1}{t_1} - k_1x_1\right) + y_2\left[\beta(1 - f)\frac{t_2 - t_1}{t_2t_1} + \frac{1}{t_2} + k_2x_2\right] \tag{5}$$

or

$$y_1 = My_2 \tag{5a}$$

where

$$M = \frac{k_2x_2 + \frac{1}{t_2} + \beta(1 - f)\frac{t_2 - t_1}{t_2t_1}}{k_1x_1 + \frac{1}{t_1} - \beta f\frac{t_2 - t_1}{t_2t_1}}$$

Then for incipient gas production

$$y_1 = AP_1\frac{1}{k_1x_1 + \frac{\beta}{t_1}\left(\frac{1}{\beta} - f - \frac{1 - f}{M}\right)} \tag{2a}$$

$$y_2 = AP_2\frac{1}{k_2x_2 + \frac{\beta}{t_2}\left[\frac{1}{\beta} - (1 - f) - Mf\right]} \tag{3a}$$

Only one of the above equations can be used — the one for the region where gas is first produced — since complete recombination in both regions is postulated. The problem of calculating H_2 concentration for incipient gas production in the remaining region while gas is coming out of solution in the other is somewhat simplified since the H_2 concentration in the other region is that in a saturated solution. Thus, if it is required to determine the H_2 concentration for bubble production in region 2 while gas is being removed from region 1, the following equations are written:

$$0 = AP - \left[k_2x_2 + \frac{1}{t_2} - \frac{\beta(1 - f)}{t_2}\right]y_2 + \frac{\beta f}{t_2}y_1 \tag{6}$$

$$y_1 = \frac{p_1^{H_2}}{\alpha_1} = \frac{2}{3}\frac{p^t - p_1^s}{\alpha_1}$$

$$= \frac{2}{3}\frac{\frac{3}{2}p_2^{H_2} + p_2^s - p_1^s}{\alpha_1}$$

$$= \frac{\alpha_2}{\alpha_1}y_2 + \frac{2}{3}\frac{p_2^s - p_1^s}{\alpha_1} \tag{7}$$

After substituting Eq. 7 into Eq. 6

$$y_2 = \frac{AP + \frac{2}{3}\frac{\beta f}{t_2}\frac{p_2^s - p_1^s}{\alpha_1}}{k_2x_2 + \frac{1}{t_2}\left[1 - \beta f\frac{\alpha_2}{\alpha_1} - \beta(1 - f)\right]} \tag{8}$$

ACKNOWLEDGMENTS

The work reported in this article was performed by the following ORNL personnel: S. E. Beall, Section Chief, HRE; D. M. Eissenberg; J. J. Hairston, Operations Group Leader; J. W. Hill, Operations Group Leader; S. I. Kaplan; V. K. Paré; T. H. Thomas, Operations Group Leader; S. Visner, Experimental Physics Group Leader; P. M. Wood; E. L. Compere, Chemical Division Consultant; H. F. McDuffie, Chemical Division Consultant; U. Koskela, Analytical Laboratory Supervisor; and C. H. Secoy, Chemical Division Group Leader.

REFERENCES

1. S. E. Beall et al., HRP Quarterly Progress Report, Report ORNL-1554, Mar. 31, 1953, p. 13.
2. J. W. Boyle, J. A. Ghormley, C. J. Hochanadel, W. R. Kieffer, and T. J. Sworski, Radiation-induced Decomposition, Reactor Sci. Technol., 3(1): 31-50 (March 1953).

3. H. F. McDuffie, E. L. Compere, H. H. Stone, L. F. Woo, and C. H. Secoy, Homogeneous Catalysis of the Hydrogen-Oxygen Reaction, Reactor Sci. Technol., 4(2): 23–42 (June 1954).
4. Reactor Handbook, 1st ed., Vol. 2, Chap. 4.7, pp. 806–812, AEC Technical Information Service, Oak Ridge, 1953.
5. P. N. Haubenreich, Use of Copper as an Internal Recombination Catalyst in the ISHR, Report ORNL-CF-53-4-292, April 1953.
6. I. Spiewak and J. O. Bradfute, Effect of Density Difference on Flow in the HRE Core, Report ORNL-CF-51-10-165, Oct. 17, 1951.
7. S. E. Beall et al., HRP Quarterly Progress Report, Report ORNL-1605, July 31, 1953, p. 5.
8. S. E. Beall et al., HRP Quarterly Progress Report, Report ORNL-1678, Jan. 31, 1954, pp. 7–11.

ABOUT THE AUTHORS

Paul N. Haubenreich is a development engineer in the Design Section of the Reactor Experimental Engineering Division at ORNL. He received the B.S. degree in mechanical engineering at the University of Tennessee in 1950. He spent the next year in the Oak Ridge School of Reactor Technology as part of the first regular group to attend the school. After completion of the ORSORT course in 1951, he joined the Laboratory staff on the Homogeneous Reactor Project. Since then he has worked on process analysis and general reactor-feasibility studies.

S. Visner is now with Combustion Engineering-Superheater, Inc. He was formerly a head physicist with the Homogeneous Reactor Project at Oak Ridge National Laboratory where he was a group leader in charge of the experimental testing of the Homogeneous Reactor Experiment. In 1941 he joined the group at Columbia University which was investigating the separation of uranium isotopes by gaseous diffusion; this group later became the SAM Laboratories of the Manhattan Project. He transferred to the K-25 Gaseous Diffusion Plant in Oak Ridge in 1945, where he was a department head in charge of nuclear safety and health physics. In 1949 and 1950 he investigated gas-transport phenomena in the Laboratory Division at K-25, receiving the Ph. D. in physics from the University of Tennessee in 1951. He had received the B.S. degree in 1937 and the M.S. degree in 1938 from the College of the City of New York with a major in physics. In 1951 he joined the Homogeneous Reactor Project at Oak Ridge.

REACTOR DATA TABLE 4

Previous issues of the Reactor Data Table have been designated as revisions of the original. In reality, the successive so-called "revisions" have superseded previous ones only in part, making it necessary for the reader to refer to all the issues. In recognition of the inappropriateness of continuing the former numbering system, a new series designation has been initiated. The correlation of the previous issues of the Reactor Data Table with their position in the new series is to be understood as follows:

Reactor Data Table 1: TID-5022, August 1951; issued as supplement to Reactor Sci. Technol., 1(2) (TID-72); [all data but those on the British Experimental Pile (BEPO) are superseded].

Reactor Data Table 2: TID-5022 (Rev. 1), August 1952; issued as supplement to Reactor Sci. Technol., 2(2) (TID-2002).

Reactor Data Table 3: TID-5022 (Rev. 2), September 1953; bound in Reactor Sci. Technol., 3(3) (TID-2010).

Table 4, presented herewith, lists revised data on the Sodium Graphite Reactor (SGR) and the Oak Ridge National Laboratory Research Reactor (ORR) and presents information on 18 reactors not incorporated in previous tables. Continuing the practice established with Table 3, the current table has been bound into this issue of Nuclear Science and Technology. A separate supplement has not been issued.

The information in this table is the best obtainable on the date shown in the first line. Many of the data are tentative since several of the reactor designs are undergoing frequent changes.

The editors welcome your criticism and suggestions. We are especially indebted to G. A. Young of the Technical Information Service, Oak Ridge, for his assistance in the preparation of this table.

REACTOR DATA TABLE 4

		ORNL Pressurized-water Package Power Reactor	Homogeneous Reactor Test (HRT or HRE-2)	Thermal Breeder Reactor (TBR-K23)	Oak Ridge Research Reactor (ORR), new design
General	Date of data	Sept. 17, 1954	Oct. 1, 1954	Oct. 1, 1954	Sept. 29, 1954
	Location & operator	Fort Belvoir, Va; Corps of Engineers, U. S. Army	ORNL	ORNL	ORNL
	Purpose	Power & heat at remote base	Experimental power	Power production	Research
	Neutron energy	Thermal	Thermal	Thermal	Thermal
	Status	Const. contract to be awarded Dec. 1954	Design and construction	Reference design	Detailed design (const. to start Feb. 1955)
Power	Reactor heat, kw	10,000	5000 (core) + 220 (refl.)	320,000 (core) + 130,000 (blanket)	5000
	Net electric, kw	1700 or 1000 + 3535 steam	300 (existing turbogenerator limit)	125,000	
	Steam temp. & pressure	382°F; 200 psia	470°F; 520 psia	478°F; 560 psia	
	Heat flux: Btu/sq ft/hr Max./av.	 55,900 4			 32,000 av. 2.1
	Power density, kw/liter	71.1	17.3 (av. core); 10 (av. core + circ. system)	100 (core); 17 (core + circ. system); 11 (blanket); 7 (blanket + circ. system); 11 (over-all)	50
	Specific power, kw/kg of FM	565	2300 (av. core); 1300 (av. core + circ. system)	77,000 (core); 13,000 (core + circ. system); 2300 (blanket); 1300 (blanket + circ. system); 3600 (over-all)	~1250
Materials & amounts	Fuel & enrichment	U (93.5%)	UO_2SO_4 in D_2O (93% U^{235})	Core: UO_2SO_4 (U^{233}) soln. in D_2O; blanket: U-Th oxide in D_2O	U (93.4%)
	Amount of fuel, kg	18.9	5.0	Core: 25 (U^{233}); blanket: 100 (U^{233}); 21,000 (Th)	3–4
	Fuel elements	Plates: UO_2-s.s.-ZrB_2 matrix			MTR type (plates: 17% U; 83% Al; 0.050 × 2.8 × 24.5 in.)
	Fuel-element jacket	S.s.			Al
	Moderator	H_2O	D_2O (700 kg)	D_2O (19,000 liters in core & circ. system; 21,000 liters in blanket & circ. system)	H_2O
	Reflector	H_2O	D_2O (2000 kg)		Be & H_2O
	Shield	Concrete	Barytes concrete + H_2O	Concrete	H_2O & barytes concrete
	Primary coolant	H_2O	Circulating fuel	Circulating fuel	H_2O

Fuel	Temperatures: Max., °F Sheath, °F	 566 554			 ~200 ~200
	Consumption, g/day	1.4 g/Mwd	6.6	540 (Th)	~6.5
	Av. cycle time	15 Mw-yr; 2.5 yr at 0.6 load demand		Core: 1–10 days (filtration), 100 days (Thorex); blanket: 270 days (Thorex)	~6 months
	Burn-up per cycle, %	42 (U^{235} atoms)			~15
Coolant	Temperatures: Inlet, °F Outlet, °F	 432 450	 494 572	 510 572	 120 135
	Velocity: Ft/sec Gpm Cfm	 4.3 (core) 4000	 10–20 (core + circ. system); 5–10 (refl. + circ. system) 400 (core + circ. system); 230 (refl. + circ. system)	 12–25 (core); 10–15 (blanket) 32,000 (core); 13,000 (blanket)	 4.0 2500
	Pumping power req'd	~30 kw	15 hp (core); 3 hp (refl.)	1200 hp (core); 600 hp (blanket)	75 hp
	System pressure, psia	1200	2000	2000	Nonpressurized
Neutron-flux density	Thermal: Max., $n/cm^2/sec$ Av., $n/cm^2/sec$	 $\sim 10^{14}$ $\sim 2.7 \times 10^{13}$	 1.1×10^{14} (core); 7.3×10^{13} (refl.) 8.2×10^{13} (core); 3.8×10^{13} (refl.)	 6×10^{15} (core); 9×10^{14} (blanket) 3×10^{15} (core); 9×10^{13} (blanket)	 8×10^{13} 3×10^{13}
	Fast: Max., $n/cm^2/sec$ Av., $n/cm^2/sec$	 $\sim 3 \times 10^{13}$	 2.0×10^{14} (core); 7.5×10^{13} (refl.); (total above thermal)	 2×10^{15} (core); 7×10^{14} (blanket); (total above thermal energy)	 1.7×10^{13}
	Intermediate (av.), $n/cm^2/sec$				
	Production rate, g/day			45 (net U^{233})	
Dimensions	Core	Cylinder: 22 in. dia. × 22 in. high	Sphere: 32 in. dia.; ¼ in. Zircaloy-2 wall; 290 liters soln.	Sphere: 6 ft dia.; ½ in. Zircaloy-2 wall; 3200 liters soln.	30 × 53 × 60 cm
	Reflector thickness	13 in.	13¾ in.; 1550 liters D_2O	2 ft blanket; 11,800 liters slurry	7.5–15 cm
	Shield thickness	8.5 ft for tolerance levels	Roof: 5 ft barytes concrete; operating-gallery wall: 5½ ft barytes aggregate & H_2O; around reactor: 2 ft H_2O or aggregate & H_2O	8–9 ft	H_2O, 4 ft; concrete, 7 ft
	Over-all dimensions	Reactor & shield: 32 × 27 × 19 ft; building: 82 × 45 × 39 ft	Pressure vessel: 60 in. I.D.; 4 in. carbon steel clad with 0.4 in. s.s.; shield inside dimensions: 54 × 26 × 20 ft high; pit: 54 × 31½ × 25 ft deep	Pressure vessel: 10 ft I.D., 6 in. carbon steel clad with 0.4 in. s.s.	Pool: 10 × 20 × 26 ft deep, surrounded by barytes concrete
	Control method	5 rods; absorber: B_4C–Cu, s.s. cladding	Fuel concn.; neg. temp. coeff.	Fuel concn.; neg. temp. coeff.	Cd-U^{238} shim safety rods
	References	ORNL-1613	ORNL-1678; ORNL-1753; ORNL-1780	ORNL-1642	ORNL, CF-54-3-49
	Remarks	See footnotes a & b	See footnote c		See footnote d

		Borax Reactor (Borax-I)	Borax-II	Boiling Experimental Reactor (BER)	Central Station Water Reactor (CSWR)
General	Date of data	Sept. 1954	Sept. 1954	Sept. 1954	Sept. 1954
	Location & operator	NRTS; ANL	NRTS; ANL	Not determined; ANL	Not determined; ANL design
	Purpose	Boiling experiment	Boiling experiment	Experimental power	Power production
	Neutron energy	Thermal	Thermal	Thermal	Thermal
	Status	Operation	Construction; operation scheduled Nov. 1954	Design	Inactive pending completion of BER
Power	Reactor heat, kw	1400 (26,000 in excursions)	6000 est.	20,000	1,000,000
	Net electric, kw			5000 (gross)	280,000
	Steam temp. & pressure			488°F; 600 psig	
	Heat flux: Btu/sq ft/hr	20,000 max.	120,000 max.	130,000 max.	400,000 max. final (unflattened); 300,000 initial (flattened)
	Max./av.	1.85	~2	2.7	2.5 final; 1.85 initial
	Power density, kw/liter	10		13 (av. core); 22 (av. coolant); 35 (max. core); 60 (max. coolant)	20 av.
	Specific power, kw/kg of FM	330	1.0 est.	420	2000 av.
Materials & amounts	Fuel & enrichment	U-Al (93%)	U-Al (93%)	U-Zr-Nb (natural & 93%)	U-Zr-Nb (natural or depleted)
	Amount of fuel, kg	4.2	6–7	5 tons natural U; 15 kg U^{235}	39 tons natural U; 41.7 tons fuel alloy
	Fuel elements	MTR type	MTR type, 10 plates per element	Natural U plates: 0.25 in. thick × 4 ft long; enriched U plates: 0.10 in. thick × 4 ft long	Twisted ribbon
	Fuel-element jacket	Al	Al	Zircaloy-2	Zircaloy-2
	Moderator	H_2O	H_2O	H_2O	D_2O (120 tons)
	Reflector	H_2O	H_2O	H_2O	D_2O
	Shield	Earth	Concrete & earth	Concrete	Concrete
	Primary coolant	H_2O	H_2O	H_2O	D_2O

Fuel	Temperatures: Max., °F Sheath, °F	400 (640 max. in excursions) 360	~450 ~450	610 520	600 545
	Consumption, g day	Not operated on continuous basis	6 (est.)	23	31 tons yr
	Av. cycle time			Natural U plates: 9 yr; enriched U plates: 2 yr	
	Burn-up per cycle, %			Natural U plates: 1; enriched U plates: 40	
Coolant	Temperatures: Inlet, °F Outlet, °F	 355 (steam)	 425	 110 488	 92 486 (steam)
	Velocity: Ft/sec Gpm Cfm	Natural circulation	Natural circulation	3 (in core channels)	 8000
	Pumping power req'd			50 hp	
	System pressure, psia	130 or atmospheric (rebuilt to operate at 300 psig)	300 psig		600; steam pressure, 600
Neutron-flux density	Thermal: Max., $n/cm^2/sec$ Av., $n/cm^2/sec$	 2×10^{13} 1×10^{13}	 6×10^{13} (est.) 3×10^{13} (est.)	 3×10^{13} 10^{13}	
	Fast: Max., $n/cm^2/sec$ Av., $n/cm^2/sec$	 Not measured Not measured		 8×10^{12} (virgin) 3×10^{12} (virgin)	
	Intermediate (av.), $n/cm^2/sec$	Not measured			
	Production rate, g/day				103,000 g Pu^{239}/yr; 13,600 g Pu^{241}/yr
Dimensions	Core	Approx. cylinder: 1.5 ft dia. × 2 ft long	Approx. cylinder: 2 ft dia. × 2 ft high	4 ft dia. × 4 ft high	Cylinder: 13.5 ft dia. × 12 ft high; 295 fuel assemblies
	Reflector thickness	12 in. av.	10 in. av.	12 in.	Radial: 1.25 ft; vert.: 1.5 ft
	Shield thickness	Variable	3–5 ft concrete + earth	8 ft	8 ft
	Over-all dimensions	Reactor vessel: 4 ft dia. × 14 ft high	Reactor vessel: 4.5 ft dia. × 20 ft high	Reactor tank: 6 ft I.D. × 22 ft high	Pressure vessel: 16 ft I.D., 43 ft high, 4 in. thick walls
	Control method	Steam voids; control rods	Steam voids; Cd rods	Hf rods; steam voids	Steam voids
	References	ANL-5211; ANL-5272		ANL-5261; ANL-5272	ANL-5208; ANL-MT-45
	Remarks			See footnote e	See footnote f

		Experimental Breeder Reactor-2 (EBR-2)	Power Breeder Reactor (PBR)
General	Date of data	Sept. 1954	Sept. 1954
	Location & operator	Probably NRTS; ANL	
	Purpose	Experimental; breeding & power prod.	Power production
	Neutron energy	Fast	Fast
	Status	Design & development	Reference design (ANL)
Power	Reactor heat, kw	62,500 (total); 50,000 (core)	940,000 (total); 800,000 (core)
	Net electric, kw	15,000+	300,000
	Steam temp. & pressure	900°F (superheat 280°F); 1800 psig	900°F (superheat 280°F); 1800 psig
	Heat flux: Btu/sq ft/hr	1.3×10^6 max.	1,250,000 max.
	Max./av.	1.5	1.4
	Power density, kw/liter	1000 (core)	1000 (core)
	Specific power, kw/kg of FM	550 (Pu); converter, 330 (U^{235})	1800
Materials & amounts	Fuel & enrichment	Pu-U^{238} (29% Pu)(converter, 45% enriched U)	Pu-U^{238} (9.1% Pu)
	Amount of fuel, kg	90 (Pu); converter, 150 kg (U^{235})	450
	Fuel elements	Pin type	Pin type
	Fuel-element jacket	S.s. (perhaps Zr)	S.s.
	Moderator		
	Reflector	Depleted U blanket	Depleted U blanket
	Shield	Concrete	Concrete
	Primary coolant	Na	Na

Fuel	Temperatures: Max., °F Sheath, °F	 1390 1025	 1325 1025
	Consumption, g/day	48	700
	Av. cycle time	130 days	140 days
	Burn-up per cycle, %	2	2
Coolant	Temperatures: Inlet, °F Outlet, °F	 822 1000	 618 1000
	Velocity: Ft/sec Gpm Cfm	 35 max. 9000	 35 63,000
	Pumping power req'd		
	System pressure, psia	Atmospheric	Atmospheric
Neutron-flux density	Thermal: Max., $n/cm^2/sec$ Av., $n/cm^2/sec$		
	Fast: Max., $n/cm^2/sec$ Av., $n/cm^2/sec$	 4.5×10^{15} 3×10^{15}	 1.2×10^{16} 9×10^{15}
	Intermediate (av.), $n/cm^2/sec$		
	Production rate, g/day	81	1200
Dimensions	Core	Cylinder: 1.4 ft dia. × 1.2 ft long; V., 50 liters	Cylinder: 3.5 ft dia. × 3 ft long; V., 800 liters
	Reflector thickness	2 ft (blanket)	2 ft (blanket)
	Shield thickness		
	Over-all dimensions		
	Control method	Movable fuel rods	Movable fuel rods
	References	ANL-5208	ANL-5208
	Remarks	See footnote g	See footnote h

		Los Alamos Omega West Reactor	Los Alamos Power Reactor Experiment (LAPRE)	Sodium Reactor Experiment (SRE)	Sodium Graphite Reactor (SGR) Reference Design
General	Date of data	Sept. 1954	Sept. 1954	Sept. 15, 1954	Sept. 15, 1954
	Location & operator	LASL	LASL	Santa Susana, Calif.; North American Aviation, Inc.	Not determined
	Purpose	Research	Experimental; power production	Experimental; power reactor dev.	Power production
	Neutron energy	Thermal	Thermal	Thermal (400°C)	Thermal (400°C)
	Status	Construction; completion scheduled early 1955	Construction; completion scheduled Dec. 1954	Construction	Reference design (NAA)
Power	Reactor heat, kw	5000 max.	2000	20,000	1,000,000
	Net electric, kw				300,000
	Steam temp. & pressure				
	Heat flux: Btu sq ft hr Max. av.		177,000	340,000 (max.) 1.7	872,000 (max.) 2.24
	Power density, kw liter		46.5	4.2 (av.)	15.6 (av.)
	Specific power, kw kg of FM		470	290 (av.)	1250
Materials & amounts	Fuel & enrichment	U (93.2%)	UO_3 (93.4%) dissolved in H_3PO_4	U (2.75%)	Th-U (2.24% U^{233})
	Amount of fuel, kg	~6	3.9 in core; 8.4 total	58	0.885 tons U^{233}
	Fuel elements	MTR type		Rods	Rods
	Fuel-element jacket	Al	S.s. tank, type 347, Au-plated	S.s.	Zr
	Moderator	H_2O	H_2O	Zr-canned graphite	Zr-canned graphite
	Reflector	H_2O	Steel & H_2O shield	S.s.-canned graphite	Zr-canned graphite
	Shield	H_2O & magnetite concrete	H_2O; Pb; concrete	Fe & concrete, toluene-cooled	Fe & concrete
	Primary coolant	H_2O	H_2O, supercritical & 2-phase (internal heat exchanger)	Na	Na

Fuel	Temperatures: Max., °F Sheath, °F		850	1200 1000 (max.)	1800 1000 (max.)
	Consumption, g/day			26.2 (at 20 Mw)	1150
	Av. cycle time		1.2 sec (fuel circul. rate, 1200 gpm)		800 to 1200 days
	Burn-up per cycle, %			0.3 (max.)	2–3 total Th-U
Coolant	Temperatures: Inlet, °F Outlet, °F		100 825	500 960 (mixed mean)	500 1000 (mixed mean)
	Velocity: Ft/sec Gpm Cfm	2700	Inlet, 15; outlet, 120 12	5 1200 (primary system)	15 max. 60,500
	Pumping power req'd		15 hydraulic hp	53 hp (all Na pumps)	
	System pressure, psia		Inlet, 3900 psi; outlet, 3600 psi; 5000 psia max.	3 psig	3 psig
Neutron-flux density	Thermal: Max., $n/cm^2/sec$ Av., $n/cm^2/sec$	$\sim 5 \times 10^{13}$	2.6×10^{13} 1.7×10^{13}	1.3×10^{14} 5.3×10^{13}	1.1×10^{14} 5×10^{13}
	Fast: Max., $n/cm^2/sec$ Av., $n/cm^2/sec$		1.4×10^{14} (all neutrons above thermal); 9.9×10^{13} (above 20 kev) 9×10^{13} (all neutrons above thermal); 6.4×10^{13} (above 20 kev)	3.1×10^{14} 1.25×10^{14}	2.5×10^{14} 1.2×10^{14}
	Intermediate (av.), $n/cm^2/sec$		3.4×10^{13} (between thermal & 20 kev)		
	Production rate, g/day			13	
Dimensions	Core	24 × 27 × 15 in.	Cylinder: 15 in. dia. × 16 in. high	Cylinder: 6 ft dia. × 6 ft high	Cylinder: 17 ft dia. × 10 ft high
	Reflector thickness		Steel, 3 in.; H_2O, 4 ft	2 ft	30 in.
	Shield thickness	Concrete, 5 ft min.; H_2O, 17 ft top	H_2O, 4 ft; Pb, 10 in.; concrete, 5.5 ft	Fe, $7\frac{3}{4}$ in.; insulation, 9 in.; concrete, 5 ft 4 in.	Fe, 6 in.; concrete, 7 ft 7 in.
	Over-all dimensions	Octagon: 18 ft face to face × 23 ft high	Reactor vessel: cylinder, 21 in.; top flange, 32 in.; ht. includ. circulator, 12.6 ft; over-all vol., 119 liters	Reactor tank: cylinder, 11 ft dia. × 21 ft high	Reactor tank: cylinder, 23 ft dia. × 25 ft high
	Control method	Rods, B^{10} in steel sheath	B^{10} rods; temp. coeff.; vessel geometry; sol. removal	B-Ni rods & falling balls	B-Ni rods & balls
	References	LA-1648	LAMS-1611, LA-1610	NAA-SR-956; NAA-SR-1027; NAA-SR-1049	NAA-SR-266; NAA-SR-283
	Remarks		See footnote k	See footnote l	See footnote m

		Ground Test Reactor (GTR)	Tower Shielding Facility (TSF)	Pressurized Water Reactor (PWR)
General	Date of data	Sept. 17, 1954	Sept. 1954	Apr. 22, 1954
	Location & operator	Fort Worth, Tex.; Consolidated Vultee	Oak Ridge, Tenn.; ORNL	Shippingport, Pa.; Duquesne Light Co.
	Purpose	ANP shielding & radiation-effect research	Shielding research	Power production
	Neutron energy	Thermal	Thermal	Thermal
	Status	Operation	Operation	Preliminary design (WAPD)
Power	Reactor heat, kw	100	500 (max.)	232,000, 3-loop operation
	Net electric, kw			60,000 net based on 3 coolant loops in operation, 4 loops provided
	Steam temp. & pressure			
	Heat flux: Btu/sq ft/hr Max./av.			118,000 av. 3.17
	Power density, kw/liter	0.91		91.2
	Specific power, kw/kg of FM	25		700–1400
Materials & amounts	Fuel & enrichment	U (93.5%)	U (93.4%)	U–12% Mo (1.5–3.0% U^{235})
	Amount of fuel, kg	4.0	3.5–4.0	
	Fuel elements	Plates: 22% U; 78% 2S Al; 0.060 × 3 × 24 in.	MTR type with 2 in. Pb shielding in upper end boxes	Rods, 0.3 in. O.D. × 10.3 in. long
	Fuel-element jacket	72S Al	Al	Zircaloy-2, 0.030 in. thick
	Moderator	H_2O		H_2O
	Reflector	H_2O	H_2O	H_2O & steel
	Shield	H_2O in pool surrounding reactor; H_2O + add'l mat. as desired when in portable shield tanks		H_2O & concrete
	Primary coolant	H_2O		H_2O at 2000 psi

Fuel	Temperatures: Max., °F Sheath, °F			1070 630 max.
	Consumption, g day			234
	Av. cycle time			~115 days at full power
	Burn-up per cycle, %			3000 Mwd ton average
Coolant	Temperatures: Inlet, °F Outlet, °F	55–70 75–90		508 542
	Velocity: Ft sec Gpm Cfm	Natural convection when in pool; 35 gpm when in portable tanks		17.9 51,300; 19.4×10^6 lb hr
	Pumping power req'd			3100 hydraulic hp
	System pressure, psia			2000 psi
Neutron-flux density	Thermal: Max., n/cm² sec Av., n/cm² sec	1.1×10^{12} 6×10^{11}		$8 \times 10^{13} - 16 \times 10^{13}$ $2.5 \times 10^{13} - 5 \times 10^{13}$
	Fast: Max., n/cm² sec Av., n/cm² sec	$\sim 4 \times 10^{11}$ $\sim 3 \times 10^{11}$		
	Intermediate (av.), n/cm² sec	3.8×10^{11} (Au resonance)		
	Production rate, g day			
Dimensions	Core	15 × 21 × 24 in. high		Cylinder: 4.33 ft dia. × 6.08 ft long
	Reflector thickness	4 in. min. in portable tanks; 8 ft in pool		8 in. H_2O; ½ in. steel
	Shield thickness	8 ft H_2O in pool; 4 in. H_2O + add'l H_2O or other materials in portable tanks		Fe, 11 in.; H_2O, 30 in.; concrete, 5 ft
	Over-all dimensions	22 in. × 30 in. × 16 ft high, bare reactor	Reactor tank: 12 ft dia. × 12 ft high; total wt.: 55 tons; tower ht.: 315 ft; tower separations: 200 & 100 ft; reactor pool: 20 × 20 × 25 ft deep	Pressure vessel: cylinder, 9.1 ft dia. × 28 ft long
	Control method	Cd-Pb rods		Homogeneous chem. control with mech. shutdown rods
	References	CVAC-38; CVAC-163; CVAC-215; CVAC-234	ORNL-1550; ORNL-1740	WAPD-MRP-44
	Remarks	See footnote o	See footnote p	See footnote q

FOOTNOTES

[a]Also known as the Army Power Package Reactor (APPR).

[b]The contract for the design, construction, and testing of the reactor has been awarded to the American Locomotive Co.

[c]D_2O reflector may be replaced with a ThO_2 slurry blanket for breeding or a UO_2SO_4 solution blanket for plutonium-production studies. Facilities will be installed for continuous removal of insoluble fission products from core system.

[d]Information given is preliminary.

[e]Flow of steam: 60,000 lb/hr; flow of condensate: 120 gpm.

[f]Supplies two turbogenerators with 3.8×10^6 lb of steam per hour.

[g]The data given are the preliminary design specifications for EBR-2. Many of the variables are being optimized and refined and are, therefore, subject to change.

[h]The data given are based on preliminary design studies which were made to provide a basis for the design of EBR-2.

[i]Two duplicate reactors to be installed in submarine. The information given applies to only one of these.

[j]The values given after "alt. design" represent an alternative reactor design being considered.

[k]Experimental facilities limited; 13 ports 1 to 8 in. dia. available. No turbine operation at present; steam exhausted to atmosphere.

[l]Secondary coolant: Na; heat will be discharged to atmosphere.

[m]Supplies 800°F psig steam.

[o]Reactor is portable and can be operated in various shield tanks. A crane permits operation at heights up to 75 ft above ground.

[p]Core is identical with BSF except for Pb shielding.

[q]Dry saturated 600 psia steam produced in heat exchangers.

REACTOR FUTURES

A Conceptual Design for the Army Package Power Reactor

ROBERT S. LIVINGSTON

Oak Ridge National Laboratory

October 15, 1954

ABSTRACT

Small compact "package" reactor power plants have been proposed for use in remote locations. Such a package reactor power plant, rated at 1000 kw of net electric power and 3500 kw of steam for heating purposes, has been designed at the Oak Ridge National Laboratory. The total thermal output of the reactor is 10,000 kw. The fuel plates consist of highly enriched UO_2 embedded in a matrix of stainless steel, with stainless-steel cladding. The core is moderated and cooled with circulating water, pressurized to 1200 psia. The saturated steam that drives the turbogenerator is produced in a heat exchanger at 200 psia. Steam from the heat exchanger is also used, at a reduced pressure, for space heating.

The reactor is loaded with approximately 18 kg of U^{235} and will supply 15 Mw-years of energy before refueling is required. This corresponds to 2.5 years of operation at an average load factor of 60 per cent. Burn-out poison in the form of B_4C is incorporated to reduce the reactivity excursion and thus facilitate control.

The major objective was to design a reactor that would require a minimum of development effort and yet be reliable and inexpensive. The estimated capital investment, exclusive of development work and exclusive of uranium, is $1,700,000. The estimated cost per kilowatt-hour for net electric and steam power at the bus, based on a 60 per cent average load demand, is 5.33 and 1.23 cents, respectively.

1. INTRODUCTION

The concept of the "package" reactor was advanced in 1952 by L. R. Hafstad of the Atomic Energy Commission (AEC), Reactor Development Division, and by A. M. Weinberg of the Oak Ridge National Laboratory (ORNL). It was suggested then that a small compact power-producing reactor might be designed to supply power in inaccessible or remote locations. Shortly thereafter a small group was established at ORNL, under the leadership of W. H. Jordan, to evaluate various reactor types and to select one that appeared to be sufficiently developed to permit the design of a thoroughly reliable sys-

tem that could run for long periods of time without reloading. The package reactor work was later continued under the direction of R. S. Livingston and A. L. Boch, after Jordan became head of the Aircraft Nuclear Propulsion (ANP) Project at the Laboratory.

It appeared at an early date that a package reactor such as was being studied would admirably suit the requirements of the Army for use at certain of its remote arctic bases. The study was then oriented more specifically toward this objective. Parallel studies were made by the Corps of Engineers and by the Operations Research Office at the Johns Hopkins University to determine which specific class of military installations would be most suitable for the efficient use of the nuclear power system and its singular characteristic of compact fuel.

In July 1954, a report was issued, summarizing the design and development work done at ORNL on the reactor system deemed most adaptable to the package concept. This report, ORNL-1613,* A Conceptual Design of a Pressurized-water Package Power Reactor, is now being used by a large group of private firms who have indicated an interest in, and a competence for, designing and constructing a reactor similar to the ORNL concept. The Army Reactors Branch of the AEC, in cooperation with the Corps of Engineers, now plans to build a prototype reactor at Fort Belvoir, Virginia, to be used in establishing a firm engineering design for an arctic unit and to provide a training center for military personnel who will be required to operate the equipment at remote bases.†

This article has been prepared as a summary of the contents of the larger ORNL report. It describes the work done by the small group of engineers and physicists on the design of a reactor to supply heat and electricity specifically to an arctic military base. The electric power and heat generated are specified to be 1000 and 3535 kw, respectively.

*As of the date of the preparation of this manuscript, Report ORNL-1613 has not been issued to the Reactor General distribution. Following receipt of proposals for design and construction of the Army Package Power Reactor (APPR) at Fort Belvoir, it is planned to issue the report to the customary distribution.

†Certain changes in the specifications to be described herein were made to adapt the reactor installation to the special conditions at Fort Belvoir. It is not the purpose of this article to review changes or to comment further on this aspect of the project.

The reactor described in this report is only one of a number of types being studied at this laboratory and elsewhere for this type of application. The particular reactor design that was chosen is a heterogeneous water-cooled and water-moderated stainless-steel system. It was selected primarily because of the advanced stage of engineering knowledge in this area and the small amount of development work which would be required. The fuel plates are similar in structure to the Materials Testing Reactor (MTR) plates; they consist of highly enriched UO_2 embedded in a matrix of stainless steel and clad with stainless steel. The choice of stainless steel was governed by the objective of holding the initial costs of the reactor to a minimum. Although the critical mass is somewhat higher than for zirconium-clad fuel plates, the cost of fabrication of the stainless steel is believed to be very much less than for zirconium. The penalty for the larger critical mass is not serious in view of the various factors contributing to the gross cost of power in this system.

The principal objective of this design study was to establish a conceptual design for a complete system in sufficient detail to provide assurance of the feasibility of the reactor and to permit the preparation of realistic cost estimates. Standard components were used wherever possible. Special components, such as the pressure vessel, heat exchangers, and control-rod mechanisms, were designed to be well within the limits of present-day technology. Much of the design was done in conjunction with equipment manufacturers, who supplied courtesy bids on all the major components. It is realized that many factors have not been completely optimized in this conceptual design. This task should be undertaken when the detailed working plans for the reactor are prepared. The estimated costs are based on construction at Oak Ridge and do not include any development costs. Therefore the cost of construction at another site would of course need to be adjusted appropriately.

2. GENERAL DESCRIPTION OF REACTOR

2.1 Site Conditions

A major factor influencing the design of the reactor power plant, in addition to the basic

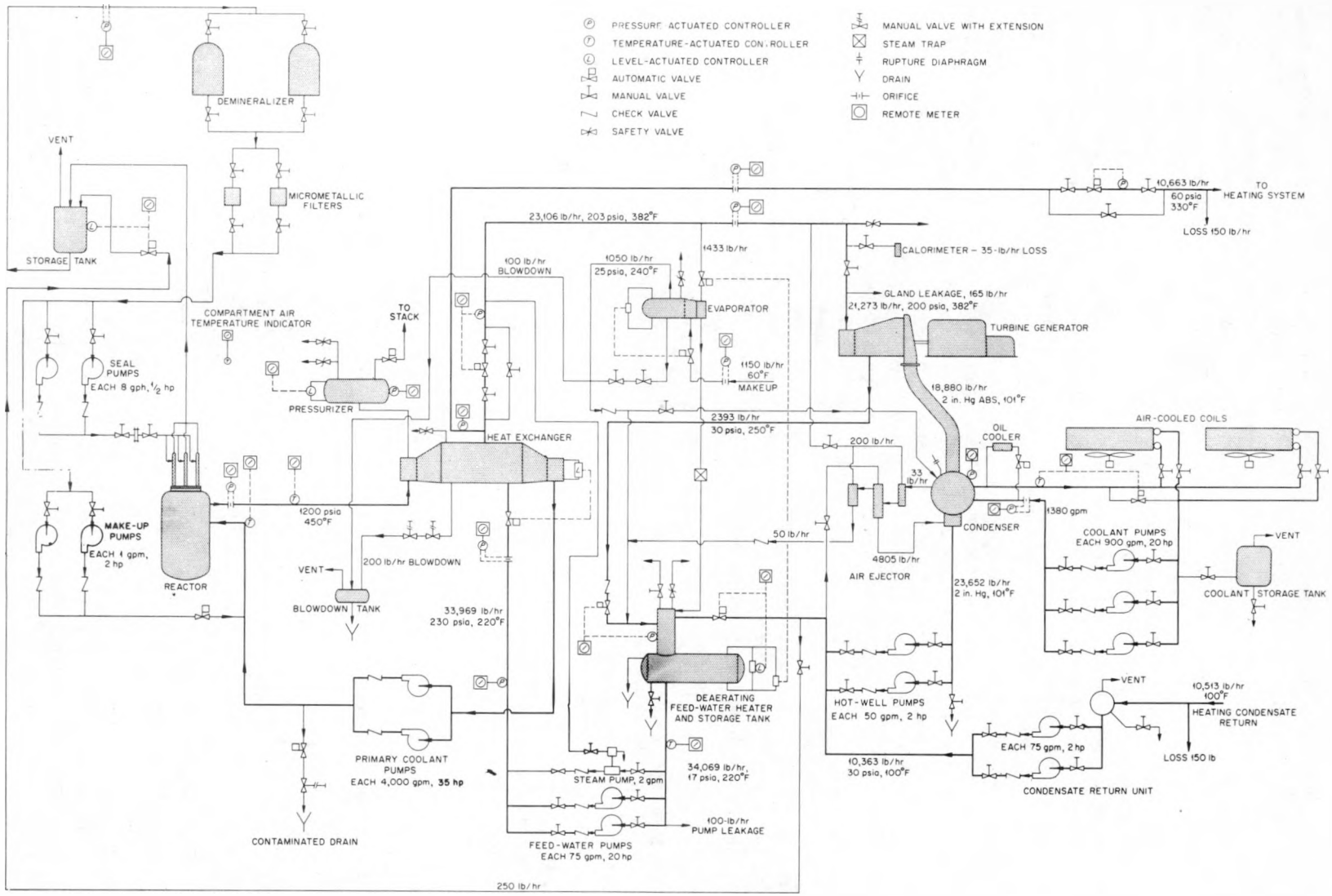

Fig. 1—Flow diagram of the reactor power cycle.

power output requirement, is its intended location. The chief usefulness of the package reactor lies in the fact that it can be located in an extremely remote place where transportation of fuel is difficult or perhaps impossible for extended periods of time. A typical application for which a nuclear-powered plant would be well suited has been taken to be an AC&W station. These installations are often in remote locations where accessibility may be limited to air transportation and where the construction period may be as short as three months per year. If the reactor is to be used at these stations, such physical characteristics of the site as weather conditions and the terrain must be properly considered insofar as they will directly affect reactor performance. The following site conditions were considered in the design of the plant:

1. The water supply is limited to amounts that can be hauled by trucks.
2. All structures must be constructed above grade, owing to the existence of permafrost.
3. The ambient-air temperature range is from −50 to +75°F.
4. The maximum wind velocity is 50 mph.
5. All equipment and materials for construction and operation must be transportable by air, with the exception of aggregates for concrete, which are available at the site.

Although these conditions did not impose serious limitations in reactor design, their effect can be noted in various parts of the reactor system.

2.2 *Reactor Cycle*

The power cycle for the APPR is composed of two main systems, the primary coolant and the secondary steam systems. Associated with these are the ancillary systems for the primary coolant make-up, the pressurizer, the space heating, the condenser coolant, and the boiler water make-up. A flow diagram of the entire reactor power cycle is shown in Fig. 1. The reactor vessel, the primary coolant system, the radiation shielding, the steam turbine, the forced-air-cooled condenser, and the reactor building are shown in an artist's sketch of the plant in Fig. 2.

Water circulating through the primary coolant system serves to transfer heat from the reactor core to the main heat exchanger, where it is transferred to the secondary system. Steam generated in the heat exchanger drives the turbogenerator and also provides heat for barracks and other space heating requirements at the station. The primary system includes the reactor pressure vessel, the pressurizer tank, two canned-rotor circulating pumps with their associated check valves, the demineralizer, a storage tank for make-up water, two filters, two make-up water pumps, and two seal pumps.

The secondary system includes the turbogenerator with its associated condenser and condenser cooling system, the heating-system condensate return unit, a steam-jet air ejector, two hot-well pumps, a deaerating feed-water heater and storage tank, two feed-water pumps, and the evaporator. The main heat exchanger is a component of both systems, the primary coolant passing through the tube side and steam being generated in the shell side.

Water for the primary system is obtained by periodically transferring a portion of the condensate from the steam cycle to a small make-up storage tank. A fixed amount of water is bled continuously from the primary coolant system and is discarded in order to maintain a low concentration of corrosion products in the system. To replace this, an equal amount of water from the make-up storage tank is passed through the demineralizer unit and filters and then is injected into the primary coolant cycle by the make-up pumps. The hot primary coolant leaves the reactor core at the rate of 4000 gal/min at 450°F, passes through the tube side of the main heat exchanger, where heat is transferred to the steam cycle, and is returned to the reactor by the primary coolant circulating pumps. An electrically heated pressurizer attached to the high point of the system maintains a pressure of 1200 psi and thus prevents boiling in the pressure vessel.

Raw water for make-up in the steam cycle is converted to steam in the evaporator; in the deaerator this steam is combined with and helps heat the feed water before it enters the heat exchanger. Steam generated in the main heat exchanger passes through the turbine and is condensed in the turbine condenser. The condensate is then returned to the deaerating feed-water heater by the hot-well pumps. Steam is also used to heat the evaporator and is used in the

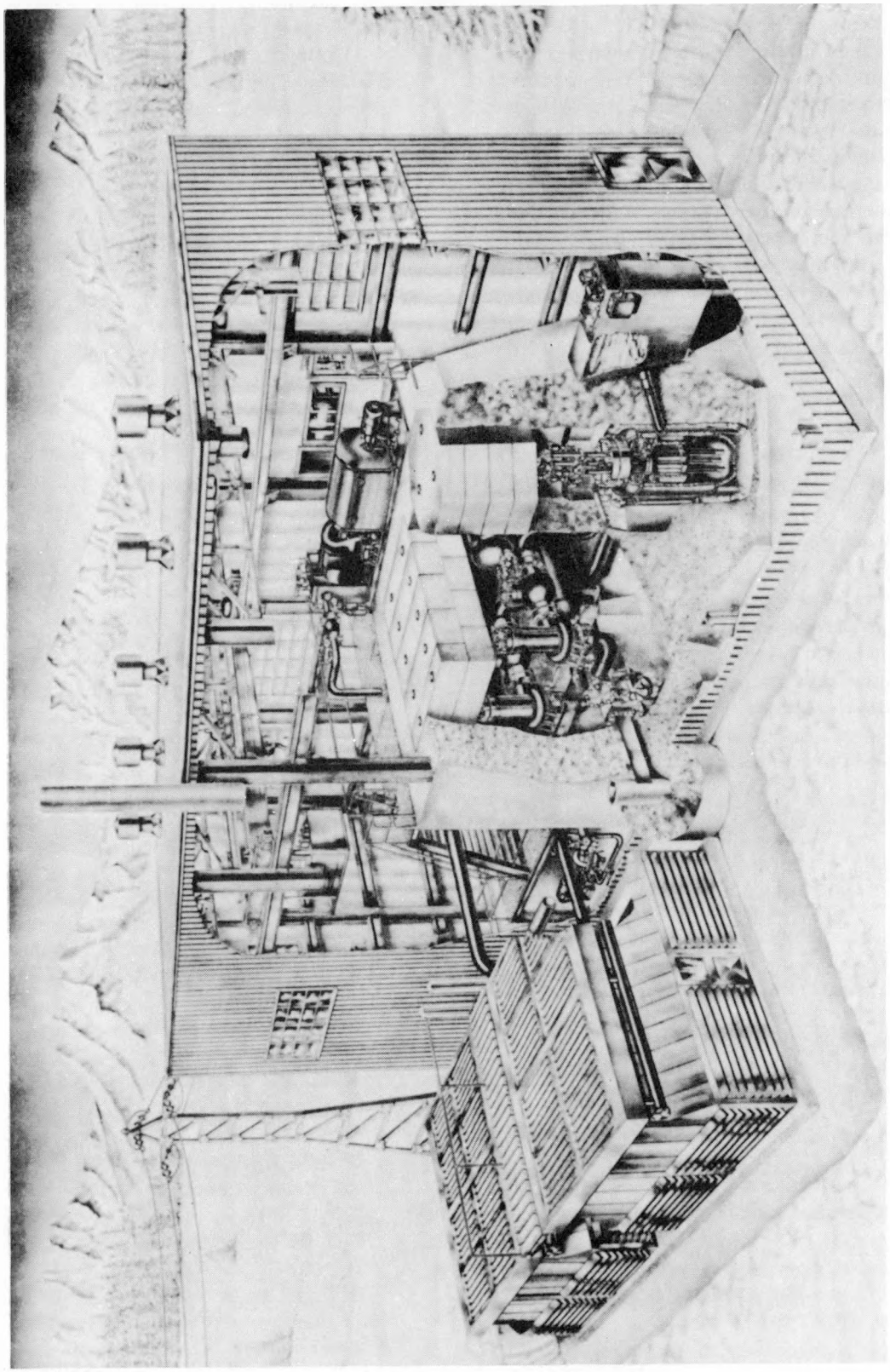

Fig. 2—Artist's sketch of the plant.

steam-jet air ejector, which maintains a vacuum in the turbine condenser.

Steam for the building heating load is taken directly from the heat exchanger, in parallel with the turbine load, and passes through a pressure-reducing valve to the building heating system. Condensate from this system is collected in a condensate return unit consisting of a storage tank and the two pumps that force the condensate back into the secondary system. Air coolers are provided to remove heat from the main turbine condenser coolant.

3. DESIGN DATA

The following is a partial summary of design data on the core characteristics, fuel-element and control-rod specifications, reactor performance, and thermal properties of this pressurized-water reactor.

Over-all plant performance:

- Thermal power developed in reactor, 10,000 kw; 34.1×10^6 Btu/hr
- Electric power generated, 1300 kw
- Net electric power delivered, 1000 kw
- Power required for auxiliaries, 300 kw
- Steam-heat load delivered, 3535 kw; 12×10^6 Btu/hr
- Over-all thermal efficiency, 45.4 per cent
- Thermal efficiency of net-electric-power generation, 15.5 per cent
- Power density of reactor core, 71.7 kw/liter
- Core life before refueling, 15 Mw-years

Reactor data:

- Core:
  - Average diameter, 22.2 in.
  - Height, 22.0 in.
  - Volume of core, 139.5 liters; 8513 cu in.
  - Uranium content (93.5 per cent U^{235}) of new core, 18.9 kg; 17.7 kg U^{235}
  - Critical mass after 15 Mw-years, 10.2 kg U^{235}
  - Stainless-steel content, excluding matrix, 110.06 kg
  - Stainless-steel content in matrix, 98.04 kg

Reactor data (Cont'd)

- Poison content, natural boron, 0.172 kg
- B_4C content, 0.220 kg
- UO_2 content (1.136 kg/kg of uranium), 21.47 kg
- Water content, 111.1 liters:
  - At 0.83 g/cm^3 (450°F), 92.2 kg
  - At 1.0 g/cm^3 (70°F), 111.1 kg
- Ratio of metal to water, 0.256
- Excess reactivity (new cold clean core), 10 per cent
- Maximum reactivity during the operating period:
  - Hot, 7 per cent
  - Cold, 16 per cent
- Neutron flux (average, thermal, at end of 15 Mw-year cycle), 2.7×10^{13} neutrons/cm^2/sec
- Reflector thickness (water), 7 in.

Fuel plates:

- Type of plates: rectangular, flat, UO_2-stainless steel-B_4C core, clad in 304L stainless steel

Geometry of plates:

	Fuel core	Over-all
Thickness, in.	0.020	0.030
Width, in.	2.50	2.760
Length, in.	22.0	23.0

- Stainless-steel cladding:
  - Thickness, 0.005 in.
  - Spacing between plates, 0.134 in.
- Composition of fuel section of plates:
  - UO_2, 17.94 wt. %
  - Stainless steel, 81.88 wt. %
  - B_4C, 0.18 wt. %
- Geometry of side plates:
  - Thickness, 0.050 in.
  - Width, 2.912 in.
  - Length, 23.0 in.
- Atom ratios in reactor core:
  - U^{235}, 1 atom
  - H_2O, 68 molecules
  - Fe, Ni, Cr, 48.4 atoms
  - B, 0.212 atom
- Fuel plates per fuel assembly, 18
- Number of fuel assemblies, 40
- Fuel plates per control-rod assembly, 16

Reactor data (Cont'd)
- Number of control-rod assemblies, 5
- Total number of fuel plates, 800
- Dimensions of fuel assembly (over-all):
  - Thickness, 2.912 in.
  - Width, 2.800 in.
  - Length, 35.25 in.
- Tolerances:
  - Particle size of UO_2:
    - Maximum, 86μ
    - Minimum, 44μ
  - Thickness of fuel plates, ±0.001 in.

Control rods:
- Type: rectangular, to fit fuel space in lattice; upper section absorber material; lower section fuel subassembly
- Composition:
  - Upper section, 16.3 wt. % B_4C in copper, $\frac{1}{8}$ in. thick clad with 304L stainless steel, $\frac{1}{32}$ in. thick; formed into square
  - Lower section, previously described
- Geometry:
  - Upper section, 2.750 × 2.750 × 29 in.
  - Lower section, 2.750 × 2.750 × 40 in.
- Number:
  - Shim rods, 4
  - Regulating rods, 1
- Travel:
  - Shim rods, 22 in.
  - Regulating, 22 in.
- Weight of rods, 60 lb
- Acceleration of rods after release, 32.2 ft/sec^2
- Maximum distance for rods to drop, 22 in.

Thermal data of reactor at full power:
- Operating pressure in reactor, 1200 psia
- Coolant inlet temperature at reactor, 431.6°F
- Coolant outlet temperature at reactor, 450°F
- Properties of coolant:
  - Density at 450°F, 51.75 lb/cu ft
  - Density at 431.6°F, 52.60 lb/cu ft
  - Change in density per °F, 0.046 lb/cu ft
  - Viscosity at 445°F, 0.295 lb/ft-hr
  - Thermal conductivity, 0.39 Btu/hr/sq ft/°F/ft
  - Specific heat, 1.115 Btu/°F/lb
- Coolant flow through core, 4000 gal/min; 1.66×10^6 lb/hr
- Number of flow passes through reactor, 1
- Flow area in core, 2.083 sq ft

Thermal data of reactor at full power (Cont'd)
- Velocity in core passages, 4.3 ft/sec
- Design heat output, 34.1×10^6 Btu/hr
- Heat-transfer area, 611.1 sq ft
- Average heat flux, 55,900 Btu/hr/sq ft
- Peak to average heat flux ratio used for design (assumed, actual ratio not available), 4 to 1
- Ratio of maximum to average heat flux in any one channel (cosine distribution), 1.31 to 1
- Ratio of heat absorbed in hottest channel to average channel (4.0/1.31), 3.05 to 1
- Maximum bulk water temperature, hottest channel, 487.6°F
- Reynolds number in core, 58,400
- Film coefficient of heat transfer, 2570 Btu/hr/sq ft/°F
- Maximum surface temperature, 554°F
- Boiling temperature at 1200 psia, 567.2°F
- Heat-transfer coefficient of scale (assuming 0.010-in. scale at k = 1.0 Btu/hr/sq ft/°F/ft), 1200 Btu/hr/sq ft/°F
- Maximum metal temperature:
  - With assumed scale, 742°F
  - With no scale, 565.7°F

4. REACTOR COMPONENTS

4.1 Reactor-core Assembly

The fuel assemblies, control rods, and their supporting structure make up the reactor-core assembly; there are 40 fuel assemblies and 5 control rods. The arrangement of these units in a lattice with a supporting structure can best be seen by referring to Figs. 3 and 4. The end fittings of the fuel assemblies fit into the upper and lower grids of the core assembly. The spring section of the upper fitting allows each assembly to be held firmly and still allows for expansion and tolerance limitations. The five square holes in the core-assembly grids are for the control rods, which extend all the way through the reactor core.

(a) Fuel Assemblies. The reactor is loaded with U^{235} fuel enriched to the 93.5 per cent level. The fuel, in the form of uranium dioxide, is incorporated into flat-plate type fuel assemblies (Fig. 5), which are similar in design to the fuel elements employed in the MTR.

The rectangular fuel plates consist essentially

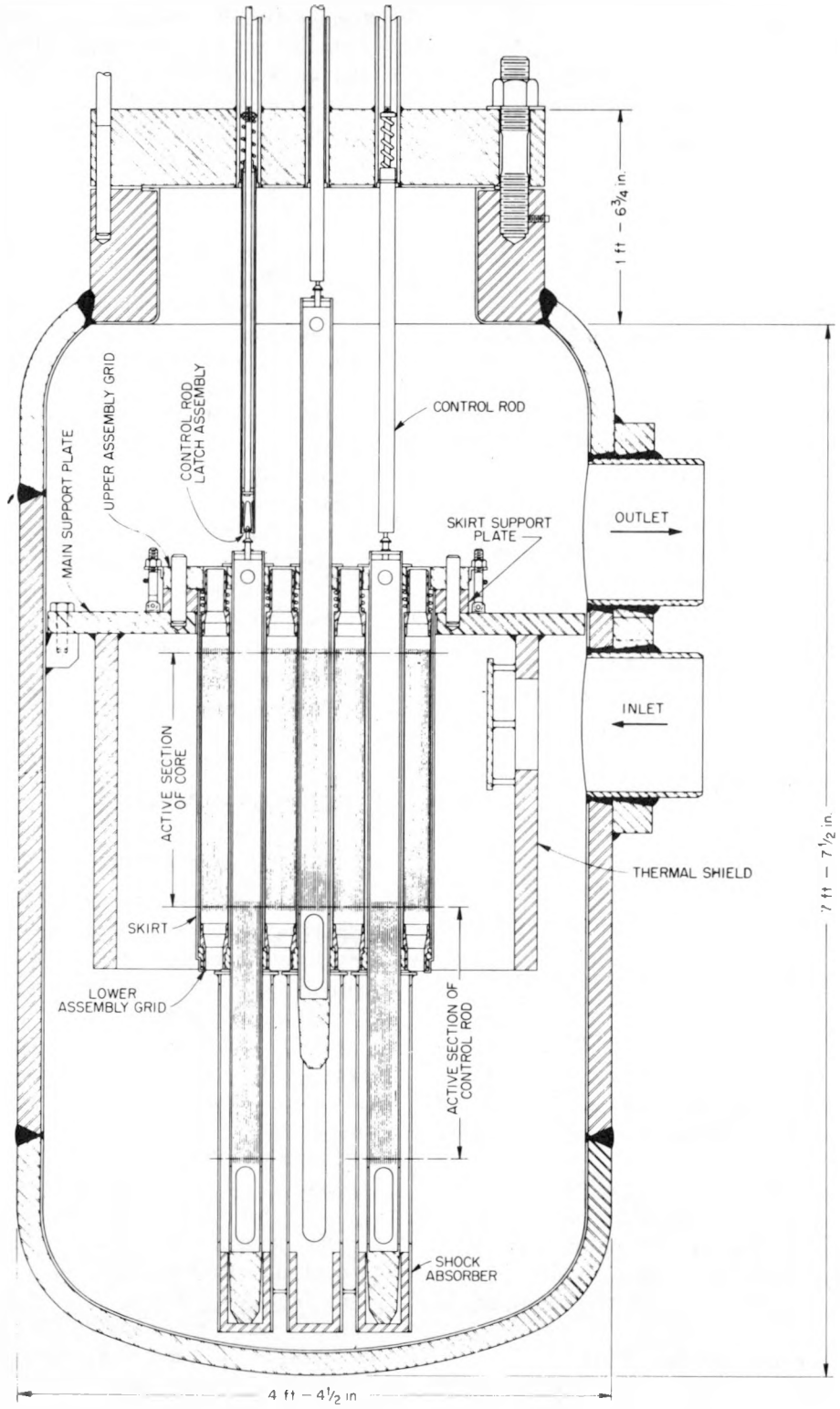

Fig. 3—Reactor assembly, vertical section.

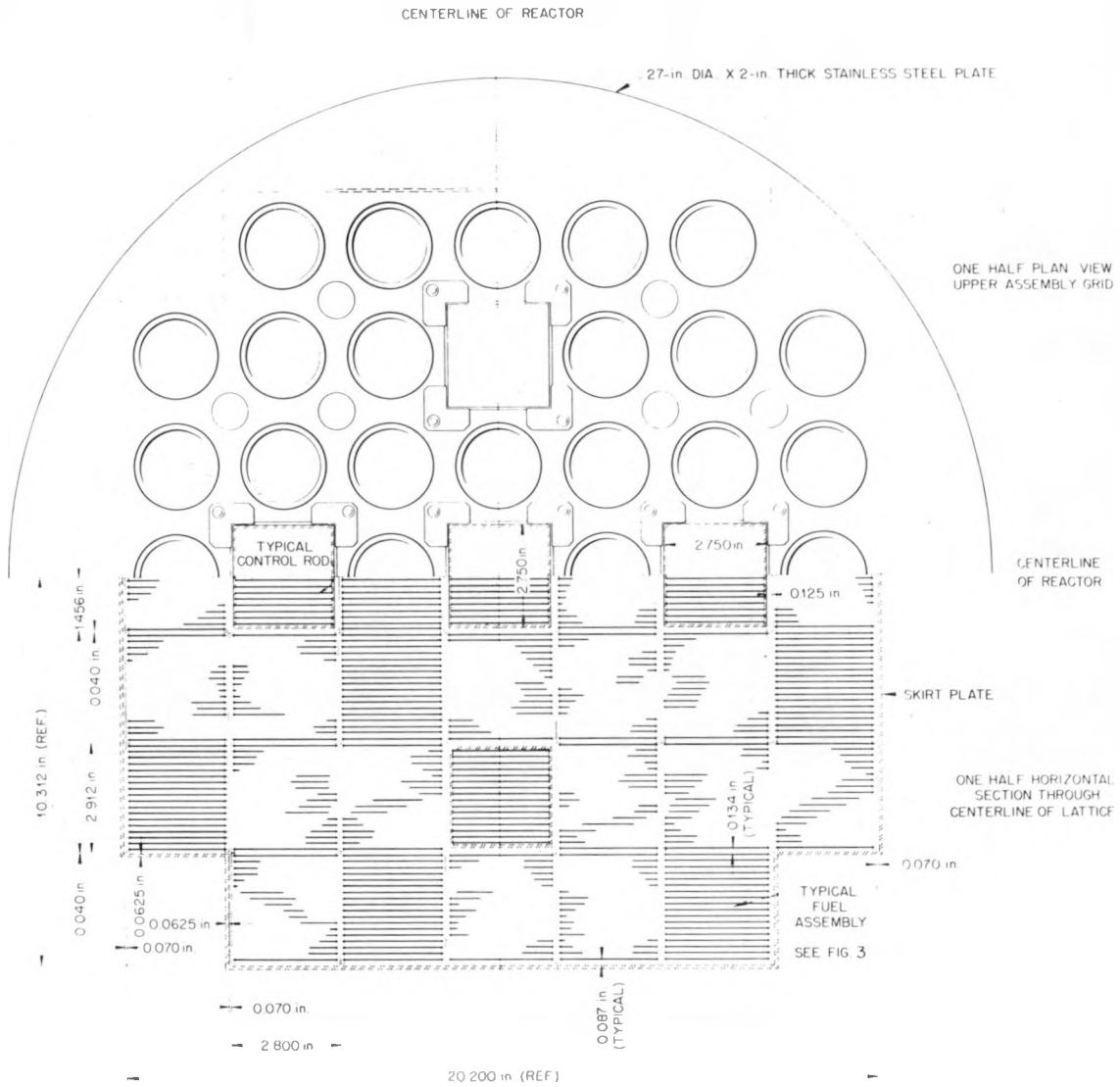

Fig. 4—Reactor core, cross section.

of UO_2 particles uniformly dispersed and embedded in a matrix of sintered stainless-steel powder which is clad on all sides with wrought 304L (low carbon) stainless steel. A small quantity of poison, B_4C, is deliberately added to the fuel mixture to facilitate reactor control.

The core of a fuel plate, when loaded for 15 Mw-years, is composed of 17.94 wt. % UO_2, 0.18 wt. % B_4C, and a matrix of 81.88 wt. % sintered stainless-steel powder. This fuel wafer measures approximately 22.00 in. long, 2.50 in. wide, and 0.020 in. thick in the finished plate. The cores are jacketed by the picture-frame technique, which seals the uranium from exposure to the cooling water and also retains the fission products. The hot-working operation results in a good metallurgical bond between clad and core. The clad-core-clad thickness in mils is 5-20-5.

Eighteen of these composite plates, each 2.76 in. wide by 23.00 in. long, over-all dimensions, are assembled into a single fuel element or assembly (see Fig. 5). The plates, with a nomi-

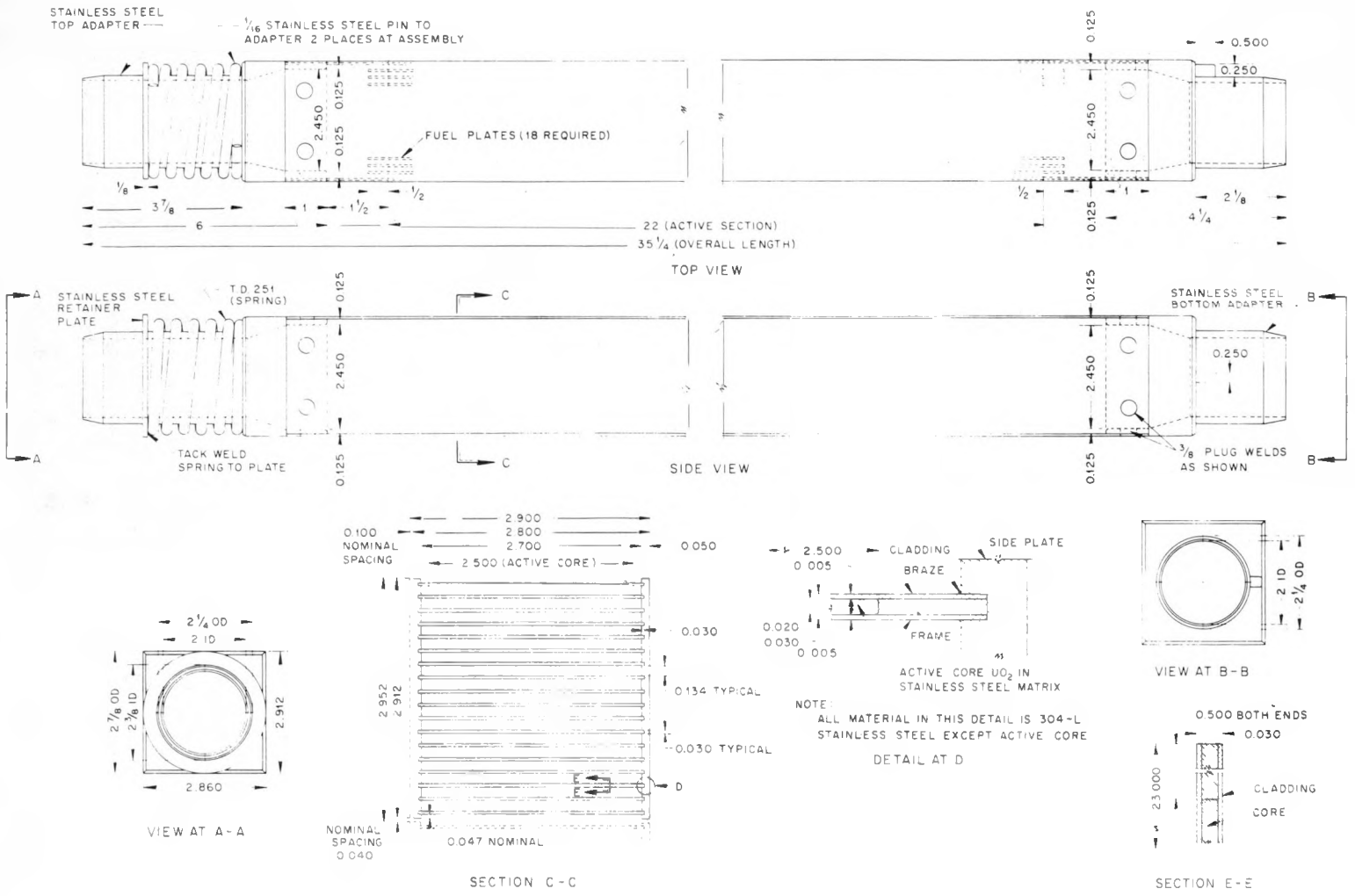

Fig. 5—Fuel assembly.

nal 0.134-in. water gap space between them, are brazed into a pair of stainless-steel side plates of 0.050-in. thickness. Stainless-steel castings are then plug welded to the ends of the fuel assembly. Each fuel assembly contains 398 g of U^{235} and 4.95 g of B_4C. For a 30-Mw-year loading the loading would be 583 g of U^{235} and 9.61 g of B_4C.

The purpose of the end fittings is to adapt the unit to the supporting grids, which in turn firmly fix the position of the element in the reactor core. A spring is provided on the upper casting to allow for expansion and tolerance limitations. These adaptors also serve as transition pieces, which convert the rectangular cross section of the fuel element to the round holes provided in the upper and lower grids; this type of construction greatly simplifies machining the grid sections. The fittings, of course, are hollow to permit free passage of water through the fuel assembly. The ratio of metal to water in the active section of the reactor core is 0.256.

The fuel plates are designed to be used in both the fuel assembly and in the fuel section of the control-rod assembly; 0.050 in. of stainless steel is trimmed from the width of the fuel plates to meet the dimensions of the control rod. Making all plates initially to one specification simplifies fabrication and permits inventory on only one type of plate. The total number of fuel plates in both the fuel assemblies and the control rods in the reactor core is 800. They contain 17.7 kg of U^{235} for a 15-Mw-year life or 26.0 kg for a 30-Mw-year loading.

(b) Control Rods. The reactivity of the reactor is lowered when the control rods are inserted to the "in" position, i.e., resting on their shock absorbers. The rods will overcome the maximum reactivity. The five control rods in the loading are identical; only one rod is used as a regulating rod. The rods are constructed in two segments, jointed by a quick-release connection (Fig. 6). The upper segment contains boron sheet;[1] this section resides in the lattice when the rod rests on the shock absorbers. The lower segment, containing a fuel element with 16 fuel plates, is raised into the lattice when the control rod is up. The control rods extend from the shock absorber up through the upper assembly grid to the top of the reactor vessel where they are driven by rack and pinion; a magnetic clutch is released in case of a scram.

The segments of the control rod can be uncoupled by rotating the upper segment approximately 30 deg in relation to the lower segment. This can be accomplished easily while the rod is in the core since, during unloading, the upper assembly grid is removed, permitting the upper segment of the control rod to be rotated while the lower segment is contained in the lower assembly grid. The control rod was designed with a quick-release connection for the following reasons:

1. Fabrication and assembly of the rods is simplified.
2. Handling of the rods is easier during reactor unloading. The shielding requirements at the top of the reactor are less rigid during unloading since the distance that the top of the rod must be raised for removal from the reactor is minimized.
3. One transfer-coffin design is sufficient to handle any of the assemblies in the reactor core.

The grid and support structure also provide bearings and shock absorbers for the control rods; bearings are located in both the upper and lower assembly grids. A bearing assembly (Fig. 7) consists of eight Stellite rollers, two rollers making up one side of a square. The rollers are mounted so as to give a clearance of $\frac{1}{16}$ in. The shock absorbers are simply cylinders which engage the piston-like ends of the control rods and which dissipate the energy of the control rods during a scram or when the rods are driven to their low position. The absorbers are attached to the lower assembly grid and are slotted to ensure proper flow of water through the core.

4.2 Control-rod Drive Mechanism

The rods are driven by a rack and pinion located inside the pressure-vessel cover. Motion is transmitted to the pinion through a commercial rotary spindle seal. A motor unit mounted on top of the reactor cover provides the motive force; the detailed design is shown in Fig. 8. The unit consists of three main subassemblies: the motor unit, the seal assembly, and the rack-latch assembly.

(a) Motor Unit. The motor unit consists of a primary drive, a magnetic clutch, gear box, and

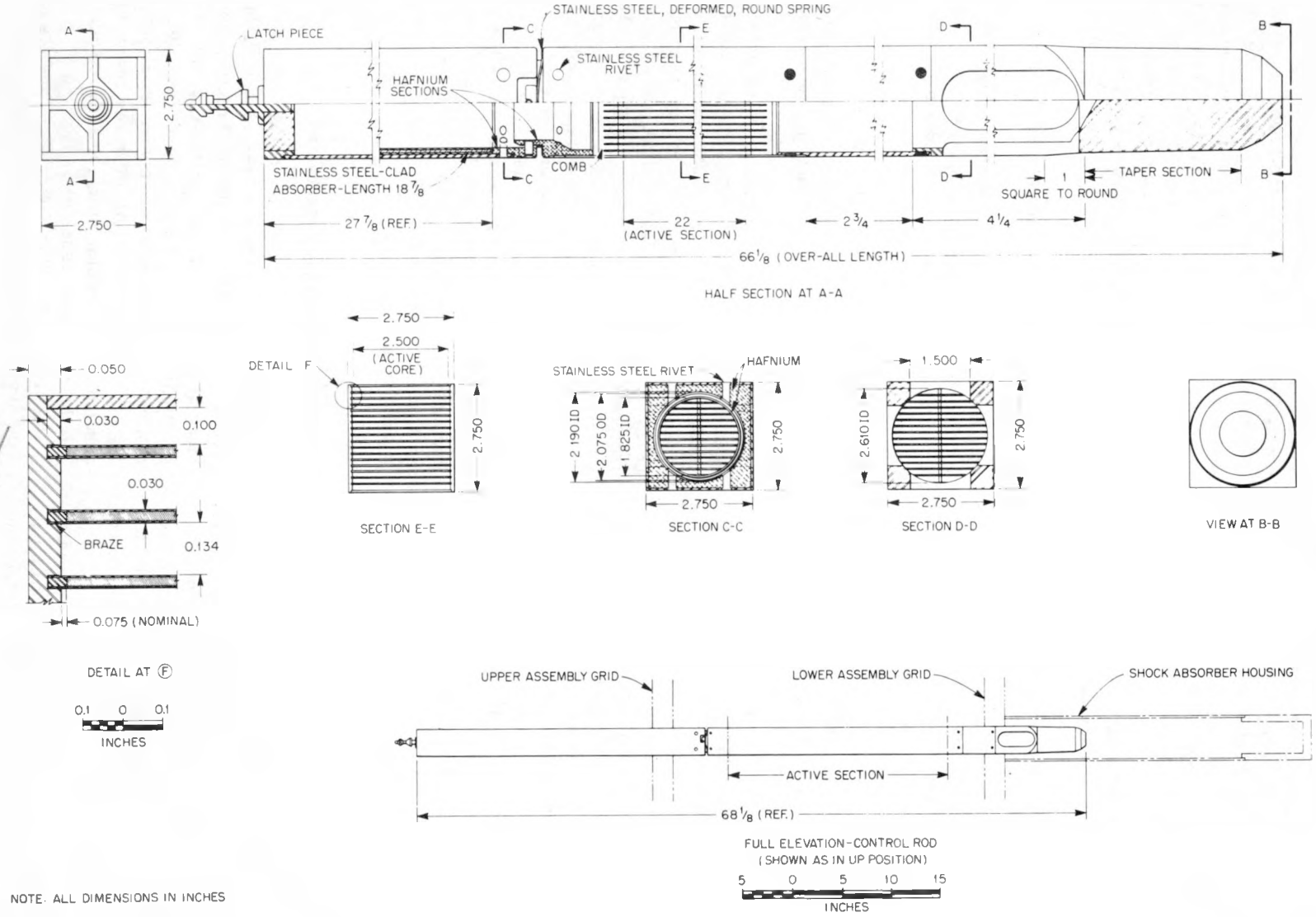

Fig. 6 — Control-rod assembly.

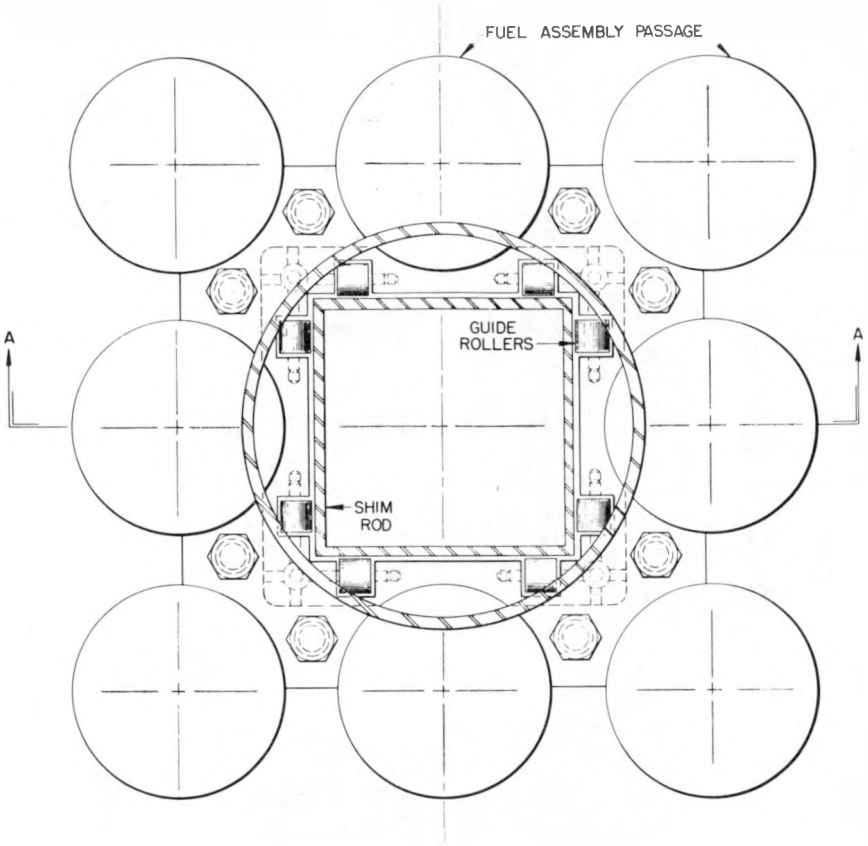

BOTTOM VIEW – LOWER ASSEMBLY GRID

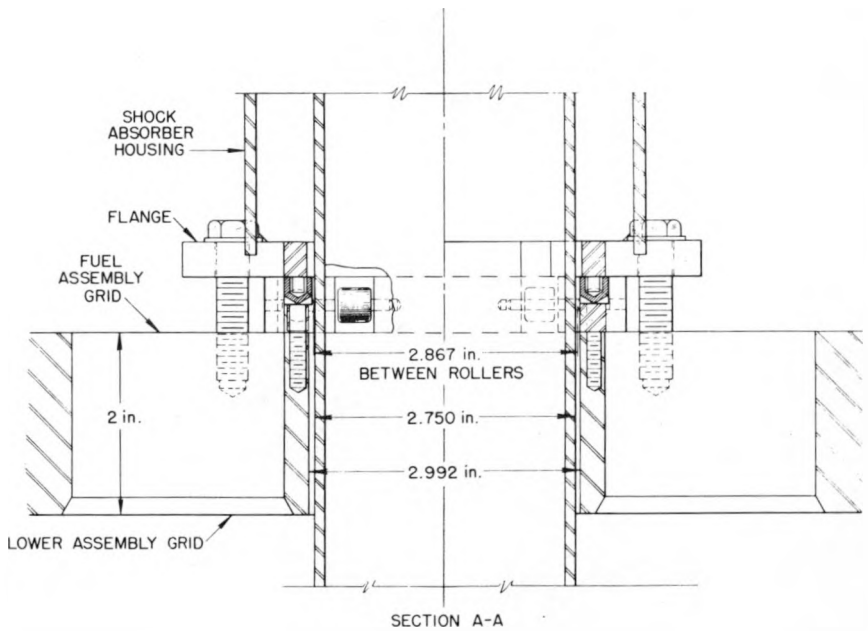

Fig. 7 — Control-rod bearing, lower.

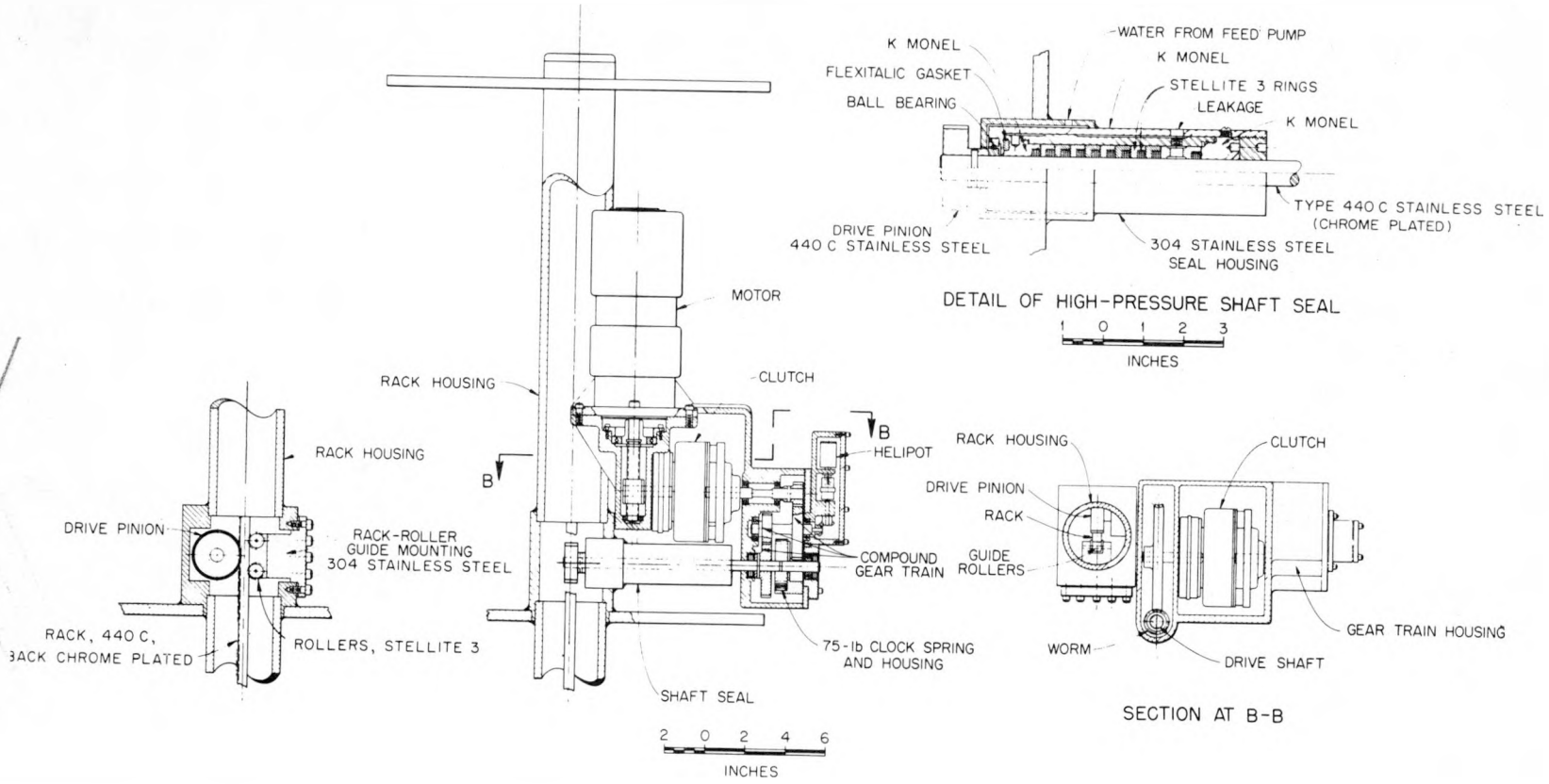

Fig. 8 — Control-rod drive, section and details.

an indication system. The design specifications are as follows:

1. Control rod to move up or down with speed of 1 ft/min.

2. Rod to move in increments of 0.02 in. by proper switch actuation.

3. Position of rod indicated at all times, including during and after scram, with an accuracy of 0.2 per cent.

4. Automatic scram rods with an acceleration equal to that of gravity.

(b) Seal Assembly. The decision to drive the rod through a seal was determined by the fact that the system can tolerate a nominal amount of leakage, provided this leakage is collected and returned to the system. The seal assembly consists of the seal and leakage collection unit (Fig. 8). The seal is a spindle type rotary seal developed by the Kuchler-Huhn Co., Inc., Philadelphia, Pa. It is a complete breakdown type and is designed for a leakage rate of 10 lb/hr. Calculations were made for a water pressure of 1200 psi and a water temperature of 600°F. These calculations resulted in an over-all seal length of 6.00 in. and a shaft clearance of 0.0003 in. It should be noted that the leakage rate varies approximately as the cube of the clearance. The torque required to overcome the calculated operating friction of the seal is 3 to 4 in.-lb, and the maximum breakaway torque is 12 in.-lb.

A fitting included in the design of the seal serves as the outlet for the leakage of the collection unit; tubing runs from each of the five seals to a common receptacle. The seal consists of a number of floating rings, made of Stellite-3 and a series of K-monel guide bushings. These are assembled in a type 304 stainless-steel housing. The number of rings, as well as the clearance, determines the pressure breakdown and resultant leakage. The shaft is 440C stainless steel, chrome plated, and must be ground to close tolerance, ±0.0001 in.

(c) Rack-latch Assembly. At the pressure side of the seal a 440C stainless-steel pinion is mounted on the shaft. This pinion in turn drives a 440C stainless-steel rack that is latched to the control element, thus giving the required linear motion.

The latch unit is attached to the lower end of the rack. The latch must be capable of transmitting linear motion to the control rod; it must automatically release the control rod when the rod is in its lowest position, thus allowing removal of the pressure vessel cover while the rod remains in the reactor; and, finally, the latch must automatically grip the rod when the pressure-vessel cover is replaced. The latch performs its required functions by relative motion between a center rod and an outside sleeve. The upper end of the center rod is attached to the rack, and the lower end contains the gripping jaws. The jaws have spring properties and are normally in the open position. As the outer sleeve moves in relation to the center rod, it locks the jaws in the closed position, or allows them to open.

In normal reactor operation the outer sleeve is held against a flange on the center rod by a strong spring. The opposing force of the spring is taken by a pin through the center rod at its upper end. In this position the rack is latched and locked to the control rod. The control rod, latch, center rod, and latch sleeve move as a single unit. When the control rod has been lowered to approximately ¼ in. from its lowest position, the motion of the outer sleeve stops owing to the engagement of a collar on the outer sleeve with a ring installed in the reactor cover. The center rod and control rod continue to be driven down by the rack, compressing the sleeve spring. When the control rod is in its bottom position, it is still latched and locked to the rack. In order to remove the pressure-vessel cover, the rack must be driven to a lower overtravel position. This further compresses the sleeve spring, and the jaws leave the sleeve and spring open. The vessel cover can then be removed, and the control elements remain in the reactor. The position-indication gauge in the control room shows whether or not the rack is in the overtravel position and whether the pressure-vessel cover can be removed.

4.3 Pressure-vessel Design

The reactor pressure vessel was designed according to the 1952 edition of "ASME Code for Unfired Pressure Vessels." It has a design pressure of 1250 psi and a design temperature of 650°F. The shell material is ASME type-SA 212, grade-B, fire-box quality boiler-plate steel. This material was selected because of its good welding and mechanical properties.

The vessel is 9 ft 2¼ in. high and has an in-

side diameter of 4 ft. The cylindrical side wall is 2¼ in. thick, including a 125-mil stainless-steel cladding, and is welded at the bottom to a standard ASME ellipsoidal head. The cylindrical section is approximately 6½ ft long. The top end of this section is welded to an elliptical head, which is, in turn, welded to a 2⅓-ft-I.D. cylinder with a 6-in. wall thickness to provide sufficient area for mounting the studs for attaching the cover plate. Five 1½-in.-diameter stainless-steel pipe sleeves are welded into the 7-in. cover plate for mounting the control-rod drives. The vessel is to be stress relieved, and all weld joints are to be examined by X ray. The entire surface exposed to the primary coolant is clad with stainless steel, AISI type 304.

The thermal stresses induced by nuclear reactions in the pressure-vessel wall were calculated as a function of wall thickness. As the total stress appeared excessive, a 2-in. thermal shield was included in the geometry, and the stresses in the shell opposite the reactor centerline were again calculated. For operation at 450°F the 2-in. stainless steel reduces the tensile stress in the 2¼-in. vessel wall from 24,000 to 17,000 psi. The thermal shield also reduces the thickness of concrete in the radiation shield; the most economical location for a given thickness of thermal shield is adjacent to the reflector.

The cylindrical shield is welded to the upper support plate and extends downward 2 ft 7⅛ in. from this plate to shield the pressure vessel from the hot core. The support plate and shield are constructed of AISI type 304 stainless steel. An 8-in.-diameter baffled opening is placed in juxtaposition to the coolant inlet to permit cooling water to flow downward on either side of the shield before entering the fuel subassemblies.

5. SELECTION OF MATERIALS

The suitability of any material of construction for use in the APPR is based upon these prime factors:

1. It must have the proper physical properties to perform its function over long periods of time.

2. It must resist radiation damage and perform satisfactorily under radiation and in contact with transported materials that have been irradiated.

3. It must withstand the corrosive action of contact with and submersion in water at 500°F.

The following materials were examined through information generally available in the unclassified literature and that available in AEC reports.

304 stainless steel	K-monel
304L stainless steel	Inconel
316 stainless steel	Inconel-X
347 stainless steel	Armco 17-4 PH
410 stainless steel	Armco 17-7 PH
440L stainless steel	USS 322 W
Stellite-3	A-nickel
Stellite-6	Hastelloy C
Stellite-12	Vascoloy-Ramet 166
Graphitar-14	Chrome plate
Monel	

Stainless steel 304 was selected as the basic material to be used, except as noted in certain special instances. Most of the previous reactor and corrosion loops to date have employed 347 stainless steel as the basic corrosion resistant material. For the APPR it is more important to select an optimum material rather than just the "best" material. The selection of such an optimum material is a function of the ability of the material to perform what is required of it, evaluated on the basis of cost, availability, ease of fabrication, etc. Since 347 stainless steel costs more (about 25 per cent), contains the strategic material columbium, is more difficult to fabricate, and is only slightly superior to type 304 in corrosion resistance, the 304 stainless steel was selected.

The materials for the primary loop are, then, as follows:

Reactor vessel, 304 stainless steel clad to ASME type-SA 212, grade B fire-box quality steel
Gasket, dead soft nickel or monel
Studs, 304 stainless steel
Nuts, 303 stainless steel
Piping, 304 stainless steel, welded with 304L stainless steel or 25-20 stainless steel
Fuel elements:
Cladding, 304 or 304L stainless steel; matrix, 304 or 304L stainless steel, sintered with suitable fuel

Control mechanisms:
- Rack and gear, 400C stainless steel
- Seal, disks, Stellite-3; diaphragm, K-monel
- Shaft, Armco 17-4 PH or 440C chrome plated
- Bearing, rollers and races, Stellite-3
- Retainers, Armco 17-4 PH
- Springs, Inconel-X

Heat exchanger:
- Tubes and headers, 304 stainless steel

Pumps:
- Canned rotor
- Frame, block, and position indicator, 347 or 304 stainless steel
- Bracket and bearing carrier, 304 stainless steel
- Shaft, 410 or 440C stainless steel chrome plated
- Lamination ring, monel

Valves, gate:
- Body, 347 or 304 stainless steel, Stellite-3 runners
- Gate, Armco 17-4 PH

Valves, check:
- Body, 347 or 304 stainless steel
- Pin, Stellite-3
- Facing, Stellite-3

It should be noted that the 304 stainless steel can be replaced by 304L, 316, 321, or 347 stainless steel, if necessary.

6. PHYSICS

6.1 General Considerations

Some general features of the core behavior may be predicted by qualitative analysis or by comparison with other reactors. If the core contains, in addition to its critical mass, enough fuel for several years of operation, the reactivity may be quite high, especially at room temperature. (In order to reduce the initial reactivity, boron is incorporated in the fuel matrix as a burnable poison.) Multigroup calculations of a number of hydrogenous reactors with ratios of fuel to moderator in the range expected for the package reactor indicate that an appreciable fraction of fissions will be caused by neutrons with energies up to a few hundred electron volts. These resonance absorptions are not properly described by ordinary two-group diffusion theory.

6.2 Methods of Calculation*

The physical characteristics of the package reactor core have been evaluated by one or more of the following three methods: modified two-group diffusion theory (with multiplication in the fast group), performed with desk calculators; three-group three-region diffusion-theory calculations, coded for the ORACLE; and thirty-group nine-region diffusion-theory calculations, coded for the UNIVAC.

The modified two-group method was chosen for desk calculations because the resonance absorptions occur at sufficiently low energies to have little effect on the spatial distribution of neutrons slowing down to thermal energy.

The UNIVAC program employs the Goertzel-Selengut method for describing neutron energy loss in hydrogen collisions. It has yielded very satisfactory results when applied to a number of aqueous homogeneous critical assemblies.

6.3 Results of Critical Calculations

The results of the calculations by the three methods are shown in Table 1. All three methods give comparable results for critical mass for the cold clean reactor; the hot poisoned reactor; and the hot fully loaded reactor containing boron burnable poison. The greatest difference is about 10 per cent in critical mass, or about 4 per cent in reactivity. The discrepancies are qualitatively understood in terms of approximations made in one or another of the methods.

6.4 Control Rods

Control-rod calculations were made in two ways. Modified two-group calculations were made for an equivalent bare cylindrical reactor, employing, at the rod surface, a fast-group boundary condition based on diffusion of the fast neutrons into the moderator within the rod. In addition, the ORACLE three-group three-region calculation was applied to a central rod in a cylindrical side-reflected reactor. The rod is regarded as a moderating region, surrounded by a thin absorbing shell that is opaque to thermal neutrons, semitransparent to resonance neutrons, and transparent to fast neutrons. The

*The methods of calculation are described in more detail by A. M. Perry et al. in Report ORNL-1819.

modified two-group method gives 0.058 for the reactivity worth of the central rod and 0.194 for the worth of the five rods in the configuration planned. The ORACLE method gives 0.067 for the central rod.

Since the maximum reactivity excursion of the reactor is 0.14, the rods planned should be adequate with a comfortable margin of safety.

6.5 Temperature Dependence of k

The temperature coefficient of reactivity has been calculated by the UNIVAC thirty-group method. The multiplication constant was calculated at 432°F for two reactor cases that are critical at 450°F, i.e., at the beginning and at the end of the operating cycle. In both cases $dk/dt = -2.2 \times 10^{-4}/°F$. From modified two-group calculations at 68 and 450°F, the average temperature coefficient between these two temperatures was $-1.68 \times 10^{-4}/°F$. Because of the shape of the density vs. temperature curve for water, the latter figure is considerably smaller than the coefficient at 450°F.

Table 1—Critical Calculations

Quantity	UNIVAC	ORACLE	Modified 2-group
Critical mass for cold clean reactor, kg	8.03	7.40	7.26
Critical mass for hot reactor, end of cycle (fission products for 15 Mw-years), and peak xenon, kg	10.60	10.35	10.16
Initial loading, U^{235}, kg	18.10	17.85	17.7
Mass of B^{10} required for criticality; hot reactor, beginning of cycle, peak xenon, g	38.18	34.9	32.4
k of cold reactor, beginning of cycle, no xenon	1.0625	1.0888	1.096

7. OPTIMUM REFUELING CYCLE

In order to evaluate the effect of length of core life on the economics of the reactor operation, a study was made in which the total fuel and related costs were computed with varying reactor loadings. The results, plotted in Fig. 9, were arrived at by adding costs of uranium actually burned, inventory charges on unburned uranium held up in the core, core fabrication costs, shutdown costs, transportation costs, and chemical processing costs for the uranium remaining in the burned-out core. Fuel burn-up cost is based on a charge of $20 per gram of U^{235} fissioned. The amount of U^{235} required initially was computed as a function of operating time. Thus, for a 15 Mw-year cycle, 18 kg of U^{235} is required as initial loading. It is assumed that, after the burned-out core is chemically processed, the unburned uranium would be sold back to the AEC at a value that would be the same as that of partially enriched fuel with an equivalent percentage of U^{235} (reference 2). Annual inventory charges are assumed to be 10 per cent of the value of the uranium held up.[3] This holdup period was estimated at $1\frac{1}{6}$ years beyond the actual fuel-cycle length; it includes time spent in fabrication and chemical processing plus a one-year cooling period for the burned-out core. The core fabrication cost is estimated to be $42,500. Shutdown costs are based on an estimate of labor requirements for a shutdown of two weeks. Chemical processing costs represent a charge of $3 per gram of uranium remaining in the burned-out core, although there are indications that this charge can be decreased as a result of development work currently under way in the fuel-plate processing field. The $2\frac{1}{2}$-year cycle chosen (15 Mw-years) is near the minimum, but longer cycles are not unattractive.

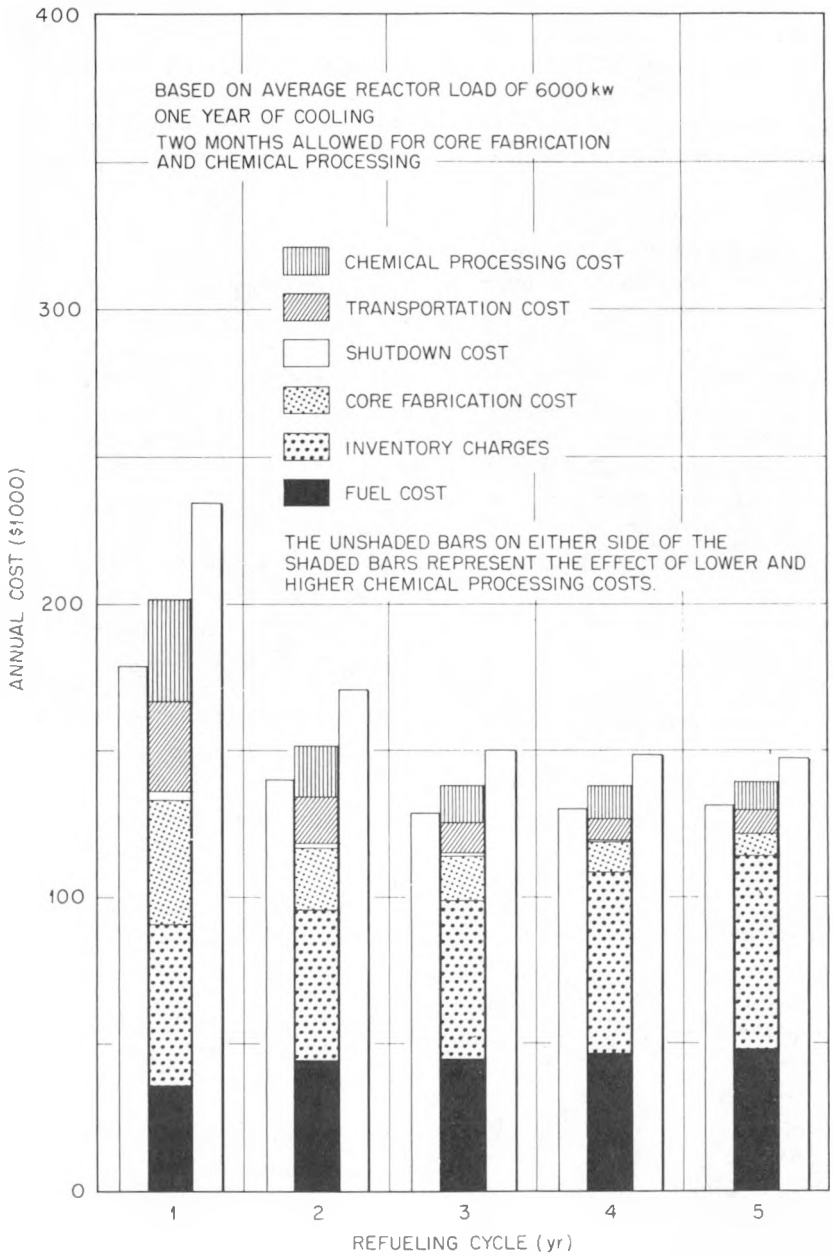

Fig. 9 — Effect of fuel-cycle length on fuel costs.

8. COST ANALYSIS

8.1 Bases of Cost Estimates

The difficulty of preparing cost estimates at the design study stage are well recognized. In order to make these estimates as realistic as possible, all major components were engineered sufficiently to enable several reliable manufacturers to quote fabrication costs. In the absence of direct quotations from manufacturers, costs on some items were estimated by comparing the component to similar existing items.

The cost estimates were prepared for construction at a developed site similar to Oak Ridge, Tenn. No attempt was made to estimate the added costs for construction of the plant at an arctic base, where labor costs and transportation could be expected to run much higher. The cost of the plant is estimated at $1,703,000, including a 10 per cent engineering charge. Additional costs would be required to cover any excessive development type engineering deemed necessary.

8.2 Capital Costs

The principal items are as follows:

Reactor	$ 148,000
Primary coolant system	357,000
Steam system	171,000
Main condenser cooling system	61,500
Evaporator system	22,000
Primary coolant water purification system	32,000
Pressurizer system	40,500
Instrumentation and controls, reactor	82,000
Instrumentation and controls, process	38,500
Electrical systems	82,000
Building, including crane, platforms, and ventilating equipment	260,000
Reactor shielding (500 cu yd)	70,500
Miscellaneous	42,000
Contingencies, 10 per cent	140,700
Engineering, 10 per cent	155,300
Total plant cost	$1,703,000

8.3 Installed Plant Costs per Kilowatt

The reactor will produce 1000 kw net electrical power and 12.1×10^6 Btu/hr (3535 kw) in the form of steam for heating purposes. An analysis of the plant costs indicates that 45 per cent should be charged to steam and 55 per cent to electric power. This gives $936 per kilowatt net electric power and $216 per kilowatt steam heat.

8.4 Kilowatt-Hour Costs

In calculating the costs per kilowatt-hour for net steam and electricity delivered (Table 2), the following assumptions were used:

1. The plant amortization rate would be 13.5 per cent.
2. The fuel inventory rate would be 10 per cent.
3. The charge for U^{235} burn-up would be $20 per gram.
4. There would be a $3.00 per gram charge for chemical reprocessing of the fuel.
5. The initial fuel loading would be approximately 18 kg of U^{235}.
6. The operating costs would be based on a core life of 15 Mw-years before refueling.
7. During reactor operation consumption of U^{235} would be 1.4 g/Mwd.
8. Operation and routine maintenance of the reactor plant would cost $150,000 per year.

8.5 Summary of Costs

A summary of the above estimates is as follows:

Plant construction costs	$1,703,000
Installed plant cost per kilowatt:	
Electric	936
Steam	216
Cost per kilowatt-hour (60 per cent average load):	
Electric	5.33 cents
Steam	1.23 cents
Cost per kilowatt-hour (100 per cent average load):	
Electric	3.59 cents
Steam	0.83 cents

Table 2 — Kilowatt-hour Costs, Mills

Item	60% average load		100% average load	
	Electric	Steam	Electric	Steam
Capital costs:				
Complete plant (rate, 13.5%)	24.06	5.57	14.43	3.34
Fuel inventory (rate, 10.0%)	3.76	0.87	2.25	0.52
Subtotal	27.82	6.44	16.68	3.86
Operating costs:				
Fuel burn-up	6.42	1.49	6.42	1.49
Fuel fabrication	1.78	0.41	1.78	0.41
Chemical reprocessing	1.58	0.37	1.58	0.37
Labor and maintenance	15.70	3.63	9.42	2.18
Subtotal	25.48	5.90	19.20	4.45
Total costs	53.30	12.34	35.88	8.31

ACKNOWLEDGMENTS

The report, A Conceptual Design of a Pressurized-water Package Power Reactor, ORNL-1613, upon which this condensation is based, represents the work of many people. The largest part of the work was done by A. L. Boch, W. R. Gall, and G. F. Leichsenring.

In addition, many important contributions to the final report were made by R. B. Briggs, W. H. Jordan, F. H. Neill, and R. C. Robertson, who assisted in the preparation of the preliminary draft of the report, ORNL CF-53-10-106. H. J. Bolwell and S. Oestreicher (American Machine & Foundry Co.) also assisted in the preparation of the preliminary draft.

The nuclear calculations are the result of work done by A. M. Perry, R. L. Murray (North Carolina State College), Capt. R. R. Bate (Corps of Engineers), and M. C. Edlund. The material on fuel-element fabrication was contributed by J. E. Cunningham, R. J. Beaver, E. S. Bomar, Jr., and E. J. Boyle, of the Metallurgy Division. Reactor simulator tests were performed by E. R. Mann and E. P. Green. L. Scheib (American Machine & Foundry Co.) assisted in the studies of corrosion. W. R. Pearce (Bendix Aviation Corp.) performed the shielding calculations.

Credit is due the Army Reactors Branch of the Corps of Engineers, under the direction of Col. J. B. Lampert, for substantial assistance in establishing the proper basis for the design study and in obtaining much necessary information. Credit is also due the members of the ORNL Package Reactor Steering Committee, A. M. Weinberg, J. A. Swartout, W. R. Chambers, J. A. Lane, and R. A. Charpie, who provided a steady flow of sound advice and guidance.

REFERENCES

1. J. H. Coombs and E. S. Bomar, Report ORNL-1463.
2. J. A. Lane et al., Feasibility and Economics of Aqueous Homogeneous Reactors, Report ORNL-1096, 1951.
3. J. A. Lane, personal communication, Aug. 12, 1953.

ABOUT THE AUTHOR

Robert S. Livingston is Director of the Electronuclear Research Division of the Oak Ridge National Laboratory and also is Chairman of the Package Reactor Project Committee. He received the Ph. D. degree from the University of California, Berkeley, in 1941; his research was in the field of nuclear physics. He joined the staff of the Tennessee Eastman Corporation at Oak Ridge in 1943 and has continued in the research program there since the laboratory was established. His chief interest has been in the fields of research connected with the development and application of cyclotrons and other heavy nuclear machinery.

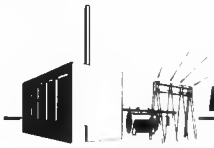

REACTOR FUTURES

A Gas-cooled Liquid-metal Reactor

H. L. FALKENBERRY,* C. J. RASEMAN, W. A. ROBBA, T. V. SHEEHAN, and L. D. STOUGHTON

Brookhaven National Laboratory

November 1954

ABSTRACT

This article describes a helium-cooled liquid-metal-fuel reactor with a graphite core structure. The fuel is a solution of uranium in molten bismuth. The graphite is composed of blocks containing vertical holes for the fuel and horizontal holes for the helium coolant, which passes directly through the core to the turbine. The liquid-metal fuel circulates slowly at a rate sufficient for fuel processing. The reflector material is graphite, and, if breeding is desired, the fertile material is a thorium-bismuth slurry.

A major advantage of this system lies in the ability of the closed-cycle gas turbine to efficiently utilize the clean inert high-temperature gas from a nuclear reactor in the direct production of useful power. The power-plant equipment can be made compact by the use of elevated pressures. As suitable materials of construction for higher temperatures are developed, further increases in efficiency can be realized by the closed-cycle plant.

The system studied will produce 60 megawatts at the generator terminals at an over-all efficiency of 40.4 per cent. The turbine inlet temperature is 1400°F, and the maximum system pressure is 1000 psi. The reactor core is a 5-ft cube contained in a 14-ft-diameter spherical vessel, and the maximum fuel temperature is 1800°F.

1. INTRODUCTION

This article describes a nuclear power plant that combines the advantages of a liquid-metal-fueled reactor with those inherent in a closed-cycle gas turbine. In this plant a common supply of helium serves as reactor coolant and power-plant working fluid. The high temperatures available in a nuclear reactor can be utilized to the fullest advantage in a closed-cycle gas-turbine power plant since it is possible to use the heat energy at a temperature close to that at which it is available without danger of chemical attack on power-plant components.

The present experimental and developmental work at Brookhaven National Laboratory (BNL)

*On loan to Brookhaven National Laboratory from the Tennessee Valley Authority.

is directed toward an externally cooled, or circulating fuel, liquid-metal-fuel reactor that works in conjunction with a steam-turbine cycle.[1] This article shows another method of utilizing some of the advantages of the uranium-bismuth liquid-metal fuel, such as continuous fuel make-up and processing, unlimited burn-up, no radiation damage to fuel, high specific power, and satisfactory properties at elevated temperature. The reactor would be internally cooled, graphite moderated, and liquid-metal fueled, with the heat transferred directly to the cycle working fluid, i.e., helium. Although many of the basic problems are similar to the externally cooled Liquid Metal Fuel Reactor (LMFR), the ultimate feasibility of the gas-cooled liquid-metal-fuel reactor is dependent on several unknown factors that have yet to be studied.

The reactor for this power plant consists of a pressure vessel containing cross-drilled graphite shapes as the core, with a similar reflector or breeding blanket surrounding the core. The graphite core structure contains horizontal rows of gas passages with alternate vertical rows of fuel passages. The fuel passages carry molten uranium-bismuth alloy. This molten fuel is stagnant, except for a small processing stream of uranium-bismuth leaving and reentering the reactor at a rate of approximately 0.2 gal/min. This stream is processed by contacting with fused salts, as proposed and developed by BNL for the LMFR. Nongaseous fission products are removed by the salt, whereas gaseous fission products are removed by suitable degassing equipment.

If breeding is desired, a fertile material would be inserted in an appropriate set of passages in the graphite blanket region, with diverted helium from the core coolant stream passing through the other set of passages. The breeder fluid would be the thorium bismuthide slurry that is being developed at BNL. The slurry would be periodically circulated for the removal of the bred fissile material.

The closed-cycle gas-turbine power plant, as proposed by the Escher Wyss Engineering Works, Zurich, Switzerland,[2,3] has been under development by that firm since 1936. The results to date have given promise of the advantageous application of the closed-cycle gas-turbine system to power-plant requirements. The range of useful output of the system would be tremendously enhanced if a nuclear reactor were to replace the conventional fuel-fired gas heater.

Major equipment items of the power plant are the machinery set, the heat-transfer apparatus, and the control system. The machinery set consists of a two-stage axial-flow compressor, with intercooling between stages, driven by a high-pressure turbine at constant speed. Helium leaves the high-pressure turbine and flows directly to a low-pressure turbine that generates the useful power. The heat-transfer apparatus is of the extended surface type, plate fin, plate pin, or tubular, depending on the application. The control system consists of a regulator to set a constant system pressure and a low-pressure receiver–high-pressure accumulator system and transfer pump.

The major advantage of the closed-cycle system is its ability to use a clean inert high-pressure gas as the working fluid. The rotating machinery is not subject to corrosion and deposition problems, and it can be made compact because turbine exhaust is at a relatively high pressure. Heat-exchange-equipment size would be reduced by the use of small hydraulic passageways. Other advantageous characteristics include (1) load-control equipment external to the main working-fluid stream because the load can be varied, while maintaining an essentially constant efficiency, merely by changing the pressure level in the system and (2) lower cooling-water requirements because of sensible heat rejection from the system instead of latent-heat rejection.

The net effect of these advantages is the potential reduction of gas-turbine equipment costs below steam equipment costs.

The system to be described will produce 60 megawatts at the generator terminals. Helium will enter the turbine at 1400°F and 1000 psia. The required heat output of the reactor will be 148.5 megawatts, giving a system heat rate of 8460 Btu/kw-hr. The proposed layout of the system is shown in Fig. 1. The turbogenerator and its associated equipment will be located out-of-doors with the reactor and fuel-processing equipment located in an underground shielded room.

A system of this size could be used to supply a block of electrical power in regions where normal transmission costs or conventional fuel-

supply costs are high. It could be operated with or without a breeder blanket, depending on the over-all economic considerations. A similar system would be applicable as a central-station type breeder reactor with a single gas-turbine plant providing a net electrical output within the limits of present-day steam-turbogenerator

When a gas-turbine cycle is considered, turbine inlet temperatures in the range of 1200 to 1500°F are required to produce optimum efficiency. This means that reactor fuel temperatures in the range of 1400 to 2000°F are necessary. Present technology offers very few materials that can contain the uranium-bismuth

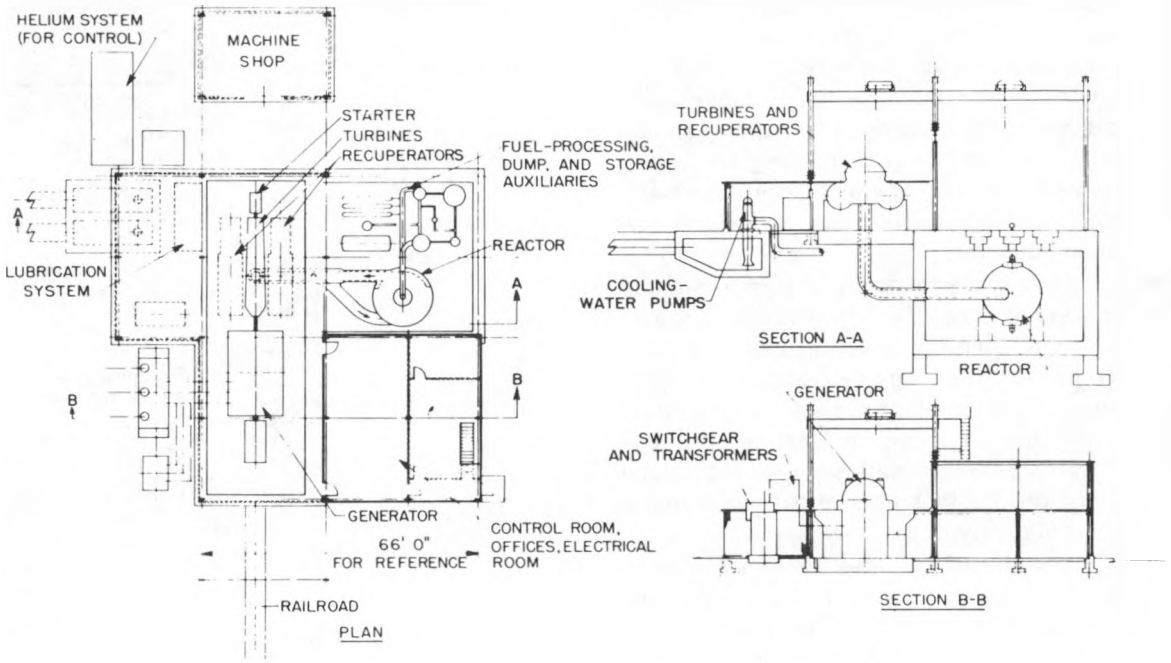

Fig. 1 — Plant layout for a 60-megawatt nuclear gas-turbine power plant.

equipment. In the field of the so-called "package reactors," this system would have the advantage of requiring only the supply of fresh fuel and salt and the return or disposal of contaminated salt. It would not require mechanical replacement of the core at a remote base.

2. REACTOR DESIGN

2.1 Heat Transfer

The use of a liquid fuel permits heat to be removed either internal or external to the reactor core. In the externally cooled LMFR the liquid fuel transports heat from the core to an external water boiler at a top fuel temperature of 1000°F. In this case core design is relatively simple, but the fuel inventory is increased owing to holdup in the external equipment.

fuel at these temperatures, much less to circulate it. An internally cooled liquid-metal-fuel reactor core would offer the best possibility of properly containing the liquid fuel. In order to include sufficient heat-transfer surface, core design would be relatively complex, but external fuel holdup would be reduced to a minimum.

To achieve the optimum power-conversion cycle, it is necessary that there be minimum temperature degradation between the reactor fuel and the turbine inlet. To accomplish this, it is proposed to circulate the coolant directly through the reactor core to the turbine inlet. Helium is a suitable coolant because of its good heat-transfer, nuclear, and chemical properties. The graphite core structure must be designed to give sufficient heat-transfer surface with a minimum resistance to gas flow and to prevent

contamination of the helium. A relatively high gas pressure will be required by the system in order to keep pressure losses low and equipment sizes moderate. Since the basic elements of the core are each potentially suitable in the higher temperature range, the upper temperature limit of the system, and consequently the extent to which the performance of the system can be improved, will probably be set by interactions between the basic elements, i.e., graphite–uranium–fission product reactions.

Heat-transfer design of the reactor core depends on many variables. Some of these variables are mutually dependent on other considerations, such as criticality requirements, gas-turbine-cycle requirements, and mechanical-design requirements. For example, the gas-coolant channels should be designed to (1) provide a heat-transfer surface to gas volume ratio for a given core size that will not seriously affect the net density of the graphite moderator; (2) handle the required gas flow while sustaining only a small pressure loss, as dictated by the turbine-cycle studies; and (3) provide sufficient graphite wall thickness between the fuel and the coolant channels to assure the mechanical stability of the core.

Initial consideration was given to finned graphite tubes for containing the fuel within the core. This scheme was abandoned because of the inability of the tubes to provide sufficient heat-transfer surface in a reasonable core size. Instead, large blocks of graphite drilled with two sets of holes, one set for the fuel and one set for the coolant, are proposed. This allows a compact array of fuel and gas channels, as shown in Fig. 2. Alternate rows of rectangular slots contain the uranium-bismuth fuel and the helium coolant.

Coolant channels of small hydraulic radius are desirable because they give a large heat-transfer surface to coolant volume ratio. The use of a clean inert gas coolant imposes no restrictions in this direction. However, since the pressure loss of the coolant going through the reactor core has a direct effect on the gas-turbine-cycle efficiency, it is necessary to optimize the size of the coolant channel.

It is desirable to express the heat-transfer capabilities of a reactor core in terms of parameters such as gas volume and allowable pressure loss in order that they may be readily optimized with the criticality calculations and the gas-turbine-cycle calculations. After an apparent optimum has been established, a detailed design may follow.

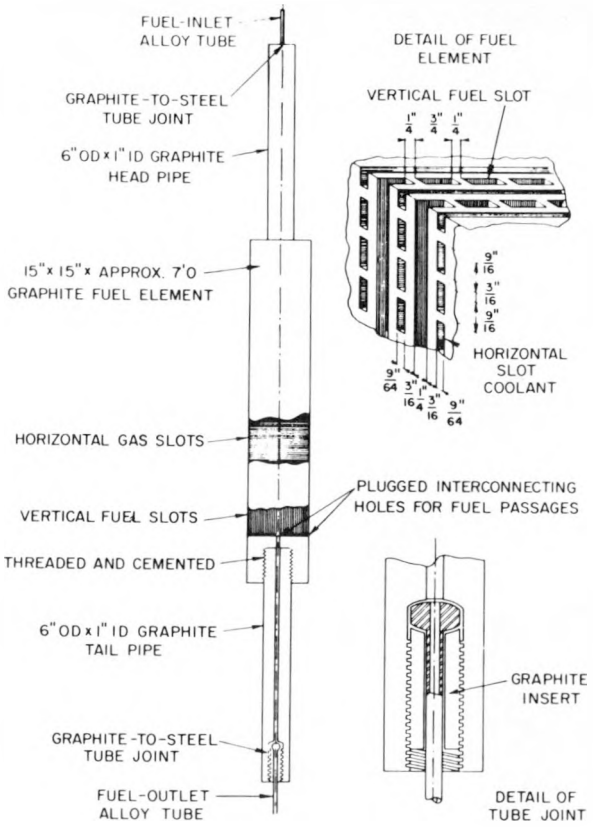

Fig. 2—Fuel and gas channels.

The criterion of fixed pressure loss of the gas coolant indicates that the equation for heat-transfer surface (see Table 1 for definitions of symbols)

$$S = \frac{Q}{h\,\Delta t} \tag{1}$$

and the equation for pressure loss

$$\frac{\Delta P}{P} = e = \frac{G^2 f V_m L}{2gr(144P)} \tag{2}$$

should be combined in order to optimize the coolant-channel size.

Table 1 — Definitions of Symbols Used for Heat-transfer Design

Symbol	Definition
A	Total face area of core, sq ft
C	Specific heat (1.25 Btu/lb/°F for helium)
D	Equivalent diameter, ft
e	Pressure-loss fraction of inlet pressure ($\Delta P/P$)
f	Friction factor
G	Mass velocity, lb/hr/sq ft
g	Gravitational constant (32.2 ft/sec^2)
h	Gas-film heat-transfer coefficient, Btu/hr/sq ft/°F
L	Length along coolant channel, ft
P	Pressure at reactor inlet, psi
Q	Total heat generation, Btu/hr
R	Gas constant (386 ft/°R for helium)
r	Hydraulic radius, ft
S	Total heat surface, sq ft
ΔT	Coolant temperature rise through reactor, °F
Δt	Temperature drop across gas film, °F
T_m	Average gas temperature, °F
u	Viscosity lb/hr/ft
V_m	Average specific volume, cu ft/lb
W	Total weight flow, lb/hr
x	Ratio of gas-flow area to total face area of core
y	Ratio of effective heat-transfer perimeter to total perimeter
Z	Ratio of maximum to average heat generation

Let the gas-film coefficient

$$h = 0.027CG^{0.8}\left(\frac{u}{D}\right)^{0.2} 3600$$

and the friction factor

$$f = 0.045\left(\frac{u}{DG}\right)^{0.2}$$

Introduce a factor x (ratio of gas-flow area to total face area of core) and a factor y (ratio of effective heat-transfer perimeter to total perimeter) for any coolant channel.

Solving both equations for hydraulic radius to length ratio gives

$$\frac{r}{L} = \frac{0.027C\left(\frac{u}{D}\right)^{0.2}(xA)^{0.2}yW^{0.8}\,\Delta t\,(3600)}{Q} \qquad (3)$$

$$\frac{r}{L} = \frac{0.045\left(\frac{u}{D}\right)^{0.2} RT_m W^{1.8}}{2ge(144P)^2(xA)^{1.8}} \qquad (4)$$

Solving Eqs. 3 and 4 simultaneously and substituting $W = Q/3600C\,\Delta T$ gives

$$Q = 3.22 \times 10^6 \frac{C}{R^{0.5}}\left(\frac{e\,\Delta T}{T_m}\right)^{0.5} P\,\Delta t^{0.5}\,xAy^{0.5} \qquad (5)$$

It is now possible to fix these parameters and find the core size as a function of power output. For the 60-electrical-megawatt case the following values are used: total heat generation Q, 506×10^6 Btu/hr, and coolant-temperature rise ΔT, 514°F, with an average coolant temperature of 1140°F and a pressure loss of 1.5 per cent of the inlet pressure. Since we are concerned for the moment only with the core, a value for e of 0.01 will be used. For helium the specific heat C is 1.25 Btu/lb/°F and the gas constant R is 386 ft/°R. As reactor operating parameters, let the reactor inlet pressure P be 1000 psi. For the gas-film temperature drop Δt, a value of 200°F will be used. Because of the good heat-transfer properties of helium, the gas film will not be the controlling resistance between the fuel and the coolant. Consideration of the thermal conductivities of the graphite wall, the bismuth-to-graphite film, and the uranium-bismuth fuel indicates a reasonable estimate of the ratio of over-all temperature drop to gas-film temperature drop to be 2.0. Therefore, by assuming gas-film Δt to be 200°F, a fuel-to-gas temperature drop of 400°F is implied. Based on a reactor coolant-outlet temperature of 1400°F and uniform heat generation along the coolant channel, this would give a maximum fuel temperature of 1800°F.

Substituting these values in Eq. 5 gives

$$xAy^{0.5} = 3.09 \qquad (6)$$

If a core shape is selected wherein all coolant channels are of the same length, then the coolant area factor x becomes the percentage of gas voids in the moderator for the entire core. Typical of this shape would be a cubical or cylindrical (axial flow) core. A cubical core was selected as the simplest shape to form with the core blocks. The penalties of an increased

critical mass and a somewhat larger core vessel remain to be evaluated.

To find the required core size, let the coolant-area factor x be 0.15 per cent. The effective heat-transfer perimeter of a rectangular slot could be assumed to include both long sides that face the fuel channels and only one short side. Using a value for y of 0.8 in Eq. 6 gives the required face area A of 23 sq ft, which is equivalent to a 4.8-ft cube.

Substituting these values in either Eq. 3 or 4 will give the proper hydraulic radius of the coolant channel. To find the actual dimensions of the coolant slots, the percentage of fuel volume in the core and the minimum practical thickness of graphite between fuel and coolant slots must be considered. From nuclear calculations a fuel-volume fraction of approximately 20 per cent is desired. The minimum graphite thickness was set at $^3/_{16}$ in. Detailed consideration of all these factors leads to the following slot dimensions:

Fuel: 0.250 by 0.75 in., with 0.250 in. between slots
Gas: 0.141 by 0.565 in., with 0.187 in. between slots
Fuel-volume fraction: 24.5 per cent
Gas-volume fraction: 13.8 per cent
Graphite-volume fraction: 61.7 per cent
Core size: 5-ft cube

These calculations have been made on the basis of uniform heat generation throughout the core in order to simplify the preliminary calculations. A number of possibilities present themselves for approaching a uniform coolant-outlet temperature while accounting for the realities of reactor operation.

1. Apply a factor Z in Eq. 5 which would be inversely proportional with the first power of Q. This factor is defined as the ratio of maximum heat flux to average heat flux. Design all channels uniformly, and employ external orificing to account for the variation in heat flux.

2. Flatten the flux distribution by varying the widths of the fuel channels, i.e., nonuniform fuel distribution.

3. Vary the spacing between adjacent coolant channels.

Although arbitrary values have been assigned to the many variables in Eq. 5 in order to illustrate the 60-megawatt case, this equation affords a rapid method for optimizing these variables with respect to other components of the entire system. Further studies toward improving the performance of the system would include increasing the gas voids at the expense of fuel inventory and increasing the allowable pressure loss and reducing the inlet temperature to the reactor at the expense of cycle efficiency.

It is of interest to take a quick look at a system generating 200 megawatts of electricity at 40 per cent thermal efficiency. If the same assumptions are used, except that $Q = 1.71 \times 10^9$ Btu/hr, gas film $\Delta t = 300°F$ (over-all $\Delta t = 600°F$), and coolant-area factor x = 0.2, then substituting these values in Eq. 5 gives the required face area A of 47.6 sq ft. This is equivalent to a 6.9-ft cube.

2.2 Mechanical Features

(a) Reactor Vessel. The reactor core and reflector are installed inside a pressure vessel. Two cases have been considered, a cylindrical vessel and a spherical vessel. The obvious advantage of a spherical vessel is that the wall thickness is halved.

Design conditions selected for the reactor vessel are:

Operating pressure: 1000 psig
Design pressure: 1250 psig
Shell design temperature: 900°F
Proposed material: carbon–0.5 per cent molybdenum (ASTM A204 or equal)
Allowable working stress: 13,000 psi

Since the vessel is exposed to helium on the inside and air on the outside, there is little corrosion or oxidation with which to contend.

The reactor outlet temperature is 1400°F, and the inlet temperature is 886°F. The design is such that the vessel wall is exposed to reactor inlet gas only. The high-temperature gas leaving the reactor is carried in internally insulated piping that begins with a hood at the reactor outlet, thereby preventing any direct contact of the outlet gas with pressure parts. The hood and inner shell of the internally insulated pipe are made of suitable alloys to resist the temperature. These parts operate essentially stress free.

The reactor core considered for this study is

a 5-ft graphite cube surrounded generally by 4-ft graphite reflector. If the corners of the resultant cubical graphite structure are rounded off so that not less than a 2-ft 6-in. reflector is provided, it can be installed in a 12-ft 6-in. cylinder or a 14-ft 3-in. sphere. The corresponding thicknesses of these vessels, using a

(b) Graphite Arrangements. An arrangement drawing (Fig. 3) has been prepared which shows the method of installing the graphite parts inside a spherical vessel. The core, together with fuel-inlet and -outlet pipes and the reflector surrounding the core, is shown. The gas flows horizontally through the reactor core,

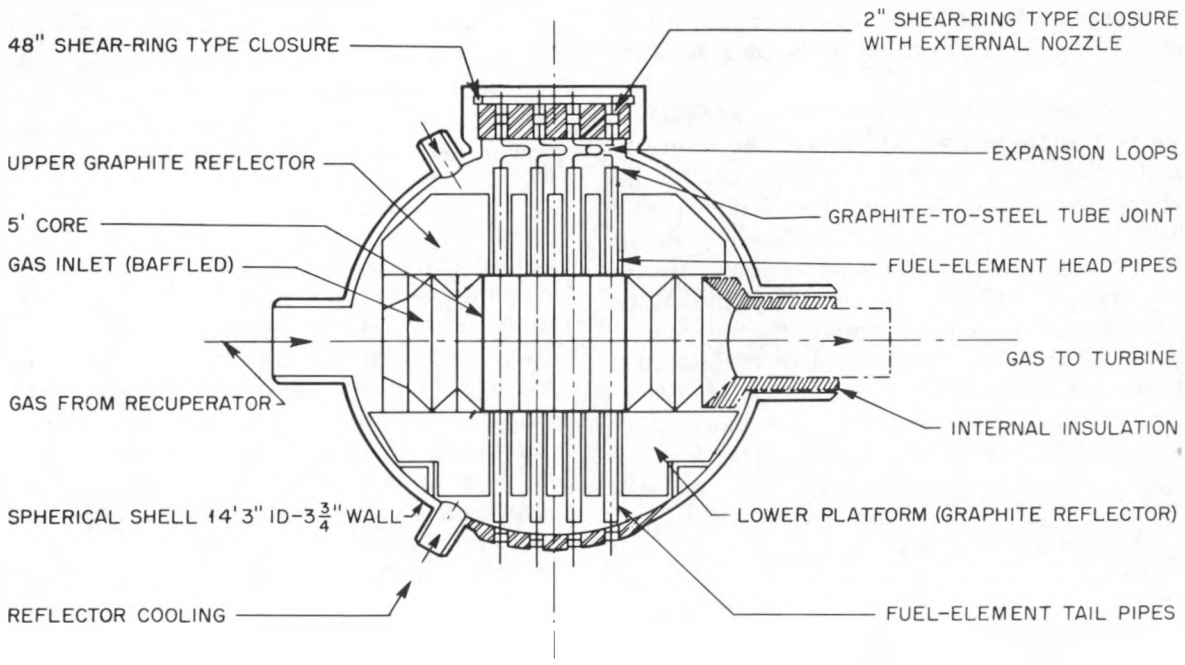

Fig. 3—Graphite arrangement.

joint efficiency, E, of 95 per cent, calculated from the simple relations $t = PR/SE$ and $t = PR/2SE$ are

12-ft 6-in. I.D. cylinder—t = 7⅝ in.
14-ft 3-in. I.D. sphere—t = 3¾ in.

The pressure-vessel industry will be able to fabricate either of these vessels; moreover it is entirely feasible to internally insulate the vessel and to take advantage of presently available higher strength alloys to further reduce wall thicknesses if desired. To permit installation and repair or replacement of core parts, a fairly large opening with a high-pressure closure is required. Again several types of closures of 36 in. to perhaps 60 in. are available for this service; furthermore, welded closures could be used.

whereas the fuel flows from top to bottom through the reactor-core elements, which will be described in Sec. 2.2f.

The general assembly of the graphite is described below and will apply to an arrangement using either a spherical vessel (see Fig. 3) or a cylindrical vessel.

The lower graphite reflector consists of graphite beams 4 ft deep and 15 in. wide, of a length sufficient to span the inside of the vessel from shelves provided on the inside wall. Such beams will be of adequate strength to support the entire graphite structure in the vessel without exceeding the allowable graphite stresses in bending. Should there be any difficulty in this respect, the shelves can be extended to reduce the span where necessary.

The fuel element consists of a central body

15 in. square and about 7 ft long, with 6-in. head and tail pipes about 5 ft long protruding from the ends. All these parts are of graphite and are shown in Fig. 2. The core contains 16 such fuel elements standing on end on the lower graphite reflector platform. The tail pipe from each fuel element passes through holes in the beams, and the alloy-steel fuel-pipe connection from the bottom of each tail pipe passes through a suitable high-pressure closure in the bottom head, thus providing a fuel connection to the outside of the vessel.

The side-reflector graphite blocks are stacked beside the 16 fuel elements, and the inlet and outlet graphite diffusers are stood up at the inlet-gas face and outlet-gas face of the reactor core, respectively. These diffusers contain gas passageways like louvers to provide some reflection of neutrons at the inlet and outlet connections. Moreover, it may be desirable to arrange the inlet- and outlet-gas ports so that there is a right-angle turn at each location to permit more effective reflection and neutron economy. The internally insulated hood at the reactor outlet makes good contact with the faces of the reflectors to prevent excessive hot-gas leakage against the vessel wall.

The upper graphite reflector is now installed. It may consist of small blocks keyed together to some extent to prevent shifting with temperature. Otherwise it is not called upon to resist particular stresses.

The alloy-steel inlet pipe protruding from the head pipe of each fuel element is sealed in a small high-pressure closure in the closure plate for the large high-pressure closure. Both inlet- and outlet-fuel pipes may be wrinkled, bent, provided with bellows, or otherwise arranged to provide for thermal expansion between the graphite and the steel vessel. Furthermore, since the graphite is much hotter than the steel, these motions may almost cancel.

(c) Reflectors and Reflector Cooling. As noted above, the upper and lower reflectors are 4 ft. The corners are rounded off to a 2 ft 6 in. minimum, and the side reflectors are 4 ft at the thickest point. In the case of the cylindrical vessel, upper and lower reflectors could be made 6 to 8 ft if desired since it is only necessary to increase the length of the cylindrical part of the vessel. In the case of the spherical vessel, the reflectors cannot be increased materially above 4 ft without increasing the size of the sphere.

The drawings do not indicate any special provisions for reflector cooling, other than inlet and outlet pipes in the heads of the vessels to inject a portion of the entering gas into these spaces. It is intended to drill the reflector blocks as necessary to permit sufficient gas to flow through these blocks to remove the heat generated in the reflector.

Outside of the considerable design, drafting, and machining time necessary to make all these graphite blocks perform as required, no unusual problems in the reflector cooling are foreseen.

(d) Graphite Shapes. It will be noted that the graphite shapes contemplated for the parts of this reactor are quite large. We believe all these parts are within the capability of the graphite industry. In some cases they may be made with power-operated tools, such as air tampers, the mix being rammed into appropriate molds. In other cases extrusion heads attached to existing machines can probably handle the problem. Furthermore, some changes in the design will permit less massive parts. For instance, the bottom platform can be more fully supported by steel shoes, thus bringing the whole reflector into a situation where no particular bending stresses would be encountered and permitting a block structure to be used.

In the case of the fuel elements, which are 15 in. square (12 or 6 in. square could be used as well), 15 in. round stock about 7 ft long would be needed. Such shapes are currently extruded for electrode work; however, a coarse mix is used for electrodes. This design will need a fine-grained mix, cured and graphitized more slowly than is the present practice.

(e) Drilling Graphite. For the reflector cooling channels, owing to the low-heat duty, we think ordinary drilled holes will be sufficiently accurate. Milled slots will be needed in some cases. All these are within present machining-practice capabilities.

In the case of the fuel elements, small and very accurately spaced slots are required (see Fig. 2). There are several proposed methods of doing this, four of which are described below.

1. Use stock 24 in. long and 15 in. square. Drill pilot holes and broach the slots to the re-

quired dimensions, then cement three pieces together and regraphitize into a seamless piece. Chase slots after regraphitizing. Plug ends of slotted holes after making end portholes.

2. The more promising method, subject to some development work, is to use sonic drilling for the slots both crosswise (15 in.) and lengthwise (60 in.). Any shape of hole can be drilled with this method, and there are no rotational forces to deflect the drill. The harder the material the better it works. We see every promise that once a set of drills is started into a piece, with the hole just made serving as a guide, very great accuracy for long distances should be easily obtained.

3. Extrude shapes around a core structure that, on being burned or melted out, will provide passages as necessary. Passages may need to be chased or broached for cleanup purposes.

4. Extrude or ram the graphite matrix over pins that will leave pilot holes in the structure for further drilling or broaching.

(f) Fuel Element. The complete fuel element is shown in Fig. 2. The main body of the element is about 7 ft long and 15 in. square, with 16 such elements comprising the 5-ft cubical core.

The gas slots are drilled crosswise through the element in the 5-ft active section.

The fuel slots are drilled lengthwise through the element, bottoming at the lower boundary of the active section. Cross holes intersect each row of fuel slots at the bottom, and a single cross hole intersects the afore-mentioned cross holes and the central outlet channel, thus connecting all vertical fuel slots to a single outlet. The outer ends of connecting cross holes are plugged.

A similar interconnection arrangement of holes will be used at the top; however, owing to the threaded connection for the head pipe, it will be necessary to cement, plug, and regraphitize the unnecessary holes at the top of the element before the recess for the head pipe can be machined and threaded.

Rugged head and tail pipes are screwed into the top and bottom of each fuel element. Connections to alloy-steel inlet and outlet fuel pipes are made by means of a special spherical seated graphite-to-tube joint.

(g) Breeding Blanket. The arrangement described in this article does not have a blanket; however, it would be possible to install, in appropriate holes in the reflector, vertical tubes containing fertile fluid. Such tubes may be cooled by gas passing in the same general manner as that described for reflector cooling which would extract both reflector and blanket heat. Provisions would be required to permit slow circulation of the fertile fluid to a processing plant and back to the blanket.

2.3 Fuel Processing

The use of a liquid-metal fuel in this reactor offers the usually mentioned advantages of fluid-fueled reactors, i.e., continuous processing, good neutron economy because of the immediate removal of fission products, high fuel burn-up, and no radiation damage to the fuel. The particular advantage offered by the liquid-metal fuel is its high-temperature low-vapor-pressure characteristics.

The fuel-processing plant under development at BNL for the externally cooled version of the LMFR should be applicable in practically every detail to the reactor described here. The processing may be carried out in the 900°F temperature range and under negligible pressure, compared with that in the reactor. Basically the processing scheme consists in continuous removal of gaseous fission products from the surfaces of the liquid-metal fuel and removal of nongaseous fission products by salt extraction. Of the gaseous fission products, Xe^{135} is by far the most objectionable; its solubility in bismuth has been estimated to be in the range of a few parts per billion, based on work by Bonilla[4] at Columbia University. It should therefore be possible to desorb the xenon by applying a vacuum or sparging the fuel with helium. Xenon thus removed or sparged would be separated out in a cold trap containing activated charcoal.

Most of the higher cross section nongaseous fission products are removed from a small processing stream by contacting with molten salts at the proper oxidation-reduction potential. Even under optimum conditions some uranium is transferred to the fused salt, and a uranium-recovery extraction column in the exit salt stream appears necessary to reduce uranium losses to acceptable quantities. For a reactor generating 150 megawatts of heat, approximately 150 g of fission products will be formed per day. If breeding is considered, it may be

necessary to maintain a fission-product concentration in the fuel stream of 20 ppm or less. If the fission-product concentration in the processing stream is reduced to 5 ppm, then the processing stream will be 267 gal of uranium-bismuth per day. Since the salt leaving will contain approximately 400 ppm of fission products, the salt quantity per day will be 830 lb.

There is the possibility of pressurizing the fuel-processing system. This can be done by moving the system inside the pressure vessel or using a suitable pressure enclosure outside. This has the double advantage of eliminating the graphite-to-steel joint and the need for a small high-pressure pump for hot radioactive fuel.

2.4 Nuclear Considerations

The nuclear calculations were done on the basis of a two-group two-region model, the second region being considered infinite. The first set of reactor calculations were for a fully reflected core. In this case breeding was eliminated in favor of simplicity of design. Here a 5-ft reflected reactor is capable of producing 150 megawatts of heat with a critical mass of 3.2 kg and a resulting specific power of 46,800 kw/kg. However, it should be realized that the graphite reflector considered here must be at least 4 ft thick to match the nuclear assumption of infinite thickness. If the reflector were beryllium, this thickness would be cut in half. In a mobile application, where size is important, either of these reflector thicknesses could be halved with a reduction in specific power of not more than one-half. The reactor cores in the first set of calculations can be considered thermal down to about 3 ft, the graphite to uranium ratio for this size being 3800. At 5 ft the ratio is 12,000.

In the second set of calculations the reflector was replaced by a breeding blanket consisting of graphite, a thorium-bismuth slurry, and the helium coolant. The thorium concentration in the bismuth was assumed fixed at 10 wt. %, and thus an increased thorium concentration in the blanket can only be achieved at the expense of replacing graphite by bismuth. Neither neutron economy nor breeding gain was calculated at this time, but calculations from the externally cooled LMFR indicate that a gain of over 1 is certainly possible with the gas-cooled version. In the case of the blanketed reactor, the minimum uranium critical mass is three times that of the reflected reactor. However, since the minimum has moved to a larger core, the mass has only doubled; consequently the specific power for a 5-ft breeder is 23,000 kw/kg. Owing to the reduction in diffusion length in the blanket, a 2-ft-thick blanket can now be considered infinite.

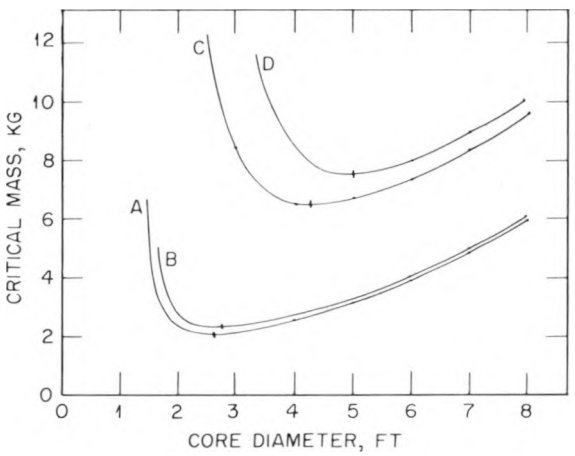

Fig. 4—Graph of critical mass vs. core diameter. A, infinite reflector of 90 per cent graphite and 10 per cent helium; for a core with 65 per cent graphite, 20 per cent bismuth, and 15 per cent helium. B, infinite reflector of 90 per cent graphite and 10 per cent helium; for a core with 61.7 per cent graphite, 24.5 per cent bismuth, and 13.8 per cent helium. C, blanket with 0.2 g of thorium per cubic centimeter of blanket; same core as A. D, blanket with 0.3 g of thorium per cubic centimeter of blanket; core same as A.

Figure 4 is a graph of the critical masses of the two cases considered. The critical concentrations of fuel in the bismuth for the 5-ft cores are 470 ppm for the reflected reactor and 1100 ppm for the blanketed reactor. The 1100-ppm concentration is less than one-half the maximum solubility for the 886°F low-temperature point for the fuel.

2.5 Reactor Safeguard

We believe that this reactor can be designed to meet safeguard requirements. Inherent in the LMFR is a negative temperature coefficient of reactivity on the order of $-2 \times 10^{-4} \Delta K/°C$.

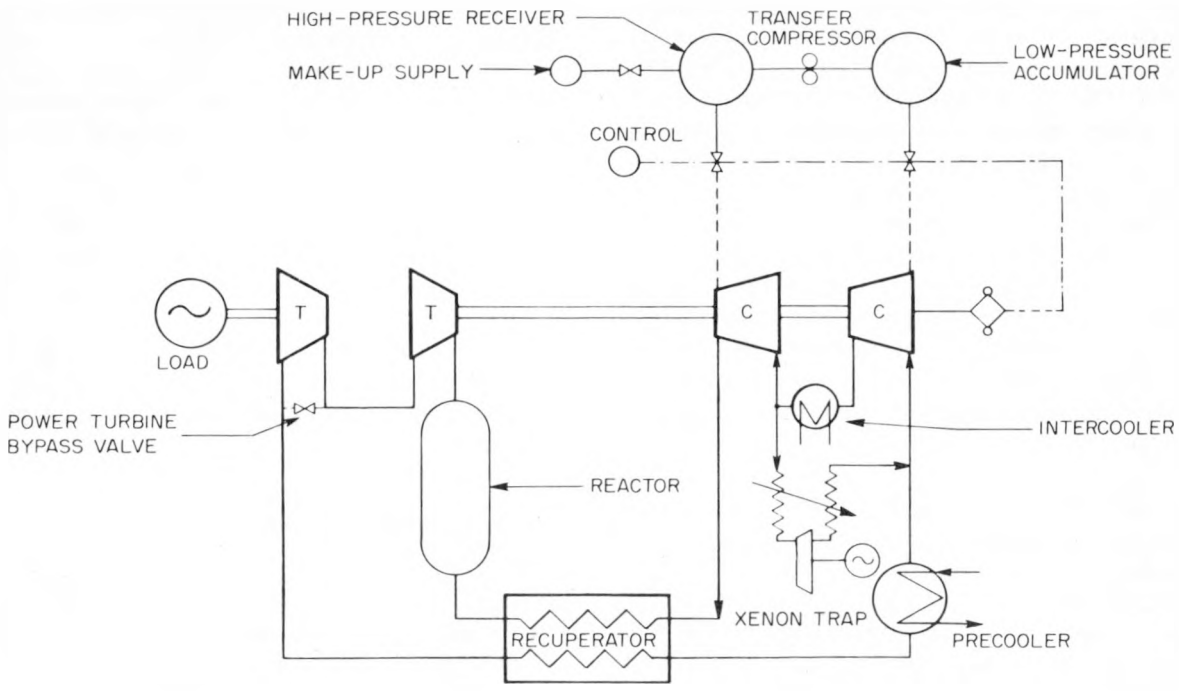

Fig. 5 — Flow diagram of power-plant cycle and control system.

Although the drawings do not indicate safety rods, these can be installed if they are deemed necessary. Control of the reactor power is achieved through the temperature coefficient and the bypassing of the helium.

Safeguard requirements might necessitate enclosing the entire reactor vessel and piping in another vessel. Probably the simplest solution would be to place the reactor in a room or basement of such volume that the entire system pressure could be released without raising the pressure of the room appreciably. The room would require impervious walls, but provisions for the chamber to withstand high internal pressures would not be necessary.

3. POWER-PLANT DESIGN*

3.1 Power-plant Cycle

A flow diagram of the power-plant cycle and control system is shown in Fig. 5. At design output helium at 90°F and 426 psia pressure enters the low-pressure compressor, where its pressure is raised 155 per cent, to 661 psia. The helium passes through an intercooler, where the heat of compression is removed, and the helium is returned to the second-stage compressor at 656 psia. Further compression occurs, raising the helium to 1015 psia and 210°F. From the compressor system the helium passes to the recuperator, where its temperature is raised to 886°F by the heat rejected from the power turbine. From the recuperator the helium passes through the reactor, where its temperature is raised to 1400°F. It then flows to the high-pressure turbine, where it expands, driving the compressor set at a constant speed. From the high-pressure turbine the gas flows to the low-pressure or power turbine at 1160°F and 665 psia. The gas expands through the power turbine, and useful work is extracted. The gas leaves the power turbine at 942°F and 440 psia to enter the recuperator, where it releases heat to the helium leaving the compressor. Finally, the gas passes through the precooler, where its temperature is lowered to 90°F, and the cycle is repeated.

The basic design principles of a closed-cycle

*Information in this section has been submitted by the American Turbine Corporation. A detailed analysis of the power cycle is contained in Report ATC-54-12 (unclassified), copies of which may be obtained from the American Turbine Corporation, 52 William Street, New York 5, N. Y.

power plant require the extensive use of heat-transfer surface for the recovery of heat available in the working fluid after expansion. The high system pressure at which a closed-cycle gas-turbine power plant operates, coupled with the fact that the working fluid is uncontaminated by products of combustion, makes this objective relatively easy to attain through the use of heat-transfer surface having flow passages of small hydraulic diameter and/or the use of extended surface. All chemically fired closed-cycle power plants built to date use air as the working fluid. The use of helium with its different gas properties makes necessary the reevaluation of the generally accepted cycles as used with air.

Compared to air, helium exhibits a considerable improvement in heat-transfer properties, the film coefficient being about 180 per cent higher under the same conditions of pressure level, pressure drop, and passage geometry. This results in heat-transfer equipment approximately 55 per cent of the size required for air or, where the equipment is the same size, an appreciable increase in the quantity of heat that can be transferred, the exact amount depending upon the effectiveness of the surface with air. For example, if the recuperator in the air-cycle machine has an effectiveness of 80 per cent, the same surface will have an effectiveness of 86 per cent in a helium cycle. If the effectiveness in an air-cycle machine is 90 per cent, which is more of the order used in a closed-cycle power plant, the same surface will have an effectiveness of 95 per cent in a helium-cycle machine.

On the other hand, the high specific heat of helium (1.25 Btu/lb/°F) and the fact that it is a monatomic gas make the design of the turbomachinery difficult, the number of stages required for the same temperature rise being roughly proportional to the specific heat or, compared to air, in the approximate ratio of 5 to 1 (1.25 to 0.24). However, a cycle analysis will show that the compressor temperature ratio required for maximum cycle efficiency decreases with increasing recuperator effectiveness. This fact is made use of in the design of a closed-cycle plant using helium as a working fluid, trading static heat-transfer surface for stages of turbomachinery.

In order for any closed-cycle nuclear power plant to be attractive economically, it is necessary that the power plant have a high thermal efficiency, which can be achieved only in a high-temperature machine, i.e., one operating at cycle temperatures in excess of approximately 1200°F. All experience to date with closed-cycle power plants has been at cycle temperatures ranging from 1250 to 1300°F, as dictated by limiting tube-wall temperatures in a chemically fired air heater. In a nuclear power plant this restriction is removed, and turbine inlet temperature is only limited, within reason, by reactor outlet temperature. However, our present experience would limit such temperatures to about 1500°F for a power plant of conservative design.

3.2 Design Assumptions

The current state of the art of designing turbomachinery of high stage loadings indicates that it is possible to obtain polytropic stage efficiencies of 89 per cent in compression and 88 per cent in expansion. Although stage efficiencies of turbines would normally be higher than compressors for the same work per stage, in an effort to reduce the number of stages in the turbine to an acceptable level, the work output per stage is about three times that of the compressor stage. This accounts for the lower turbine stage efficiency. Compression work is equally divided between the high- and low-pressure compressor, and each has a pressure ratio of 1.55 to 1, resulting in an over-all pressure ratio of 2.4 to 1.

Pressure losses in the plant have been assessed at 7 per cent, resulting in an over-all expansion ratio of $2.4 \times 1 - 0.07 = 2.23$ to 1. Pressure losses are distributed as follows:

Intercooler	−0.75 per cent
High-pressure recuperator	−1.50 per cent
Reactor	−1.50 per cent
Low-pressure recuperator	−2.25 per cent
Precooler	−1.00 per cent

Although these pressure losses may appear to be optimistic, they can be attained with careful design and without excessively large heat-transfer surface. Referred to an air-cycle plant this is the equivalent of a total over-all pressure loss of 11 per cent, assigning 5.5 per cent total pressure loss to the reactor, which would be the equivalent pressure loss in a fired heater.

Compressor inlet-air temperature is assumed at 90°F, based on 75°F cooling water. If cooling water is available at, say, 55 to 60°F, the efficiency of the plant would increase about 2 per cent.

A recuperator effectiveness of 93 per cent has been selected for the design since a plant of this type would be a base-load machine. This is slightly less than the maximum used in closed-cycle plants (94 per cent in the experimental Escher Wyss plant of 2000 kw) and is believed to be reasonable for a plant of this type.

3.3 Turbomachinery

Modern fluid mechanics and gas dynamics (upon which turbomachinery design is based) are founded upon the concepts of perfect fluid, potential flow, and real fluid corrections to this flow. Both the theoretical and experimental developments of the science are expressed in terms of kinematic nondimensional parameters and such nondimensional groups as Reynolds number and Mach number. Therefore, if the effects of these nondimensional variables are properly applied, much of the existing work on turbomachinery for air can be used for the design of units for another gas, such as helium.

The expected performance of the proposed 60-megawatt machine has a strong foundation in reality since the blading and proportions of the set have been closely patterned on an existing successfully tested development compressor and a successful turbine. The units chosen were selected as good examples of present-day practice for machines now running on industrial test and in service. The compressor and turbine were designed for air and tested in air, with air Mach-number limitations an important factor. The helium design is so closely patterned on the air machines that no attempt was made to take advantage of the release from Mach-number limitations. Hence there should be a slight unaccounted for performance bonus that follows the conservative design pattern adopted for this unit with the idea of providing as nearly guaranteed performance as is possible in the preliminary design of an unconventional machine.

In all cases tip speeds, solidity ratios, and blade diagrams are essentially identical to those of the reference machines. Hub-tip diameter ratios are made similar to those of the models, except where some modifications are needed to match the speed and volume flow of the helium machine.

(a) Compressors. Both the high- and low-pressure compressors are discussed at the same time since each has the same over-all pressure ratio and blading design. The only difference is an increase in the hub-tip diameter ratio and a decrease in the length of the high-pressure unit owing to the greater density and consequent reduced volume flow in this machine.

The blading is the standard free-vortex axial-stator inlet type pioneered by Escher Wyss of Zurich, Switzerland. This type of blading is conservative in concept and application but provides outstandingly high efficiencies and numerous constructional advantages for the many gas-turbine and industrial blower installations in service. This blading is especially attractive for a helium machine since the Mach-number restrictions, which provide the limiting conditions for the pressure-rise coefficient in air, do not apply in the less compressible helium.

Both compressor units are based directly on test data[5] in air. It should be emphasized that this test work, reported in 1945, represents conservative but efficient practice which resulted from many years of research and industrial application with this type of machine and which has been further proved in service in the years since 1945.

(b) High-pressure Turbine. The high-pressure turbine supplies the power for operation of the compressors. It is mounted with the compressors as a single-shaft three-bearing self-running turbocompressor set. No useful output torque comes from this turbine.

The turbine blading is a high-efficiency type based on aircraft gas-turbine practice. Absolute exit velocity from the rotor is axial, and experimental results show close agreement with a free-vortex radial distribution of velocity through the stage.

(c) Low-pressure Power Turbine. The low-pressure power turbine is mechanically independent of the compressors and high-pressure turbine, but it is directly coupled to the generator. The power turbine therefore rotates at a constant speed of 3600 rpm and produces the entire useful work output for the plant.

The blading is basically the same as that in the high-pressure turbine and derives from the same test data. However, the tip speed is only about one-half that of the high-pressure machine, and the gas velocities are reduced proportionally.

3.4 Heat-exchange Apparatus

Efficient heat-exchange apparatus plays an important role in the design of a closed-cycle power plant. All exchangers operate at an effectiveness of at least 80 per cent and may exceed 90 per cent. This requires that the units be of a special design if their dimensions are to be kept within reason. The problem is alleviated somewhat by the fact that the working fluid is clean, thus permitting the use of compact surfaces with flow passages of small hydraulic diameter.

The recuperator design is based on the Ferrotherm pin-fin flat-plate heat exchanger. The low-pressure passages are formed of rows of biconvex pins sandwiched between thin parting sheets. The high-pressure passages are formed of thin ribbons that are edge brazed to the low-pressure parting sheets. After assembly the entire unit is furnace brazed. The completed recuperator, which is rectangular in shape, is mounted inside a cylindrical pressure shell.

The precooler is constructed of a standard tube-in-shell design using fin tubes of the type manufactured by the Heat-X-Changer Company, Inc., to carry the helium. Cooling water flows through the shell in a four-pass cross flow.

The intercooler is a conventional tube-in-shell heat exchanger with a hairpin tube bundle and a divided tube sheet. The partially compressed helium flows through the tubes, and water flows across the tubes in the shell.

3.5 General Arrangement

A general arrangement of the 60-megawatt closed-cycle gas-turbine machinery set and heat-transfer apparatus is shown in Fig. 6.

The high-speed compressor and turbine set and the low-speed power turbine are arranged in a single case, split on the horizontal center line. The high-speed shaft, consisting of the two compressor stages and the high-pressure turbine, is mounted on three bearings, one at each end of the shaft and one between the low- and high-pressure compressor. The center bearing is a combination thrust and journal bearing. The low-pressure power turbine is located downstream from the high-pressure turbine, and it is supported on two bearings, the one at the turbine exhaust being a combination thrust and journal bearing. There is but one opened shaft in the machinery set, that being at the discharge end of the power turbine from which the generator is driven. A viscosity on contact type seal is used at this point to prevent the escape of helium from the system. The system pressure at this point is approximately 150 lb. Seals of this type are currently being used in compressors handling hydrocarbon gases at pressures far in excess of this level. When piston bearings of the type currently being used in canned rotor pumps, where the fluid being pumped is used as the lubricant, are fully developed, their use will make it possible to dispense with the lubrication and oil scavenger system.

The intercooler between compressor stages is designed to be an integral part of the machinery set, thus eliminating the necessity for external lines and their associated joints, which are a source of leakage. The intercooler is a hairpin tube type, with helium in the tubes and water in the shell. The tube sheet, to which the tubes are welded, is bolted directly to a mating flange on the bottom of the machinery-set casing between the low- and high-pressure compressors. The helium is conducted, by suitable diffusers, from the discharge of the low-pressure compressor through the intercooler and back to the high-pressure compressor inlet.

Through a system of internal ducts, helium leaving the compressor flows in an annular passage around the high-pressure turbine inlet pipe. In this way, openings in the machinery-set casing are reduced to a minimum.

3.6 Control System

The subject plant is designed for base-load operation on a network where the frequency (speed) control is from another source. Therefore only power-output (pressure-level) control is required, together with a means of synchronizing the speed of the output turbine to the reference source of the time of starting. Power, or pressure-level control, is effected by the

addition or withdrawal of working fluid from the circuit. Speed control of the power turbine is effected by bypassing.

Helium that is not being circulated in the power-plant cycle is stored in accumulators for subsequent use, i.e., this is a no-loss system. The accumulator system consists of two, or two groups of, storage bottles; one is the receiver, and the other is the accumulator interconnected by a transfer pump. In this system the total amount of helium in the power plant and tanks is constant at all times. Leakage losses are made up by the addition of helium to the receiver from time to time as required. A simplified diagram of this system is shown in Fig. 5.

Over the range of power output at which this plant will operate, assumed to be ±10 per cent of normal rating, power output varies directly with system pressure. Therefore the power-output control consists of a set of variable-datum pressure-reducing valves between the system and the receiver and accumulator tanks which are designed to maintain a constant preselected pressure level in the system.

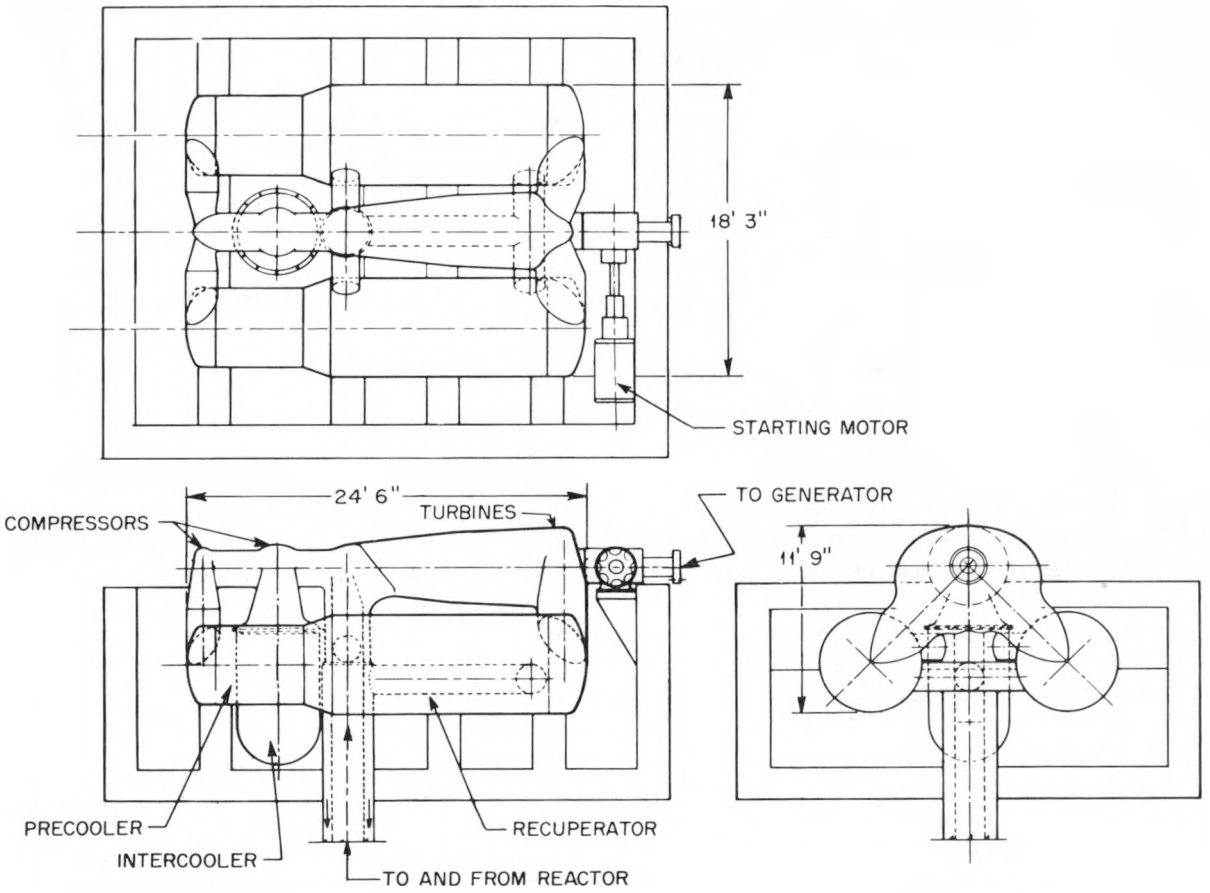

Fig. 6—General arrangement of the 60-megawatt closed-cycle gas-turbine machinery set, including heat-transfer apparatus.

An overspeed governor is provided on both the high-pressure compressor-turbine set and the power turbine. The governor on the compressor-turbine set is a top-speed governor only, tripping a compressor bypass valve when this set exceeds a predetermined speed limit. The governor on the power turbine is designed to come into play only in the event of an emergency, the presence of which makes it necessary to shut the plant down. In action the power-turbine governor opens the power-turbine bypass

valve, immediately reducing the weight flow through the power turbine. Since this reduces the back pressure on the compressor-drive turbine, it tends to overspeed, thus activating the compressor bypass valve. Furthermore, the power-turbine-overspeed governor trips the system-pressure regulator, resulting in the discharge of the contents of the system to the receiver.

When the power-plant load is dumped and the reactor activity level is reduced, a means must be provided to cool the reactor for a period of about 1 hr after shutoff. During the normal procedure of shutting off the plant and the emergency condition previously discussed, the compressor-turbine set will circulate helium through the reactor until the minimum self-running speed is reached. At that time a secondary motor-driven circulating compressor with an auxiliary cooling loop is energized, circulating helium through the reactor until activity is reduced to a point resulting in a safe temperature level.

3.7 Xenon Removal

The helium used in this plant is available commercially at a purity of 99.99 per cent. Impurities consist of argon, carbon dioxide, and nitrogen; none of these are in sufficient quantities to be of any concern. There is, however, the possibility of contamination of the system by gaseous fission products escaping from the reactor fuel elements. The principal volatile radioactive impurity of the fission process is xenon, and removal of the xenon from the working fluid is desirable to reduce the activity of the working fluid to an acceptable level and avoid the necessity of extensive shielding.

The xenon can be effectively removed to any degree desired by activated charcoal in a cold trap. This is accomplished by withdrawing a small stream of helium from the cold end of the compressor intercooler and passing it through a heat exchanger in which it is cooled to the temperature necessary to reduce the xenon content to a permissible level. Since the xenon is present in such small amounts, even its complete removal leaves the helium essentially undiminished in amount. This cold helium stream passes through a turboexpander, where its pressure is dropped to essentially the suction pressure of the compressor. In passing through the expander the helium is cooled sufficiently so that it can act as the refrigerant for cooling the xenon cold-trap exchanger. A typical flow diagram for this cold-trap system is shown in the general flow diagram (Fig. 5).

4. DEVELOPMENT WORK

The major premise in this proposal is that the graphite core structure will be a suitable container for the uranium-bismuth fuel. The ideal container material would prevent any passage of the fission products into the coolant stream and would be completely inert to any reaction with the uranium or its fission products.

Experimental work on the diffusion of gaseous and nongaseous fission products through uranium-impregnated graphite is being done by North American Aviation, Inc.[6,7] Results show relatively slow diffusion rates at 1000°C, with appreciable diffusion rates in the range from 1500 to 2200°C.

Fission-product diffusion rates through impervious graphite from uranium-bismuth solutions remain to be evaluated. Factors that might tend to retard fission-product contamination of the coolant stream include the effect of fission-product removal by the circulating fuel stream and the effect of high-density graphite.

Pending a study of this problem, certain alternate features can be considered. A fraction of the helium stream could be diverted through a turboexpander and cold-trap arrangement, as described in Sec. 3.7, in order to reduce the level of activity in the helium circuit. Another possibility would be to add an intermediate gas-to-gas heat exchanger and isolate the leakage fission products in the primary coolant circuit.

Present experimental work at BNL indicates the formation of uranium carbide in a uranium-bismuth-graphite system and shows that the formation of UC or UC_2 is favored by increasing temperature. This problem may be solved by adding a suitable inhibitor to the uranium-bismuth which would have a greater tendency than uranium to react with carbon. Zirconium may be such a suitable inhibitor, particularly if all the fuel passageways are lined with zirconium carbide.

Another matter to be considered would be the tendency of helium to diffuse from the coolant channels into the fuel channels. However, by maintaining the fuel pressure only slightly below the helium pressure, the leakage rate would be minimized. The leakage helium would be restored to the main coolant stream after aiding in the sparging of fission-product gases from the uranium-bismuth fuel.

The research work at BNL directed at the externally cooled LMFR will be of some value in predicting the performance of gas-cooled uranium-bismuth cores operating at higher temperature; in addition, BNL will pursue where possible some of the problems to a limited degree. It is hoped that those interested in the gas-cooled reactor and gas turbine will examine some of the problems mentioned in this article.

REFERENCES

1. Nucleonics, 12(7): 11-42 (July 1954) (a series of seven articles on the liquid-metal-fuel reactor); and Chemical Engineering Progress Symposium Series, Vol. 50, Nos. 11 to 13 (1954).
2. C. Keller, The Escher Wyss AK Closed-cycle Turbine, Its Actual Development and Future Prospects, Trans. Am. Soc. Mech. Engrs., 68(8): 791-822 (1946).
3. S. T. Robinson, The Closed-cycle Gas-turbine Plant, Am. Soc. Mech. Engrs., Preprint Paper 52-A-137 (1952).
4. C. F. Bonilla and C. R. Mitra, Solubility and Stripping of Rare Gases in Molten Metals, Columbia University, Reports CU-3-54 and BNL-S229, Chem. Eng., May 18, 1954.
5. Escher Wyss Report TK-45-046, 1945.
6. Diffusion of Xenon from Uranium-impregnated Graphite at High Temperatures, Report NAA-SR-194, Oct. 13, 1952.
7. High-temperature Diffusion of Individual Fission Elements from Uranium Carbide-impregnated Graphite, Report NAA-SR-255, Sept. 11, 1953.

ABOUT THE AUTHORS

Harold L. Falkenberry is a development engineer from the Tennessee Valley Authority, Division of Power Supply, on loan to the Nuclear Engineering Department of Brookhaven National Laboratory. He graduated in 1948 from Alabama Polytechnic Institute with the B.S. degree in chemical engineering. He also received the B.S. degree from the United States Merchant Marine Academy in 1946. Prior to coming to BNL in 1953, he was laboratory supervisor at the TVA Shawnee Steam Plant, Paducah, Kv.

C. J. Raseman is leader of the Fuel Processing Group of the Nuclear Engineering Department of Brookhaven National Laboratory. He graduated from Wayne University in 1941 with the B.S. degree in chemical engineering and from the University of Michigan in 1943 with the M.S. degree. He received the Ph. D. degree from Cornell University in 1951. He entered the nuclear-energy field in 1943 as an officer on active duty with the Naval Research Laboratory at Philadelphia and Oak Ridge. Later he was a group leader with The Kellex Corporation.

William A. Robba is an associate physicist in the Nuclear Engineering Department of Brookhaven National Laboratory. He graduated from Fordham University in 1950 with the B.S. degree in physics and received the M.S. degree in nuclear physics in 1951 from the Agricultural and Mechanical College of Texas. During 1951 and 1952 he attended the Oak Ridge School of Reactor Technology at Oak Ridge National Laboratory. Prior to joining the staff at Brookhaven, he was employed at the Consolidated Vultee Aircraft Corporation as a nuclear engineer on reactor design with the Nuclear Powered Aircraft program. His present work at Brookhaven is concerned with reactor design and evaluation.

Thomas V. Sheehan is employed by the Standard Oil Company of Indiana and has been on loan to the Nuclear Engineering Department at Brookhaven National Laboratory since 1947. He received the B.S. degree in mechanical engineering from the University of Illinois in 1929. Since that time he has been affiliated with Standard Oil, working on the design and operation of chemical-processing equipment. His work at Brookhaven in the past has been on the mechanical design of the Brookhaven reactor, and at present he is mechanical consultant to the Nuclear Engineering Department.

Lincoln D. Stoughton has been with the Mechanical Engineering Division of the Nuclear Engineering Department at Brookhaven National Laboratory since 1951. From 1948 to 1951 he worked on the design and construction of the 3-bev cosmotron at Brookhaven. He received the B.S. degree in mechanical engineering from the University of Rochester in 1946. From 1946 to 1948 he was an instructor of mechanical engineering at the University of Rochester, where he received the M.S. degree in mechanical engineering in 1948.

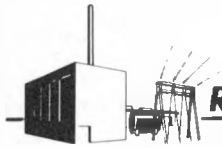

REACTOR FUTURES

A Hybrid-reactor Proposal

GEORGE SAFONOV

The RAND Corporation
Santa Monica, California

October 28, 1954

ABSTRACT

A hybrid reactor which incorporates the stability of the homogeneous reactor with the high conversion ratio of a Kouts-Chernick lattice is proposed.

The technology of water-cooled and water-moderated reactors has been advanced by recent work at two of the national laboratories. The Homogeneous Reactor Experiment (HRE) at Oak Ridge National Laboratory (ORNL) has demonstrated that systems with fuel in aqueous solution will operate with remarkable stability. At Brookhaven National Laboratory (BNL), Kouts and Chernick[1] have shown experimentally that systems with slightly enriched uranium in an approximately equal volume of water exhibit high fast fission factors ($\sim 1.1 < \epsilon < \sim 1.2$). The BNL team has suggested that such a large fast fission effect may make it possible to breed plutonium in a substantially thermal-neutron spectrum. Such a thesis was strengthened at the recent Symposium on Fission Physics and Classified Nuclear Physics for Reactors and Shielding held at Oak Ridge where Kouts reported an initial U^{235} to Pu^{239} conversion ratio of approximately 1.3. In this paper a hybrid reactor that would incorporate features of the above ORNL and BNL reactor concepts is proposed.

It is not possible to hold uranium as a salt solution in an equal volume of water. However, if the uranium is only slightly enriched in U^{235}, this isotope alone, or a large part of it, may be held in solution. By moving the primary fissionable material from the metal to the water, the high conversion ratio of a Kouts-Chernick lattice should not be appreciably altered, and, with the fissionable material in solution, the condition for HRE type stability is satisfied. Such a reacting system, therefore, is truly hybrid. It is not only a composite heterogeneous-homogeneous machine but it also operates with a "fast-slow" neutron spectrum.

Moving the fissionable material from the metal to the water converts a one-region reactor into a two-region machine. The liquid region with its expensive fissionable material forms a cooling and moderating bath about the solid region with its inexpensive depleted uranium. Two-region operation may offer benefits other than HRE type stability and a high conversion ratio.

Since the solid region contributes a small fraction of the total power, it may be possible

to relax the rigid fuel-element specifications on all-solid fuel systems. The escape of fission products is no longer a problem since the liquid region continuously removes such poisons. With a lower fission rate in the metal, this region tends to operate at lower maximum temperatures. Also, the solid region is less subject to fission-fragment damage, and the in-pile life of the metal may be increased. Corrosion is a problem, but larger amounts of corrosion might be tolerated in a system that continually purges its liquid of foreign matter.

It is not the purpose of this paper to speculate on possible operational schemes for an over-all plant employing a hybrid. However, a particular scheme might be worth mentioning. This scheme involves two reactor tanks, A and B, each containing their charge of depleted uranium. The working fluid is pumped in a loop containing tank A and an external heat exchanger. When A is ready for processing or servicing, the expensive working fluid is pumped through B. That is, B replaces A in the circulating-fluid loop. Such an operational scheme would keep the expensive fuel solution earning its keep in a more or less continuous manner.

REFERENCE

1. Herbert Kouts and Jack Chernick, Reactor Sci. Technol., 3(3): 119 (September 1953).

ABOUT THE AUTHOR

George Safonov is a physicist with the Nuclear Energy Division of The RAND Corporation. He received the B.S. degree in electrical engineering in 1943, the M.S. degree in physics in 1948, and the Ph. D. degree in physics in 1949 from the California Institute of Technology. Dr. Safonov has been with RAND since 1949, where he has worked on the theory of chain-reacting systems. In the summer of 1954 he was in charge of the reactor group of Project Separation at Massachusetts Institute of Technology.

TID-2506 (Del)

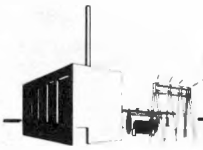

REACTOR FUTURES

Plutonium Power Reactor with Oxide Fuel and Blanket Elements

J. B. SAMPSON and E. A. LUEBKE

General Electric Company
Knolls Atomic Power Laboratory
Schenectady, New York

January 26, 1955

ABSTRACT

Increased capital costs of a reactor power system make it desirable to seek reduced fuel charges below the 2 to 4 mills/kw-hr of coal- or oil-fired systems. An inexpensive procedure for recovering plutonium from the core and blanket of a breeder and for refabricating it into fuel structures offers an attractive possibility for reducing fuel costs. A fuel element consisting of plutonium and uranium oxide in steel tubing and capable of a large fraction of fuel burn-up is described. This fuel element makes possible recovery and refabrication with fewer steps than are required for a metal fuel element and, therefore, results in lower recycle costs.

Breeders with fuel and fertile material in both oxide and metallic form were analyzed by the multigroup method on the UNIVAC for the purpose of comparing characteristics. A summary is presented of the nuclear data assumed, the method of calculation, and the results obtained. The decrease in the breeding ratio resulting from the replacement of the metal core by oxide is only 0.2, which is a small effect in a future nuclear power economy, where plutonium has a low value as fuel rather than a high value as weapon material. Use of an oxide blanket may reduce the breeding ratio by 0.05.

An illustrative design is presented which has five atoms of uranium per atom of plutonium in the core and 45 per cent sodium and which has a breeding ratio of 1.4 and a critical mass of 400 kg. Incremental refueling is assumed to reduce the control range required for 50 per cent burn-up of the original fuel loaded.

1. INTRODUCTION

At this stage in the development of reactor power systems, it is generally considered that the substitution of the reactor for the firebox of the boiler results in a higher capital cost per unit of electrical capacity when compared to conventional power plants. It is desirable to

reduce the power cost attributable to fuel below the 2 to 4 mills/kw-hr of coal- or oil-fired systems in order to achieve a competitive position with a reactor system. Each mill per kilowatt-hour reduction in fuel cost compensates for an approximate $50.00 per kilowatt increase in capital cost.

The recycling of plutonium from the core and blanket of a breeder type reactor offers an attractive possibility for reducing fuel costs. Its success depends on determining an inexpensive procedure for recovering the plutonium from the core and blanket and for fabricating it into fuel structures. The sale of excess plutonium is desired to compensate for fuel-inventory charges and a high fuel charge during the start-up phase of a breeder cycle.

If the fuel-fabricating cost is expressed in terms of cost per unit length, we have the following relation[1] for the contribution of fuel fabrication to the cost of electricity. Power conversion efficiency is taken as 30 per cent.

$$\frac{\text{Mills}}{\text{Kw-hr}} = \frac{0.14}{\text{burn-up frac.}} \left(\frac{\$/\text{ft to fabricate}}{\text{g Pu loaded/ft}} + \frac{\$}{\text{g chemical recovery}} \right)$$

A fuel element that costs $5.00 per foot to fabricate, has 3 g of plutonium per foot, and is capable of a burn-up fraction of 50 per cent contributes about 0.5 mill/kw-hr to the cost of electricity, exclusive of the cost of the plutonium, which is expected to be small in a future plutonium-power production economy. If chemical recovery costs $1.00 per gram, it contributes another 0.25 mill/kw-hr, making a total of only 0.75 mill/kw-hr. The factor-of-10 reduction due to a 50 per cent burn-up fuel instead of a 5 per cent burn-up fuel is very important.

A fuel element that shows great promise is the concept of uranium and plutonium oxide in steel tubing. The recovery and fabrication procedure has fewer steps and is therefore less expensive. Because of the chemical stability of the oxide, this form of plutonium is believed to present the fewest materials-compatibility problems with uranium compounds and tubing materials. It makes possible exploitation of the high-temperature potentialities of sodium as a reactor coolant for efficient power conversion. The porous mixture is desired to achieve a large fraction burn-up per pass of the fuel loaded, thus reducing the refabrication frequency and expense. The porosity provides space for accumulation of the additional fission atoms and permits escape of fission gases to a reservoir. The design is also applicable to U^{235} fuel, which may be used during the start-up phase of a breeder cycle or as a converter type power and plutonium producer.

A possible method of constructing the fuel element is to slide an oxide rod or oxide pellets into a tube. A large diameter of fuel compact is desirable in order to reduce fabrication costs per gram of plutonium loaded. As a result of operation at high specific power, it is expected that densification of the compact will occur, with the formation of a small central void. Most of the cylindrical compact will be sintered, a small region near the outer edge will remain powdered, and at high specific powers it is reasonable to expect that a region near the center will be fused. Irradiation tests[2] of powder-filled fuel elements indicate that this condition would be satisfactory.

One of the questions concerning the use of oxide fuel and fertile material is their effect on the breeding ratio and fuel loading. Multigroup calculations were made to explore the breeding ratio and critical mass of oxide reactors with variations in the composition. The effect of replacing oxide for metal in both core and blanket has been studied. Results concerning critical mass and breeding ratio have been obtained for a variety of cases having different ratios of fertile material to fuel and varying sodium content. Enough cases have been calculated to indicate the feasibility of a reactor having both core and blanket made of oxide.

Control effectiveness has been studied together with an incremental reloading scheme. This scheme makes possible high burn-up of individual fuel rods with a small operating control range. Some safety considerations indicate the oxide fuel rod is as safe or more safe than the metal for a wide range of accidents. The nuclear data assumed in this multigroup analysis and the compositions studied will be described and results will be given.

2. NUCLEAR EVALUATION

Nuclear characteristics have been calculated for the various reactor compositions which are listed in Table 2. It is not intended that each composition have complete technical and engineering feasibility. The compositions were chosen as being typical of an area of interest in which to explore the nuclear properties that would serve as a basis for a more detailed mechanical design.

2.1 Method of Calculation

The multigroup calculations were carried out on the UNIVAC, using codings developed at Argonne National Laboratory (ANL). Nine energy groups were used. The highest seven energy groups were identical with the highest seven of a previous calculation.[3] The eighth and ninth groups extended over lethargy intervals 7.0 to 8.5 and 8.5 to 10.0, respectively. Elastic degradation was treated similarly to inelastic scattering, except that each scattered neutron is transferred into the next lower energy group. To determine this elastic transfer requires knowledge of the ratio of flux at the bottom of a group to the average flux in the group, which is estimated from experience with similar problems previously done. This estimate is checked after flux distributions are obtained, and the problem can be iterated if agreement is unsatisfactory. It is assumed that there is no degradation to energies below the lowest group.

To obtain answers to cases rapidly enough for exploratory work, some simplification must be made to the end-enclosed cylindrical geometry of practical reactor construction. Therefore cases have thus far been treated in one of two geometries that permit analysis by a single spatial variable. These simpler geometric forms are a sphere and a bare-ended cylinder, in each of which a reflector and blanket are wrapped around a central core; however, the wrapping is omitted from the ends of the cylinder.

Critical masses and breeding ratios calculated in these simpler geometries have been corrected to values applicable to the practical end-enclosed cylindrical geometry. These corrections are sufficiently well known in the case of the sphere, which has been applied to several most interesting cases. A greater number of cases have been treated as bare-ended cylinders, simply because a UNIVAC coding in this geometry was available earlier.

2.2 Nuclear Data Used

Much of the input information, including fission cross sections, was obtained from publications of the cross-section committee, particularly the BNL-170 report series.[4]

A curve for α (ratio of radiative capture to fission) of Pu^{239} vs. energy deduced several years ago at Knolls Atomic Power Laboratory (KAPL) was used. These data are given in Fig. 1. This curve is based on two types of experiments carried out at KAPL. The first experiments were exposures of thin plutonium foils in a Hanford flux with different degrees of shielding to cut off the low-energy flux at various energies; results of these measurements are labeled "Hanford" in Fig. 1. The second type of experiment involved exposure of 20-mil-thick plutonium foils in various preliminary pile assemblies (PPA in Fig. 1) having intermediate- and fast-neutron spectrums. These PPA data gave the lower curve of Fig. 1, for which self-shielding caused some reduction in the α of Pu^{239}. The PPA points indicated on the upper curve were obtained by estimating the effect of self-shielding and correcting accordingly. The upper curve of Fig. 1 is, therefore, an extrapolation to those foils having no self-shielding.

The α data for Pu^{239}, therefore, are consistent with a number of experiments having semiquantitative validity. The important energy range for oxide reactors lies between 10 and 200 kev.

The inelastic-scattering data for U^{238} are taken from reference 5, Fig. 1. The iron and Pu^{239} inelastic data used are given in Table 1, where σ_{inel} is the inelastic-scattering cross section.

Inelastic scattering of iron is deduced from measurements by Jennings, Weddell, and Hellens.[6] Inelastic scattering of Pu^{239} is described by figures used in previous calculations at KAPL.[3]

The degradation effect of various inelastic scatterers is given by the energy-group trans-

fer functions listed in reference 3 or reference 7, p. 29.

The capture cross section of iron assumed is taken from reference 7, p. 34.

The scattering resonances in oxygen above approximately 0.4 mev were not included in detail, but a more smoothed-out function was assumed, which was carried over from older calculations.[3]

The neutrons per fission were assumed to be 2.91 in the case of Pu^{239} and 2.48 for both U^{235} and U^{238}. These are conservative figures which give little credit for recently reported increases above several million electron volts neutron energy. Pu^{240} was assumed to have the same cross sections and number of neutrons per fission as U^{238}. The average poisoning per fission product was assumed to be 0.1 of the Pu^{239} fission cross section at that energy. This ratio is suggested in reference 7.

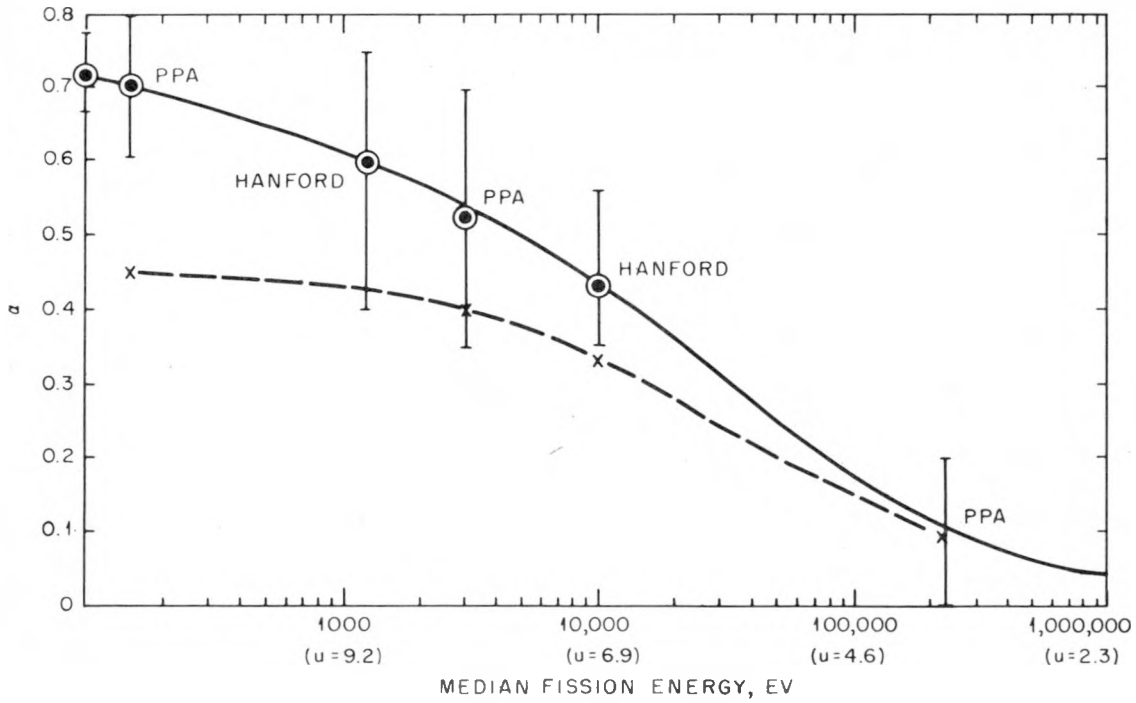

Fig. 1—Curves for α of Pu^{239} vs. fission energy.

Table 1—Iron and Pu^{239} Inelastic Data

Lethargy*	Mev	σ^{Fe}_{inel}, barns	$\sigma^{Pu^{239}}_{inel}$, barns
1	3.68	1.45	1.8
2	1.35	0.59	1.2
2.5	0.82	0	1.1
3	0.50	0	0

*Lethargy, u, $\ln(10^7 \text{ ev}/E)$, where E is neutron energy.

An assumption has to be made concerning the effect of self-shielding on the α of Pu^{239}. The fuel rods visualized are about $\frac{1}{8}$ to $\frac{1}{4}$ in. in diameter.[1] This gives an equivalent thickness of about 5 to 10 mils of pure plutonium. In the case of oxide reactors having considerable scattering intimately associated with the fuel, the self-shielding effect would be slight. For this reason we have made the conservative assumption that for oxide cores the α of Pu^{239} is entirely non-self-shielded or that the upper curve of Fig. 1 applies. For metal cores we have assumed values of α for Pu^{239} intermediate between the two curves of Fig. 1, where the lower curve applies to 20-mil foils.

2.3 Results of Analysis for Various Reactor Cases

Results based upon the sphere are assumed to be directly applicable to the practical end-covered cylindrical geometry, provided the critical mass and size are increased 10 per cent. This recipe has been found reliable from past experiments and calculations, provided the channeling effect in the end reflectors and blankets in the actual geometry is low.

Results for bare-ended cylinders are "calibrated" by comparison with calculations for spheres of the same material composition. It has been found that the breeding ratio for bare-ended cylinders agrees to within a few per cent with that for spheres and, therefore, with that for a practical geometry if a blanket is provided at the ends to receive the escaping neutrons. The correction of the critical masses from bare-ended cylinders to spheres is apparently dependent upon composition since a correction factor applicable to an oxide reactor predicts a critical mass for a metal reactor which is about 30 per cent too large. The interpretation adopted here is that applicable to an oxide reactor. Larger critical masses and dimensions are given here than those previously reported[8] for some cases. These increases have resulted from a recent comparison of spherical and bare-ended cylindrical results for an oxide composition together with an allowance for conversion to the practical geometry.

To restate, all results given in this report are those applicable to a practical end-enclosed cylindrical geometry. These results are believed to be valid, except that critical masses and sizes predicted by the bare-ended cylindrical geometry for a metal reactor are probably somewhat high.

Table 2 lists the more important reactor compositions that have been studied together with results obtained for each composition by the multigroup analysis.

Each reactor in Table 2 is designated by a descriptive code. Reactor M-4-M(C), for example, designates a reactor having metal core, four uranium atoms per plutonium atom in the

Table 2—Composition and Results of Analysis for Various Reactors*

	Reactor M-4-M(C)	Reactor O-4-M(C)	Reactor O-5-M(C)	Reactor O-6-M(C)	Reactor O-6-O(C)	Reactor O-6-O(S)	Reactor Op-5-OP(S)
U/Pu atomic ratio in core	4	4	5	6	6	6	5
Core composition, vol. %							
Pu^{239} metal	3.56	0	0	0	0	0	0
U metal	14.1	0	0	0	0	0	0
$Pu^{239}O_2$	0	4.50	3.99	3.84	3.80	4.11	4.15
UO_2	0	18.7	20.8	24.0	23.8	25.7	21.7
Na	53.8	44.0	45.4	42.5	43.0	38.4	44.4
Fe	19.7	20.0	16.5	14.8	14.8	16.0	15.6
Pu^{240}	0	0	0	0	0	0	14.2
Fission products	0	0	0	0	0	0	
Void	9.0	12.8	13.3	15.0	14.6	15.6	
Core diameter and height, cm	84	101	114	123	123	112	108
Critical mass of Pu^{239}, kg	308	366	465	564	558	456	412
Blanket type	Metal†	Metal†	Metal†	Metal†	Oxide†	Oxide†	Oxide‡
Blanket thickness, cm	45	45	45	80	80	80	45
Internal breeding ratio	0.39	0.43	0.55	0.66	0.66	0.66	0.55
External breeding ratio	1.26	1.03	0.94	0.88	0.83	0.86	0.90
Total breeding ratio	1.65	1.46	1.49	1.54	1.49	1.52	1.45

*Code explained in text.
†Clean.
‡Exposed.

core, and a metal blanket (analyzed in cylindrical coding). Reactor O-6-O(S), for example, designates one having an oxide core, six uranium atoms per plutonium atom in the core, and an oxide blanket (spherical coding). Reactor Op-5-OP(S) is a special and important case. It has an oxide core with some poisons of burn-up due to Pu^{240} and fission products, five atoms of uranium per atom of plutonium in the core, and an oxide blanket containing some Pu^{239} due to exposure (spherical coding). This reactor is discussed further below. In this report U, as well as uranium, designates natural uranium. Plutonium designates Pu^{239} unless stated otherwise.

Table 3 — Blanket Compositions

Blanket	Material	Vol. %
M (metal)	U	67
	Na	23
	Fe	10
O (oxide)	UO_2	67
	Na	23
	Fe	10
OP (oxide; Pu included)	UO_2	66.3
	$Pu^{239}O_2$	0.7
	Na	23.0
	Fe	10.0

Each reactor has a reflector 12 cm thick, composed primarily of lead, with the following composition: lead, 60 vol. %; iron, 23 vol. %; and sodium, 17 vol. %. This reflector was found[3] to represent a good compromise between reducing critical mass and providing some reflector control without much sacrifice in breeding.

The composition of the blankets of the reactors listed in Table 2 are given in Table 3.

The densities used were as follows:

Material	Density, g/cm^3
PuO_2	11.4
UO_2	10.9
Pu metal	18.6
U metal	18.8
Fe	7.8
Na	0.85
Pb	10.5

Comparison of oxide-core reactor O-4-M(C) with metal-core reactor M-4-M(C) shows the decrease in breeding ratio resulting from replacing the metal core by oxide to be only 0.2. The oxide core is larger and can have a smaller sodium fraction to remove the same amount of heat. Therefore reactors M-4-M(C) and O-4-M(C) are similar in power characteristics.

A comparison of oxide-blanket reactor O-6-O(C) with metal-blanket reactor O-6-M(C) points out that a decrease in breeding ratio of only 0.05 results from replacing a metal blanket by an oxide blanket. The gain in economy in reprocessing oxide-blanket elements is to be balanced against this reduction in breeding.

The dependence of breeding ratio and critical mass upon composition is indicated by comparing results for the various reactors listed in Table 2. To determine the effect of sodium content, a modification of reactor O-6-O(C) was calculated which had the sodium fraction reduced sufficiently to reduce the critical radius about 10 per cent. This reactor turned out to have 37.6 instead of 43.0 vol. % sodium and a critical mass 23 per cent less. The breeding ratio was changed by a negligible amount (less than 1 per cent). This information was used to reduce all reactors to the same sodium fraction of 40 vol. % in order to study the dependence of breeding ratio and critical mass upon changes in only the uranium to Pu^{239} atomic ratio in the core. Results for breeding, assumed to be unaffected by changes in sodium fraction, are, however, revised by a few per cent in each case so as to be applicable to an infinite blanket; this removes the small effect of differences in blanket thickness upon the breeding ratio. The critical mass was revised according to the formula

$$\frac{\Delta\ (\%\ \text{critical mass})}{\Delta\ (\text{Na vol. \%})} = \frac{23}{43.0 - 37.6} = 4.3$$

The dependence of breeding ratio and critical mass upon the uranium to Pu^{239} ratio is illustrated in Fig. 2. Both the breeding and critical mass increase with increasing ratio, but for a ratio larger than 5 the critical mass increases very rapidly. Therefore, an optimum design is indicated in the vicinity of a ratio of 5, above which the additional increase in breeding is not worth the excessive increase in critical mass.

The spectrums of neutron distribution, core fissions, and U^{238} captures are given in Figs. 3 and 4 for reactors O-6-M(C) and O-6-O(C). These spectrums apply to oxide reactors having a uranium to Pu^{239} ratio of 6. Reactors having the more desirable value of 5 for this ratio have very similar spectrums. The maximum in the fission distribution (Fig. 3) in an oxide core lies at about 100 kev. The smaller peak at about 2 mev is due to U^{238} fissions. The distribution of fissions and to a lesser extent of other captures extends over a considerable width. The difference in blankets has a trivial effect in the core, but the spectrum in the oxide blanket (Fig. 4) is significantly lowered.

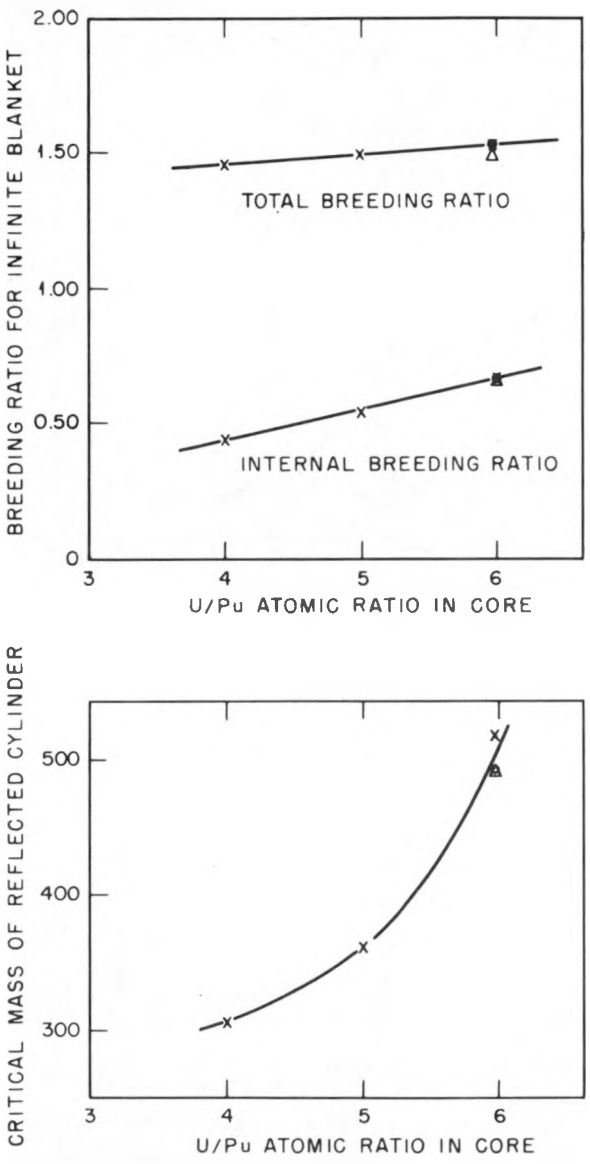

Fig. 2—Effect of uranium to plutonium atomic ratio for oxide cores each containing 40 vol. % sodium. ×, metal blanket, cylindrical calculation. △, oxide blanket, cylindrical calculation. ○, oxide blanket, spherical calculation.

The spatial distribution of Pu^{239} production in the blankets is given in Figs. 5 and 6. Figure 6 points out that the blanket relaxation lengths are fairly short, even in the oxide blanket, which has less than half the atomic uranium density of the metal blanket. Therefore, the 80-cm thickness is greater than necessary. A reasonable thickness for the oxide blanket is 50 cm. This thickness permits an escape out of the blanket of about 3 per cent of the neutrons which enter the blanket. The external breeding ratio is reduced about 0.024 in the 50-cm blanket as compared to the 80-cm blanket.

To determine the reactivity loss in a reactor operated up to 50 per cent burn-up of its original plutonium, an estimate was made of the isotopic constitution and the reactivity after such burn-up, assumed uniform throughout the core, for a reactor having originally six uranium atoms per plutonium atom. The burned-out reactor lost 13 per cent in reactivity, of which fuel depletion and Pu^{240} accumulation was responsible for 9 per cent and fission products for 4 per cent.

To sustain such a reactivity loss in a single loading run to 50 per cent burn-out would require a 30 per cent increase in the plutonium originally loaded. Moreover, about 5 per cent of the neutrons would be parasitically lost, a large control range would be required, and too little space would be available for coolant. A practical way to minimize these difficulties and yet take advantage of the long burn-out possibilities of oxide fuel rods is to include fuel rods of all exposures in the reactor and at discharge to replace only a fraction (say, 0.1) of the most exposed rods by unexposed rods.

An analysis has been completed of such an incremental refueling or steady-state reactor having a uranium to Pu^{239} content of 5 to 1 and having maximum exposure for each rod sufficient to burn out 50 per cent of the original fuel. This reactor is Op-5-OP(S) of Table 2. The

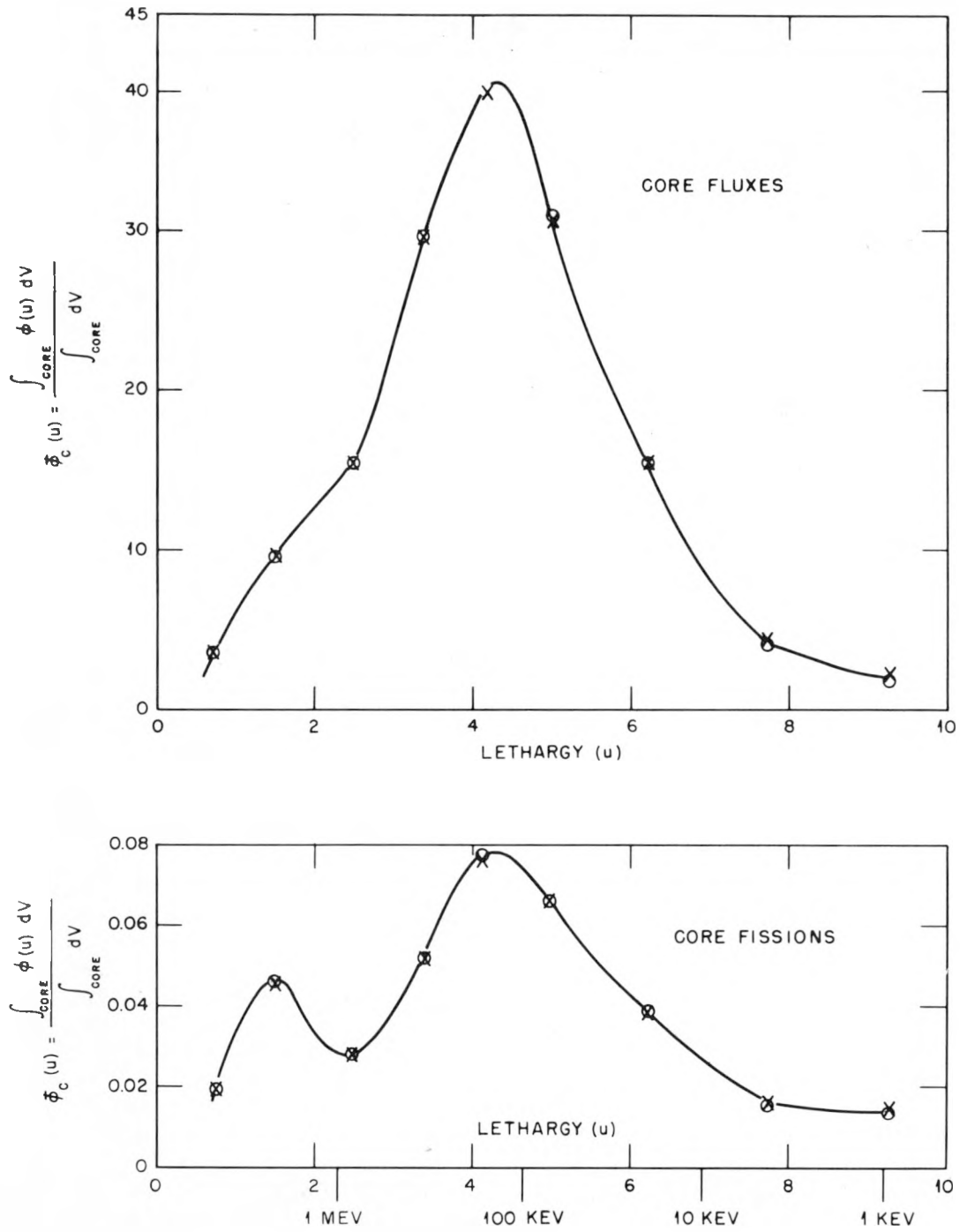

Fig. 3—Core spectrums fission distribution curves. O, metal blanket. ×, oxide blanket. $\phi(u)$ is neutron flux per unit logarithmic energy interval measured in neutrons per square centimeter per second and normalized to one source neutron per cubic centimeter per second in the core.

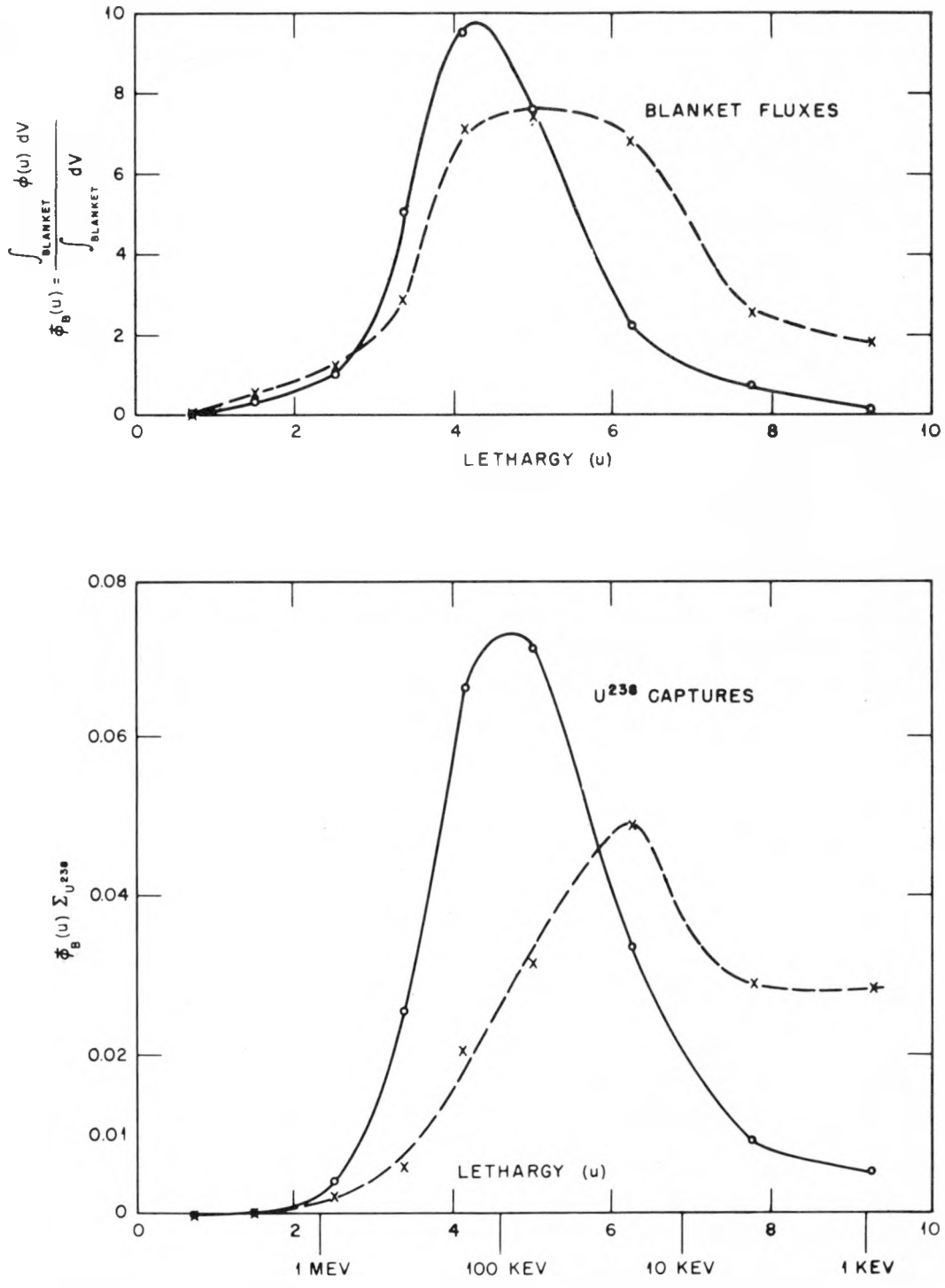

Fig. 4 — Blanket spectrums fission distribution curves. ○, metal blanket. ×, oxide blanket. $\phi(u)$ is the same as for Fig. 3. $\Sigma_{U^{238}}$ is the capture cross section of U^{238} measured in cm^{-1}.

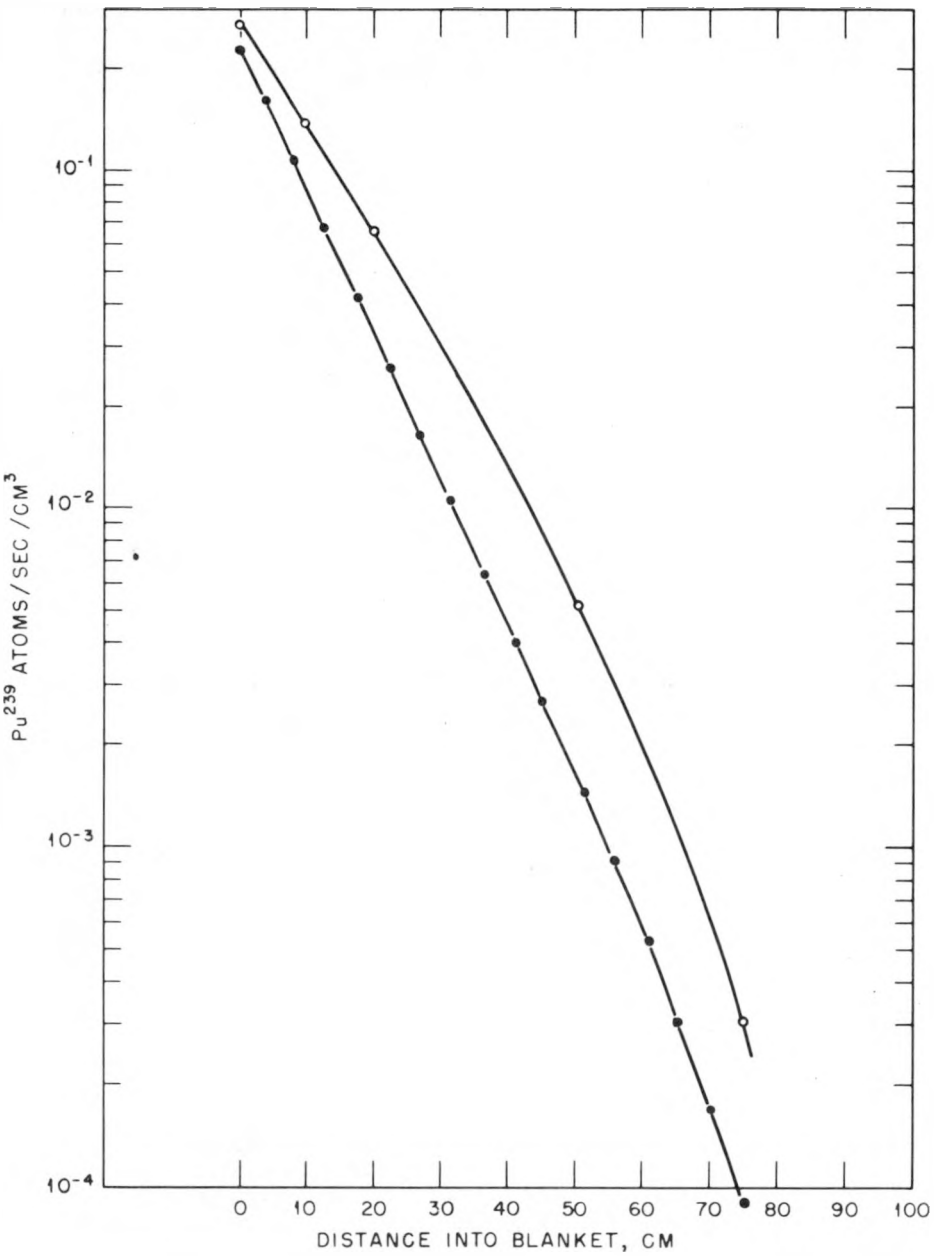

Fig. 5—Spatial distribution of Pu^{239} production in blankets. –·–, metal blanket. ——, oxide blanket. Normalization is the same as for Fig. 3.

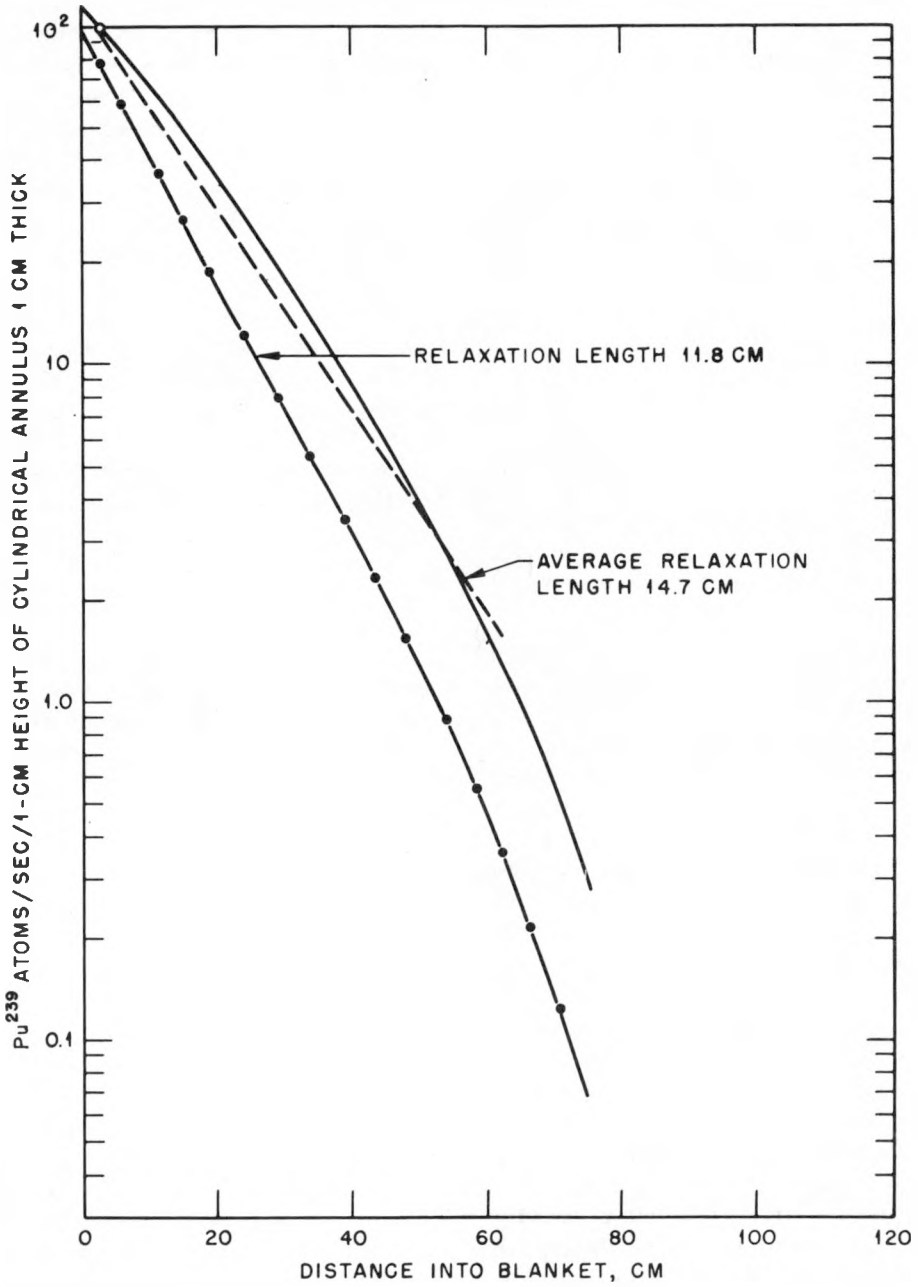

Fig. 6—Spatial distribution of Pu^{239} production in blankets. –·–, metal blanket. ——, oxide blanket. Normalization is the same as for Fig. 3.

critical mass is about 400 kg, and its breeding ratio is at least 1.4. Consistent with an average burn-up of 25 per cent per rod, Pu^{240} and fission products were included in the core to the extent of 0.00040×10^{24} atoms/cm^3 and 0.00106×10^{24} atoms/cm^3, respectively.

The control available by replacing the lead in the reflector with sodium is 4 per cent, which was found by a separate multigroup calculation. The approximate control requirements in terms of percentage may be outlined as follows:

Temperature	0.5
Burn-up (incremental refueling)	1.3
Tolerances	0.2
Total	2.0

The use of 2 per cent in operational control leaves 2 per cent in the reflector for shutdown safety. Additional elements for shutdown and safety will be required.

An accident analysis has been made for both an oxide and a metallic fuel rod under the conditions that reactivity is added to the reactor at a constant rate and that the negative coefficient of reactivity of each rod results from the thermal expansion, which reduces fuel density. It was assumed that both oxide and metal rods can expand until a condition of failure is reached, which for metal was assumed to be melting of fuel at 860°C and for oxide was assumed to be melting and vaporization, both of which were assumed to occur near 4000°C. For reactivity increase rates up to 1 dollar/sec, both metal and oxide elements appear controllable. The oxide element is superior, owing principally to its larger heat capacity before melting, even though its temperature coefficient of reactivity is slightly less negative. At the 1 dollar/sec rate, for example, the times between reactivity bursts are 0.10 and 0.14 sec, respectively, for metal and oxide; the metal can withstand only one or two such bursts and the oxide about five. Only at very high rates of increase in reactivity, probably about 5 dollars/sec, can the metal be preferable. In this case the time before melting or bursting is in the range 10 to 100 msec even for the metal, and it is questionable whether a reactor with either type of fuel element can be saved.

3. ILLUSTRATIVE DESIGN

The illustrative design is based on the results of reactor Op-5-OP(S) calculation. Incremental refueling, whereby the reactor is composed of fuel rods of a progressive degree of burn-up from 0 to 50 per cent of the original fuel loaded, is assumed. This reduces the control range that must be provided for fuel depletion and fission-product and Pu^{240} accumulation. For this reactor, with a 5 to 1 uranium to Pu^{239} content, the fuel loading is about 400 kg of plutonium. The core volume corresponds to that of a cylinder 42 in. in diameter and height.

The mixture of PuO_2 and UO_2 is pressed to 65 per cent density and is inserted in steel tubes 0.2 in. in diameter. Suitable blanket and reflector inserts are added at each end and are sealed, with some additional void space allowed for a fission-gas reservoir.

Some provision must be made to arrange the fuel elements in subassemblies as a larger fuel rod, with means for separating individual fuel elements from each other. Solid metal rib or spiral wire spacers have been used in some reactor designs. The use of larger size fuel elements in this reactor, $\frac{1}{8}$ to $\frac{1}{4}$ in. in diameter, makes possible the consideration of thin-walled tubular spacers between fuel rods, as illustrated in Fig. 7. An important feature of this arrangement is that the coolant sodium is allowed to flow through the separator tubes as well as in the usual space between the fuel elements. Because of the good thermal conductivity of sodium and the thin tube wall of the spacers, this arrangement permits better heat transfer than is possible with solid wire or rib separators.

The fuel rods and separator tubes are suspended on one end from narrow support strips, as illustrated in Fig. 8. This is arranged so as to provide low impedance entrance and exit conditions for coolant flow. Many fuel elements and separator tubes are grouped together in a subassembly, which may be hexagonal, square, or another shape, depending on special features of the general reactor design. In the illustrative design the fuel elements are 0.2 in. in diameter. For this case the tubular spacers are about $\frac{1}{8}$ in. in diameter, and with a 0.005-in. thickness they represent only 2 per cent volume fraction of steel in the core; 0.010-in.-thick walls would

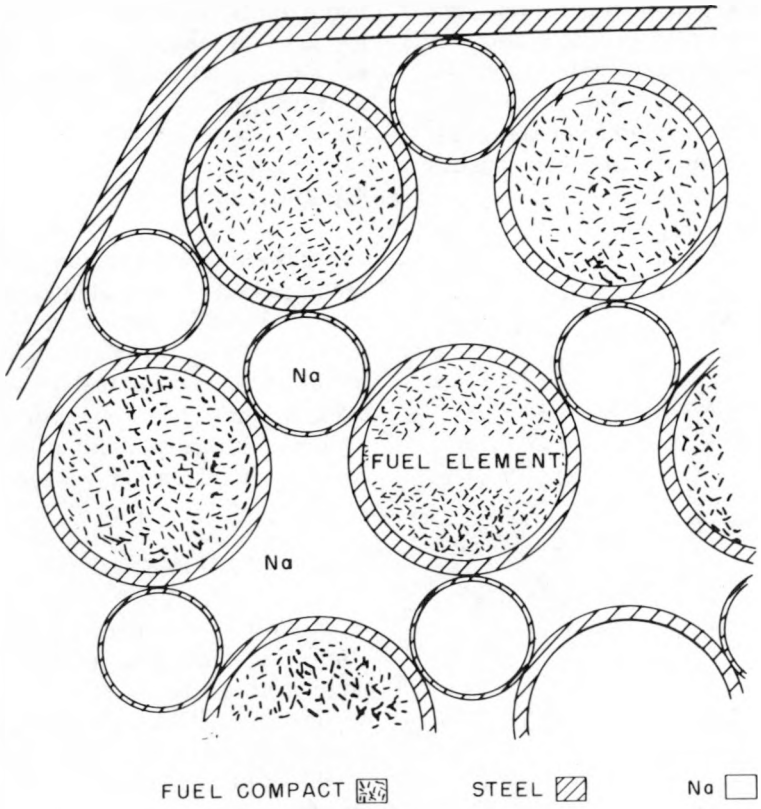

Fig. 7 — Fuel-rod arrangement.

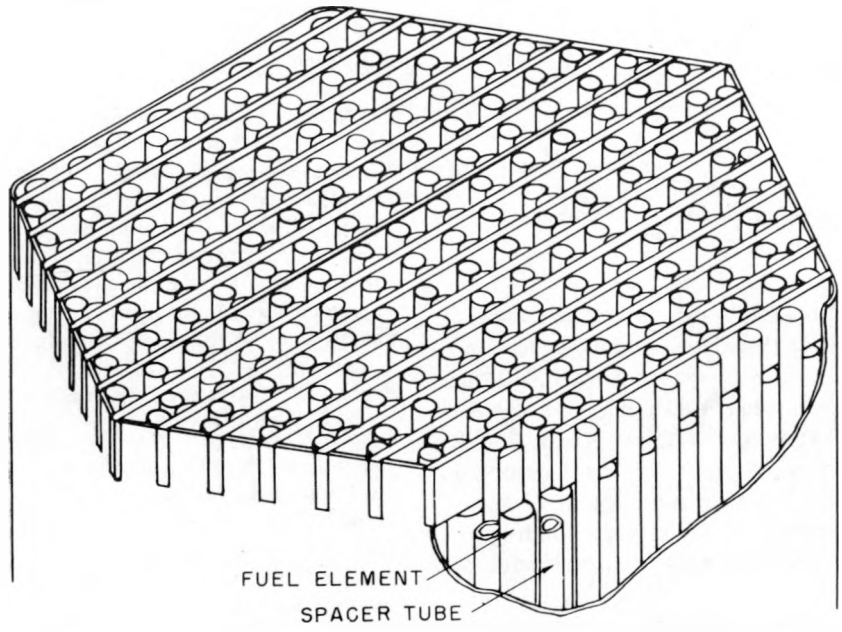

Fig. 8 — Fuel-rod assembly.

increase the steel fraction to 4 per cent. The larger hexagonal tubes surrounding a group of fuel elements and spacers, approximately 4 in. across flats, with 0.020-in. walls account for another 2 per cent steel volume in the core. Allowing 2 per cent steel for tubular spacers

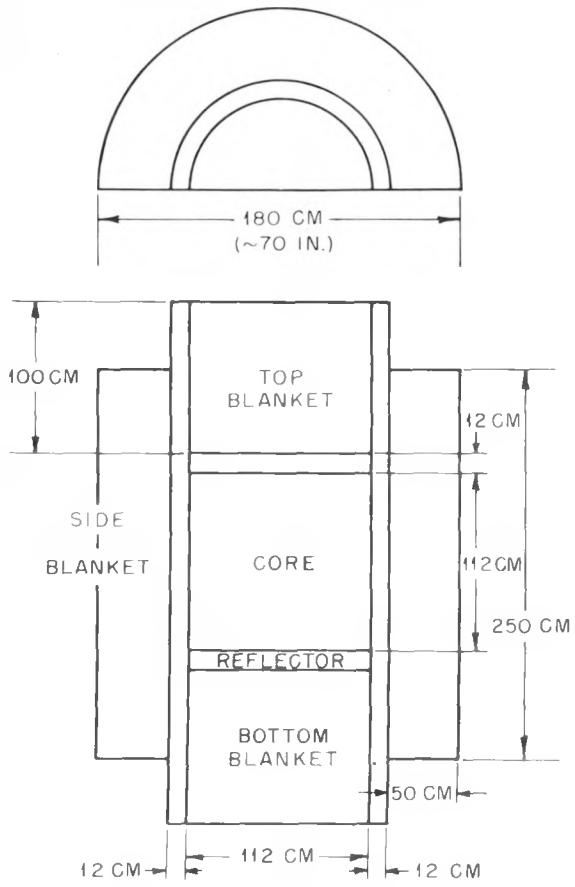

Fig. 9—Geometry of reactor regions.

and 2 per cent for the 4-in. hexagonal tubes, 11.6 per cent steel fraction remains for the fuel-element wall. This results in a 0.013-in. wall thickness for the fuel element.

With a sodium flow of 30 ft/sec and a 300°F temperature rise in the core, the heat removal is 160,000 watts/cm^2 of flow area, or 660 megawatts from the core. With a fuel loading of 400 kg, this is a specific power in the core of 1650 watts/g.

The general reactor geometry is illustrated in Fig. 9. The side blanket is 50 cm thick. The end blanket, which has a larger sodium fraction because of coolant channels to the core, is shown as 100 cm thick to reduce leakage of neutrons.

4. CONCLUSION

A power breeder having fuel and fertile material in both core and blanket can be designed with a breeding ratio of 1.4 and a fuel investment of 400 kg. The effect of oxide instead of metal is to reduce the breeding ratio by only 0.25, a small effect in a future nuclear power economy where plutonium has a low value as fuel rather than a high weapon value.

ACKNOWLEDGMENTS

This work was made possible by the cooperation of a number of people. We are particularly grateful to R. Avery of ANL for helping us to apply a UNIVAC coding developed there. Miss C. Hibbert, C. J. Habetler, and R. H. Stark of the KAPL Machine Calculation Unit have provided both labor and valuable suggestions. R. Ehrlich and T. M. Snyder have contributed nuclear information and helpful guidance.

ABOUT THE AUTHORS

Emmeth A. Luebke is Supervisor, Reactor Evaluation Unit, Knolls Atomic Power Laboratory, General Electric Company. During the period 1950 to 1953 he was associated with the Submarine Intermediate Reactor project staff. From 1946 to 1950 he was Technical Coordinator of the KAPL Power Breeder Reactor Project. He was at the radiation laboratory of Massachusetts Institute of Technology for five years and joined the General Electric Company Research Laboratory in 1945. In 1941 he received the Ph.D. degree in physics from the University of Illinois.

John B. Sampson is a physicist with the Technical Department, Knolls Atomic Power Laboratory. From 1946 until 1954 he was a member of the KAPL Theoretical Physics Unit. During 1950 he was on loan to the Pile Technology Unit at Hanford. He received the Ph.D. degree in physics from the University of Pennsylvania in 1942. He joined the General Electric Company in 1946 after several previous positions involving both teaching and industrial research.

REFERENCES

1. E. A. Luebke, Plutonium-Power Reactor with Oxide Fuel Elements, Report KAPL-1133, May 24, 1954.
2. Knolls Atomic Power Laboratory, Reactor Materials Progress Report, Report KAPL-655, September–November, 1951, p. 107; Report of Metallurgy Section for March, April, May, 1953, Report KAPL-930, July 30, 1953, p. 127.
3. R. Ehrlich and E. A. Luebke, KAPL Study of Heterogeneous Plutonium-Power Reactors, Report KAPL-908, May 1, 1953, p. 79.
4. Neutron Cross Section Advisory Group, Neutron Cross Sections, Reports BNL-170, 170A, 170B, and 170C, 1952.
5. J. W. Weil, Fast Effect in Uranium-Water Lattices, Report KAPL-1043, Jan. 15, 1954.
6. B. Jennings, J. B. Weddell, and R. L. Hellens, Inelastic Scattering of 4.3-mev Neutrons by Fe^{56}, Phys. Rev., 95: 636 (1954).
7. C. Goodman, J. L. Greenstadt, R. M. Kiehn, A. Klein, M. M. Mills, and N. Tralli, Nuclear Problems of Nonaqueous Fluid-fuel Reactors, Report MIT-5000, Oct. 15, 1952.
8. J. B. Sampson and E. A. Luebke, Multigroup Analysis of PuO_2 Power Breeder: Preliminary Results, Report KAPL-1197, Aug. 17, 1954.

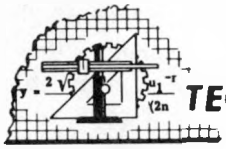

TECHNICAL NOTES

Radioactivity in Reactor Cooling Water

W. S. LYON, JR., and S. A. REYNOLDS

Analytical Chemistry Division
Oak Ridge National Laboratory

December 7, 1954

1. INTRODUCTION

The Oak Ridge National Laboratory (ORNL) Low Intensity Test Reactor (LITR) is a beryllium-moderated water-cooled reactor using enriched-uranium fuel. It was of interest to the ORNL Operations Division to determine what radioactive species are present in the cooling water when the reactor has reached a steady state. Induced activity from impurities in the water or from dissolved metal from the reactor components or lines would be expected. In addition, some slight fission-product activity might be expected. Table 1 lists the impurities found in the LITR cooling water.

Three different types of determinations were made in assaying the radioactivity present in the LITR water. Each of these experiments, together with the results therefrom, is described in the following sections.

2. SHORT-LIVED ACTIVITY

The only activity with a half life greater than a few seconds and less than 1 min was N^{16}, which is produced by the reaction $O^{16}(n,p)N^{16}$. The identification of N^{16} in LITR water and the estimation of its concentration were performed as described below.

Since N^{16} has a quite short half life, it was decided to make energy measurements on a steady-state system containing the activity. Beta-absorption data were chosen for the activity measurement since N^{16} has two extremely hard beta rays, 4 and 10 mev.[1]

The experimental assembly used to measure the N^{16} in LITR water is shown schematically in Fig. 1. A three-way stopcock was attached to the outlet line from the LITR water system. Water entering the stopcock could then be sent either through the counter assembly or directly to the drain. The counter assembly consisted of a proportional argon-methane–filled beta counter connected through an Instrument Development Laboratories model 162 scaler to a linear count-rate meter and Brown recorder with fast response. A standard aluminum sample card holder was placed between the counter tube and the sample tube through which the active water passed. The sample tube was made of aluminum tubing about 1 cm in diameter with a wall

Table 1—Impurities in LITR Cooling Water as Determined by Spectrographic Analysis

Element	Approximate concentration, ppm
Silver	<1
Beryllium	0.05
Calcium	4
Chromium	5
Copper	10
Iron	20
Magnesium	0.3
Manganese	<1
Sodium	<100
Nickel	<4
Silicon	2
Titanium	3
Zinc	<30
Zirconium	<1.5

assembly of counter, shelf, and sample tube was held in place on a table by clamps and screws and was surrounded on all sides by lead brick. The experimental procedure was to allow LITR water to flow through the tube for several minutes until a steady-state activity had been reached. Aluminum absorption data were then obtained by placing aluminum absorbers below the counter tube and observing the decrease in counting rate. Data were taken on water from two outlets from the LITR, valves 12 and 25. The shape of the absorption curve obtained in each experiment was the same. Figure 2 is an absorption curve obtained in this manner. The counter was calibrated by clearing the sample tube of LITR water and filling it (through the third arm of the stopcock) with a solution of radioactive Ru^{106}-Rh^{106} (3.5-mev beta) of known concentration and obtaining aluminum absorption data in a similar manner. The efficiency of the counter tube was thus obtained by dividing the observed counting rate of the known ruthenium-rhodium solution by the true disintegration rate (disintegrations per

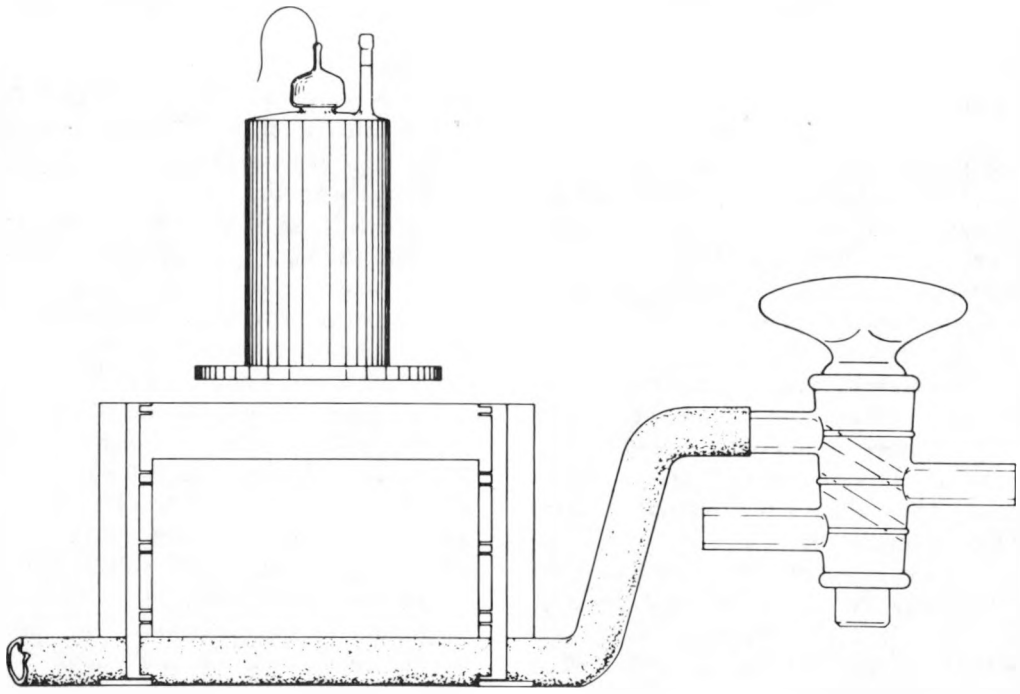

Fig. 1—Counter assembly for measurement of N^{16} in LITR water.

thickness of about 1 mm everywhere except directly below the tube window, where the aluminum wall had been filed down to approximately 0.40 mm thickness for about 1 cm along the length of the aluminum tubing. The entire

minute per milliliter) of the standard solution. The activity of the LITR water was found by dividing the observed counting rate of the water by the tube efficiency.

Decay data were obtained on the water to ascertain what activities were being counted in the counter. These data were obtained by first closing the stopcock so that no more water entered the tube and then following the decay of the water in the sample tube by use of the Brown recorder. Figure 3 indicates the short-lived decay of LITR water and shows the presence of N^{16} and a longer lived background.

The activity observed from the absorption data had then to be corrected to the time of leaving the LITR. This time was found by opening the stopcock and measuring the time required for the active water to reach the counter. This time was observed to be 18 sec. With this figure and the half life for N^{16} (7.3 sec), the absorption data were corrected to the time of leaving the LITR. The activity found was calculated to be 1.7×10^8 dis/min/ml for valve 12 and 1.9×10^8 dis/min/ml for valve 25.

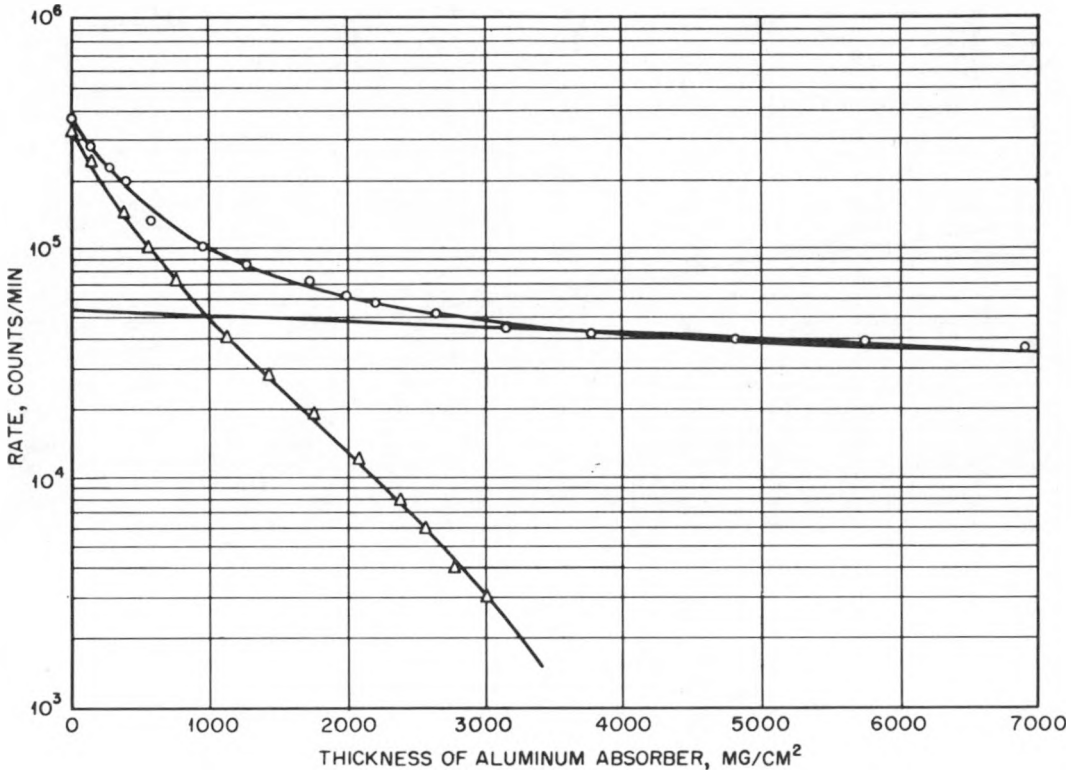

Fig. 2—Aluminum absorption data for LITR water.

3. GAMMA EMITTERS OF INTERMEDIATE HALF LIFE

It was of interest to find what gamma-emitting nuclides having a half life greater than 1 min and less than 1 day were present in LITR water. For the identification of electromagnetic radiation an NaI(Tl) gamma-ray spectrometer is most useful.[2] Fred C. Maienschein provided such a spectrometer for these experiments. The counter consisted of a 3- × 3-in. cylindrical NaI crystal with an approximately $1\frac{1}{2}$- × $\frac{3}{4}$-in. well. This well type crystal was cemented to a Dumont 3-in. photomultiplier tube. Pulses from the Dumont phototube were fed through an A-1-A preamplifier and an A-1 amplifier and thence to a 40-channel differential pulse analyzer. The counting rate in each channel was recorded on a mechanical register. Data were obtained from

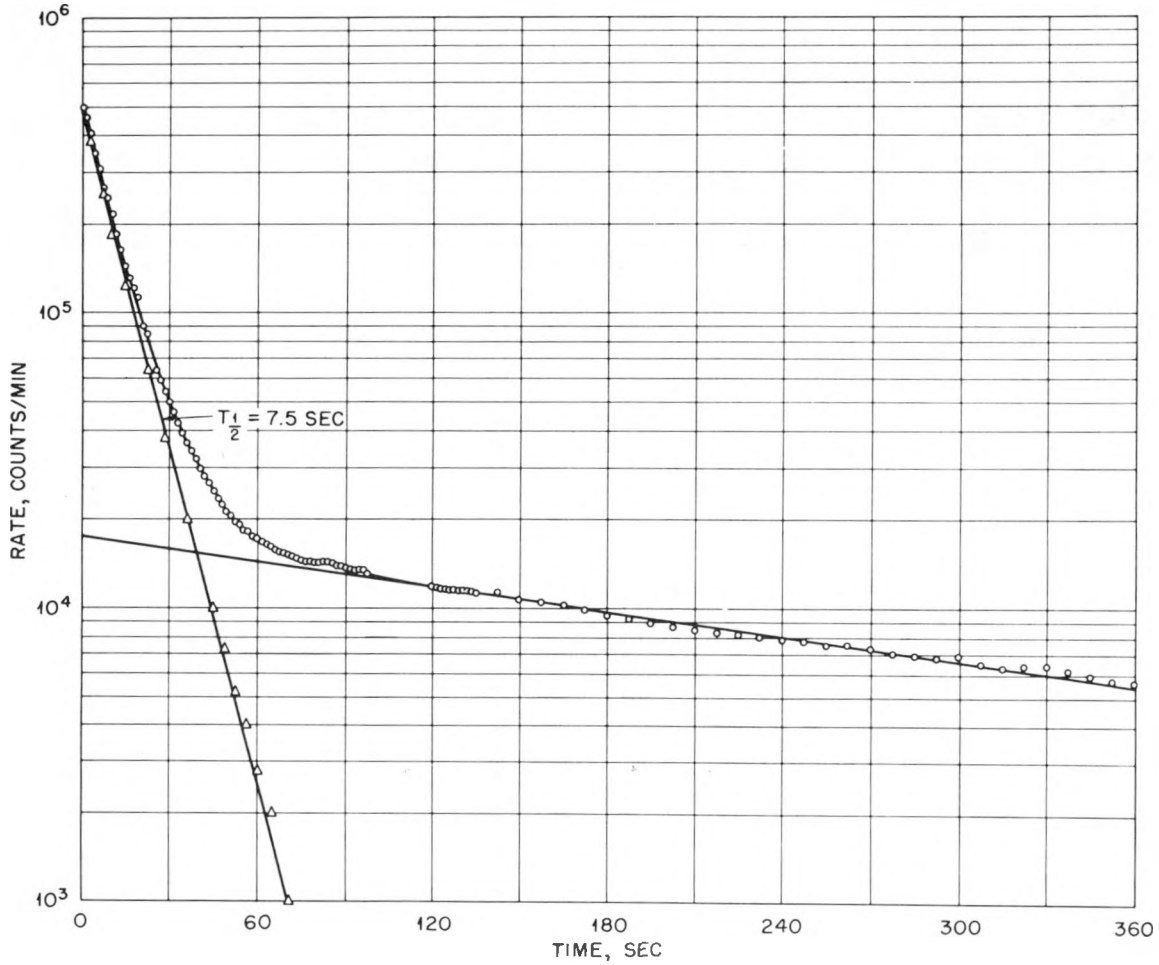

Fig. 3—Short-lived decay of LITR water.

300 kev to 4.3 mev with each channel width being 100 kev, and again from 150 kev to 2.15 mev with each channel width being 50 kev.

A hollow cylindrical aluminum shield (about 1.3 g/cm^2) was placed in the crystal opening to absorb most of the beta radiation from the sample. Samples of LITR water were obtained, made to 2 ml in volumetric flasks, and placed within the crystal. The decay of the gamma spectrum of the water was followed on the multichannel analyzer. Figure 4 shows the decay data obtained with the analyzer set for the range 300 kev to 4.3 mev. Figure 5 shows similar data for the range 150 kev to 2.15 mev. From the data of Fig. 4 it was concluded that there was no gamma radiation of energy greater than the 2.8-mev gamma from Na^{24}. The peak at 4.1 mev is a "pile-up" peak caused by the coincidence summing of the Na^{24} 2.8-mev and 1.3-mev gamma rays. Decreasing the geometry of the counter by moving the sample away from the crystal removed this peak; in addition, known samples of Na^{24} gave a peak with the ratio, (2.8-mev gamma)/(4.1-mev gamma), identical to that of the water sample.

The areas beneath the photopeaks observed in Figs. 4 and 5 were obtained by graphical integration, and the decay of each peak was plotted.

An energy and efficiency calibration of the counter was made by measuring aliquots, of known disintegration rate, of Na^{24} (1.37- and 2.75-mev gamma energy) and Cs^{137} (0.661-mev gamma energy) in the scintillation-counter assembly in a manner similar to that used for the

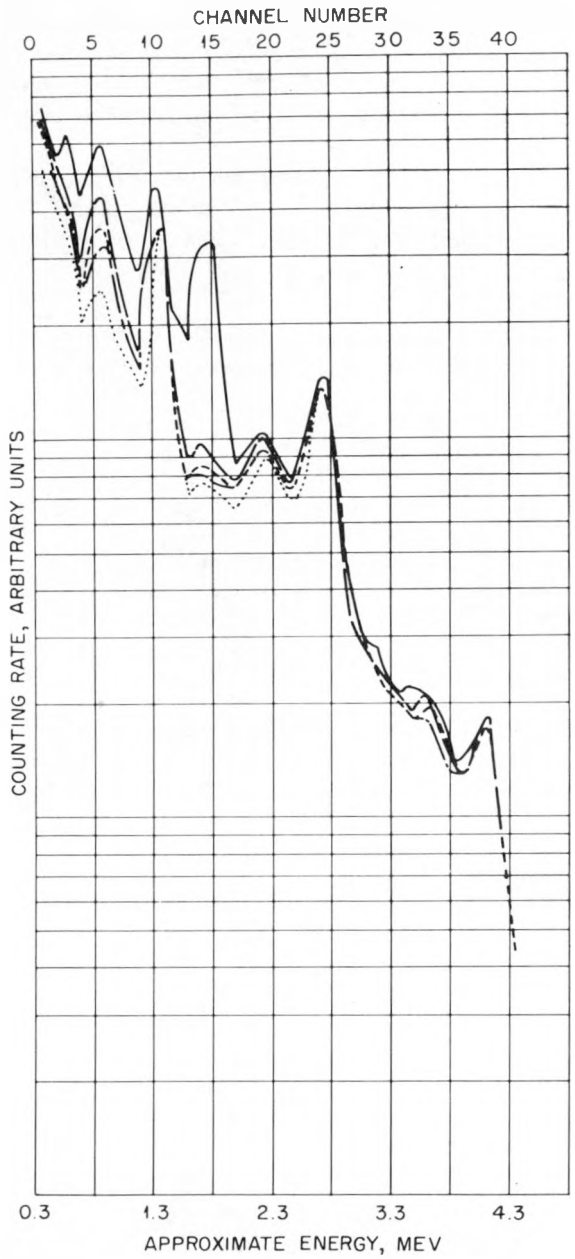

Fig. 4—Decay of gamma-ray spectrum (0.3 to 4.3 mev) of LITR water. Time out of LITR: _____, 250 sec; — — —, 980 sec; _ _ _ _, 1480 sec; — . — . —, 1820 sec; ·····, 3680 sec.

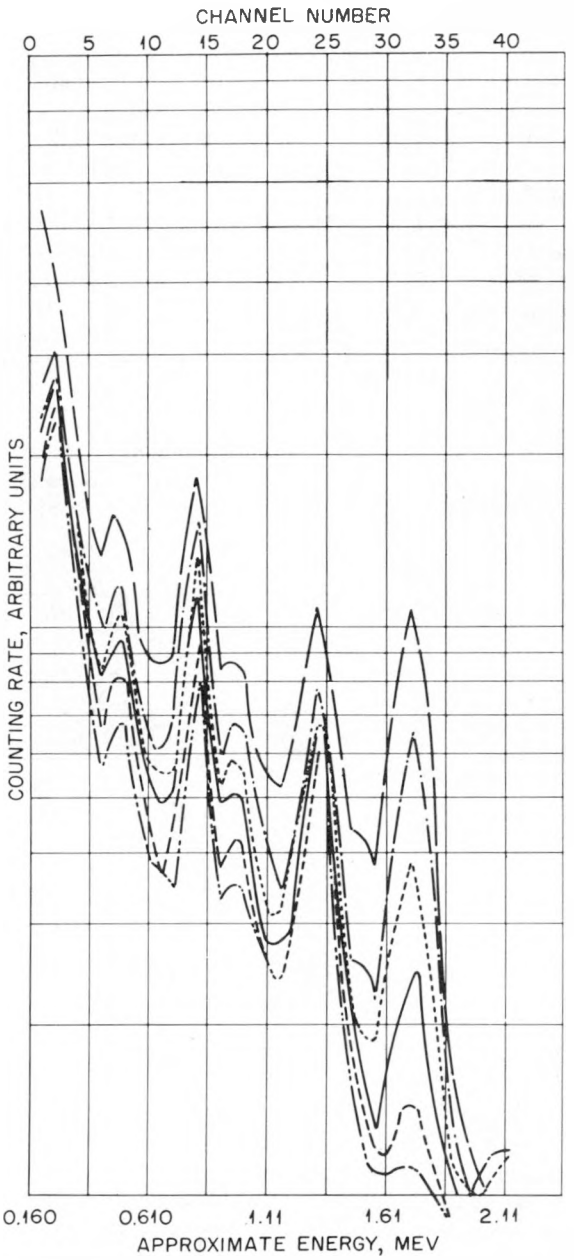

Fig. 5—Decay of gamma-ray spectrum (0.15 to 2.15 mev) of LITR water. Time out of LITR: — — —, 65 sec; — · —, 185 sec; ·····, 320 sec; _____, 440 sec; _ _ _ _, 740 sec; — · · —, 1040 sec.

Table 2—Gamma Emitters Observed in LITR Water

Nuclide	Energy, mev	Half life	Rate, dis/min/ml
Na^{24}	1.38	15.1 hr	1.3×10^5
	2.7	15.1 hr	1.3×10^5
Mg^{27}	0.84 (42%)	9.5 min	1.4×10^5
	1.01 (58%)	9.5 min	1.4×10^5
Al^{28}	1.78	2.3 min	6×10^5
Np^{239}	0.21	2.33 days	2×10^5
Uncertain	0.46	~16 min	5×10^4 γ dis/min

The values given in the last column of Table 2 for the disintegration rates are absolute disintegration rates of the nuclides. These are identical with the emission rates of the gamma rays with the exception of Mg^{27}, which has relative gamma intensities, as indicated in the second column.[3]

The Na^{24} is formed by the $Al^{27}(n,\alpha)Na^{24}$, $Na^{23}(n,\gamma)Na^{24}$, and $Mg^{24}(n,p)Na^{24}$ reactions. Mg^{27} is formed by $Mg^{26}(n,\gamma)Mg^{27}$, and perhaps a small amount is formed by $Al^{27}(n,p)Mg^{27}$. Al^{28} is formed by $Al^{27}(n,\gamma)Al^{28}$.

No assignment has been made for the approximately 16-min 0.46-mev gamma activity since the literature reveals no nuclide with this half life and gamma energy.

Table 3—Radiochemical Analysis of LITR Water 5 Hr After Removal from the Reactor

Activity	Half life	Rate, dis/min/ml	% of total dis/min	Method references[5]
Np^{239}	2.3 days	2.0×10^5	59.1	6
Na^{24}	15.1 hr	8.7×10^4	25.2	7
Cu^{64}	12.8 hr	2.7×10^4	7.8	8
Mn^{56}	2.6 hr	5.4×10^3	1.6	9
Ag^{110}	270 days	2.8×10^3	0.8	9
	Fission products			
I		4.8×10^3	1.4	10
Sr		4.6×10^3	1.3	11
Zr		6.2×10^3	1.8	12
Ba		1.4×10^3	0.4	13
Nb		1×10^3	0.3	14
Total rare earths		1×10^3	0.3	15
Total		3.45×10^5	100	

samples. The area beneath the photopeak obtained from the gamma spectrum of each nuclide, when divided by the true disintegration rate, gave the efficiency of the counter for that energy gamma. These true points were used to construct an efficiency vs. energy curve, from which efficiencies for the various observed energy photopeaks were obtained.

The area beneath the photopeaks, when divided by the appropriate efficiency, yielded the absolute gamma-emission rate of each gamma ray. From the energy, intensity, and decay data,[1] the radioactivity listed in Table 2 was identified.

4. LONGER LIVED RADIOACTIVITY

The radioactive contaminants remaining in LITR water after a decay of several hours were determined by radiochemical analysis. These analyses were performed under the supervision of G. W. Leddicotte and were done by the standard radiochemical methods in use by the ORNL Analytical Chemistry Division.

Table 3 summarizes the results of these analyses. These are in agreement with data

previously reported by Reynolds.[4] All counting was done on a well type gamma scintillation counter, and the percentages are percentages of gross gamma counts per minute observed. The accuracy of each individual analysis is unknown. The presence of such a large amount of Np^{239} and of such a small amount of fission-product activity is quite mystifying. Np^{239} has been positively identified through chemical separation of the neptunium and physical measurements. These have included gamma-ray spectroscopy and decay measurement. Repeated attempts to find the 23-min U^{239} parent of the Np^{239} have been unsuccessful. These methods have included an attempt to find the 23-min decay period in the gross-decay curve of the LITR water by use of a scintillation counter as detector and chemical separation followed by decay counting. This work was done under the supervision of E. I. Wyatt. The procedure used was to extract, using diethyl ether, an aqueous phase of 20 ml of LITR water containing a few milligrams of natural uranium as carrier, together with $FeSO_4$ and hydroxylamine to keep the neptunium reduced and thus nonextractable. The ether phase was then evaporated, and decay followed. No U^{239} was found in this decay. Since the chemistry of neptunium and uranium should be quite similar in an aqueous solution such as this, it seems unlikely that uranium is "falling out" within the system. These considerations suggest that Np^{239} may actually be diffusing through the fuel element and into the circulating water. In any event the presence of Np^{239}, and its large contribution to the total activity present, is quite surprising.

Table 4 — Radioactivity Present in LITR Cooling Water

Activity	Half life	Rate, dis/min/ml	% of total dis/min*
N^{16}	7.5 sec	1.8×10^8	
Al^{28}	2.3 min	6×10^5	50.9
Mg^{27}	9.5 min	1.4×10^5	11.9
Uncertain	~16 min	5×10^4	4.2
Mn^{56}	2.6 hr	2×10^4	1.7
Cu^{64}	12.8 hr	2.7×10^4	2.3
Na^{24}	15.1 hr	1.1×10^5	9.3
Np^{239}	2.3 days	2.1×10^5	18.1
Ag^{110}	270 days	2.8×10^3	0.2
Total fission product		1.9×10^4	1.6

* Excluding N^{16}.

5. SUMMARY

The presence of radioactivity in LITR cooling water has been quantitatively established. Table 4 is a summary of the data obtained.

REFERENCES

1. J. M. Hollander, I. Perlman, and G. T. Seaborg, Revs. Mod. Phys., 25: 469 (1953).
2. B. Kahn and W. S. Lyon, Nucleonics, 11(11): 61 (1953).
3. H. Daniel, L. Koester, and Th. Mayer-Kuckuk, Z. Naturforsch., 8A: 447 (1953).
4. S. A. Reynolds, Report ORNL-CF-53-4-12, Apr. 3, 1953.
5. C. D. Coryell and N. Sugarman, "Radiochemical Studies: The Fission Products," National Nuclear Energy Series, Division IV, Volume 9, McGraw-Hill Book Company, Inc., New York, 1951.
6. J. E. Hudgens, Report MonN-13, Sept. 24, 1945.
7. G. W. Leddicotte, Report ORNL-1113, Nov. 27, 1951, p. 37.
8. G. W. Leddicotte, Report ORNL-1129, Feb. 12, 1952, p. 38.
9. G. W. Leddicotte, unpublished methods.
10. D. N. Hume, N. E. Ballou, and L. E. Glendenin, Report CN-2815, Sept. 25, 1945, p. 45.
11. Reference 10, p. 23.
12. Reference 10, p. 27.
13. Reference 10, p. 19.
14. Reference 10, p. 31.
15. Reference 10, p. 48.

ABOUT THE AUTHORS

W. S. Lyon is a member of the Radiochemistry Group of the Analytical Chemistry Division, Oak Ridge National Laboratory. He attended the University of Virginia and received the B.S. degree in chemistry in 1943. After employment as a chemist in the Polychemicals Division of the Du Pont Company in 1943, he transferred to the Manhattan Project in 1944. He has been employed at several Project installations, and since 1947 he has been with the Radiochemistry

Group at ORNL. Here his principal investigations have been in beta- and gamma-ray spectroscopy, radioactivity measurements and standards, nuclear decay schemes and cross-section measurements.

S. A. Reynolds is leader of the Radiochemistry Group of the Analytical Chemistry Division, Oak Ridge National Laboratory. He received the A.B. degree in chemistry from Emory University in 1942 and the M.S. degree from the University of Tennessee in 1953. His research has included radioactivity measurements and standards, activation analysis, fission-product and heavy-element methods, and electroanalysis.

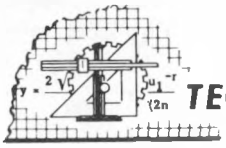

TECHNICAL NOTES

A Method of Estimating the N^{16} Content in the Cooling System of an MTR Type Reactor

F. T. BINFORD

Reactor Experimental Engineering Division
Oak Ridge National Laboratory

February 8, 1955

N^{16} is produced by the reaction $O^{16}(n,\gamma)N^{16}$. This reaction takes place above a neutron threshold energy of the order of 9.3 mev.[1,2] Although the half life of N^{16} is only 7.3 sec,[1,3,4] the high-energy gamma rays that accompany the decay of this nuclide present a major shielding problem in cases where circulation of aqueous reactor coolant outside the main reactor shield is a design requirement. The gamma energies are reported by Millar[5] to be 6.13 mev (100 per cent) and 7.10 mev (8 per cent).

Lansing[6] has calculated the linear absorption coefficients for these photons to be 0.06 cm^{-1} in 2.3 g/cm^3 of concrete and 0.026 cm^{-1} in water. Curves showing the thickness of 2.3 g/cm^3 concrete which is required to reduce to tolerance the radiation from pipelines carrying various concentrations of N^{16} in water have been calculated by the method of the equivalent-line source.[7] The results are presented graphically in Fig. 1.

For a reactor through which a coolant is circulated at a constant rate, the gain in concentration per pass through the reactor of any radioactive nuclide produced, may be represented by an equation of the form

$$\Delta C = \overline{\Sigma\phi}(1 - e^{-\lambda t_r}) \qquad (1)$$

where ΔC is the increment of activity concentration gained during a single pass through the core, $\overline{\Sigma\phi}$ is the average cross section–flux product over the neutron energy and space distribution in the core, λ is the decay constant of the nuclide under consideration, and t_r is the residence time in the core.

If C is taken to be the concentration of activity (disintegrations per unit time per unit volume) of the nuclide under consideration in the coolant at the exit from the core, and if a fraction α of the total flow is continuously purged from the system and is continuously replaced by an equal amount of coolant that is free of activity, then at equilibrium

$$C = C(1 - \alpha)e^{-\lambda t_c} + \Delta C \qquad (2)$$

where here t_c is the total circuit time. Thus the activity concentration in the core effluent becomes

$$C = \frac{\overline{\Sigma\phi}(1 - e^{-\lambda t_r})}{1 - (1 - \alpha)e^{-\lambda t_c}} \qquad (3)$$

The times t_c and t_r may be expressed in terms of the volume flow rate Q (volume per unit time), which is considered constant over the entire system, and of the water-containing volumes, V_r and V_c, of the reactor core and the entire system, respectively. Thus

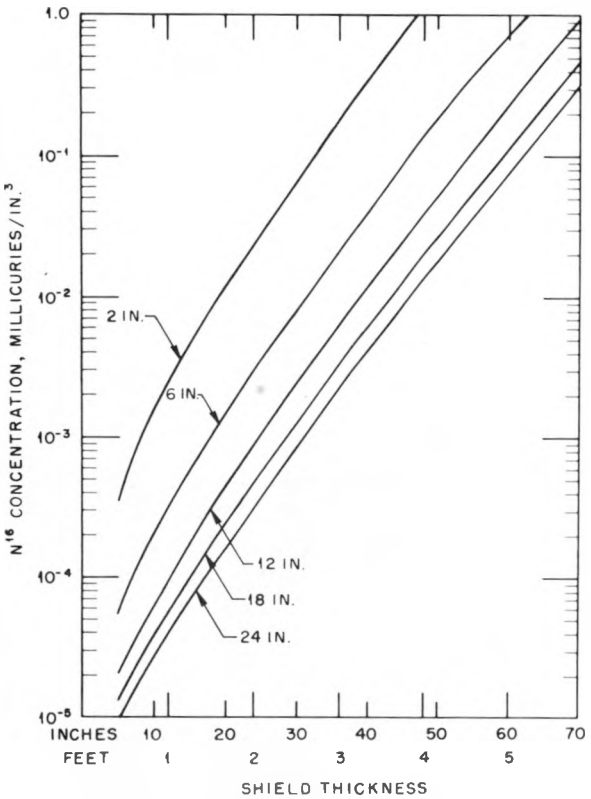

Fig. 1—Curves for 2-, 6-, 12-, 18-, and 24-in. pipe, showing concrete-shield thickness required to reduce radiation from pipelines carrying N^{16}-bearing water to tolerance (~0.75 mr/hr). (UNCLASSIFIED)

$$C = \frac{\overline{\Sigma\phi}(1 - e^{-\lambda V_r/Q})}{1 - (1 - \alpha)e^{-\lambda V_c/Q}} \qquad (4)$$

For the particular case of N^{16} the value of λ is 0.095 sec^{-1}, and for most practical cases V_c/Q is greater than 500 sec. Thus, since $0 \leq \alpha \leq 1$, the second term in the denominator is negligible compared to unity. On the other hand, V_r/Q is generally quite small, being of the order of 1 sec or less. Thus Eq. 4 becomes

$$C \cong \overline{\Sigma\phi}\ \lambda V_r/Q \qquad (5)$$

It can be seen from Eq. 5 that purging has virtually no effect on effluent activity in those cases where the half life of the nuclide in question is short compared to the time required for an increment of coolant to traverse the entire cooling circuit.

The factor

$$\overline{\Sigma\phi} = \int_E \int_{vol} \phi(\bar{r},E)\ \Sigma(\bar{r},E)\ d\bar{r}\ dE$$

is just the average production rate of N^{16} atoms per unit volume per unit time. For any given core configuration this quantity is proportional to the specific power. That is,

$$\overline{\Sigma\phi} = \frac{\varkappa P}{m} \qquad (6)$$

where $\varkappa$ is a constant of proportionality, P is the power level in convenient units, and m is the mass of fissionable material present.

The assumption is now specifically introduced that $\varkappa$ has essentially the same value for all MTR type reactors having similar fuel elements and similar ratios of metal to water. This is equivalent to the assumption that the form of the energy and of the space dependence for both the cross section and the flux is essentially the same in all such reactors. Under this assumption Eq. 5 becomes

$$C \cong \frac{\varkappa\lambda V_r P}{mQ} \qquad (7)$$

In many cases of practical interest the flow rate of the coolant, Q, is also proportional to the power level. Thus, if K is the flow per unit power,

$$Q = KP \qquad (8)$$

whence

$$C \cong \frac{\varkappa \lambda V_r}{mK} \tag{9}$$

For a given type of fuel element, the ratio V/m is constant. Thus, if the expression $\varkappa\lambda V_r/m = A$,

$$C \cong \frac{A}{K} \tag{10}$$

where A is a constant for all the systems considered and K is characteristic of the particular reactor under consideration.

This relation is quite useful since it permits measurements taken in an operating reactor to be extrapolated for the purpose of estimating the N^{16} activity to be expected in the coolant of another reactor of similar type but of different size, provided only that the values of K are known.

Let K_0 be the flow rate per unit power for the reference reactor in which the effluent-activity concentration is known. Then, if K_1 is the corresponding value for the reactor for which the concentration estimate is required,

$$C_1 = \frac{K_0}{K_1} C_0 \tag{11}$$

where C_0 is the measured reference concentration and C_1 is the estimated concentration.

Lyon and Reynolds (page 197) have measured the maximum N^{16} concentration in the cooling-water effluent from the Low Intensity Test Reactor (LITR) at 3-megawatt operation to be 3×10^6 dis/sec/ml. The average concentration then is 2.6×10^6 dis/sec/ml, where the ratio of average to maximum flux laterally across the LITR core has been taken as 0.87. $K_0 = 400$ gal/Mw-min. Then for any similar reactor the concentration of N^{16} in the effluent in disintegrations per second per milliliter is given by

$$C_1 = \frac{1.04 \times 10^9}{K_1} \tag{12}$$

where K_1 is the flow rate per megawatt in gallons per megawatt-minute. Conversion to millicuries per cubic inch may be accomplished by multiplying by 4.43×10^{-7}.

It is interesting to compare the result obtained experimentally by Lyon and Reynolds for the LITR with the concentration of N^{16} obtained by a calculation based on measured constants.

The cross section for the $O^{16}(n,p)N^{16}$ reaction has been tabulated as a function of energy from the threshold to 18 mev by Martin.[1] This cross section is indicated by the solid-line curve in Fig. 2. The broken-line curve represents a correction[2] of the threshold to 9.3 mev and a correction at 18 mev which is noted in a footnote of reference 1. Because of the high threshold it is reasonable to consider, as a first approximation, that only the uncollided flux is effective in producing the reaction. Measurements by Trice,[8] in both the LITR and the Bulk Shielding Facility (BSF), indicate that the high-energy spectrum in these reactors does not differ sensibly from the fission spectrum. Accordingly normalization of the cross section for $O^{16}(n,p)N^{16}$ over Watts's fission spectrum yields a value of 0.026 millibarn for the average cross section. The macroscopic cross section thus becomes 8.66×10^{-7} cm^{-1}. The N^{16} concentration in the LITR effluent is given by

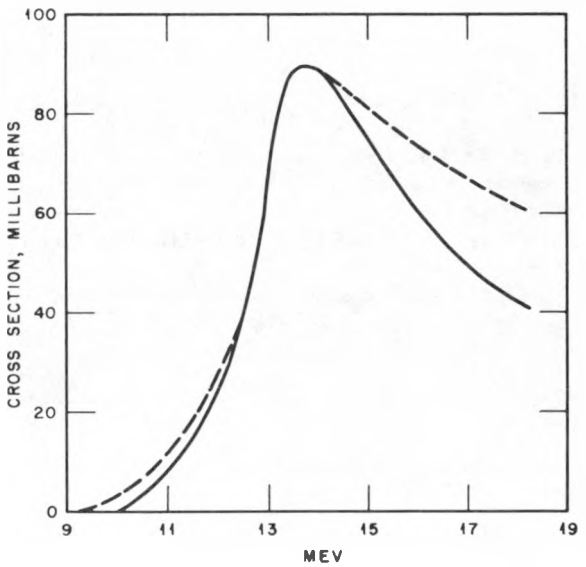

Fig. 2—Cross section for $O^{16}(n,p)N^{16}$. ——, cross section reported by Martin.[1] – – – –, correction to 9.3-mev threshold and to footnote given in reference 1.

$$C = 8.66 \times 10^{-7} \overline{\phi_u} \frac{\lambda V_r}{Q} \quad (13)$$

where here $\overline{\phi_u}$ is the average uncollided flux. For the LITR, $V_r/Q = 0.75$ sec and $\lambda = 0.095$ sec^{-1}. Measurements by Trice[8] in the BSF indicate that the ratio of uncollided to thermal flux is approximately unity for this type of core. Thus, since in the LITR at 3 megawatts the average thermal flux is 2.6×10^3,

$$C = 1.6 \times 10^6 \text{ dis/sec/ml} \quad (14)$$

which is in fair agreement with the experimental value of 2.6×10^6 dis/sec/ml.

REFERENCES

1. H. C. Martin, Cross Sections for the $O^{16}(n,p)N^{16}$ Reaction from 12 to 18 Mev, Phys. Rev., 93(3): 498 (1954).
2. B. Cohen, (n,2n) and (n,p) Cross Sections, Report NP-1254, 1949.
3. H. S. Sommers, Jr., and R. Sherr, Activity of N^{16} and He^6, Phys. Rev., 69(1-2): 21 (1946).
4. E. Bleuler, P. Scherrer, M. Walter, and W. Zünti, β-Zerfall von N^{16}, Helv. Phys. Acta, 20: 96 (1947).
5. C. H. Millar, G. A. Bartholomew, and B. B. Kinsey, γ-Rays from the Decay of N^{16}, Phys. Rev., 81: 150 (1951).
6. N. F. Lansing, The Oak Ridge National Laboratory Research Reactor Safeguard Report, Vol. 2, ORNL-1794, 1954, p. 3.
7. Project Handbook V.
8. J. B. Trice, private communication.

ABOUT THE AUTHOR

F. T. Binford is a development engineer with the Reactor Experimental Engineering Division of the Oak Ridge National Laboratory. He became affiliated with the Laboratory in 1948, after spending six years in heavy-chemical and explosives production with the U. S. Rubber Company. Mr. Binford served as Assistant Superintendent of the Radioisotope Sales Department from 1950 to 1952. In 1953 he attended the Oak Ridge School of Reactor Technology and at that time was assigned to the Reactor Experimental Engineering Division. He received the B.S. degree in chemistry from Pennsylvania State in 1941 and has pursued a course of graduate study in applied mathematics at the University of Tennessee since 1951.

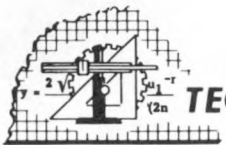

TECHNICAL NOTES

Continuous Repurification of LITR Cooling Water

J. A. COX, W. R. CASTO, and W. H. TABOR

Oak Ridge National Laboratory

March 9, 1955

The cooling water used in the Low Intensity Test Reactor (LITR) has presented a number of problems because the relatively small volume in the system has caused the concentration of radioactivity to be rather high. Also, the system contains large amounts of exposed carbon steel and cast iron, which has increased the problems of corrosion, turbidity, and radioactivity of the water. The water has been much improved in quality by the use of a combined cation and mixed-bed bypass demineralizer, and at the same time the corrosion rate of the steel and the radioactivity of the water have been reduced.

The cooling-water system of the LITR has a total capacity of about 10,000 gal and includes the reactor tank (holding about 4000 gal), a seal or surge tank (having a 7000-gal capacity but generally operated with about 4000 gal of water), pumps, heat exchangers, a demineralizer and filter, and connecting pipelines. The steel tanks and some of the pipelines were originally painted with Amercote 33, but this has come off in many places, especially where it is exposed to high radiation. A schematic diagram of the system is shown in Fig. 1.

When routine operation of the LITR began in 1951 at 770 kw, the water could only be purified, whenever it became turbid or the radioactivity became high, by purging into retention basins located about 200 yards away. It was possible, using this method of operation, to maintain the specific resistance of the water at about 200,000 ohm-cm and the concentration of the radioactivity at about 50,000 counts/min/ml (counted in a well type gamma scintillation counter with approximately 45 per cent efficiency for Na^{24} and 39 per cent efficiency for Np^{239}).

In 1952 the power of the reactor was increased to 1500 kw, the purge rate was increased from 25,000 to 50,000 gal/month, and the radioactivity of the cooling water rose to about 150,000 counts/min/ml. The flow rate of the cooling water was increased from 300 to 1100 gal/min, and the increased water flow carried a sufficient quantity of N^{16} ($T_{1/2}$ = 7 sec) out of the reactor tank to require 2½ in. of lead shielding on the exit-water line. (At the previous water flow of 300 gal/min, the linear velocity of the water was so low that the N^{16} decayed before it reached the exit-water line.)

The high radioactivity of the cooling water

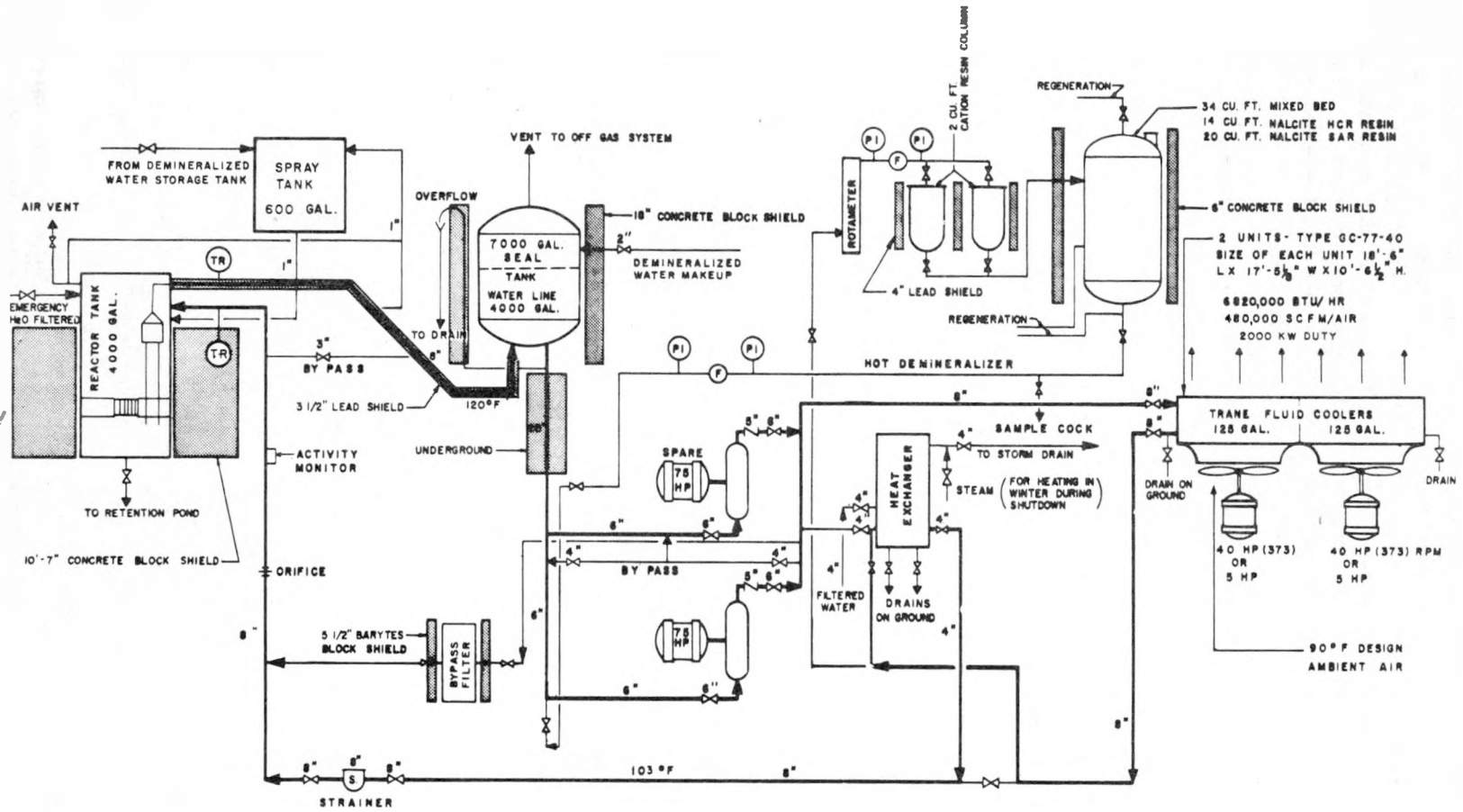

Fig. 1 — Schematic diagram of the LITR cooling-water system.

presented a considerable disadvantage in operation for other reasons also; for example, tools used in the reactor during shutdown became highly contaminated. Occasionally it is necessary to lower the water level in the reactor tank about 8 ft in order to work inside the tank, and under these conditions radiation fields of 500 mr/hr are sometimes encountered. The radioactivity of the pumps and pipelines was in proportion to the amount of long-lived radioactivity (half life greater than a few minutes) in the circulating water.

For these reasons it was decided to install a bypass demineralizer, which would reduce the radioactivity and increase the purity of the water, thus reducing corrosion and the need for purging the system with fresh demineralized water. The demineralizer concentrates the radioactivity so that it can be sent to a hot-waste system in a small volume, whereas the purging method put large volumes of radioactive water into retention ponds. The latter method is much less desirable than the hot-waste system, where the radioactivity can be stored indefinitely.

A mixed-bed demineralizer with a 3-cu ft capacity was designed for purifying the water. Two of these units were fabricated, and it was hoped that one unit would keep the system purified for several months, at which time a second unit could be inserted into the system and the resin from the first unit dumped to the hot-waste system or buried. Operation of the units using Rohm and Haas resins IR-120 and IRA-410 began in January 1953, and the water quality in the system was quickly increased from about 250,000 to 500,000 ohm-cm. The radioactivity in the cooling water was reduced somewhat, although the main effect was the reduction of the amount of purge water used. It quickly became apparent that the demineralizer was too small for the system. The radioactivity of the cooling water was not reduced as much as had been hoped, and the life of the unit was too short (3 to 4 weeks) to permit the use of new resin each time the units were regenerated. Since the columns had not been designed to be regenerated intact, it was necessary to open them, remove the radioactive resin, separate it into cation and anion components, and then regenerate each component. Because the columns were very radioactive (about 10 r/hr at 1 ft), this system of operation was quite difficult, and it was decided to enlarge the capacity of the system and provide for regeneration in place.

The effect of the increased water quality on corrosion was marked. Corrosion samples* were inserted into the water system on a rack suspended from the top plug approximately 15 ft above the active lattice. These were samples of beryllium, 2S aluminum, and 1030 carbon steel which were attached to the rack in sets of three. One of each set was insulated from contact with any other metal; another was in contact with aluminum, and the third was in contact with type 347 stainless steel. The samples were defilmed and weighed* after being removed. The results showed that aluminum and beryllium had negligible corrosion rates; aluminum, for example, was shown to corrode at a rate of only 0.2 or 0.3 mil per year and sometimes less than this, and the beryllium corrosion rate was usually less than 0.2 mil per year. However, carbon steel, which had a corrosion rate before installation of the bypass demineralizer of approximately 14 mils per year, showed a decrease in the corrosion rate to approximately 4.1 mils per year after the installation of the demineralizer. Both tests were maintained for about 1500 hr. Little difference was noted between the samples insulated from other metals and those in contact with aluminum or stainless steel.

In February 1953, an analysis† was made of the major radioactive components in the water, which were found to be approximately 58 per cent Np^{239}, 27 per cent Na^{24}, and 3 per cent Mn^{56} (these of course represent only the longer lived components). The Na^{24} and Mn^{56} can be explained by well-known nuclear reactions on sodium, aluminum, and iron, but the presence of Np^{239} could not be explained since it implies the presence of depleted U^{238} in the LITR cooling water. Following this, S. A. Reynolds and others in the Analytical Chemistry Division, ORNL, confirmed the presence of Np^{239} and performed a more comprehensive analysis of the radioactivities in 1954; their results have been reported in this journal.[1] There has been considerable speculation that the Np^{239} may be produced in the small amount of U^{238} in the fuel elements and

*By J. L. English, Reactor Experimental Engineering Division, ORNL.

†By A. R. Brosi, Chemistry Division, ORNL.

then diffuses through the fuel-plate cladding into the water. The water was analyzed for U^{239} with negative results. However, no satisfactory explanation has been found for the presence of Np^{239} in the water, which is relatively free from fission products.

In September 1953, the power of the reactor was increased from 1500 to 3000 kw. The effect of this change on the water system was immediately apparent in a decreased specific resistance and increased radioactivity in the cooling water. The amount of radioactivity in the cooling water increased to about 200,000 counts/min/ml and sometimes ran 300,000 counts/min/ml. This, of course, increased the difficulty of working in and around the reactor water tank. It was decided to press ahead with the design of a larger bypass demineralizer that could be regenerated in place and would process a larger portion of the cooling water, reducing the radioactivity and increasing the quality of the water. A mixed-bed column of 20 cu ft was decided upon as the minimum size that could be used, and bids were solicited from several companies. After consideration of the equipment offered by bidders, a standard-sized tank holding 30 cu ft of resin was chosen instead of building a tank of special design.

Considerable difficulty had been encountered in regenerating the anion resin taken from the 3-cu ft columns then in use, and investigation disclosed that the anion resin was apparently being damaged by radiation; therefore it could not be regenerated properly. It was decided,

Table 1 — Radiochemical Analysis of LITR Water Before and After Passing Through Demineralizer

Radiochemical analyses	Process water entering demineralizer: Gamma, counts/min/ml	Process water entering demineralizer: Gross gamma, %	Exit from 2-cu ft cation column,[a] gamma, counts/min/ml
Gross gamma	21,700		475[b]
Np^{239} gamma	12,000	55.3	< 10
Na^{24} gamma	6,950	32.0	< 10
Cu^{64} gamma	1,620	7.5	< 5
Mn^{56} gamma	380[c]	1.8	[d]
Sr^{91} gamma	272[e]	1.2	< 2
I[f] gamma	230[g]	1.0	[g]
Total rare earths	138	0.6	< 2
Ba^{140} gamma	36	0.1	< 2
Zr^{95} gamma	Not detected[h]		< 2
Nb^{95} gamma	< 10		Not detected
Material balance		99.5	

[a] The exit from the 30-cu ft column was too low to be successfully measured.

[b] This activity was not identified, but it is believed to be predominantly radioiodine isotopes.

[c] The decay study showed that the manganese activity was predominantly, but not pure, Mn^{56} (half life 2.6 hr).

[d] Activity showed up in the manganese precipitate but it was not Mn^{56}.

[e] The decay study indicates pure Sr^{91} (half life 9.7 hr).

[f] Fission-product iodine.

[g] It is possible that radioiodine was volatilized during the evaporation.

[h] The radiochemical procedure does not appear to give a very good decontamination factor for neptunium. In spite of the fact that the zirconium precipitate contained much activity, the spectrometer showed that it was neptunium instead of zirconium.

Considerable difficulty had been encountered in regenerating the anion resin taken from the 3-cu ft columns then in use, and investigation disclosed that the anion resin was apparently being damaged by radiation; therefore it could not be regenerated properly. It was decided,

in order to protect the resin in the 30-cu ft mixed-bed column, to install cation columns before the mixed-bed column so that most of the activity (which is in cationic form) would be removed before the water entered the mixed-bed demineralizer. This design was carried out, and the mixed-bed unit was installed in September 1954, using approximately 20 cu ft of Nalcite SAR anion resin and 14 cu ft of Nalcite HCR cation resin. The two columns formerly used as mixed-bed columns were installed with 2 cu ft of cation resin each so that they could be operated singly, in series, or in parallel ahead of the mixed-bed column. The volume of water going through the demineralizer was increased from about 3 to 15 gal/min. This arrangement proved very successful and reduced the radioactivity in the cooling water from about 250,000 to about 50,000 counts/min/ml. At the same time the specific resistance has been increased from about 300,000 to 500,000 ohm-cm. The increased water quality made it much easier to do work in and around the reactor tank; the radiation immediately above the open tank was lowered from 100 to about 30 mr/hr. It is quite likely that further reductions in radiation level will be noted as the radioactivity adsorbed on the tank walls gradually decays.

A typical radioactive analysis of the water going through the demineralizer is as follows:

Inlet water	55,000 counts/min/ml
Exit water from 2-cu ft cation column	4,000 counts/min/ml
Exit from 30-cu ft mixed-bed column	1,500 counts/min/ml

Another typical analysis,* showing the different radioactive components, is given in Table 1.

Table 2 — Data on LITR Water for Different Methods of Operation*

Date	Flow rate, gal/min	Specific resistance, av. ohm-cm	Radioactivity in cooling water, av. counts/min/ml	Power, kw	Corrosion rate of 1030 carbon steel, mils/year	Method of operation
3/51	300	~200,000	~50,000	770		Purging
3/52	1100	~250,000	~150,000	1500	15	Purging ~25,000 gal/month
1/53	1100	~500,000	~100,000	1500	4	3-cu ft mixed-bed; bypass demineralizer, 3 gal/min
9/53	1200	~300,000	~200,000	3000		3-cu ft mixed-bed; bypass demineralizer, 3 gal/min
9/54	1200	~500,000	~50,000	3000		30-cu ft mixed-bed; bypass demineralizer preceded by 2-cu ft cation column

*Temperature of water, 100 to 120°F; pH, 5.5 to 6.5.

It was found desirable to install a filter capable of handling several hundred gallons per minute to remove flocculent corrosion products to reduce the turbidity of the water. The filter selected contains cloth filter elements; it was installed in bypass piping around the pump.

Decomposition of water required that the seal tank be operated with an off-gas suction to prevent the build-up of explosive mixtures of hydrogen and oxygen.

Table 2 gives typical values of important operating data for the different methods of operation of the LITR water system.

*By E. L. Wyatt, Analytical Chemistry Division, ORNL.

REFERENCE

1. W. S. Lyon, Jr., and S. A. Reynolds, Radioactivity in Cooling Water, Nuclear Sci. Technol., 1(2): 197 (April 1955).

ABOUT THE AUTHORS

William R. Casto is a department supervisor in the Operations Division at ORNL. He received the B.S. degree in chemistry in 1940 from West Virginia Wesleyan College. Before coming to ORNL in 1948, he was engaged in chemical-engineering work with industrial organizations.

J. A. Cox, who is now superintendent of the Reactor Operations Department in the Operations Division at ORNL, received the B.S. degree in chemical engineering from Washington State College in 1940. He came to ORNL after two years at Brown University and four years in the U. S. Army.

William H. Tabor is a supervisor in the Operations Division at ORNL. He received the B.S. degree in physics in 1948 from Tennessee Polytechnic Institute and has been associated with ORNL since that date.

LETTERS TO THE EDITORS

To the Editors:*

When the reactor business was in its infancy, the primary problem was one of physics. Later, mechanical design problems involving such components as pumps, valves, and control-drive mechanisms began to stand out. Now we are beginning to realize that one of our major problems in the design of power reactors lies in the field of heat transfer, especially since we have found that the limiting factors in reactor design are certain transient conditions rather than steady-state conditions.

As an illustration, consider the so-called "loss-of-flow accident." This situation, which is of concern in the design of several reactors now under consideration, arises when all pumping power is lost with the reactor at full power. Although the flow of coolant is rapidly diminishing, the reactor will continue to produce a significant amount of heat owing to the length of time it takes the control system to scram the reactor. The question now is: "At what heat flux will the fuel element burn out owing to the reduced flow?" This is a question which has not yet been given a satisfactory answer, and as a result we are forced to be overly conservative in our designs.

I doubt if most people in the heat-transfer field appreciate the extremely high price that we have to pay for this conservatism. The entire design of the power plant, including the detailed design of its components, is affected. For example, one conservative solution made necessary by the lack of heat-transfer data is to have a much larger flow through the core than is necessary for steady-state conditions. This, in turn, requires developing larger size pumps with their associated bearing and material problems; it means having larger generators to provide the power required for the increased flow; it also means using larger pipes. All this results in a heavier and larger plant.

Another approach is to operate the reactor at lower temperatures and lower heat fluxes. The penalty for this is an increase in the size and cost of the core, the size of the pressure vessel, etc. Our lack of heat-transfer knowledge also forces us to develop quick-responding scram mechanisms. However, this type of control instrumentation and mechanism is extremely difficult to develop since we are talking of the order of a few hundred milliseconds. The point I would like to emphasize is that our lack of burn-out data requires us to accept undesirable alternatives that decrease the reliability of our plants and make them bigger and heavier than necessary.

Closely allied with the question of fuel-element burn-out is the question of flow stability during a power transient. Conceivably a flow channel could develop a hot spot at which boiling might occur. The increased resistance to flow due to the presence of the vapor might so restrict the flow that the hot-spot temperature would continue to rise and fuel-element burn-out would occur. Today little is known of this effect.

Of considerable interest is the effect of local boiling on the corrosion properties of fuel elements and on the rate of deposition of crud. A good knowledge of this effect would be of great value to the reactor designer.

[*Editors' Note: This is a summary of remarks made by Admiral H. G. Rickover at the Reactor Heat-transfer Meeting held at Brookhaven National Laboratory, Oct. 18 and 19, 1954.]

Even in the nonboiling region the lack of data is felt since investigations of over-all and local heat-transfer coefficients and pressure drop have been limited largely to over-simplified geometries and to temperatures, pressures, and flow rates below those currently being considered.

The reactor heat-transfer program is lagging in two respects. Not only do we lack an understanding of the basic mechanism of such things as burn-out but of more immediate concern to the core designer is the need for raw experimental data for the reference fuel-element geometries and coolant conditions.

Several things must be done without delay if we are to hope for any improvement in the situation.

1. The various organizations throughout the country engaged in building or designing reactors must place a much greater emphasis on heat transfer and must support expanded heat-transfer experimental programs.

2. The heat-transfer people must learn more about core design and the particular problems facing the reactor designer since the limiting factors in design are transient problems unique to the reactor field.

3. The experimenter in heat transfer must chart his program to obtain this urgently needed information on a "cash" basis and must look for novel approaches to this admittedly difficult problem.

4. The experimenter must publish his findings quickly and must overcome his reluctance to release results which to him appear erroneous or difficult to explain.

The situation is a serious one. The United States today is deeply committed in the field of power reactors; the heat-transfer people hold one of the vital keys to the solution of many of our reactor problems. Significant advances in nuclear power will be retarded unless heat-transfer people make a concentrated effort to solve the pressing thermal problems I have enumerated above.

H. G. Rickover
Naval Reactors Branch
Division of Reactor Development
U. S. Atomic Energy Commission

To the Editors:*

I would like to make some comments on the status of general reactor theory and then to discuss some of the special problems of slightly enriched uranium–water lattices. To begin with, it is evident that the volume of effective work in reactor theory has been increasing at an exponential rate during the past few years. While this rapid development is due in part to an increase in personnel and to the adaptation of high-speed computing machines to reactor problems, to an even greater extent is it due to improvements in our knowledge of nuclear constants afforded by integral experiments and cross-section measurements.

For example, it was not until large-scale D_2O–natural uranium lattice studies were initiated at North American Aviation, Inc., (NAA) and the data on thermal-neutron cross sections were improved that it became worth while to go beyond diffusion theory to calculate the flux distribution within a lattice cell. There now exist a number of alternate attacks on this common problem. At Brookhaven National Laboratory (BNL), the spherical-harmonics method[1–3] and mesh methods of solving one-velocity equations[4] have been adapted to this purpose for use on the AEC UNIVAC at New York University. At Knolls Atomic Power Laboratory (KAPL) the BNL work on the spherical-harmonics method has been extended to multiregion lattices by Weil.[5] At Argonne National Laboratory (ANL),[6] a Los Alamos procedure for the solution of the one-velocity Boltzmann equation for spheres has been applied to the more complex case of cylindrical geometry. Further work on this problem is in progress at Hanford, Westinghouse Atomic Power Division (WAPD), and at Du Pont where Brown and St. John[7] have made an initial attack on the difficult problem of chemical binding in hydrogenous mediums.

Similarly, it was not until large-scale H_2O–slightly enriched uranium lattice studies were undertaken at BNL that the need of refining calculations of the fast effect, resonance capture, and neutron leakage in hydrogen-moderated

*[Editors' Note: The contents of this letter were presented as a paper at the Oak Ridge Classified Nuclear Physics Meeting, Oct. 13 to 15, 1954.]

systems became apparent. With the Pressurized Water Reactor, the Submarine Advanced Reactor, and boiling reactors in various stages of design, we now have plenty of company in these investigations, including WAPD, KAPL, ANL, and others.

Finally, we owe a great deal to so-called "pure neutron physics" experiments for the steady improvement in our knowledge of cross sections and other basic data, without which reactor theory would remain in a semiempirical state.

Since we will never have the last word on cross sections or the last refinement of reactor theory, it would seem that now is as good a time as any to coordinate this knowledge and to broaden the scope of our work. We are looking hopefully to the newly revamped Reactor Physics Planning Committee to achieve this goal. We need, among other things, to fill in the large gaps in reactor theory and experiments and in the tabulation of basic reactor parameters which are evident, for example, in the present "Reactor Physics Handbook."

In addition, we need to correlate discordant results. In the past such correlation has been sporadic for lack of an effective central group among the diverse, harassed, widely separated AEC sites. For example, some years ago, in analyzing the temperature coefficients of graphite–normal uranium reactors at BNL, I. Kaplan and I came to the conclusion that the capture to fission ratio for U^{235} was essentially constant in the thermal-energy range. On the other hand, a KAPL analysis of neutron-spectrometer data[8] indicated a fairly large temperature coefficient for $\alpha^{U^{235}}$. It was not until much later, in fact not until the Chalk River meeting of January 1953, that I was able to discuss fully this discrepancy[9] with J. B. Sampson, and, thanks in part to subsequent pressure by KAPL, the experimental group under Don Hughes at BNL devised a more accurate method of measuring α which not only resolved the problem but is now being used to obtain cross-section data for other fissionable species. Some of their results have been discussed at this meeting.

There are a number of current problems of this type. Thus the Chalk River meeting disclosed a systematic difference in the buckling of D_2O–natural uranium lattices as measured at Chalk River and at NAA. Recent Snell experiments at Los Alamos and at ANL have yielded conflicting results. Fowler's measurements at Oak Ridge National Laboratory (ORNL) of the variation of ν of U^{235} with energy, if substantiated, would cast doubt on the traditional cross sections in use for even the simplest untamped assemblies. Again, the age of a fission-energy neutron in pure water has been going down on the basis of recent calculations. According to Zweifel and Hurwitz,[10] the best value is now 25 cm^2, or about 20 per cent below the experimental values. To avoid any possibility of ruffled feelings, I might add a current discrepancy in which BNL and WAPD are involved. Measurements of the thermal-neutron flux in the moderator of slightly enriched uranium–water lattices have been running about 10 per cent higher at Bettis Field than similar measurements at BNL.

With regard to theoretical methods, I would say that the results achieved to date by straight Monte Carlo calculations have been quite meager. Modifications of the Monte Carlo method, such as the multigroup directional network presently being tested by Schiff[11] of WAPD, appear to hold more promise. On the other hand, age-diffusion multigroup methods have been carried to a fine art with the aid of high-speed computing machines, and they remain invaluable in the treatment of intermediate reactors of complex geometry. At KAPL, for example, Stark and Roe have completed a two-dimensional multigroup code capable of handling up to 15 neutron groups and a few thousand space points in what is regarded as a reasonable amount of UNIVAC time.

Since age-diffusion theory is correct only to first order, even for nonhydrogenous systems, spherical-harmonic refinements have been suggested, for example, by Safonov[12] of RAND and Fleck[13] of BNL. For water-moderated systems these refinements become quite important, and various theoretical methods have been suggested by Goertzel[14] of Nuclear Development Associates (NDA); Selengut[15] of NDA; Zweifel, Hurwitz, and Erlich of KAPL; and Henry, Hellens, and others of WAPD.[16] At Harwell we understand that similar work is in progress, following spherical-harmonics methods devised by Davison.[17]

Of course, group methods still mask a good deal of ignorance. Group constants must still be fudged to agree with such things as experimental neutron ages, resonance integrals, and critical-mass data. Limited experimental data on clean critical assemblies make it difficult to assess the validity of these constants. As far as checking theoretical calculations of other important parameters such as conversion ratios or neutron spectrums is concerned, we have much less experimental data to go on.

Although the theory of the statics of clean homogeneous-reactor systems is therefore far from complete, reactor physicists have concentrated heavily on this particular field at the expense of other important problems. Among these are:

1. The general theory of reactor kinetics, stability, and control. There have, of course, been a number of studies of the kinetics of specific reactor systems and a few general studies, such as those of Fleck and myself[18–20] at BNL and Welton, Ergen, and Weinberg[21,22] at ORNL, but a great deal still remains to be done.

2. The hydrodynamics and heat-transfer characteristics of reactor coolants. Most of this work is presently being done by engineers, but, in questions involving fluid flow or the formation and growth of bubbles in boiling systems, the theoretical physicist could render valuable aid.

3. The application of newer models of the nucleus to reactor problems. These models cast considerable light on details of the fission process, on neutron cross sections, on the angular distribution of scattered neutrons, and so forth. Because of manpower limitations at BNL we have been able to assign only one physicist, Sophie Oleksa,[23,24] to work of this type.

4. The statics of heterogeneous reactors involving a lattice or clumped arrangement of fuel elements. Too many of these problems are still being treated by first "homogenizing" the reactor system.

In investigating the latter problems at BNL for slightly enriched uranium–water lattices, we have found that some type of mesh method is generally indicated. A typical problem is illustrated in Fig. 1. In a heterogeneous reactor a considerable increase in the interaction fast effect, and hence in the conversion ratio, can be obtained by use of a close-packed lattice or clumped arrangement of fuel elements. The

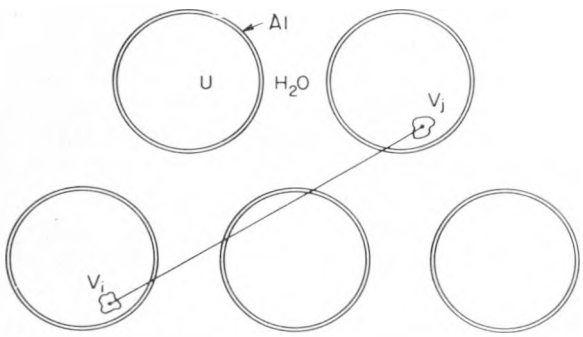

Fig. 1 — First-collision probability in rod lattices.

$$P_{ij}(E) = \frac{K_{i_1}(d'_{ij})\ V_j}{2\pi\lambda_U}$$

where d_{ij} = distance between centers of volumes V_i and V_j

d'_{ij} = corresponding distance in mean free paths

$K_{i_1} = \int_x^\infty K_0(y)\ dy$

Table 1 — Solution of Reactor Integral Equations by Mesh Methods*

One-velocity integral equations:

$$n(\vec{r}) = \int [(1 + f)\ n(\vec{r}') + S(\vec{r}')]\ K(\vec{r},\vec{r}')\ d\vec{r}' \qquad (1)$$

Equivalent set of mesh equations:

$$n(r_i) = \sum_{j=1}^{N} P_{i,j}\ [(1 + f)\ n(r_j) + S(r_j)] \qquad (2)$$

Finite slab formula for first-collision probability:

$$P_{i,i\pm k} = \frac{1}{2\delta}\{E_3[(k-1)\delta] - 2E_3(k\delta) + E_3[(k+1)\delta]\}$$

$$P_{i,i} = \frac{\delta - \frac{1}{2} + E_3(\delta)}{\delta}$$

$$E_n(\delta) = \int_0^1 e^{-\delta/\mu}\mu^{n-2}\ d\mu$$

Present applications to lattice problems:

Thermal-neutron leakage
Thermal-flux distributions

*See Report BNL-C-7953.

problem of determining the interaction fast effect is resolved, for isotropic scattering, by the essentially geometrical problem of obtaining the first slight collision probability for a neutron of given energy between two elementary volume elements. Theoretical complexities arising from the spatial variation of the thermal-fission sources, the presence of fuel cladding, and the shielding effect of intervening fuel elements limits the usefulness of analytical approaches to the problem.[25] On the other hand, if we divide the fuel elements into a suitable mesh, the solution indicated in the figure involves nothing more complicated than an accurate scale drawing of the lattice, a good ruler, and a table of the K_{i_j} function.[26]

Table 1 shows the general one-velocity integral equation which is equivalent to the exact Boltzmann equation for an isotropic scatterer. Similar integral equations have been derived by Carlson[27] and others at Los Alamos for anisotropic scatterers. In the present instance, the kernel of the integral equation has a simple physical interpretation, again representing the collision probability at $\vec{r}$ for a neutron starting a new flight at $\vec{r}'$. In place of the integral equation, which can be solved only in special cases, we can set up a mesh and solve an equivalent set of simultaneous linear equations. The method can now be used for heterogeneous as well as homogeneous systems, for reflected as well as bare reactors. We have run a number of trial neutron-leakage problems through by this method, and we have found that it gives accurate results for a fairly crude mesh.[4,28] At present we are running the problem of the flux distribution in heterogeneous slab lattices on the UNIVAC for a wide range of parameters, partly to determine the range of validity of spherical-harmonics approximations and partly with a view to the complete tabulation of this particular problem.

Table 2 — Influence of the Choice of Cross Sections on Reactor Parameters

Fast-fission factor ϵ in homogeneous U^{238}-H_2O assemblies

V_{H_2O}/V_u	Report KAPL-1043	Report WAPD-T-149 $\sigma_i^{\mu} = 2.10$	Report WAPD-T-149 $\sigma_i^{\mu} = 2.73$	Report BNL-C-7580	BNL, new σ_i values
0	1.23	1.23	1.17	1.227	1.170
1	1.091	1.11	1.080	1.093	1.081
2	1.062	1.069	1.055	1.060	1.055
3	1.047	1.051	1.042	1.044	1.042
4	1.038	1.041	1.035	1.035	1.034

Correction for more accurate treatment of energy losses in collisions with uranium

V_{H_2O}/V_u	Standard ϵ	Corrected for inelastic collisions	Corrected for elastic collisions
0	1.2274	1.2345	1.2216
1	1.0925	1.0932	1.0918

Table 1 shows the general one-velocity integral equation which is equivalent to the exact Boltzmann equation for an isotropic scatterer. Similar integral equations have been derived by Carlson[27] and others at Los Alamos for anisotropic scatterers. In the present instance, the kernel of the integral equation has a simple physical interpretation, again representing the collision probability at $\vec{r}$ for a neutron starting a new flight at $\vec{r}'$. In place of the integral equation, which can be solved only in special cases, we can set up a mesh and solve an equivalent set of simultaneous linear equations. The method

The influence of the choice of cross sections on reactor parameters, is shown in Table 2, where theoretical values of the fast-fission factor ϵ are tabulated for homogeneous U^{238}–H_2O assemblies. The methods used to obtain this important quantity are essentially exact. At BNL we obtain ϵ by iteration of the exact integral equation.[29] At KAPL a group method has been developed for the same purpose,[30] and at WAPD a successive neutron-generation treatment is employed.[31] The difference in results is mainly attributable to the choice of inelastic cross sections for U^{238}, which have not as yet been sufficiently well tied down. On the basis of Bonner's recent data, the value of ϵ for pure U^{238} is reduced from 1.23 to 1.17. The sensitivity

of the results at low water to uranium volume ratios indicates the need for additional accurate integral experiments in this region.

The value of ϵ is sensitive also to the value of U^{238} as a function of energy. However, the calculations are insensitive to the particular treatment of neutron-energy losses in collisions with the fuel. In particular, elastic collisions may be treated as involving no energy loss, and inelastic collisions, as slowing the neutron down past the fission threshold of U^{238}. The results of more accurate treatments are shown in the second part of Table 2.

The ratio of fast to thermal fissions in an isolated uranium rod is shown in Fig. 2. Theoretical curves, based on an extension of the method of Report CP-644, which takes the exact energy dependence of the neutron cross sections into account,[29] are compared with experimental data obtained by Untermyer[32] and Kouts.[33] Corrections for thermal-flux gradients and backscattering from a particular moderator may be obtained by the mesh methods previously discussed. The difference in the theoretical curves due to changes in inelastic cross sections becomes more pronounced for the thicker rods, and the desirability of extending the BNL measurements into this region becomes evident. This type of experiment is also relatively inexpensive since the material requirements are small.

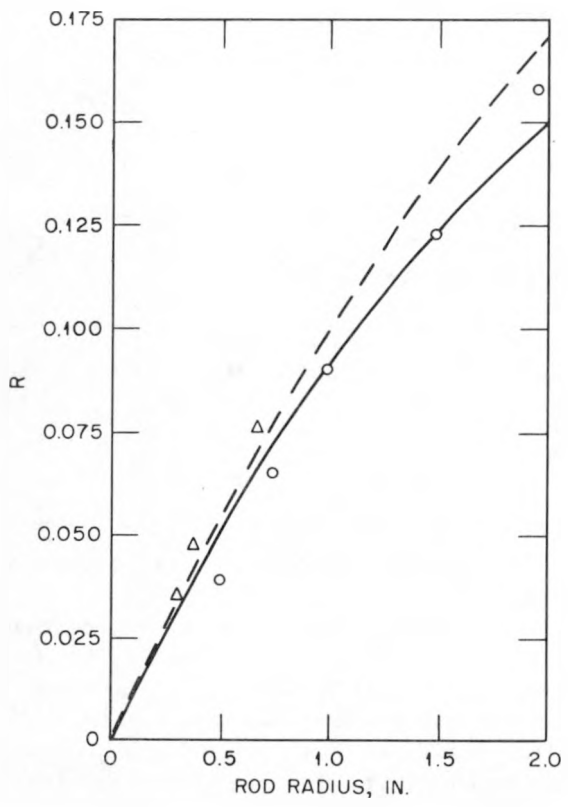

Fig. 2—Ratio of fast fissions to thermal fissions in an isolated uranium rod.

$$R = \frac{\nu^{U^{235}} \int_{E_{tres}}^{\infty} P_1\ p_f\ F(E)\ dE/(1 - P_0 p_e)}{1 - \int_{E_{tres}}^{\infty} P_1 p_f\ \nu^{U^{238}}\ F(E)\ d(E)/(1 - P_0 p_e)}$$

○, Untermyer's data. △, Kout's data. ---, old σ_i's. ——, new σ_i's. Assumptions: $\nu^{U^{235}} = \nu^{U^{238}}(E) = 2.5 \times$ flat flux. No back-scatter from moderator.

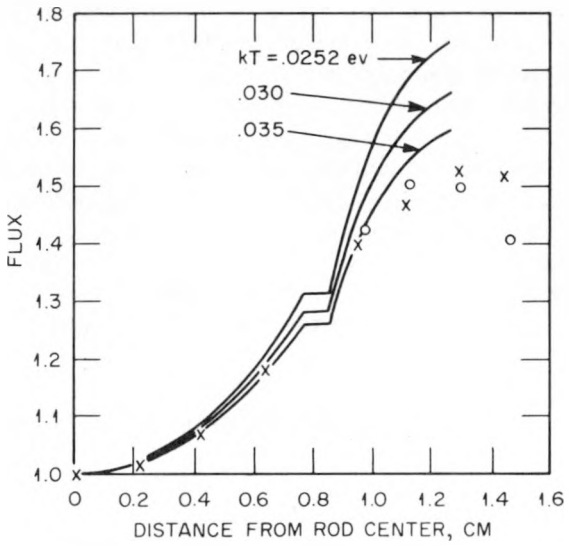

Fig. 3—Flux distribution in uranium-H_2O lattice. P_3 spherical-harmonic approximation; 1.15 per cent enriched 0.6-in.-diameter rods on triangular grid. Ratio of H_2O volume to uranium volume = 1.5. ×, experimental data along median. ○, experimental data between rod centers.

Figure 3 correlates experimental data on the intracell flux distribution in BNL H_2O–slightly enriched uranium lattices with one-velocity spherical-harmonics calculations.[3] The data indicate a strong increase in neutron temperature for close-packed lattices as contrasted with the results for more widely spaced lattices where kT values of 0.025 to 0.030 ev appear to fit the data.[29] The convenient "cylindricalization" of the lattices makes it impossible to reproduce the azimuthal variation of the flux distribution in the moderator. Relaxation calcu-

lations based on elementary diffusion theory[29] show an adequate fit of the flux distribution in the moderator, although diffusion theory yields a poor approximation for the flux distribution within the fuel rods. It may also be noted from Fig. 3 that the flux distribution does not flatten at the fictitious cell boundary as it should at the boundary of any space-filling periodic lattice. The reason is that the requirement of zero net current at the cell boundary is not synonymous with the vanishing of the neutron gradient except in elementary diffusion theory. Cylindricalization may thus introduce some error, especially in closed-packed lattices.[3]

Jack Chernick
Brookhaven National Laboratory

Nov. 9, 1954

REFERENCES

1. J. Fleck, The ψ_3 Approximation With Anisotropic Effects for Cylindrical Geometry, Report BNL-1574, Jan. 22, 1953.
2. J. Fleck, The Use of Maxwellian Averages in the Transport Equation, Report BNL-1576, Mar. 6, 1953.
3. J. Chernick, Results of UNIVAC Survey of the Thermal Utilization of BNL Experimental Lattices, Report BNL-1797, Apr. 13, 1954.
4. J. Chernick, The Solution of Reactor Integral Equations by Relaxation Methods, Report BNL-1795, Mar. 29, 1954.
5. J. Weil, Neutron-flux Distribution Calculations Using the P_3 Spherical-harmonics Method, Report KAPL-1173, July 10, 1954.
6. W. Feurzeig and B. Spinrad, Numerical Solution of Transport-theory Problems for Spheres and Cylinders, Report ANL-5049, December 1953.
7. H. Brown and D. St. John, Neutron-energy Spectrum in D_2O, Report DP-33, February 1954.
8. J. Sampson and H. Hurwitz, Dependence of Alpha (U^{235}) on Temperature, Report KAPL-511, Aug. 14, 1951.
9. J. Chernick, Temperature Coefficients of Reactivity of Reactors, Chalk River Conference on Reactor Calculations, Report CRR-546, January 1953, p.p. 46-59.
10. P. F. Zweifel and H. Hurwitz, Jr., Report of the Physics Section for September, October, and November 1953, Report KAPL-1012, p. 49.
11. D. Schiff, Multigroup Integral Network Method, Report WAPD-108, July 1954.
12. G. Safonov, Notes on Multigroup Techniques for the Investigation of Neutron Diffusion, Reactor Sci. Technol., 2(4): 63-86, December 1952.
13. J. Fleck, The Energy-dependent Boltzmann Equation Applied to Criticality Calculations for Bare Graphite-moderated Reactors, Report BNL-298, August 1954.
14. G. Goertzel, Criticality of Hydrogen-moderated Reactors, Report TAB-53, July 25, 1950.
15. D. Selengut, Critical-mass Calculations for Bare Hydrogen-moderated Reactors by Means of Transport Theory, Report APEX-121, September 1952.
16. See recent WAPD and KAPL Physics Progress Reports, e.g., Reports WAPD-MR-41, KAPL-991, KAPL-1012, and KAPL-1156.
17. B. Davison, A New Method for Calculating the Critical Radius of Systems Containing Hydrogen and Fissile Material, Report AERE T/R 826, January 1952.
18. J. Chernick, The Dependence of Reactor Kinetics on Temperature, Report BNL-173, Dec. 20, 1951.
19. J. Fleck, Kinetics of Circulating Reactors at Low Power, Nucleonics, 12(10): 52-55 (October 1954).
20. See recent BNL Quarterly Progress Reports, e.g., Reports BNL-285, BNL-297, and BNL-309.
21. W. K. Ergen and A. M. Weinberg, Some Aspects of Nonlinear Dynamics, Physica, XX(7): 413-426 (July 1954).
22. F. H. Brownell and W. K. Ergen, J. Rational Mechanics, 3(5): 565-579 (September 1954).
23. S. Oleksa, The Inelastic Scattering Cross Section of Lead, Report BNL-273, December 1953.
24. S. Oleksa, The Variation of $\alpha^{U^{235}}$ with Energy in the Intermediate-energy Range, to be published.
25. A. Radkowsky, Contribution of Fast Fissions to k, Report ANL-4476, p.p. 101-115.
26. M. Goldstein, A Table of the Function $K_{i_1}(x)$, Report LAMS-728, May 13, 1948; see also W. G. Bickley and J. Nayler, Phil. Mag., 20: 343-7 (1935).
27. B. Carlson, Neutron-diffusion Theory, Report AECD-2835, Dec. 15, 1949.
28. J. Chernick, G. Rabinowitz, and B. Mozer, Quarterly Progress Report of November 1953 to February 1954, Report BNL-285, p.p. 11-12.
29. J. Chernick, Lattice Parameters for Light-water Slightly Enriched Uranium Reactors, ANL Reactor Information Meeting, Oct. 7-9, 1953, Report ANL-5176, Pt. II, p.p. 45-54.
30. J. Weil, Fast-fission Effect in Uranium-Water Lattices, Report KAPL-1043, Jan. 15, 1954.
31. R. Hellens, Fast-fission Effect in Close-packed Lattices, ANL Reactor Information Meeting, Oct. 7-9, 1953, Report ANL-5176, Pt. II, p.p. 11-15.
32. S. Untermyer, Fast Fission in Natural-uranium Rods, Report ANL-5070, Jan. 12, 1953.
33. H. J. Kouts, K. Downes, G. Price, et al., Quarterly Progress Report of February to May 1954, Report BNL-297, p. 12.

LETTERS TO THE EDITORS

To the Editors:

The Uranium Metal Quality Working Committee (made up of representatives of E. I. du Pont de Nemours & Company, National Lead Co., General Electric Company, and Mallinckrodt Chemical Works) has become concerned over the marked variation in reported tensile properties of uranium with slight changes in test temperature. This problem has been studied by the committee, and a plan of cooperative study has been accepted. In order that additional data may be obtained, laboratories not represented on the Uranium Metal Quality Working Committee are invited to conduct tensile tests and to report data according to the system described below. It will then be possible to use all the data obtained in a solution to this problem.

To give additional background on the problem and the proposed system of testing and reporting data, the following information is taken from the report to the Uranium Metal Quality Working Committee:

At the request of the Uranium Metal Quality Working Committee, a meeting was held at Battelle on November 8, 1954, to discuss the tensile testing of uranium. This meeting was attended by Mr. Kattner and Dr. Bush of General Electric, Dr. Fellows of Mallinckrodt, Mr. Guay of National Lead, and Mr. Muehlenkamp and Mr. Saller of Battelle.

The first part of the meeting was devoted to a review of recent data as background information for defining the problems and setting up possible research programs for their solution. Recent results at Battelle, Hanford, and National Lead were presented and evaluated.

Briefly, the situation has not been changed by recent work. There is definite evidence of a very marked change in tensile properties (ultimate strength, per cent elongation, and per cent reduction in area) in the temperature range from 50 to 250°F. A peak in ultimate strength occurs in this range, and, in the same range, elongation and reduction of area increase drastically with an increase in temperature. This critical temperature range varies according to the type of uranium and condition of heat treatment of the specific sample.

Future work on impact testing has failed to reveal a similar behavior. The impact strength of uranium increases gradually with increasing temperature. While there is a change in the appearance of the fracture, there is no sudden increase in impact strength.

The problem appears to be that of determining the effect of a number of variables including test temperatures, strain rate, grain size, orientation, condition of heat treatment, method of fabrication, and chemical composition on the tensile properties of uranium. An understanding of the relationship of these variables is essential if tensile testing is to be used as a part of production control.

Three types of attack on the problem were discussed. One method could be based on a fundamental study of the effect of all the above variables on tensile properties. Such a program would of necessity start with pure uranium and would, by its very nature, be quite time consuming. Another approach would be to assemble all possible data from routine testing that is done and attempt to determine statistically the relative effect of the various factors such as grain size, etc. on tensile properties.

The group decided that neither of the above approaches seemed proper for this group to undertake. Any laboratory planning to undertake the fundamental approach to this problem should be encouraged, but this group would not attempt to sponsor or direct the program. It is believed further that a statistical approach using presently existing data would not be fruitful, since insufficient information regarding the several variables involved is available.

The group then decided to suggest a type of cooperative program which will be organized to take maximum advantage of tensile testing being done at the various sites. It is hoped that by studying the data

obtained in the next 6–9 months, some idea of the relative importance of the variables can be obtained. This could lead to a more direct approach on the important variables.

In order to get the most information from the tests that are run, it is necessary that there be some uniformity of test conditions and the way in which the data are reported. The group recommends the following.

Specimen Size: Standard 0.505-in. round specimens with 2-in. gage length. For some work, 0.250 in. will be used.

Strain Rate: 0.01 in. per in. per min to the yield strength.

The following information should be reported.

1. Specimen History: A description of melting practice, fabrication history, and heat treatment.
2. Size of Sample
3. Density of Material
4. Macrostructure
5. Microstructure
6. Degree of Orientation of Grain Structure
7. Composition: This should include values for carbon, hydrogen, iron, magnesium, nitrogen, and silicon.
8. Strain Rate
9. Test Temperature
10. Yield Strength: Based on 0.2 per cent offset.
11. Ultimate Strength
12. Elongation
13. Reduction in Area

Since it appears that test temperature is the most important single variable, it is suggested that any single lot of material be tested with duplicate samples at six temperatures. Tests should first be made at −75, +75, and 300°F. Based on the results of the first three tests, the final three tests should be made at 25-degree intervals chosen to define the critical temperature range. For example, if low values of elongation are obtained at both −75°F and +75°F while the elongation at +300°F is high, the next three tests should be run at temperatures above 75°F. Conversely, if the elongation at −75°F is low, the elongation at +75°F is moderately high and that at 300°F is high, the appropriate subsequent test temperatures might be +25°F, +50°F, and +100°F. It is hoped that the sharp break in the curve will be defined in this way.

Laboratories desiring to participate in this program should contact H. A. Saller at Battelle Memorial Institute.

H. A. Saller, Advisor to the Uranium Metal Quality Working Committee
Battelle Memorial Institute

Mar. 30, 1955

To the Editors:

A Thorex Information Meeting was held in October 1954 at Oak Ridge National Laboratory for the purpose of reviewing the latest irradiated-thorium processing technology. Irradiated-thorium processing, which provides for the recovery of more than 99.7 per cent of the fissionable U^{233} and the source Th^{232}, is essential to the economy of U^{233} breeder reactors. Procedures developed prior to Thorex merely recovered U^{233}, leaving Th^{232} and Pa^{233} plus fission products in the extraction waste. (The newer Thorex process for recovery, decontamination, and separation of Th^{232} and U^{233} was described in the June 1954 issue of *Reactor Science and Technology*. Representatives from the Atomic Energy Commission, E. I. du Pont de Nemours & Company (Savannah River), Hanford, Mound Laboratory, National Lead Co. of Ohio (Feed Materials Processing Center), Los Alamos Scientific Laboratory, Knolls Atomic Power Laboratory, and ORNL were present to participate in the Thorex Information Meeting at ORNL.

At the meeting the Hanford representatives described their consideration of the possibilities of a dual-purpose plant that could handle either Thorex or Purex, whichever the Commission might ultimately request. They contemplated three solvent-extraction cycles to eliminate head-end and possibly digestion procedures. The first two cycles would provide codecontamination in order to ease criticality problems arising from the dual-purpose design concept.

The Savannah River representatives indicated that, if Du Pont is requested to process thorium, this would be done ultimately on a closed-cycle basis: irradiation, processing, metal fabrication, and back to irradiation. The initial fuel charge would be aluminum-silicon bonded slugs; however, subsequent charges may not include bonding. Hanford reported they already had unbonded thorium slugs in their reactors; and a hot-canning procedure being developed at the Feed Materials Processing Center (FMPC) looked very promising as a superior alternative to aluminum-silicon bonding.

Savannah River Thorex development was based on maximum use of existing plant facilities and inclusion of conservative procedures. Hence

their processing scheme included caustic dejacketing, batch dissolution with 10N HNO_3–0.1N NF, MnO_2 head-end scavenging, and 30 per cent tri-*n*-butyl (TBP) solvent extraction in mixer-settlers. Solvent extraction would include an acid-deficient aluminum nitrate (ANN) first cycle, an acid second thorium cycle, and an acid second U^{233} cycle followed by U^{233} concentration by ion exchange.

Savannah River experience with irradiated-thorium feed runs in the miniature mixer-settler using nine extraction and seven scrub stages yielded uranium and thorium losses to the 1AW stream of ~0.1 and 0.01 per cent, respectively. Protactinium and zirconium-niobium decontamination factors to the 1BT stream have ranged between 10^3 and 10^4; ruthenium and rare-earth decontamination has been poor and variable. Head-end was expected to improve all decontamination factors except for rare earths, and the second cycle was expected to give good rare-earth decontamination. Savannah River experience indicated that 20 stages would be required for good thorium-uranium partition.

The FMPC, in developing thorium nitrate-to-metal processing procedures, abandoned aqueous hydrofluorination of thorium nitrate because of the very high maintenance cost of the process equipment and is now using the "oxalate process." The latter includes calcining the thorium oxalate to thorium oxide, hydrofluorinating the oxide, reducing the fluoride with calcium in the presence of $ZnCl_2$ to thorium-zinc alloy, and finally distilling off the zinc to yield a thorium "sponge." The sponge is melted in zirconia crucibles. FMPC contracted with the Bureau of Mines to develop an arc-melting procedure. FMPC was also investigating the possibilities of the Kroll (reduction of $ThCl_4$ with molten magnesium) and electrolytic (reduction of $ThCl_4$ in a fused-salt bath of NaCl-KCl) processes for thorium-metal production.

KAPL was conducting a limited study on an "acid Thorex" flow sheet. This study was scheduled to end by mid-February 1955. The KAPL acid flow sheet incorporated caustic dejacketing of the fuel elements, thorium dissolution with 13.6N HNO_3–0.075N HF, head-end MnO_2 precipitation, followed by high-temperature (~70°C) solvent extraction in mixer-settlers. The discussion at the meeting concerning the head-end procedure brought out that Du Pont would require a purification step ahead of solvent extraction (>99 per cent protactinium and >80 per cent ruthenium are removed from the feed by the MnO_2 procedure). However, the MnO_2 procedure requires centrifugation, whereas the ORNL Thorex flow sheet includes a feed-digestion step from which the feed solution goes directly to the extraction pulse column without clarification. It was pointed out that the ORNL metal-recovery plant operations had never required either head-end treatment or feed clarification in any of the various fuel-processing jobs so far undertaken.

KAPL reported that, with respect to radiation effects on the nature of MnO_2 precipitate formation in head-end and the question of cake stability at high radiation levels, their Purex head-end studies involved gross beta and gross gamma levels in the head-end operation "which were as high, and higher, respectively, than any contemplated in short-cooled Thorex feeds." They reported, "the nature of the precipitate, carrier efficiency, and solution clarification were satisfactory and the Mn^{++} content of the resultant feed to solvent extraction was satisfactorily low." The cake, after centrifugation and washing, was immediately dissolved. KAPL felt that possible Thorex problems from heat production or criticality after protactinium decay could be overcome by further dilution.

KAPL reported thorium and uranium losses of 0.1 and <0.01 per cent, respectively, to the extraction waste in Mini mixer-settler tests using nine extraction and seven scrub stages. In 70°C non-head-ended runs they observed zirconium-niobium and ruthenium decontamination factors of 2×10^5 and 2×10^3, respectively. However, they reported emulsion troubles in the thorium-uranium separation bank; hence no separation data were reported.

At ORNL thorium-fuel reprocessing development, which was recommenced in 1951 at the request of the Commission for a process capable of recovering, decontaminating, and separating U^{233}, thorium, and protactinium, resulted in the Thorex solvent-extraction process using TBP. The pilot plant for this process, which was nearing the "cold" start-up point at the time of the October 1954 meeting, will not include protactinium recovery initially because earlier

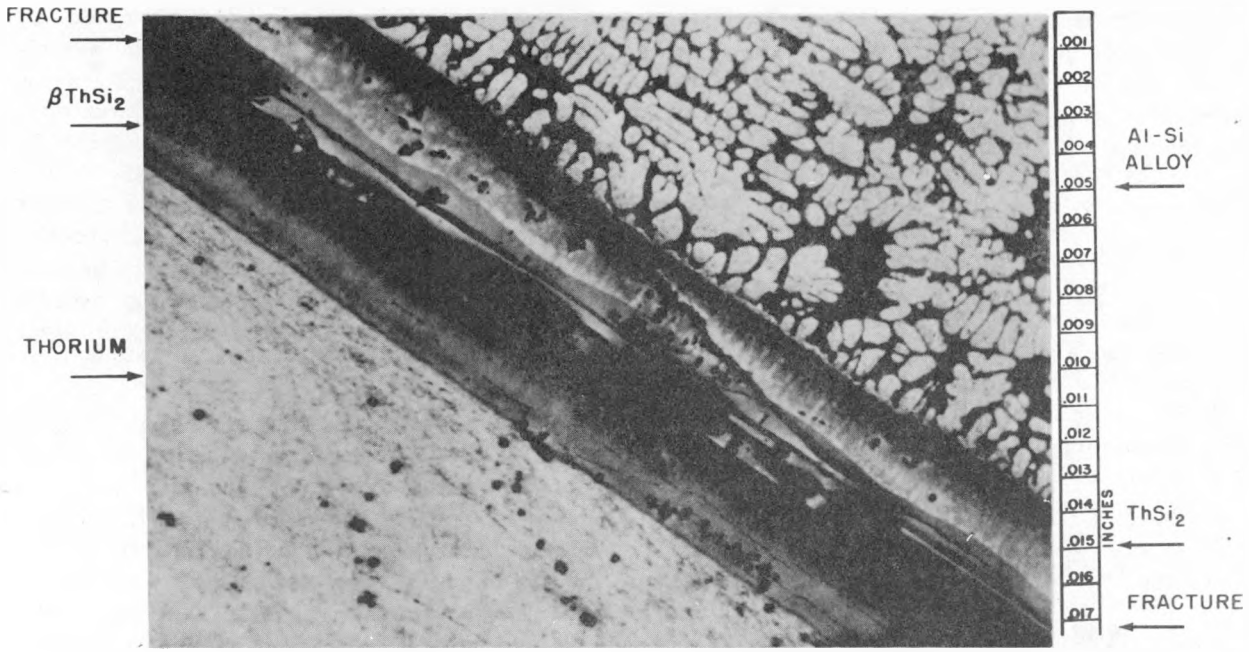

Fig. 1—Microphotograph (bright field) of bond between thorium and aluminum-silicon alloy. Note continuous fracture in intermetallic compounds.

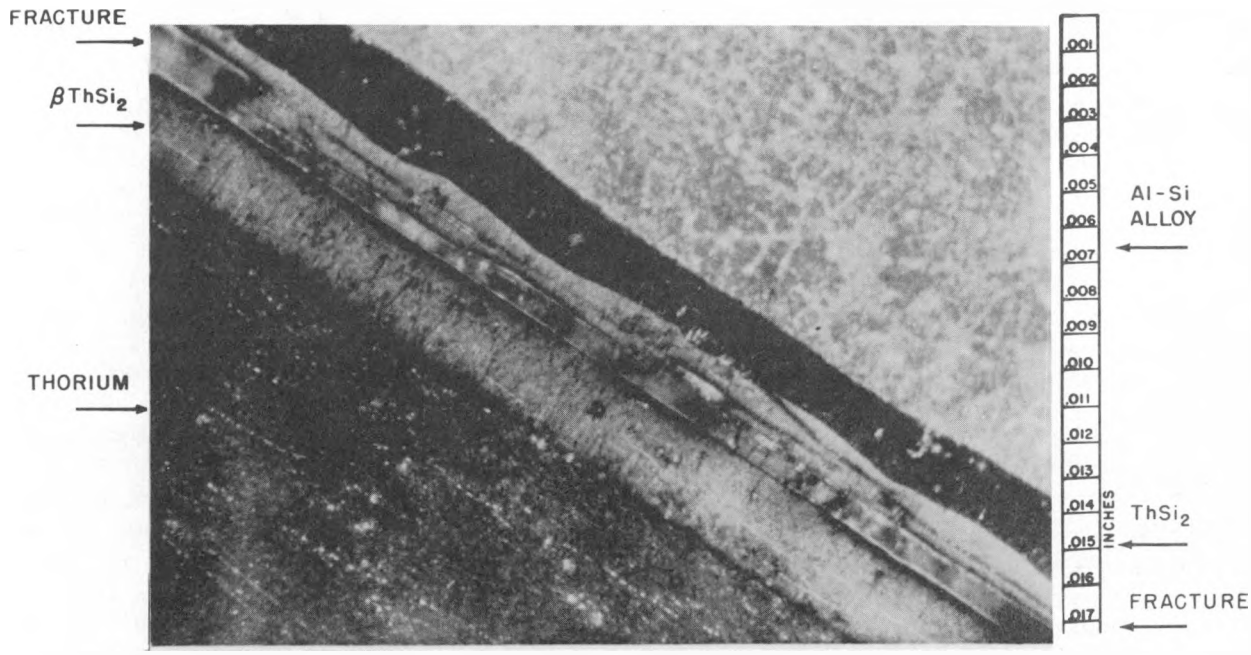

Fig. 2—Microphotograph (polarized light) of same field as in Fig. 1. Note two compound layers.

interest in protactinium has since vanished. However, the process was designed to handle short-cooled material in order to permit maintaining a low inventory of unrecovered U^{233}. It was pointed out that the Thorex process is similar to the Purex process, differing principally in that:

1. It was designed to handle short-cooled fuel (of particular interest in a power economy)
2. It does not have a fuel-dejacketing step because aluminum is used for salting and for minimizing corrosion
3. F^- ion is required for catalyzing thorium dissolution
4. A feed-adjustment step is required to
   (a) Dehydrate the hydrous oxides of zirconium and silicon that otherwise cause emulsions, thus impairing solvent-extraction contactor throughput
   (b) Dissolve any blue ThO_2 not dissolved in the dissolver
   (c) Enhance ruthenium decontamination by a factor of ~100

The development of the acid-deficient Thorex process chemical flow sheet was described in detail in the June 1954 issue of *Reactor Science and Technology*.

The use of aluminum-silicon bonded fuel elements would present some difficulty in radiochemical processing. Metallographic examination at ORNL of aluminum-silicon bonded slugs showed that the silicon in the aluminum-silicon alloy bonding agent had migrated to the surface of the thorium metal and had formed an extremely refractory thorium silicide layer about 7 mils thick. Furthermore, as shown in Figs. 1 and 2, a continuous fracture was evident between the thorium and the aluminum can. Such a fracture would have considerable effect on the heat-transfer properties from the thorium to the aluminum can if slugs canned by this procedure were used in a reactor.

Laboratory data indicated that the thorium silicide layer of the bonded slugs was extremely resistant to nitric acid and alkali attack even though the normal catalyst, mercury, was used in the former case. Concentrations of mercury four times that used in a noncoated slug dissolution failed to completely dissolve the intermetallic layer after refluxing for 25 to 27 hr in 13M nitric acid. Caustic dejacketing using 10 per cent NaOH–20 per cent $NaNO_3$ did not dissolve or disintegrate the thorium silicide layer after refluxing for 20 to 24 hr. The very passive layer of thorium silicide was not dissolved when fresh dissolvent was charged to the dissolver. As shown in Fig. 3, the intermetallic layer was so passive that the thorium metal was dissolved through the center of the slug before the surface layer was significantly penetrated. The segments of the bonded slugs shown in Fig. 3 were cut from the same slug; only specimen A received the caustic dejacketing step.

For the aluminum-silicon bonded slugs to be utilized in the Thorex pilot plant, it would be necessary to develop either (1) a more efficient dejacketing reagent or (2) a revised dissolution flow sheet dissolving aluminum, thorium, and the intermetallic compounds simultaneously. In either case centrifuges or filters would have to be installed in various feed lines to prevent any aluminum-silicon or thorium silicide particles from reaching the extraction columns. A considerable waste-storage problem would be involved since (1) disposal of the hot precipitate from the intermetallic layer would involve handling hot solids; (2) the aluminum jackets, if removed with caustic, would not be usable as salting agent in the extraction column; and (3) the filtered or centrifuged precipitate of the dissolving cycle would represent a considerable loss of thorium and U^{233} unless provisions were made to eventually reprocess this material.

ORNL laboratory-scale corrosion results presented at the meeting indicated (1) that type 309 SNb stainless steel would be best for use in the fuel-dissolver and feed-adjustment tanks but (2) that the observed corrosion notes were very much exaggerated by the build-up of chromium in the test solutions during the 200- to 400-hr exposure periods. The laboratory tests indicated peak dissolver and feed-adjustment tank corrosion rates, during the most corrosive portion of the dissolver and feed-adjustment cycles, of 30 and 55 mils/year. Because the corrosion test solutions were not replaced with fresh solutions during the extended exposure periods and because the test exposures were carried out in stainless-steel beakers, the chromium concentration built up to values exceeding by a factor of 10 the concentrations to be expected in Thorex plant operations. J. E.

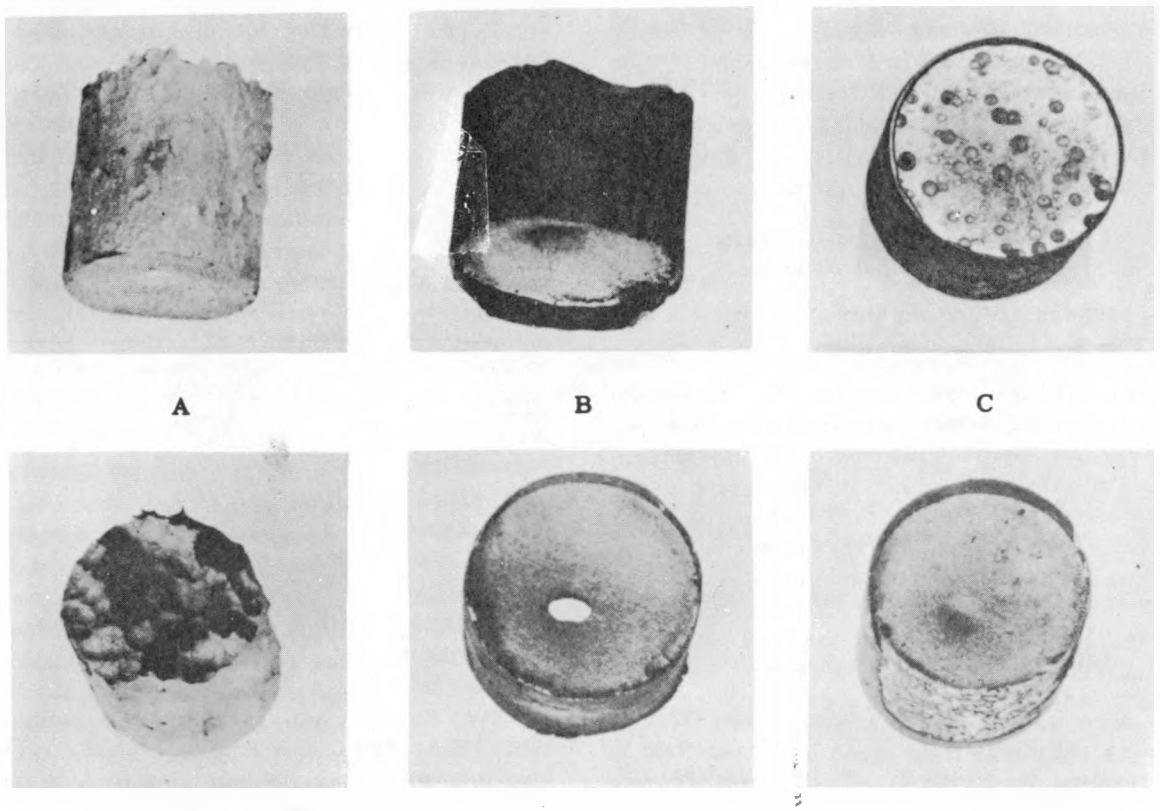

Fig. 3—Aluminum-silicon bonded thorium slug. Slug was partially dissolved in $HNO_3-F^--Hg^{++}$. A, end of slug, which was previously dejacketed with NaOH. B, center of slug. C, end of slug.

Truman [J. Appl. Chem. London, 4: 273-283 (May 1954)] showed the tremendous effect of chromium on accelerating corrosion rates in high HNO_3 concentration solutions at boiling. This effect unfortunately was not recognized prior to Thorex corrosion studies which were carried out in 1953 and early 1954. A significant corrosion program will be carried out in the Thorex pilot plant and should provide the best indication of corrosion rates to be expected in the critical parts of the Thorex process.

Mechanical performance of all major process equipment has so far been highly satisfactory. This effort indicates that the Thorex pilot-plant program can be carried out safely with a minimum of operational problems.

Performance of the Thorex pilot plant was indicated by the following data:

	Column	Per cent
Average thorium loss per column	A	0.15
	B	0.01
	C	0.01
Average uranium loss per column	A	0.03
	B	0.6
	C	0.01

The A column was operated with 9 ft of extraction in order to provide a maximum scrub length of 24 ft. The high uranium loss in the B column indicates inadequate solvent scrubbing of the aqueous phase in the bottom section of the column. (The B and C columns in this pilot plant are concatenated pulse columns; the solvent scrub section length in the B column is 15 ft.)

Incomplete decontamination data on the uranium product are as follows:

1. Protactinium decontamination varied from 1×10^6 to 6×10^6 and averaged 4×10^6.

2. Niobium-zirconium decontamination varied from 2×10^6 to 8×10^6 and averaged 4×10^6.

3. Total rare-earth decontamination varied from 2×10^7 to 1×10^8 and averaged 7×10^7.

4. Ruthenium decontamination varied from 3×10^3 to 6×10^4 and averaged 1×10^4.

The data for protactinium, zirconium-niobium, and total rare earth were consistent throughout the whole series of runs. The initial ruthenium decontamination factor was about 6×10^4 but decreased over the series of runs to 3×10^3, a value more consistent with previous data obtained in the chemical development section.

The program will attempt to establish such things as the conditions for maximum feasible ruthenium decontamination factor and B column U^{233} recovery.

KAPL has reported that recent runs using their high-temperature acid flow sheet have indicated that in such a system precipitation occurred in the partition and stripping banks. They also report precipitation was similarly observed when testing the Savannah River flow sheet under high-temperature conditions, and they will test the ORNL flow sheet in like manner next.

Following several runs using dissolved irradiated-thorium feed, KAPL observed an increase in gamma activity in the thorium product. Both KAPL (R. C. Feber, Report KAPL-1271, February 1955) and ORNL (E. D. Arnold, Report ORNL-1869, March 1955) have restudied the thorium decay scheme and found that 70-year U^{232}, which is produced in the thorium-U^{233} cycle, produces much larger concentrations of Th^{228} and its daughters than would be present in natural thorium. Results of the study indicate considerable gamma activity will be present in both U^{233} and the thorium products. Apparently the U^{233} problem can be relatively readily accommodated, but the recycle of thorium through metallurgy will become significantly more troublesome from the radiation hazards standpoint since the metal activity after infinite recycle increases by a factor approaching 2 to 3 over natural thorium activity.

A. G. Jealous
Oak Ridge National Laboratory

Mar. 10, 1955

To the Editors:

The Division of Reactor Development, U. S. Atomic Energy Commission, Washington, D. C., has commissioned Nuclear Development Associates, Inc., to issue a serial *Boiling Burnout Newsletter* presenting fresh experimental data, correlations, operating problems, critiques, and notices of new projects in this field, with the aim of contributing to the improved design of nuclear reactors and connected power plants. All organizations and institutions engaged in boiling burn-out experimental work or in need of pertinent data are invited, if not already on the mailing list for this newsletter, to write to me at Nuclear Development Associates, Inc., 80 Grand Street, White Plains, N. Y.

John E. Viscardi, Editor
Boiling Burnout Newsletter